

MYELOID SPECIFIC EGFR REGULATES CARDIAC HOMEOSTASIS AND  
PROTECTS THE INFARCTED HEART DURING REPAIR

---

A Dissertation  
Submitted to  
The Temple University Graduate Board

---

In Partial Fulfillment  
of the Requirements for the Degree  
DOCTOR OF PHILOSOPHY

---

By  
Ama Dedo Akainyah Okyere  
August 2022

Examining Committee Members:

Douglas Tilley PhD, Advisory Chair, Department of Cardiovascular Sciences  
Michael Autieri PhD, Committee Member, Department of Cardiovascular Sciences  
Sadia Mohsin PhD, Committee Member, Department of Cardiovascular Sciences  
Ying Tian PhD, Committee Member, Department of Cardiovascular Sciences  
Michael Tranter PhD, External Examiner, Department of Internal Medicine, Division of  
Cardiovascular Health and Disease, University of Cincinnati, College of Medicine

## ABSTRACT

**Background & Rationale:** Tissue residing macrophages (TRMs) guard normal physiology in the steady-state heart, and can be important for coordinating inflammatory events at the onset of injuries like myocardial infarction (MI). Following an ischemic attack though, TRMs become outnumbered by circulating myeloid cells and monocyte (mon) derived macrophages (mf), which function to clear injury debris and instruct cardiac repair to mitigate heart failure (HF) severity. The major goal of this work is to investigate how TRM and post MI mf are regulated to participate in cardiac health and post injury repair. Epidermal growth factor receptor (EGFR) is a cell surface tyrosine kinase receptor governing numerous cell processes, and though it has been historically studied as an oncogene, EGFR is implicated in cardiac physiology, and has been shown to regulate mf activation, survival and function.

**Objectives:** Here, we investigated how the loss of EGFR in mf would impact basal cardiac structure, and function, as well as post MI remodeling, repair, and HF development.

**Methods & Results:** By using a myeloid-specific cre, we generated mice with EGFR knockout in mf and other myeloid cells (EGFRmylKO), and performed comparative analyses between these and control mice. We identified that the loss of EGFR in myeloid cells, including cardiac TRMs, resulted in modest signs of stress at baseline, namely enlarged cardiomyocytes and elevated stress associated fetal gene transcripts. Though the loss of EGFR did not impact TRM subtype distribution in basal hearts, whole transcriptomic analyses of these cells revealed over 700 differentially expressed in EGFRmylKO relative to control. Among these are insulin like growth factor (IGF)

binding proteins (IGFBP) family members 5 and 7, which are known to regulate not only IGF availability, but also IGF and other cytokine receptor activation, all key players in cardiac hypertrophy. Indeed, EGFRmylKO hearts exhibited enhanced extracellular signal-regulated kinase (ERK)1/2 activation relative to control. Additionally, in response to MI, EGFRmylKO mice experienced a hastened decline in cardiac function, coupled with exacerbated hypertrophic remodeling, and limited angiogenic repair. Analyses of the inflammatory response in EGFRmylKO injured hearts revealed a greater percentage of inflammatory CCR2/Ly6C<sup>hi</sup> mf even at 7 days into the injury, resulting in significantly reduced transcripts of reparative factors like interleukin (IL)-10.

**Conclusions:** In sum, we propose novel roles for mf EGFR in cardiac physiology and pathology. TRM EGFR regulates several transcripts, required to maintain cardiac homeostatic integrity. In ischemic injury, mf EGFR is key to promoting repair and limiting HF severity.

## **FUNDING**

Ama Okyere was supported by two National Institutes of Health/Heart, Lung, and Blood Institute grants: an R01 HL136219-04 to Douglas Tilley, and Jeffrey Benovic; and an F31 HL154814-01 to Ama Okyere.

## ACKNOWLEDGMENTS

Over the last several years, I have come to understand how tough, but rewarding research can be, and I have grown so much, I could not have done it without the help of so many, who I would like to acknowledge.

First, my thesis advisor Doug. Since my rotation, you have been very encouraging, and have helped me develop as a scientist. You have given me the opportunity to work through big and small ideas, and you have provided critical guidance, feedback, excitement, and suggestions to help me stay on course. I have appreciated all of the helpful discussions about the project. You have also given me a lot of opportunities for professional advancement, and have supported my academic growth. I have learned a lot from you, and am very grateful.

Next, I would like to thank members of my committee, past and present. Dr. Wen Chen, Dr. Mike Autieri, Dr. Ying Tian, and Dr. Sadia Mohsin. You have provided ample project feedback, have shared technical solutions, have written letters of support/reference, and have discussed ideas and my progress with great enthusiasm. I am also thankful for the atmosphere you have fostered during committee meetings. I am also thankful to my external examiner Dr. Mike Tranter. I appreciate your willingness to thoughtfully review my work, and provide feedback.

I would also like to acknowledge members of my lab, and the DCVS. Postdocs Dr. Grisanti, Dr Bajpai, former student Dr. Guo, scientist Tobias T, and lab manager Rhonda. I learned so much from all of you from the beginning of this journey, from technical skills, to experiment setup. I have really appreciated all your support, and guidance. I have also appreciated all of the comradery and laughter. Thank you for answering all of

my annoying questions, and for indulging me in fun discussions. I would also like to thank Dr. Nayak, Dr. Xu, Erin, Josh, Viren, Jeanette, Nitya, FI, SS, KV, and VP. All of you have been tremendously helpful, have taught me so much, and I have been able to count on you in lab. Thank you also for answering all of my annoying questions. You have also been very spirited, and we have had great fun in lab together. Also to David HH tepidlipsky. I am very grateful for your dedication to EGFR! You were so helpful, and patient. And I appreciated your sense of humor. I am also thankful to many members of DCVS: postdocs (Drs. IK, AG, MC, Candischay, JP, KG, CdL), other students and scientists (A/JS, DK, AE, RC, JI, AML, NL, CG), and faculty (Drs. EG, JE, WK, AKS) who have contributed to my scientific, academic, and professional development.

Last, I would like to express gratitude to my friends and family. First, friends at temple Sophie, MariaBethania, Bethania, Luciana, Ron, Tiffania. You have been supportive, kind, and fun. I wouldn't want to have gone through this program without you all. Also other friends, Meg FG, Liate, Priscilla, Leigh, Mariah. You have been so supportive, and loving, and we have had great fun together. Next, to my incredible sister Jess. You are my number one hype lady. You are always on my side, and you are incredibly loving, kind, supportive, and fun. I am always inspired by how fearless you are. Next to my parents, it is great to have your support and love in life. You have been so encouraging, and always believe that I will do my best. You have been great examples of hard work, trying new things, moving forward, being organized, thinking critically, and also having fun and building community. Lastly, to my extended family everywhere, you are always so supportive and loving even from afar! I am so grateful. Thanks to you all, and many more I couldn't name.

# TABLE OF CONTENTS

|  | Page |
|--|------|
| ABSTRACT.....  | ii   |
| FUNDING.....   | iv   |
| ACKNOWLEDGEMENTS.....  | v    |
| LIST OF FIGURES.....   | xi   |
| LIST OF TABLES.....  | xiv  |
| LIST OF ABBREVIATIONS.....   | xv   |
| <br>   |      |
| CHAPTER 1: CARDIAC PHYSIOLOGY AND HEART FAILURE, CONSIDERING<br>THE ROLE OF MACROPHAGES..... | 1    |
| 1.1 Brief Epidemiology of Heart Failure .....  | 1    |
| 1.1.1 Cardiovascular Disease.....  | 1    |
| 1.1.2 Recent Heart Failure Statistics.....   | 2    |
| 1.1.3 Normal Cardiac Structure and Function.....   | 2    |
| 1.1.4 Abnormal Cardiac Function & Heart Failure Types.....                                   | 3    |
| 1.1.5 Risk Factors for Heart Failure.....  | 4    |
| 1.1.6 Current Heart Failure Therapies.....   | 7    |
| 1.2 Cardiac Cell Distribution, Physiological Function, & Post Injury Mechanisms.....         | 8    |
| 1.2.1 Cardiac Muscle.....  | 8    |
| 1.2.2 Cardiac Fibroblasts.....   | 10   |
| 1.2.3 Cardiac Vasculature.....   | 11   |
| 1.3 Cardio-immunology: Inflammation in the Healthy and Failing Heart.....                    | 12   |
| 1.3.1 Immune Cells: General Introduction.....  | 12   |

|  |   |    |
|--|---|----|
| 1.3.2  | Lymphocytes .....   | 15 |
| 1.3.3  | Myeloid Cells.....  | 17 |
| 1.3.4  | Macrophages (Mf) in Cardiac Homeostasis & Heart Failure.....                              | 18 |
| 1.4  | Epidermal Growth Factor Receptor (EGFR): A Key Factor for Macrophages in the Heart? ..... | 26 |
| 1.4.1  | Introduction to Receptor Biology.....   | 26 |
| 1.4.2  | EGFR.....   | 29 |
| 1.4.3  | EGFR Signalome.....   | 30 |
| 1.4.4  | EGFR in the Cardiovascular System.....  | 35 |
| 1.4.5  | Myeloid-Cell Specific EGFR.....   | 37 |
| 1.5  | Summary, Thesis Key Questions, and Hypothesis.....  | 41 |
| CHAPTER 2: EXPANDED MATERIALS AND METHODS..... |   | 43 |
| 2.1  | Animal Protocols.....   | 43 |
| 2.2  | Mouse Genotyping.....   | 43 |
| 2.3  | Reverse Transcription – quantitative Polymerase Chain Reaction (RT-qPCR)...               | 45 |
| 2.4  | Tissue Histology.....   | 45 |
| 2.5  | Primary Cell Isolation & Staining for Flow Cytometry.....                                 | 49 |
| 2.6  | Isolation of Cardiac Cluster of Differentiation (CD)11b Cells.....                        | 50 |
| 2.7  | Whole Transcriptome Analysis.....   | 52 |
| 2.8  | Antibody Array Analysis.....  | 53 |
| 2.9  | Neonatal Rat Ventricular Myocyte (NRVM) Isolation.....                                    | 54 |
| 2.10   | Isolation & Culture of Bone Marrow Derived Macrophages.....                               | 55 |
| 2.11   | L-cell clone 929 Culture.....   | 55 |

|   |           |
|---|-----------|
| 2.12 Bone Marrow Derived Polarization.....  | 55        |
| 2.13 Conditioned Media Assays.....  | 56        |
| 2.14 Protein Extraction and Immunoblot Analysis.....  | 56        |
| 2.15 Mouse Model of Non-Reperfused Myocardial Infarction.....   | 57        |
| 2.16 Echocardiography.....  | 58        |
| 2.17 Mitochondrial Bioenergetics Analysis.....  | 58        |
| 2.18 Statistical Analysis.....  | 59        |
| <b>CHAPTER 3: MYELOID SPECIFIC EGFR REGULATES CARDIAC HOMEOSTASIS<br/>AND PROTECTS THE INFARCTED HEART DURING REPAIR.....</b>                             | <b>60</b> |
| 3.1 Myeloid-Cell Specific EGFR Knockout Mice Show Significantly Reduced EGFR<br>in Cardiac Myeloid Cells and Bone Marrow Derived Macrophages.....         | 60        |
| 3.2 Myeloid-Cell Specific EGFR Maintains Cardiac Homeostasis During Normal<br>Physiology.....   | 65        |
| 3.3 Myeloid-Cell Specific EGFR Deletion Does not Shift Resident Cardiac<br>Macrophage Subsets in the Steady State Heart.....                              | 71        |
| 3.4 Myeloid-Cell Specific EGFR Deletion Significantly Shapes the Cardiac CD11b <sup>+</sup><br>Transcriptome in the Steady State Heart.....               | 74        |
| 3.5 Myeloid-Cell Specific EGFR Regulates CD11b <sup>+</sup> IGFBP Expression and is<br>Associated with Elevated Growth Factor Signaling in the Heart..... | 79        |
| 3.6 Impact of Myeloid-Cell Specific EGFR on Cardiac Structural Integrity During<br>Ageing.....  | 82        |
| 3.7 Myeloid-Cell Specific EGFR Deletion Aggravates Cardiac Dysfunction<br>Following Ischemic Injury.....  | 85        |
| 3.8 Myeloid-Cell Specific EGFR Limits Adverse Cardiac Remodeling Following<br>Ischemic Injury.....  | 90        |
| 3.9 Myeloid-Cell Specific EGFR Regulates the Post Ischemic Inflammatory<br>Response.....  | 94        |
| 3.10 Myeloid-Cell Specific EGFR Promotes Pro-Repair Myeloid<br>Polarization.....  | 108       |

CHAPTER 4: KEY FINDINGS AND SIGNIFICANCE, DISCUSSION, AND FUTURE DIRECTIONS.....112

    4.1 Summary and Significance.....112

    4.2 Extended Discussion.....116

    4.3 Future Directions.....127

REFERENCES CITED.....131

## LIST OF FIGURES

|  |    |
|--|----|
| Figure 1. Heart Failure (HF) Statistics.....   | 5  |
| Figure 2. Cardiac Cellular Complexity.....   | 9  |
| Figure 3. Cardiac Immune Cell Landscape.....   | 13 |
| Figure 4. Cardiac Macrophages (Mf) in Post Ischemic Injury Response.....   | 23 |
| Figure 5. Epidermal Growth Factor Receptor (EGFR) Family.....  | 28 |
| Figure 6. Major EGFR Signaling Pathways.....   | 31 |
| Figure 7. Generation of Myeloid-Cell Specific EGFR Knockout (KO) Mouse Model.....  | 44 |
| Figure 8. Myeloid-Cell Specific EGFR Deletion Results in Significant Reduction in EGFR Gene Expression and Protein Level in Bone Marrow Derived Macrophages..... | 61 |
| Figure 9. Myeloid-Cell Specific EGFR Deletion Results in Significant Reduction in EGFR Gene Expression in Cardiac Myeloid Cells.....                             | 63 |
| Figure 10. Myeloid-Cell Specific EGFR Deletion does not Result in Compensatory Changes in the ErbB2-4 Family.....  | 64 |
| Figure 11. Myeloid-Cell Specific EGFR Deletion does not Alter Canonical EGFR Signaling.....  | 64 |
| Figure 12. Myeloid-Cell Specific EGFR Deletion Results in Increased Cardiomyocyte Size in the Left Ventricle, with No Change in Total Tissue Weight.....         | 66 |
| Figure 13. Myeloid-Cell Specific EGFR Deletion Leads to Elevated Levels of Fetal Gene Transcripts in the Left Ventricle.....                                     | 67 |
| Figure 14. Myeloid-Cell Specific EGFR Deletion does not Result in Altered Cardiac Function During Normal Adulthood.....  | 69 |
| Figure 15. Myeloid-Cell Specific EGFR Deletion does not Significantly Influence Resident Macrophage Subtypes in the Heart.....                                   | 73 |
| Figure 16. Cardiac CD11b <sup>+</sup> Cells in EGFRmylKO Exhibit Unaltered Transcripts of Resident Macrophage Markers.....                                       | 74 |
| Figure 17. Cardiac CD11b <sup>+</sup> Cells in EGFRmylKO Hearts Show Significant Differential Gene Expression Compared to Control.....                           | 75 |

|  |     |
|--|-----|
| Figure 18. IPA Revealed Relevant Pathways Altered in Cardiac CD11b <sup>+</sup> Cells in EGFRmylKO Hearts Compared to Control.....             | 77  |
| Figure 19. EGFRmylKO Cardiac CD11b <sup>+</sup> Cells Differentially Express Transcripts Associated with Resident and Injured Mf Subtypes..... | 78  |
| Figure 20. Cardiac CD11b <sup>+</sup> Cells in EGFRmylKO Hearts Show Differential Expression of Igfbp5/7 Relative to Controls.....             | 80  |
| Figure 21. EGFRmylKO Hearts Exhibit Elevated Growth Factor Receptor Activation Relative to Control.....  | 81  |
| Figure 22. Impact of Myeloid-Cell Specific on Cardiac Structural Integrity During Ageing.....  | 83  |
| Figure 23. Loss of Myeloid-Cell Specific EGFR Does not Significantly Impact Survival Following Ischemic Injury.....                            | 86  |
| Figure 24. Loss of Myeloid-Cell Specific EGFR Results in Rapid Decline in Cardiac Function Following Ischemic Injury.....                      | 87  |
| Figure 25. Loss of Myeloid-Cell Specific EGFR does not Alter Cardiac Fibrosis Following Ischemia.....  | 91  |
| Figure 26. Loss of Myeloid-Cell Specific EGFR Aggravates Pathological Hypertrophy Following Ischemia.....                                      | 92  |
| Figure 27. Loss of Myeloid-Cell Specific EGFR Limits Angiogenic Repair Following Ischemia.....   | 93  |
| Figure 28. Early Following Ischemia, EGFRmylKO Hearts Exhibit Similar Loss of Cardiomyocytes.....  | 95  |
| Figure 29. Early Following Ischemia, EGFRmylKO Hearts Exhibit Similar Neutrophil Densities.....  | 96  |
| Figure 30. Early Following Ischemia, Myeloid-Cell Specific EGFR does not Significantly Impact Leukocyte Mobilization.....                      | 98  |
| Figure 31. During the Peak of Acute Inflammation, EGFRmylKO have enhanced Inflammatory Mfs.....  | 99  |
| Figure 32. During Repair & Resolution, EGFRmylKO Hearts Exhibit Reduced Reparative Macrophage Subsets.....                                     | 101 |

|   |     |
|---|-----|
| Figure 33. Deletion of Myeloid-Specific EGFR does not Impact TRM Replenishment 7d pMI.....                                | 102 |
| Figure 34. Deletion of Myeloid-Specific EGFR does not Significantly Impact Lymphocyte Density 7d pMI.....                 | 103 |
| Figure 35. Following MI, Myeloid-Cell Specific EGFR does not Significantly Impact Leukocyte Density in BM.....            | 105 |
| Figure 36. Following MI, Myeloid-Cell Specific EGFR May Influence Inflammation in the Spleen.....                         | 106 |
| Figure 37. Following MI, Myeloid-Cell Specific EGFR does not Significantly Impact Leukocyte Density in Spleen.....        | 107 |
| Figure 38. Myeloid-Cell Specific EGFR Deletion Results in Reduced Expression of Repair Promoting Factors Post Injury..... | 109 |
| Figure 39. EGFR Deletion in BMDM May Result in Reduced STAT3 activation following IL4 Induced Polarization.....           | 110 |
| Figure 40. Summary: Myeloid EGFR in Cardiac Homeostasis and Injury Repair.....  | 115 |
| Figure 41. Mf Secretome May Enhance Growth Factor Signaling in NRVMs.....   | 129 |
| Figure 42. EGFRmylKO Mf Display Altered OCR In Response to LPS or IL4, Relative to Control.....                           | 130 |

## LIST OF TABLES

|   |    |
|---|----|
| Table 1. Primer Sequences for Mouse Genotyping.....     | 45 |
| Table 2. Primer Sequences for RT-qPCR.....              | 46 |
| Table 3. Conjugated Antibodies for Flow Cytometry.....  | 51 |
| Table 4. Flow Cytometry Isotype Control Antibodies..... | 51 |
| Table 5. Immunoblot Primary Antibodies.....             | 57 |
| Table 6. 3-8 mo Echo Parameters.....                    | 70 |
| Table 7. 10-15 mo Echo Parameters .....                 | 84 |
| Table 8. Sham & MI Echo Parameters.....                 | 88 |

## **LIST OF ABBREVIATIONS**

ACK - ammonium-chloride-potassium

ACTA - actin alpha

ADAM - a disintegrin and metalloprotease

AKT - ak strain transforming/ protein kinase b

ANGPTL - angiopoietin-like proteins

Ao - aorta

AREG - amphiregulin

ATP - adenosine triphosphate

AV - atrioventricular

BM - bone marrow

BMDM - bone marrow derived macrophages

BSA - bovine serum albumin

BTC - betacellulin

BW - body weight

CCR - c-c motif chemokine receptor

CCS - cardiac conduction system

CD - cluster of differentiation

CF - cardiac fibroblasts

CHD - coronary heart disease

CLP - common lymphoid progenitor

CNS - central nervous system

CM - cardiomyocyte

CMP - common myeloid progenitor

CO - cardiac output

Col - collagen

COPD - chronic obstructive pulmonary disease

CVD - cardiovascular disease

CXCL - c-x-c motif ligand

CX43 - connexin 43

DAMP - damage associated molecular pattern

DC - dendritic cell

ECM - extracellular matrix

EDTA - ethylenediaminetetraacetic acid

EF - ejection fraction

EGF - epidermal growth factor

EGFR - epidermal growth factor receptor

EGFR<sup>f/f</sup> - epidermal growth factor receptor flox control

EGFRmylKO - epidermal growth factor receptor myeloid specific knockout

Endo - endothelial cell

EMT - epithelial-mesenchymal transition

ErbB - erythroblastic leukemia viral oncogene homolog

EREG - epiregulin

ERK - extracellular related kinase

FACS - fluorescence activated cell sorting

FBS - fetal bovine serum

FDR - false discovery rate

flox - flanked by loxP sites

FS - fractional shortening

GAB1 - GRB2 associated binder 1

GAPDH - glyceraldehyde-3-phosphate dehydrogenase

Ga - g protein alpha subunit

Gbg - g protein beta, gamma subunit

GDP - guanosine diphosphate

GEF - guanine nucleotide exchange factor

GFP - green fluorescent protein

GM-CSF - granulocyte macrophage colony stimulating factor

GPCR - g protein coupled receptor

GRB2 - growth factor receptor-bound protein 2

GTP - guanosine triphosphate

HB-EGF - heparin binding epidermal growth factor

HBSS - hanks buffered salt solution

HCC - hepatocellular carcinoma

HF - heart failure

HFmrEF - heart failure with mid range ejection fraction

HFpEF - heart failure with preserved ejection fraction

HFrfEF - heart failure with reduced ejection fraction

HR - heart rate

HSC - hematopoietic stem cell

HTN - hypertension

HW - heart weight

IACUC - institutional animal care and use committee

ICM - ischemic cardiomyopathy

IFN - interferon

IGF - insulin like growth factor

Igfbp - insulin like growth factor binding protein

IHD - ischemic heart disease

IL - interleukin

ISG - interferon stimulated genes

LA - left atrium

LV - left ventricle

LVAW - left ventricle anterior wall

LVID - left ventricle internal diameter

LVPW - left ventricle posterior wall

Mf - macrophage

MHC - major histocompatibility complex

MI - myocardial infarction

MMP - matrix metalloprotease

Mon - monocytes

MYH - myosin heavy chain

MYL - myosin light chain

MAPK - mitogen activated protein kinase

MPO - myeloperoxidase

NFKB - nuclear factor kappa b

NRG - neuregulin

OCR - oxygen consumption rate

oxLDL - oxidized low density lipoprotein

PBS - phosphate buffered saline

PCR - polymerase chain reaction

PFA - paraformaldehyde

PI3K - phosphoinositide 3 kinase

PRR - pathogen recognition receptor

PTB - phospho tyrosine binding

RA - right atrium

RAAS - renin angiotensin aldosterone system

RBC - red blood cell

RHD - rheumatic heart disease

ROS - reactive oxygen species

RT - room temperature

RT-qPCR - reverse transcription quantitative polymerase chain reaction

RTK - receptor tyrosine kinase

RV - right ventricle

SNS - sympathetic nervous system

SOS1 - son of sevenless 1

STAT - signal transducer and activator of transcription

SV - stroke volume

TAM - tumor associated macrophages

TF - transcription factor

TGF - transforming growth factor

TIM4 - t cell immunoglobulin and mucin domain containing 4

TLR - toll like receptor

TNF - tumor necrosis factor

TNNI - troponin I

TRM - tissue resident macrophages

VEGF - vascular endothelial growth factor

VSMC - vascular smooth muscle cell

WHO - world health organization

# **CHAPTER 1**

## **CARDIAC PHYSIOLOGY & HEART FAILURE, CONSIDERING THE ROLE OF MACROPHAGES**

### **1.1 Brief Epidemiology of Heart Failure**

#### **1.1.1 Cardiovascular Disease**

Cardiovascular disease (CVD) encompasses a collection of syndromes and diseases affecting normal function of the heart and major vessels, with some of the most notable and prevalent being coronary heart disease (CHD), stroke, hypertension (HTN), and heart failure (HF) (Roth et al., 2020; Virani et al., 2021). To date, CVD remains one of the leading causes of worldwide mortality and morbidity: 2019 estimates from the world health organization (WHO) indicate about 32%, or 18 million of global deaths can be attributed to CVD (Roth et al., 2020; Virani et al., 2021; Savarese et al., 2017; Ziaeeian et al., 2016; Savarese et al., 2022). In the United States alone, almost half of the population is plagued with CVD, as about 49.2% of adults aged 20 or older experience some form of CVD (Roth et al., 2020; Virani et al., 2021). Considering these statistics, it is quite clear that CVD poses a major health and economic burden.

Of all CVD, CHD is the most common, and is the leading cause of CVD death, followed by stroke, HTN, and HF (Virani et al., 2021). To note though, HF is often the end result of many CVD (Virani et al., 2021; Savarese et al., 2017). Further, HF is one of the leading causes of hospitalization in US adults; as such, HF is a global pandemic, and remains a major public health concern as its prevalence is projected to continue increasing (Roth et al., 2020; Virani et al., 2021; Savarese et al., 2017; Ziaeeian et al., 2016; Savarese et al., 2022).

### **1.1.2 Recent Heart Failure Statistics**

HF can broadly be defined as the inability of the heart muscle to orchestrate adequate perfusion to the remaining tissues, leaving them bereft of required nutrients (Virani et al., 2021; Savarese et al., 2017; Ziaeeian et al., 2016; Savarese et al., 2022). Right now, about 6 million Americans suffer with HF, and globally, this number jumps to over 37 million (Virani et al., 2021; Ziaeeian et al., 2016). Though these statistics are already staggering, recent projections suggest HF prevalence will increase 46% by 2030 in the US alone (Virani et al., 2021). This increase in prevalence stems from a few different factors: greater life expectancy and aging, improved survival following heart attacks (defined as vessel occlusion, leading to failure to receive oxygen rich blood) and improved treatments for CVD patients (Savarese et al., 2022). Though prevalence rates are on the rise, surviving HF has seen some improvements. Rates of HF mortality have declined from 1998 to 2008, although they remain astronomical at over 40% by 5 years (Virani et al., 2021). Beyond its rising prevalence and high fatality, the total costs of HF further intensify its burden. In 2012, about 30.7 billion in total was spent on HF, with about two-thirds of that being direct medical costs (Virani et al., 2021). By 2030, we can expect that to more than double, and be further compounded by a growing population (Virani et al., 2021). Consequently, understanding HF presentations, and searching for HF therapies is of utmost importance.

### **1.1.3 Normal Cardiac Structure and Function**

To critically consider novel HF therapeutic approaches, the body of this work will carefully evaluate general cardiac physiology, mechanisms contributing to HF development, and key unanswered questions. The heart is a largely post-mitotic,

muscular organ with 4 chambers: 2 atria, and 2 ventricles (Sylva et al., 2014; Buijtenlijk et al., 2020). To allow for the unidirectional flow of blood, valves lie between atria and ventricles, with the mitral on the left, and tricuspid on the right (Park et al., 2017). The heart contains 2 other valves, the semilunar valves, which allow for blood to leave the 2 major arteries: pulmonary and aortic (Buijtenlijk et al., 2020). In brief, blood flow through the heart can be described as follows. Once oxygen rich blood enters the left atrium (LA), from the pulmonary vein, it is propagated through the mitral valve to the left ventricle (LV) and pumped through the aorta (Ao) to feed the systemic circulation (Buijtenlijk et al., 2020). Oxygen deficient blood returns to the right atrium (RA) through the vena cava, and is propelled through to the right ventricle (RV) back to the lungs (Buijtenlijk et al., 2020). The coordination of blood flow relies on the heart's intrinsic electrical system, referred to as the cardiac conduction system (CCS) (Park et al., 2017). Electrical conduction generated in the CCS is highly conserved, and is critical for maintaining optimal stroke volume (SV), that is, the blood volume ejected during each contraction and relaxation cycle (Park et al., 2017).

#### **1.1.4 Abnormal Cardiac Function & Heart Failure Types**

Efficient pumping, or systolic function, in the LV is measured by the fraction of blood ejected in every contraction cycle (systole) and is denoted as ejection fraction (EF) (Savarese et al., 2022). The EF percentage reports this SV relative to blood volume at the end of the relaxation cycle (diastole) (Savarese et al., 2022). In adult men and women, values of EF range from 52 - 74 %, with the normal values laying about 62 and 64% for men and women respectively (Savarese et al., 2022). Though HF was broadly defined above, it is important to note its complexity; when the heart fails, it can present in 1 of 3

types, distinguished by EF (Savarese et al., 2022). HF statistics and types are detailed in Figure 1a-b.

HF where the EF is reduced to 40% or less (HFrEF) is to date the most characterized HF type, as it is easiest to diagnose (Savarese et al., 2022). In HFrEF, systolic dysfunction is the main driver of disease, though this is unlike HF with preserved EF (HFpEF) (Savarese et al., 2022). As its name would suggest, in HFpEF, patients EF is maintained at or above 50% (Savarese et al., 2022). Studies of HFpEF are fewer in number, but it is widely understood that HFpEF arises when the ventricle loses its ability to relax normally, typically because the muscle is stiff, leaving the heart unable to adequately fill during diastole (Savarese et al., 2022). Lastly, HF can present as that with mid range EF (HFmrEF) (Savarese et al., 2022; Andronic et al., 2016). HFmrEF has been vastly understudied and misdiagnosed largely because it can have hallmarks reminiscent of HFrEF or HFpEF (Savarese et al., 2022; Andronic et al., 2016). In recent years though, HFmrEF is starting to be defined as HF where EF is between 41 and 49 percent (Andronic et al., 2016). It is also important to note that in HFmrEF, there are both distinct, yet intermediate clinical, structural, and functional features and outcomes when compared to HFrEF or HFpEF (Andronic et al., 2016).

### **1.1.5 Risk Factors for Heart Failure**

Irrespective of type, HF can arise from a variety of risk factors and etiologies. These can include complications from several other CVDs, hereditary and genetic defects, diet and lifestyle choices, or systemic diseases (Virani et al., 2021; Ziaieian et al., 2016). It's important to note that these risk factors are not mutually exclusive: many factors can lead to HF development in patients (Virani et al., 2021; Ziaieian et al., 2016).

## HF at a Glance ...

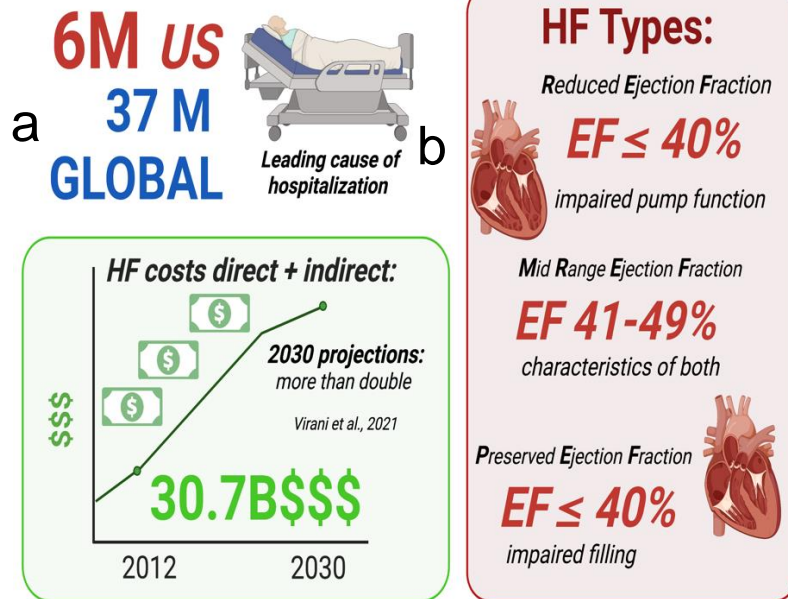


**Figure 1. Heart Failure (HF) Statistics.** a) Prevalence rates, reported, and projected costs associated with HF. b) Brief definitions of HF types. EF = ejection fraction. Figure was generated in Biorender (<https://biorender.io>) under a student premium license.

Of all risk factors though, ischemic heart disease (IHD), chronic obstructive pulmonary disease (COPD), HTN, and rheumatic heart disease (RHD) have been shown to account for about two thirds of HF cases (Ziaecian et al., 2016).

In brief, RHD can develop after an infection which, if left untreated, can trigger a chronic and excessive immune response in or near heart valves, ultimately resulting in their dysfunction (Carapetis, 2007). Dysfunctional valves due to scarring and damage can result in inadequate ventricular filling, or fluid buildup, ultimately resulting in HF (Carapetis, 2007). The incidence of valvular and RHD causing HF in the developed world is quite rare, though the developing world still experiences relatively high prevalence (Ziaecian et al., 2016; Carapetis, 2007; Virani et al., 2021).

COPD is a chronic inflammatory disease in the lungs which can result in pulmonary HTN. Of note, HTN itself is a major risk factor for HF (Kotlyarov, 2022; Ziaieian et al., 2016; Hawkins et al., 2009). With regards to the heart, HTN or high blood pressure increases the afterload, that is, the force opposing ventricular contraction (vascular resistance) (Oh et al., 2020). This increase in vascular resistance increases muscle strain, ultimately leading to grave damage and subsequent cell death (Oh et al., 2020). Since the muscle is post-mitotic, with low cell proliferation and renewal rates, cell death triggers the heart's adaptive remodeling and repair responses, namely cell hypertrophy (muscle growth) and tissue fibrosis (replacement scar tissue) (Oh et al., 2020; Bergmann et al., 2015). Though initially adaptive, these processes, coupled with continued strain ultimately decreases ventricular compliance (increased stiffness) and deteriorates ventricular function, leading to HF (Oh et al., 2020).

IHD is one of the largest contributors to HF development (Savarese et al., 2022; Moran et al., 2014). IHD develops from an imbalance between energetic demands in the tissue and coronary blood flow (Severino et al., 2020). Any dysfunction in the vasculature can disrupt coronary circulation; for instance, a myocardial infarction (MI) can occur when an obstructive atherosclerotic plaque ruptures, or the cholesterol filled plaque severely occludes the vessel (Severino et al., 2020). When the muscle near the vessel is deprived of oxygen and nutrients, there is a gross amount of cell death, resulting again in cardiac remodeling. As highlighted above, remodeling can ultimately turn maladaptive, therefore prompting HF (Oh et al., 2020).

### **1.1.6 Current Heart Failure Therapies**

Currently, the standard of care for HF focuses on improving patients' presentations and symptoms by targeting any number of the compensatory mechanisms that become initiated during disease (Mascolo et al., 2022; Machaj et al., 2019). During the onset of HF, neurohormonal systems, including the sympathetic nervous system (SNS), renin-angiotensin-aldosterone system (RAAS), and natriuretic peptides (NP) become elevated in order to improve ventricular contractile force, ventricular filling, and vascular resistance (Mascolo et al., 2022). Overtime, neurohormonal overactivation can contribute to and further aggravate adverse cardiac remodeling, ultimately worsening the progression of HF (Mascolo et al., 2022). A major class of HF drugs target neurohormonal mechanisms by preventing their synthesis, or antagonizing their cognate receptors (Mascolo et al., 2022; Machaj et al., 2019).

A major symptom of HF can be reduced pump efficiency; in order to combat this decline in systolic function, positive inotropes are often employed (Mascolo et al., 2022; Machaj et al., 2019; Okyere et al., 2022). Current drugs on the market in this class work by enhancing contractile force through activation of the cardiac muscle motor (myosin), and enhancing cell respiration (Mascolo et al., 2022; Machaj et al., 2019; Okyere et al., 2022).

Beyond these established therapies are newer drug classes on the horizon, as well as clinical trials aimed at new therapeutic avenues (Mascolo et al., 2022). Current attractive options include gene therapy, specifically, the reintroduction of key genes that regulate systolic function (Mascolo et al., 2022). Also, clinical observations and recent experimental findings have suggested potential benefits from modulating inflammation in

HF states (Mascolo et al., 2022). There has been some initial success in reducing HF associated hospitalization with clinical trials that have targeted reducing levels of inflammation, though much remains to be learned (Mascolo et al., 2022). In order to fully leverage the benefits from immunomodulation in HF, it has become imperative to explore the multifaceted and complex role of inflammation in the normal and failing heart.

## **1.2 Cardiac Cell Distribution, Physiological Function, & Post Injury Mechanisms**

### **1.2.1 Cardiac Muscle**

The mammalian heart maintains a highly specialized arrangement of cells which allow normal cardiac function and optimal physiology; cardiac cellular complexity is outlined in Figure 2a-b. Cardiac myocytes (CM) occupy the greatest volume in the tissue, though they are not the largest cell type in number (Tucker et al., 2020; Litvinukova et al., 2020; Skelly et al., 2018; Pinto et al., 2016). General CM characteristics and function include organized sarcomeric structures of actin and myosin proteins which form cross-bridges to drive muscle contraction (Squire, 1971). Muscle contraction propels the ejection of blood into distal tissues. Though actin and myosin are key components of CM, it's important to note that CM are not homogenous. Between chambers, CM heterogeneity can be observed: for instance, atrial and ventricular CM vary in gene expression patterns, ultimately allowing their unique functions (Tucker et al., 2020; Litvinukova et al., 2020). For one, within the sinoatrial node are a subset of CM termed pacemaker cells which propagate the CCS (Mangoni et al., 2008). Pacemakers exhibit low contractile activity but continuously generate action potentials, thereby driving the contractile cycle (Mangoni et al., 2008). Additionally, chamber specific CM can be

distinguished by myosin isoforms like myosin/atrial light chain 2 (MYL7), and myosin heavy chain a (MYH6) (Tucker et al., 2020).

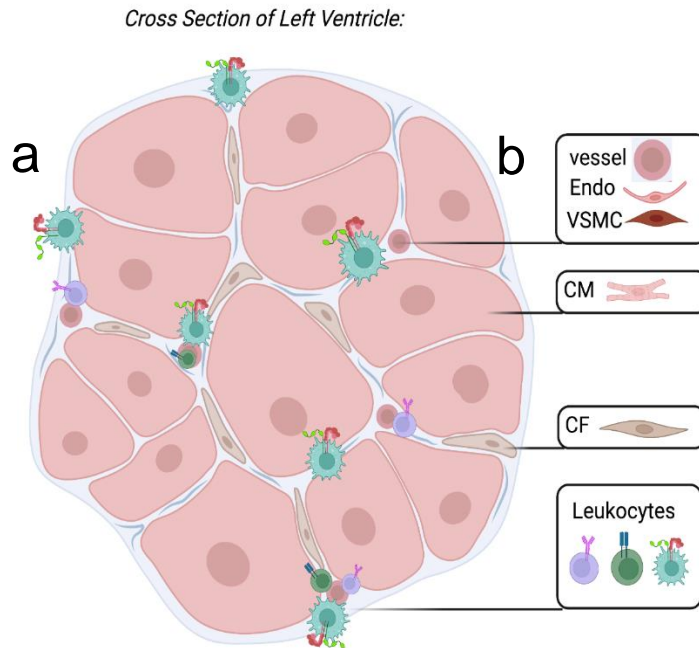


**Figure 2. Cardiac Cellular Complexity.** a) Graphic depicts a transverse cross section of the heart's left ventricle. b) The cell complexity present in the mammalian heart can be observed. Endo = endothelial cell, VSMC = vascular smooth muscle, CM = cardiac myocyte, CF = cardiac fibroblast. Figure was adapted in Biorender (<https://biorender.io>) under a student premium license.

These isoforms exhibit structural domains which allow unique biophysical and mechanical properties required for atrial contraction (Litvinukova et al., 2020; Walklate et al., 2021). On the other hand, ventricular CM are enriched with canonical contractile proteins including those required for excitation-contraction coupling, and calcium handling processes (Litvinukova et al., 2020).

In early life, CM exhibit their highest exchange rate, though intrinsic renewal drops to less than 1% by adulthood (Bergmann et al., 2015; Lazar et al., 2017). Thus, damage to, or loss of CMs is irreversible and largely irreplaceable (Bergmann et al.,

2015). To overcome severe CM loss, surviving CM can undergo cell hypertrophy (Azevedo et al., 2016). Hypertrophy describes the process whereby cells adapt morphologically, increasing in size and volume (Azevedo et al., 2016). Initiation of the hypertrophic response is exceedingly complex and can occur through numerous mechanisms (Dirkx et al., 2013; Pflieger et al., 2020). For instance, elevated neurohormones and growth factors (GF) can initiate molecular changes that then result in enhanced global gene expression to account for increased cell size (Dirkx et al., 2013; Pflieger et al., 2020). This transcriptional activation within the cell can resemble some gene programs seen during cardiac fetal development (Dirkx et al., 2013). Overtime, elevated expression of cardiac fetal genes and cell growth turn maladaptive. Dysregulated expression of fetal genes involved in CM homeostatic function like contraction, and calcium handling can catalyze ventricular dysfunction, ultimately yielding HF (Azevedo et al., 2016; Dirkx et al., 2013).

### **1.2.2 Cardiac Fibroblasts**

In the mammalian heart, CM are supported by cardiac fibroblasts (CF). Fibroblasts are cells of mesenchymal origin which primarily function to support cardiac structural homeostasis (Ivey et al., 2016; Tallquist et al., 2018). In the normal heart, quiescent resident fibroblasts are small, spindle shaped cells that produce and secrete collagens, glycoproteins, and proteases to maintain the extracellular matrix (ECM) (Tucker et al., 2020; Litvinukova et al., 2020). CF also support the myocardium through additional functions: they provide insulation of the CCS, and they secrete GF and inflammatory mediators (cytokines and chemokines) which regulate muscle growth, inflammation, or blood vessel formation (Gibb et al., 2020).

Early during stress or injury, resident fibroblasts expand in number, and transdifferentiate into myofibroblasts (Ivey et al., 2016; Tallquist et al., 2018; Gibb et al., 2020; Ivey et al., 2018). Myofibroblasts can be characterized by denovo expression of periostin, allowing them to migrate to sites of damage, and secrete even larger amounts of ECM components to build scar tissue (Ivey et al., 2016; Tallquist et al., 2018; Gibb et al., 2020; Ivey et al., 2018). Fibrosis can be a necessary adaptation for the tissue, however, excessive myofibroblast activation disrupts the intricate coordination of cells within the tissue and weakens tissue compliance (Gibb et al., 2020).

### **1.2.3 Cardiac Vasculature**

CM and CF are supported by a network of vascular cells: endothelial (Endo) and vascular smooth muscle cells (VSMC) (Tucker et al., 2020; Litvinukova et al., 2020; Skelly et al., 2018; Pinto et al., 2016). In the heart, Endo constitute the largest number of non-CM cells; with the vast majority of Endo lining the vascular endothelium (Tucker et al., 2020; Pinto et al., 2016). Endo are enriched in genes that participate in processes like vascular endothelial growth factor (VEGF) signaling, vasculogenesis, and Endo differentiation to name a few (Tucker et al., 2020; Pinto et al., 2016; Lothar et al., 2018). During normal physiology, Endo also produce paracrine factors and small molecules which regulate CM function and remodeling (Segers et al., 2018). In injury states, Endo contribute to cardiac remodeling through a few mechanisms. Endo can secrete small molecules, and upregulate the secretion of larger GF to modulate the microenvironment (Segers et al., 2018). Endo are also important in the rapid regeneration of new blood vessels which is necessary to feed working CM (He et al., 2017).

## **1.3 Cardioimmunology: Inflammation in the Healthy and Failing Heart**

### **1.3.1 Immune Cells: General Introduction**

As outlined in Figure 3a-b, the normal heart maintains resident immune cells to support optimal physiological function (Tucker et al., 2020). Immune cells, or leukocytes, are a collection of white blood cells, primarily responsible for sensing and responding to foreign pathogens or intrinsic damage with the goal of eliminating and suppressing further danger (Okyere et al., 2020; Kondo, 2010). To do so, leukocytes have several mechanisms at their disposal, with some being cell-type specific (Okyere et al., 2020; Kondo, 2010). For instance, leukocytes are highly secretory, and often release agents which are necessary for regulating different inflammatory stages. In brief, chemokines and cytokines are secreted at sites of injury; their release primarily triggers the recruitment of inflammatory cells, and activates molecular signatures to produce factors for resolution (Okyere et al., 2020; Swirski et al., 2018). Leukocytes also secrete proteases, extracellular traps, and antibodies to specifically neutralize pathogens, and help promote tissue homeostasis and repair (Okyere et al., 2020; Kondo, 2010; Swirski et al., 2018). In the context of the heart, these mediators allow leukocytes to initiate repair after injury, but also govern homeostasis.

Leukocytes can be classed by their specific function and origin, making up a few different subsets (Kondo, 2010). They all initially derive from hematopoietic stem cells (HSC), and differentiate into subclasses of lymphoid or myeloid progenitors (Kondo, 2010). Common lymphoid progenitors (CLP) can then differentiate into B and T lymphocytes, natural killer cells (NK), or a few dendritic cell (DC) subtypes (Kondo, 2010). On the other hand, common myeloid progenitors (CMP) are precursors for

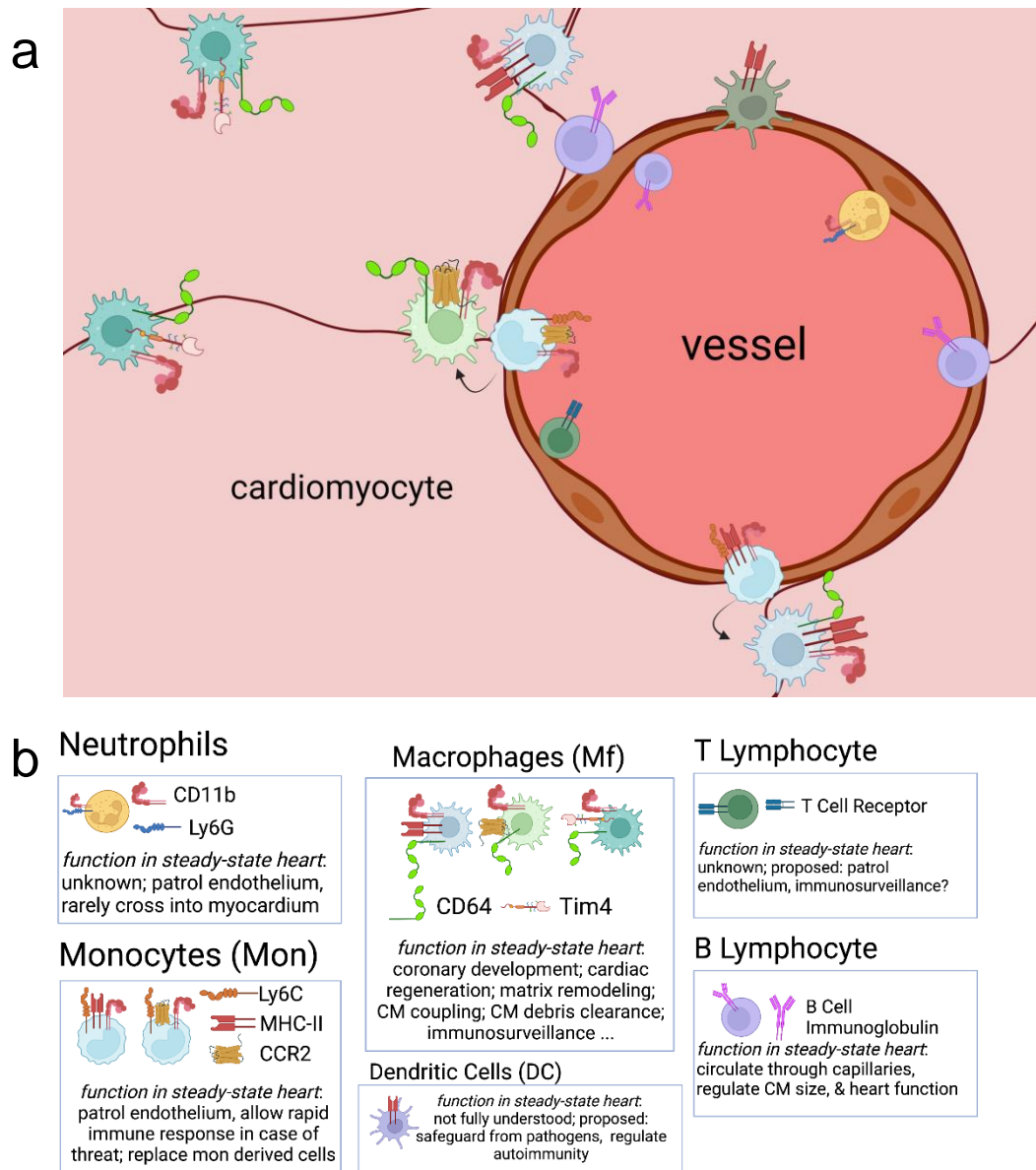


**Figure 3. Cardiac Immune Cell Landscape.** a) Magnification within the myocardium, highlighting cardiac immune cell distribution. Immune cell subsets are indicated by their expression of unique markers, pointed out in b) B and T cells are primarily associated with the endothelium. Functions of T cells in the steady state heart is not well characterized. B cells have been recently shown to contribute to regulating CM integrity, size, and cardiac function. DCs are also present within steady state hearts, though their function is not yet known. Neutrophils, and mon patrol the endothelium in steady state. Mon can transmigrate into myocardium, differentiating into mf. Cardiac mf are the most abundant leukocyte in the steady state heart, and are present in a few subtypes. Together, they function to aid in maintaining cardiac homeostasis. Figure was generated in Biorender (<https://biorender.io>) under a student premium license.

megakaryocytes, erythrocytes, granulocytes, and mononuclear phagocytes like macrophages (Mf) (Kondo, 2010)

Over the last decade or so, a combination of cell and tissue profiling studies have given greater depth to the understanding of the immune cell makeup, types, and proportions in both the normal and injured heart (Tucker et al., 2020; Litvinukova et al., 2020; Skelly et al., 2018; Pinto et al., 2016; Okyere et al., 2020; Dick et al., 2022; Swirski et al., 2018; Lafuse et al., 2021). In the steady state heart, Mf and B Lymphocytes are the most numerous immune cell type; T Lymphocytes, DC, monocytes (Mo) and neutrophils represent a much smaller percentage, with Mo and neutrophils often only identified patrolling the vessels (Okyere et al., 2020; Dick et al., 2022; Swirski et al., 2018; Lafuse et al., 2021) (Figure 3).

Following injury, the leukocyte landscape exhibits a large shift, as more immune cells are required to mount an appropriate inflammatory response and contribute to cardiac adaptation and repair, therefore limiting HF progression (Prabhu et al., 2016). For instance, once an MI incites a large volume of cell death, any number of dying cardiac cells will release intracellular contents, like mitochondrial DNA, reactive oxygen species (ROS), cytokines, and chemokines which become damage associated molecular patterns (DAMPs) (Prabhu et al., 2016). DAMPs are recognized by pathogen recognition receptors (PRR) mostly on immune cells; PRR activation by DAMPs triggers a wave of peripheral inflammatory events (Prabhu et al., 2016). Within minutes of cell death, this results in an immense amount of immune cells migrating to the injured heart. Once they arrive, extravasate into tissue and become functional, they ingest and clear cell death debris, making space for myofibroblasts to form a replacement scar (Prabhu et al., 2016).

As time goes on, these highly inflammatory cells get cleared from the tissue, and additional leukocytes continue to migrate to the site of injury to help build and stabilize a scar, promote angiogenesis, and remodel the myocardium to limit HF (Prabhu et al., 2016; Swirski et al., 2018). These functions are meticulously coordinated, and rely on the activation of major inflammatory programs through key transcription factors (TFs) like interferon regulatory factor (IRFs), signal transducer and activator of transcription (STATs), and nuclear factor kappa B (NF- $\kappa$ B) (Swirski et al., 2018). Below, each leukocyte subtype is reviewed, focusing on how they contribute to cardiac maintenance and repair.

### **1.3.2 Lymphocytes**

Lymphocytes are typically branded as the adaptive arm of the immune system because they provide targeted responses against specific antigens or danger associated peptides (Lafuse et al., 2021; Zougari et al., 2013). Once they derive from CLP in the bone marrow (BM), B cells can be subdivided into a few different classes, which allow for diverse functions (Kondo, 2010; Wu et al., 2019). For one, conventional B Cells function by making unique antibody receptors against specified antigens during injury (Kondo, 2010; Wu et al., 2019). In addition to conventional B cells are B1 cells and B “regulatory” cells (Wu et al., 2019). B1 cells function similarly to the innate arm of the immune system in that they are responsive to immune cues that are released early during injury (Wu et al., 2019). Regulatory B cells primarily work to dampen the immune response by increasing the secretion of anti-inflammatory cytokines like interleukin (IL)10 (Wu et al., 2019). T Lymphocytes make up the other major component of the adaptive immune response (Blanton et al., 2019). Similar to B cells, T cells derive from

BM CLP that populate the thymus; their maturation requires proliferation, generation of diverse T cell repertoires, and the elimination of autoreactive cells (Blanton et al., 2019). Once mature, T cells can traffick to other organs, and based on environmental cues present, can differentiate to regulate inflammation (Blanton et al., 2019).

Interestingly, B cells constitute the 2nd largest leukocyte class associated with the steady state heart (Lafuse et al., 2021). Although recent studies have identified that most myocardial B cells predominantly circulate through small capillaries, these B cells are transcriptionally unique, and play an important role in cardiac homeostasis (Adamo (a) et al., 2020). Specifically, they have been shown to regulate total myocardial mass, CM size integrity, and cardiac function, though mechanistically, it is unclear how (Adamo (a) et al., 2020). T lymphocytes are also expressed in healthy mammalian hearts (Tucker et al., 2020; Swirski et al., 2018; Lafuse et al., 2021). In terms of function relevance, not much is known, however, T cells patrolling the endothelium may partake in immunosurveillance (Swirski et al., 2018; Lafuse et al., 2021; Blanton et al., 2019).

Following injury, lymphocytes are present in the heart in much greater numbers, and there is ample clinical and experimental evidence to suggest their role in HF development (Okyere et al., 2020; Zougari et al., 2013; Weirather et al., 2014). For instance, studies involving B or T lymphocytes in mouse models of HF have linked their regulation of inflammatory cytokines like tumor necrosis factor  $\alpha$  (TNF $\alpha$ ) and interferon  $\gamma$  (IFN $\gamma$ ) to modulating fibrotic remodeling (Okyere et al., 2020; Zougari et al., 2013; Weirather et al., 2014). In addition to these mouse models, patient evidence implicates circulating T cells and infiltration of distinct T cell subsets to the heart in pathological HF remodeling (Blanton et al., 2019). Similarly, higher levels of B cells have been identified

in MI and HF patients, and suggested to play a role in fibrotic remodeling (Zouggari et al., 2013; Okyere et al., 2020).

### **1.3.3 Myeloid Cells**

Cells of myeloid origin, in particular, granulocytes and Mon derived cells, allow for the innate immune response by providing an initial defense mechanism against danger (Kondo, 2010). Consequently, myeloid cells are highly secretory: they release copious amounts of cytokines, GF, proteases, and additional inflammatory mediators in order to quickly and effectively clear damage (Swirski et al., 2018; Lafuse et al., 2021; Okyere et al., 2020). Myeloid cells can also indirectly contribute to a more specific immune response through digesting pathogens, and presenting them to adaptive immune cells (van de Borgh et al., 2018). These include myeloid dendritic cells (DC), which function as a bridge between the innate and adaptive immune system (van de Borgh et al., 2018). DCs arise from common Mon-DC precursors from the BM, once they differentiate into DC precursors, they are then able to adopt numerous DC subclasses (Mildner et al., 2014). The basal heart contains at least 2 DC subsets, and though their function is unknown, they are proposed to safeguard the heart from pathogens, and gatekeep autoimmunity (van de Borgh et al., 2018).

In addition to DCs, Mon and neutrophils have also been identified in association with the steady state heart (Swirski et al., 2018; Lafuse et al., 2021). Both of these cell types stem from the granulocyte Mf precursor, downstream of CMPs (Wolf et al., 2019). As progenitor cells, they can mature in BM as either Mon or granulocytes, based on their exposure to relevant environmental cues (Wolf et al., 2019). Their release into circulation is prompted by specific and strict chemokine gradients established at sites of injury (Wolf

et al., 2019). In the basal heart, Mon exist in very few numbers (Swirski et al., 2018; Lafuse et al., 2021). They primarily patrol the endothelium, allowing for a rapid immune response, should any threat occur (Swirski et al., 2018; Lafuse et al., 2021). Granulocytes are a subset of leukocytes with enzyme containing granular structures (Kondo, 2010; Swirski et al., 2018). Of all granulocytes, are arguably the most studied in the heart, though the presence of neutrophils in the steady-state heart is controversial and still debated (Swirski et al., 2018; Lafuse et al., 2021). It is likely that they patrol endothelium, but rarely cross into myocardium (Swirski et al., 2018; Lafuse et al., 2021).

In the event of injury, neutrophils rise in number, and provide the first defense once they infiltrate through the activated endothelium (Prabhu et al., 2016; Fine et al., 2020). Infiltrating neutrophils then release enzymes like serine proteases, matrix proteases, and other inflammatory enzymes to begin clearing cell death and matrix debris (Prabhu et al., 2016; Fine et al., 2020). DCs have been much less extensively studied, but it has been reported that their depletion in experimental MI improves outcomes (Lee et al., 2018).

#### **1.3.4 Macrophages (Mf) in Cardiac Homeostasis & Heart Failure**

Mf are a class of myeloid immune cells; here they are expanded upon because they are the most abundant leukocyte class within the steady-state heart, and take on even more roles following an ischemic injury (Tucker et al., 2020; Litvinukova et al., 2020; Skelly et al., 2018; Pinto et al., 2016; Dick et al., 2022; Swirski et al., 2018; Lafuse et al., 2021; Lavine et al., 2018). In general, Mf are the most numerous and diverse of all leukocytes; they are capable of regulating a vast array of biological outcomes (Williams et al., 2018). To name a few, Mf play major roles in sensing and processing pathogens,

they also function as APC, they engulf debris particles, and they are one of the most major producers of inflammatory cytokines, and GF (Williams et al., 2018). Since their discovery in 1882, they continue to be studied in numerous contexts because of their diverse, and at times paradoxical functions in various disease models and injuries (Williams et al., 2018).

Mf can differentiate from circulating Mon precursors based on the tissue's local microenvironment, however, it is important to note that studies from years past have shown tissue specific Mf development and origin is not due solely to BM Mon differentiation (Williams et al., 2018; Jakubzick et al., 2017). In detail, Mf can derive from at least 3 different sources (Jakubzick et al., 2017). Early in embryogenesis, yolk-sac derived progenitor cells and fetal liver Mon both contribute to populating tissue Mf, and are ontologically different from HSCs, even requiring different TFs for cell fates (Williams et al., 2018; Jakubzick et al., 2017; Schulz et al., 2012). After birth, circulating BM Mon can serve as a 3rd source for Mf in tissues (Dick et al., 2022). So then in the adult mammalian heart, tissue residing Mf (TRM) can be stratified based on their origin, which allow for diverse function (Lavine et al., 2018).

Using mice as models, we have learned that TRM that are established in embryonic development are first evident at E11.5, in association with the epicardium (Lavine et al., 2018). Unlike circulating Mon, which respond to chemokine gradients using their cognate receptors, these Mf are characterized by low expression of a C-C motif Chemokine Receptor 2 (CCR2) (Lavine et al., 2018). Maturation of these Mf will rely heavily on local cues from the epicardium, and circulating Mon can not contribute to this Mf population; epicardial ablation in development results in the loss of yolk-sac

derived TRM (Lavine et al., 2018; Stevens et al., 2016). Functionally, these TRM, starting as early as E13.5 become very important in the development and maturation of the coronary system (Lavine et al., 2018; Leid et al., 2016). In addition to yolk-sac derived TRM, at E14.5, Mf expressing CCR2 can also be observed, and are likely recruited to the heart (Lavine et al., 2018). To date, the specific roles of these recruited Mf have not been characterized, and it remains unclear if and how they are required for proper cardiac development (Lavine et al., 2018; Leid et al., 2016).

By adulthood, TRM in mouse hearts can be fully stratified into 4 distinct subsets with developmental and functional diversity (Dick et al., 2019). The first and reportedly most predominant TRM is entirely self-renewing, and can be distinguished by expression of T cell immunoglobulin and mucin domain containing 4 (Tim4) (Dick et al., 2019). Tim4 is a phosphatidyl serine receptor that mediates phagocytosis through binding of exposed phosphatidylserines apoptotic cell membranes (Miyanishi et al., 2007). The transcriptional profile of Tim4<sup>+</sup> Mf includes high expression of lymphatic vessel endothelial hyaluronan receptor 1 (LYVE1) and insulin-like growth factor 1 (IGF1) (Dick et al., 2019). LYVE1 allows Mf to interact with the vascular endothelium, therefore supporting vessel health; IGF1 is a potent GF capable of stimulating cell growth (Dick et al., 2019). Tim4<sup>+</sup> TRM gene expression patterns suggest that functionally, these Mf participate in processes like endocytosis, vessel health, muscle cell regeneration, muscle cell proliferation, cell chemotaxis, and regulation of leukocyte migration (Dick et al., 2019). Tim4<sup>+</sup> TRM are unlike the 3 other TRM subsets in the steady state heart, which have been shown to receive at least partial renewal input from monocyte differentiation (Dick et al., 2019).

The 2nd subset of TRM are distinguished by their enrichment in major histocompatibility complex II (MHC-II) (Dick et al., 2019). MHC-II hi TRMs have limited self-renewal capacity, and thus, are partially replenished by circulating Mon (Dick et al., 2019). MHC-II molecules are able to bind fragments of digested pathogens, then traffick them to the cell membrane for T cell recognition, allowing antigen presentation (van de Borgh et al., 2018). Additional functions of MHC-II hi TRMs include cell killing, and regulation of molecular signaling upstream of master regulatory TFs like NF- $\kappa$ B (Dick et al., 2019). The remaining 2 subsets of TRM are CCR2+, and are entirely maintained by circulating and recruited Mon (Dick et al., 2019). They can be distinguished from one another by one's expression of IFN stimulated genes (ISG) (Dick et al., 2019). Functionally, ISG TRM are involved in the response to IFN  $\gamma$ , and type 1 IFN (Dick et al., 2019). They also function in the response to foreign invaders by recognizing cytotoxic pathogen fragments and viral pathogens (Dick et al., 2019). The final subset, CCR2 TRM are enriched in genes involved in glycolysis, (the preferred metabolic pathway of inflammatory Mf (Van den Bossche et al., 2015). CCR2 TRM also function in the response to hypoxia/ischemia, they regulate fibroblast proliferation through cytokine production, and they respond to the release of inflammatory cytokines (Dick et al., 2019).

A few studies have delved into examining Mf function in the steady state heart. Beyond their proposed functions, we have come to appreciate that Mf are important in overall cardiac homeostasis. For instance, it was recently shown that Mf form gap junctions with CM through connexin 43 (Cx43) expression (Hulsmans et al., 2017). Mf and CM coupling allows for regulation of the CCS, as loss of Mf, or Mf specific Cx43

delays AV conduction (Hulsmans et al., 2017). Loss of Mf and CM coupling is also associated with mild abnormalities in the atria and ventricles (Hulsmans et al., 2017). Beyond these findings, a second study has also shown Mf to be key in supporting mitochondrial homeostasis in the heart. When CM eject dysfunctional mitochondria and cargo, Mf phagocytose them (Nicolas-Avila et al., 2020). Depletion of Mf or the loss of major Mf phagocytic receptors results in impaired clearance of these defective mitochondria and cargo, leading to activation of the inflammasome, metabolic alterations, and ventricular dysfunction (Nicolas-Avila et al., 2020). These studies illuminate what Mf can do in the steady- state heart, although this is just the beginning. Currently, the long-term contributions of Mf and other cardiac cells cross talk is still unknown. Furthermore, the mechanisms necessary for Mf contribution to homeostatic function within basal hearts is still unknown.

Following MI, Mf subtype, distribution, and function grows far more complex beyond the TRM scope, as detailed in Figure 4a-c (Dick et al., 2019). Ischemia results in the loss of a large percentage of TRMs, meaning additional Mf will be recruited to the ischemic zone early after injury to initiate injury resolution (Dick et al., 2019; Bajpai et al., 2019). In detail, the large volume of cell death will result in enhanced hematopoiesis in peripheral tissues like BM and spleen, leading to continued CCR2 dependent Mon migration to the heart (Prabhu et al., 2016; Dick et al., 2019, Bajpai et al., 2019). Once Mon enter the tissue, they differentiate into Mf, and earlier following injury, can be characterized by their high expression of lymphocyte antigen 6 complex locus c1 (Ly6C) (Peet et al., 2020). The function of Ly6C is not entirely understood, though it's thought to be important in cell trafficking (Hanninen et al., 2011). In the first few days, CCR2+ and

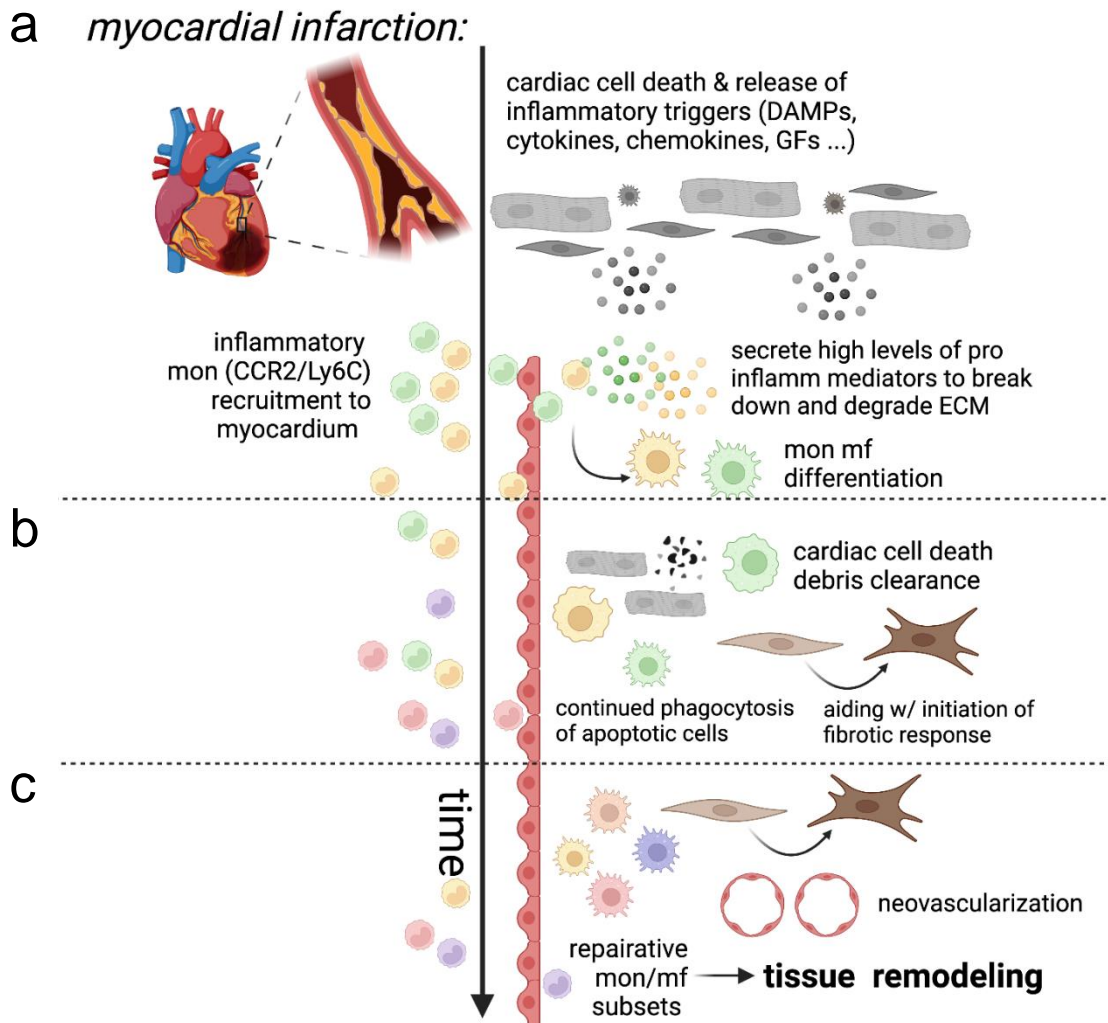


**Figure 4. Cardiac Macrophages (Mf) in Post Ischemic Injury Response.** a) Following myocardial infarction (MI) cardiac cell death leads to the release of damage associated molecular patterns (DAMPs), cytokines, chemokines, and growth factors, which trigger inflammatory responses. Inflammatory monocytes from the periphery infiltrate the myocardium, and secrete factors to break down ECM, and support inflammation/mf differentiation. b) Early post MI mf clear cardiac cell death; mf continue to clear cell death from early immune cell responders. c) As time progresses, mf dynamics shift, where they support building and stabilizing scar tissue to prevent rupture, support angiogenesis, contribute to muscle remodeling. Figure was generated in Biorender (<https://biorender.io>) under a student premium license.

Ly6C high Mf are tasked with a few different roles; for one, they are responsible for clearing ischemia induced cardiac cell death and debris, as well as short-lived inflammatory neutrophils (Prabhu et al., 2016; Peet et al., 2020). This can occur through receptor mediated or independent endocytosis and phagocytosis; for instance scavenger receptors like MER Proto-Oncogene, Tyrosine Kinase (MERTK) have been shown to regulate these roles (Howangyin et al., 2018). Additionally, early post MI (pMI) Mf are responsible for the production of cytokines, proteases, and GF which are integral to the remodeling heart; once debris is cleared, scar expansion becomes the next priority (Peet et al., 2020). pMI Mf express key PRRs like toll like receptors (TLR), nod like receptors (NLR), and receptor for advanced glycation-end products (RAGE), which can be activated by DAMPs in the infarct microenvironment (Prabhu et al., 2016; Peet et al., 2020). PRR activation then results in the induction of NF-kB, STATs, IRF, and other TFs, leading to the production of IL1b, IL6, IL12, IL18, TNFa, IFNg, MMP9, collagens, and transforming growth factor b (TGFb) to name a few (Swirski et al., 2018; Peet et al., 2020). These factors can activate neighboring CM and CF through paracrine mechanisms to initiate CM hypertrophy and fibrotic remodeling. In brief, CM express receptors for cytokines like IL6, and TNFa; activation of these receptors triggers molecular signaling events which lead to cell growth (Yokoyama et al., 1997; Zhao L et al., 2016). Similarly, CF, which begin expanding 1-3 days following MI can be activated to differentiate by factors like TGFb, leading to scar formation (Fu et al., 2017). As time progresses, and these repair mechanisms take place, Mf continue to switch phenotypes, allowing for additional functions (Peet et al., 2020). Later stage pMI Mf can be distinguished by lower expression Ly6C and CCR2 (Peet et al., 2020). This wave of Mf can derive from

differentiating CCR2<sup>+</sup> Mon that exhibit expression and activation of particular TF like nuclear receptor subfamily 4 group A member 1 (NR4A1) (Dehn et al., 2018; Hilgendorf et al., 2014). Mf in this phase of repair will produce factors like IL10, VEGF, and TGF $\beta$  (Swirski et al., 2018). Functionally, these Mf and their mediators focus on limiting the early inflammatory response, stabilizing the expanding scar through continued fibroblast activation, and helping to stimulate vessel growth to feed the surviving tissue (Swirski et al., 2018; Peet et al., 2020). Following this repair phase, in the weeks pMI, inflammation begins to subside, and interestingly, Mf populations begin to mirror baseline TRMs, although their origin and genetic signatures may differ greatly (Swirski et al., 2018; Peet et al., 2020; Dick et al., 2019). For one, the few TIM4<sup>+</sup> TRMs that were able to survive the ischemia, in areas remote to the infarct, will proliferate and repopulate the heart (Dick et al., 2019). Additionally, once repair mechanisms are stabilized, Mon recruitment will not occur at such high volumes (Dick et al., 2019). Mf in the heart will then revert to homeostatic functions (Swirski et al., 2018; Dick et al., 2019).

Currently, it is understood that TRM homeostasis, and the biological processes of pMI Mf are critical to adequate cardiac repair; this is because several studies show that a disruption in any of these functions can severely alter pMI HF development in mice. For one, selective depletion of TRM prior to MI results in adverse events, namely, mice lacking TRM experience greater mortality pMI (Dick et al., 2019). This reduction in survival may be the result of excessive fibrosis, and hypertrophy, ultimately triggering a greater loss of LV function (Dick et al., 2019). In addition to TRM loss, it has recently been shown that modulating Mf phenotype, function, and or dynamics, through the deletion of key scavenger receptors, metabolic regulators, or TFs, can greatly impact pMI

HF development outcomes (Mia et al., 2020; DeBerge et al., 2021; Zhang et al., 2019; Galuppo et al., 2017; Liu et al., 2021; Chen et al., 2019; Song et al., 2020). These studies begin to link Mf to HF development, but also highlight the need to critically examine how Mf, from TRM to recruited Mf pMI, can impact the heart as a whole, and as it is failing. A greater understanding of how Mf subtypes influence heart homeostasis and pMI repair is of utmost importance. In particular, it could shed light on functional roles of Mf in patients with ischemic cardiomyopathy (ICM), for instance, where an abundance of CCR2+ Mf have been associated with worse cardiac function (Bajpai et al., 2018). Remaining questions include: *are there factors key to Mf activation, survival, function, or dynamics that could have huge impacts in post MI HF development?*

## **1.4 Epidermal Growth Factor Receptor (EGFR): A Key Factor for Macrophages in the Heart?**

### **1.4.1 Introduction to Receptor Biology**

Within tissues, cells are constantly exposed to signals, which need to be translated and integrated appropriately in order to maintain homeostasis, survival, protection, and adaptation of any kind (Holbro et al., 2004). This primarily occurs through cell surface receptors, which can take signals, or ‘ligands’ from the extracellular space, with the goal of inducing some biological outcome (Holbro et al., 2004). In general, cell surface receptors come as 1 of 3 types, these being ion channel receptors, G Protein Coupled Receptors (GPCR), or enzyme linked receptors (Deller et al., 2000; Miller et al., 2021). Briefly, ion channel receptors are typically activated by ligand binding, which results in structural changes in the receptor to allow for the exchange of ions between the extracellular and intracellular space (Miller et al., 2021). The second class, GPCR,

typically have an orthosteric ligand binding pocket in the extracellular space, and in their intracellular domain, GPCR bind the heterotrimeric (alpha, beta, gamma) protein, termed G protein (Miller et al., 2021). When inactive G protein alpha is bound to guanine diphosphate (GDP) (Miller et al., 2021). Ligand binding or activation of GPCR results in guanine nucleotide exchange of GDP to guanine triphosphate (GTP) on G alpha, allowing for subsequent activation of proteins downstream, to modulate cell function (Miller et al., 2021). The third and final class of cell surface receptors are enzyme linked receptors. These receptors are differentiated by the presence of catalytic sites within their intracellular domains (Miller et al., 2021). Their most common mechanism follows as such: after ligand binding, single receptors come in close proximity, forming dimers (Miller et al., 2021). This dimerization then activates the catalytic site, resulting in some enzyme activity (Miller et al., 2021).

The Erythroblastic leukemic viral oncogene (ErbB) family make up one family of enzyme linked receptors, functioning as tyrosine kinase receptors (Holbro et al., 2004; Deller et al., 2000; Miller et al., 2021). The ErbB family is evolutionarily conserved, as it is observed from *caenorhabditis elegans* (*C. elegans*) to large mammals, though in greater complexity in higher organisms (Holbro et al., 2004). Specifically, in *C. elegans* the ErbB network consists of 1 receptor and ligand, however, in mammalian cells, the family includes 4 receptors, with an expansive combination of ligands, detailed in Figure 5a (Holbro et al., 2004). The complexity of the mammalian ErbB family expands the signaling network, adding a great deal of receptor signaling diversity (Holbro et al., 2004). The 4 receptors include ErbB1, more commonly referred to as the Epidermal Growth Factor Receptor (EGFR), ErbB2, ErbB3, and ErbB4 (Holbro et al., 2004). ErbB2

and ErbB3 are also often referred to as human EGFR 2 and 3 respectively (HER2, HER3) (Holbro et al., 2004). Ligands in the ErbB family include epidermal growth factor (EGF), transforming growth factor a (TGFa), heparin-binding EGF (HB-EGF), amphiregulin (AREG), betacellulin (BTC), epigen (EPG), epiregulin (ERG), and neuregulins (NRG) 1-4 (Holbro et al., 2004). These ligands bind ErbB members with unique specificity, outlined in Figure 5a. Of all ErbB receptors, EGFR and ErbB2 are most highly expressed in heart tissue (Okada et al., 2022 ). Interestingly, data from the human protein atlas database indicates EGFR as being most highly expressed in heart immune cells. This makes EGFR an interesting and critical factor to consider.

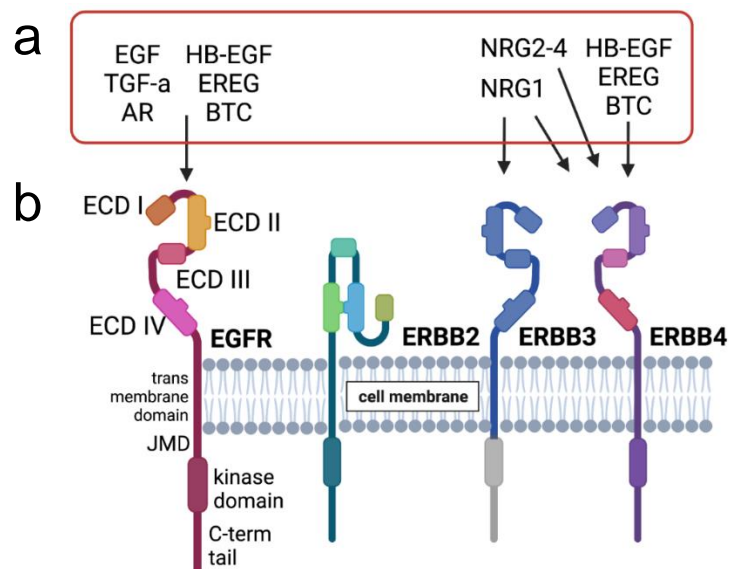


**Figure 5. Epidermal Growth Factor Receptor (EGFR) Family.** a) ErbB1-4 family of cell surface receptors can be activated by a total of 10 ligands combined (circled in red): epidermal growth factor (EGF) transforming growth factor alpha (TGF-a), amphiregulin (AR), heparin-binding EGF (HB-EGF), epiregulin (EREG), betacellulin (BTC), neuregulins 1-4 (NRG1-4). Arrows specify which ligands activate which receptors. b) General ErbB structure includes extracellular domain (ECD) comprising of 4 parts, transmembrane spanning domain, juxtamembrane domain (JMD), kinase domain, and carboxy terminal (C-term) tail. Structural features of other ErbB members presented. ErbB2 does not bind ligand. Kinase domain of ErbB3 functionally impaired. Figure was generated in Biorender (<https://biorender.io>) under a student premium license.

### 1.4.2 EGFR

ErbB receptors share functional and structural homology, though each receptor has unique features, allowing for differential receptor signaling kinetics and thus, biological outcome (Figure 5b) (Holbro et al., 2004). In detail, the extracellular domain (ECD) of EGFR can be divided into 4 domains, which cooperate to maintain the receptor in an open or closed state depending on ligand availability (Holbro et al., 2004; Kovacs et al., 2022). Ligand binding to the receptor induces major conformational changes, a necessity for receptor dimerization and subsequent activation (Lemmon et al., 2014 ). Specifically, beta helical domains 1 and 3 rearrange to bind ligands, allowing for the cysteine rich domain 2 to bind and dimerize another receptor molecule (Ogiso et al., 2002; Burgess, 2009). Following the ECD are the membrane spanning portion, and the intracellular domain, consisting of the tyrosine kinase, and carboxyl terminal (C-term) tail, rich with autophosphorylation sites (Burgess, 2009; Makki et al., 2013).

EGFR dimerization and activation is best exemplified by ligand dependent activation of the receptor. ErbB family ligands are typically synthesized as membrane bound precursors, which are cleaved by proteases in the MMP or A disintegrin and metalloprotease (ADAM) family, to make soluble GF (Burgess, 2009; Makki et al., 2013). Once cleaved, ligands bind EGFR, leading to clustering of receptors on the membrane (Burgess, 2009; Makki et al., 2013). Receptor monomers are unable to initiate downstream molecular signaling, therefore, 2 receptor molecules form a dimer in order to stimulate intrinsic kinase activity within the intracellular domain (Holbro et al., 2004; Burgess, 2009). Typically, activated ErbB family receptors can form homo- or heterogenous dimers, though dimerizing properties differ between receptors; in

particular, ErbB2 and 3 can only signal through heterodimers (Lemmon et al., 2014). EGFRs in dimer form are brought in closer proximity, where their juxtamembrane domains (JMD) and C-term tails can interact, resulting in receptor activation (Burgess, 2009; Jura et al., 2009; Patwa et al., 2021; Zhang et al., 2006 ). In total, the EGFR intracellular domain contains 20 tyrosine residues, many of which become autophosphorylated upon ligand stimulation (Purba et al., 2017; Lemmon et al., 2014; Wee et al., 2017). Autophosphorylated tyrosine residues can then act as docking sites, allowing for the recruitment of many intracellular adaptor proteins, most of which contain phospho tyrosine binding domains (PTB) (Prenzel et al., 2001; Ogiso et al., 2002; Wee et al., 2017 ).

### **1.4.3 EGFR Signalome**

Of all ErbB receptors, the EGFR signaling network is perhaps the most expansive (Wee et al., 2017). Some of the most common molecular signaling pathways downstream of EGFR are highlighted below, and represented in Figure 6a (Burgess, 2009). Interestingly, many of these pathways are interconnected, with several points of cross talk (Wee et al., 2017). Additionally, these molecular signaling events can occur simultaneously, leading to biological outcomes like cell proliferation, growth, and differentiation (Wee et al., 2017).

a

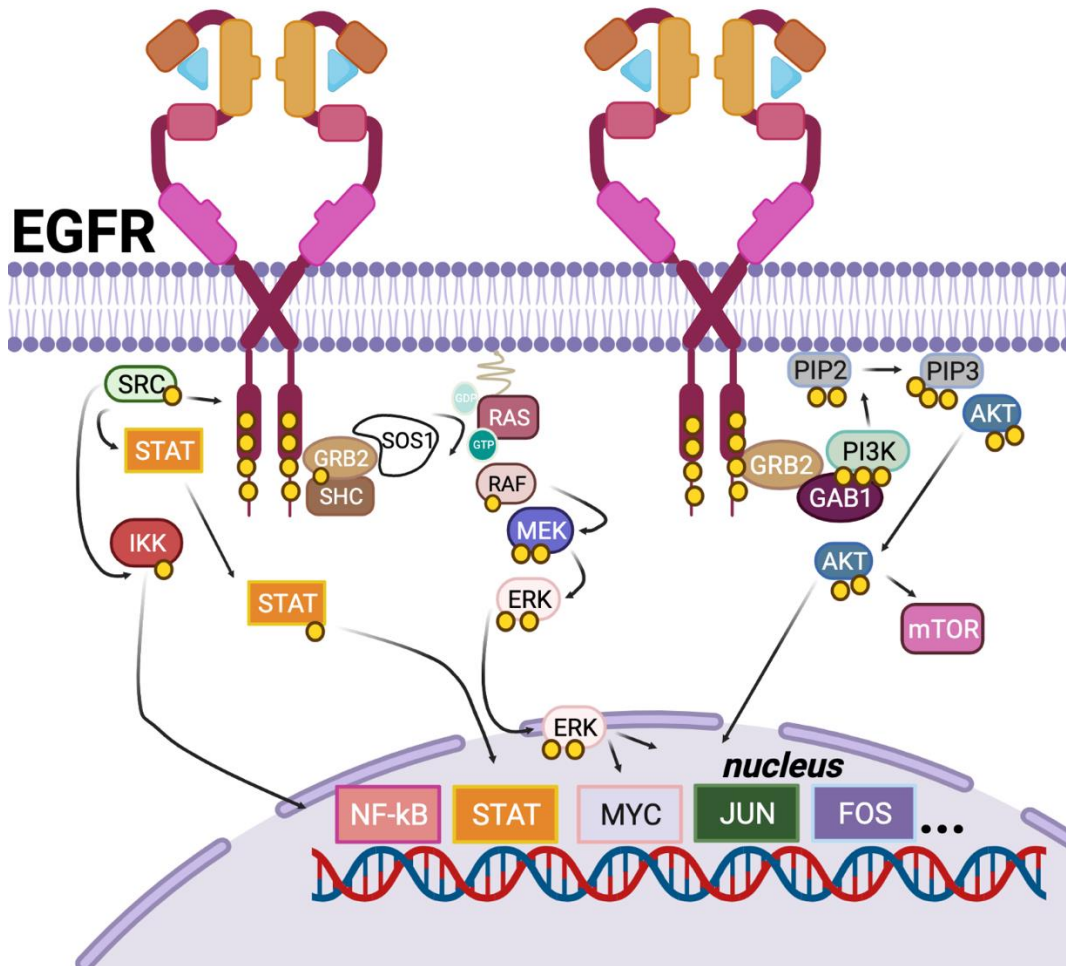


**Figure 6. Major EGFR Signaling Pathways.** a) Graphic depicts major signaling pathways downstream of EGFR, these being MAPK and PI3K/AKT. Activation of these pathways is best exemplified following EGFR ligand activation, leading to dimerization and trans/autophosphorylation at particular tyrosine (Y) residues. SHC and GRB2 can bind phosphorylated (yellow circles) EGFR, leading to SOS1 recruitment. SOS1, a guanine nucleotide exchange factor (GEF), activates RAS, which initiates the MAPK cascade (RAF, MEK, and ERK). ERK activation can result in the activation of numerous other cytosolic kinases, or nuclear transcription factors (TF) like JUN/FOS and MYC. SRC belongs to a family of kinases that mediate molecular changes downstream of EGFR. SRC can activate TFs like STATs or NF-kB. PI3K activation follows its binding to GAB1. PI3K phosphorylates PIP2, yielding PIP3, which leads to the recruitment and activation of AKT. AKT then regulates a large number of cytosolic substrates, including mTOR. AKT activation also leads to the activation of additional nuclear TFs. Figure was generated in Biorender (<https://biorender.io>) under a student premium license.

Canonical EGFR pathways:

The mitogen-activated protein kinase (MAPK) pathway is arguably the most activated pathway following EGFR activation; MAPK activation mediates a significant number of biological responses ranging from cell proliferation, and migration, to cell survival, and more (Wee et al., 2017). MAPK activation is initiated after growth factor receptor binding 2 (GRB2) binds phosphorylated tyrosine residues within the EGFR intracellular domain (Wee et al., 2017). GRB2 functions as an adaptor protein, capable of binding son of sevenless 1 (SOS1), a guanine nucleotide exchange factor (GEF) for the small GTPase rat sarcoma virus (Ras) (Wee et al., 2017). SOS1 GEF activity results in the exchange of GDP for GTP on Ras (Wee et al., 2017). GTP bound Ras then interacts with Raf1, resulting in its translocation to the membrane (Wee et al., 2017).

Translocation of Raf1 to the membrane is an initial requirement in its activation mechanism (Wee et al., 2017). Once fully activated, Raf1 kinase activity phosphorylates the MAPK kinase (MEK); MEK continues the phosphorylation cascade by activating extracellular signal-regulated kinases (ERK) 1 and 2 (Wee et al., 2017). The activation of the MAPK signaling pathway induces such a vast array of biological outcomes predominantly because of the large number of substrates that are targeted by ERK 1/2 (Yoon et al., 2006 ). For instance, ERK 1/2 substrates include nuclear transcription factors, additional cytosolic kinases, or phosphatases, cytoskeletal proteins, and proteins involved in other key signaling pathways (Yoon et al., 2006).

Another major canonical pathway that is activated downstream of EGFR activation involves phosphatidylinositol 3 kinase (PI3K) and protein kinase B (AKT), which are key regulators of processes like metabolism, proliferation, growth, survival,

and motility (Vanhaesebroeck et al., 2012). PI3K is a family of kinases, capable of phosphorylating membrane phospholipids, which then act as potent second messengers in a number of cell signaling events (Wee et al., 2017). Following EGFR activation, PI3K is recruited to the receptor, though it does not bind directly (Wee et al., 2017). GRB2 and GRB2 associated binder (GAB1) bind activated EGFR, and allow for PI3K docking (Wee et al., 2017). In this canonical pathway, PI3K then phosphorylates phosphatidylinositol - 4 - 5 - biphosphate (PIP2), yielding phosphatidylinositol - 3 - 4 - 5 - triphosphate (PIP3) (Vanhaesebroeck et al., 2012). PIP3 can recruit pleckstrin homology (PH) domain containing proteins to the membrane, including the serine threonine kinase AKT (Wee et al., 2017). AKT translocation to the membrane is the first step in its activation; once phosphorylated, AKT in turn targets a large number of cytosolic substrates to mediate a number of physiological outcomes (Manning et al., 2017).

The Src family of kinases are non receptor tyrosine kinases that mediate molecular changes downstream of EGFR (Sen et al., 2011). Of the 11 members, c-Src is most commonly associated with EGFR activation (Wee et al., 2017). Ligand stimulation of EGFR is known to mediate c-Src activation (Wee et al., 2017). Functionally, EGFR/c-Src signaling may be important for activation of major TFs like STATs and NF- $\kappa$ B, which are key regulators of inflammatory mediators (Wee et al., 2017; Shostak et al., 2015).

#### Noncanonical EGFR Functions:

In addition to activating intracellular molecular protein pathways, EGFR can regulate physiology through non canonical mechanisms. For instance, EGFR has been

shown to impact distinct biological outcomes following translocation to different compartments of the cell (Wee et al., 2017). In this context, EGFR nuclear and mitochondrial signaling have been most extensively studied (Lin et al., 2001; Waugh et al., 2001; Brand et al., 2013; Demory et al., 2009). EGFR nuclear translocation and function was first reported over 20 years ago when evidence pointed to EGFR's ability to bind unique DNA sequences commonly seen in some TFs that regulate proliferation (Lin et al., 2001). Though initially controversial, these early reports have since been followed by additional supportive studies, which altogether indicate the potential for EGFR as a TF, or TF co-activator (Waugh et al., 2001; Brand et al., 2013). Nuclear EGFR translocation is argued to add a layer of specificity to EGFR signaling, as it allows for more direct modulation of specific TF targets (Waugh et al., 2001). EGFR is also reported to translocate to the mitochondria, where it can associate with and phosphorylate mitochondrial proteins, and also regulate mitochondrial dynamics through inhibition of mitochondrial fission proteins (Demory et al., 2009; Che et al., 2015).

#### EGFR Internalization:

Ligand activated EGFR homodimers, or EGFR/ErbB heterodimers can be internalized, a mechanism which was first thought to terminate receptor signaling, as internalized receptors could be targeted to the lysosome for degradation (Sorkin et al., 2009). Receptor dimers are internalized through endocytosis, with differing kinetics based on dimer makeup (Brand et al., 2013; Sorkin et al., 2009; Holbro et al., 2004). Homodimers of EGFR are internalized most rapidly, while ErbB heterodimers are internalized at slower rates (Brand et al., 2013). Additionally, it has been shown that receptors in endosomes can continue the recruitment of additional protein effectors

(Sousa et al., 2012). This highlights receptor endocytic trafficking as a potential mechanism through which EGFR/ErbB signaling can be more robust, and specifically localized to initiate necessary molecular changes (Sousa et al., 2012; Sorkin et al., 2009).

EGFR transactivation:

An additional layer in the complexity of EGFR signaling stems from its ability to be transactivated by other receptors (Grisanti et al., 2017). Some of the most commonly studied EGFR transactivation pathways are those secondary to GPCR activation (Grisanti et al., 2017). This was first reported after evidence of GPCR ligands inducing EGFR phosphorylation (Daub et al., 1996). Since these findings, EGFR transactivation has been extensively investigated, and mechanisms leading to GPCR mediated EGFR transactivation have been identified (Grisanti et al., 2017). For one, effector proteins like G proteins or b Arrestins, downstream of GPCR can activate proteases which cleave EGFR ligands, allowing for their potential binding to EGFR (Grisanti et al., 2017; Overland et al., 2015). GPCRs may also interact with EGFRs in microdomains, leading to receptor cross-talk and transactivation (Grisanti et al., 2017). Functionally, transactivation can engage any number of canonical receptor signaling pathways, but is also unique in that it can alter the kinetics of receptor signaling, ultimately yielding differential biological outcomes (Grisanti et al., 2014).

#### **1.4.4 EGFR in the Cardiovascular System**

Historically, EGFR signaling has been the target of cancer research as it is highly expressed in tumor tissue, and can be a major driver of tumorigenesis (Holbro et al., 2004). Within this context, aberrant ligand production, receptor overexpression, or mutated forms of the receptor can lead to excessive proliferation and tumor survival

(Holbro et al., 2004). Consequently, several EGFR inhibiting strategies have been employed as cancer therapeutics and also in clinical trials, with some success (Holbro et al., 2004). Currently however, it is well documented that EGFR has physiological roles outside of oncogenesis (Burgess, 2009). For one, EGFR is critical for development, as its loss in mice is embryonic, or postnatally lethal (Burgess, 2009). The difference in lethality can be explained by differences in strain and genetic backgrounds (Burgess, 2009; Sibilina et al., 1998). However, these early studies reveal that EGFR is clearly needed for implantation of the embryo, and development of the central nervous system (CNS) (Burgess, 2009; Sibilina et al., 1998).

In addition to roles in development, EGFR is important in the cardiovascular (CV) system, as it is expressed in virtually all cardiac and vascular cell types (Makki et al., 2013). Since loss of the receptor is lethal, early studies employed dominant negative or pharmacologic strategies to understand how EGFR regulates CV homeostasis. In one such model, mice expressing mutant EGFR with receptor autophosphorylation 5-10 fold lower exhibit significant cardiac hypertrophy, and systolic dysfunction, with 50% mortality by 12 months (Barrick et al., 2009). Similarly, chronic infusion of an EGFR inhibitor also leads to cardiac dysfunction in mice, accompanied by elevated fetal gene expression, and cardiac cell death (Barrick et al., 2008).

In more recent studies, the advent of mouse models with promoter specific cre recombinases has allowed for the analysis of the distinct roles of EGFR within particular cells in the CV system. For example, although Endo specific deletion of EGFR is dispensable for basal vascular function, VSMC deletion of EGFR alters vascular tone (Schreier et al., 2021; Schreier et al., 2013). In VSMC, EGFR is a critical factor

regulating proliferation and migration; its loss results in a modest reduction of the vessel media layer, with a concomitant increase in lumen diameter (Makki et al., 2013; Schreier et al., 2013). Beyond general vascular homeostasis, manipulating the expression or activation of EGFR can also regulate disease outcomes; for instance, EGFR inhibition has been shown to limit the severity in models of vascular proliferative disorders like restenosis (Makki et al., 2013).

Cell specific models have also been employed to study the function of EGFR in cardiac muscle. In a model of VSMC EGFR deletion, cre promoter overlap in cardiac muscle results in 50% reduction in CM EGFR (Schreier et al., 2013). This reduction in CM EGFR results in ventricular hypertrophy (Schreier et al., 2013). Further analysis of specific CM EGFR deletion shows its importance in maintaining cardiac contractile homeostasis and dynamics (Guo et al., 2021). Here, the loss of CM EGFR in mice results in progressive systolic dysfunction, and adverse cardiac remodeling by 10 months of age (Guo et al., 2021). These phenotypes result in 50-60% mortality by 16 months of age (Guo et al., 2021).

#### **1.4.5 Myeloid-Cell Specific EGFR**

Currently, there have been no full scope reports detailing the role of EGFR in cardiac immune cells, especially with regards to their contribution in normal physiology, but also in post MI HF development. Interestingly, Mf EGFR has been examined in other disease models, raising the question then: *do cardiac Mf, which are a critical cell type in physiology and pathology, rely on EGFR to function.* Each of these studies have used the LysMcre model, where a nuclear-localized cre recombinase is inserted into the first coding sequence of the lysozyme 2 (Lyz2) gene (Clausen et al., 1999; Shi et al., 2019).

Lyz2 is expressed in innate immune cells of myelomonocytic origin, these include Mon, Mf, and granulocytes (Shi et al., 2019). As a result, deletion of EGFR is not strict to Mf, although, owing to shared precursor cells, and common genetic markers, this is a major limitation in virtually all myeloid (myl) targeting cre/lox systems (Shi et al., 2019). However, using this model is myl specific, and it is often the case that Mf expression of cre and Mf density is greatest relative to Mon or granulocytes (Shi et al., 2019; Hoyer et al., 2019). Below, key findings regarding the role of myl/Mf EGFR are discussed; these key findings provide rationale for examining whether EGFR ties Mf to cardiac physiology/HF development.

Initial studies of Mf EGFR have examined its role in contributing to tumorigenesis in hepatocellular carcinoma (HCC) and a few types of gastrointestinal cancer. LysM mediated EGFR deletion has been shown to reduce key cytokines that promote hepatocyte malignant growth (Lanaya et al., 2014). In detail, during the development of HCC, liver resident Mf, or so called kupffer cells, upregulate EGFR (Lanaya et al., 2014). Hepatocytes also undergo damage, resulting in their release of DAMPs, which can activate Mf to produce EGFR ligands (Lanaya et al., 2014). This induction of EGFR ligands likely contributes to activating EGFR in kupffer cells, which then regulates the production and secretion of IL6, allowing for the malignant growth of hepatocytes through hepatocyte IL6 receptor (Lanaya et al., 2014).

Mf EGFR regulation of cytokine production is also observed in other models of chronic inflammation and associated cancers. Although it's important to note, the mechanisms contributing to, and the physiological outcomes following, are still up for debate. This is because, for instance, in similar models of colitis, different outcomes have

been observed following lysm mediated EGFR deletion (Srivatsa et al., 2017; Lu et al., 2014; Hardbower et al., 2017). One group has observed that myl EGFR protects against the development of severe colitis, as EGFR myeloid knockout mice (EGFRmylKO) exhibit enhanced inflammation and reduced epithelial barrier integrity during disease (Srivatsa et al., 2017). The specific mechanisms leading to this phenotype are not identified. On the other hand, using similar mouse models, another group has shown that myl EGFR deletion improves colitis outcomes and limits inflammation in the colon (Lu et al., 2014). Mechanistically, they provide evidence, suggesting that the loss of Mf EGFR leads to prolonged NF-kB activation through enhanced degradation of its upstream inhibitor, IkbA (Lu et al., 2014). Here, they reason that prolonged NF-kB activation, in response to reduced Mf EGFR activity, results in elevated IL10, which combats inflammation in the colon (Lu et al., 2014). Finally, a third group has observed Mf EGFR to play no role in colitis severity (Hardbower et al., 2017). Regardless of colitis outcomes however, two of the studies mentioned above indicate that in models of colitis associated cancer (CAC), Mf EGFR is detrimental, and its deletion reduces tumor burden (Srivatsa et al., 2017; Hardbower et al., 2017). In CAC, Mf EGFR activates the TF STAT6, leading to the enhanced production of cytokines and growth factors like CXCL9, 10, IL4, 10, 13, and VEGF, all of which promote tumor cell survival and angiogenesis (Srivatsa et al., 2017; Hardbower et al., 2017). Additionally, Mf EGFR also regulates the production of pro-inflammatory cytokines, namely IL1b, and IL6, contributing to enhanced inflammation and tumorigenesis in CAC (Hardbower et al., 2017).

The ability of Mf EGFR to regulate the production of both pro and anti inflammatory cytokines has also been shown to similarly drive gastrointestinal cancer

subsequent to bacterial infection (Hardbower et al., 2016). It is important to note, that in this context, Mf EGFR plays no role in pathogen induced apoptosis, or pathogen clearance mechanisms (Hardbower et al., 2016). On the other hand though, another group has shown, that Mf EGFR may protect against tumor development in gastrointestinal cancers (Zhao G et al., 2016). In brief, EGFR in tumor associated Mf (TAM) can be transactivated in the tumor microenvironment, in response to elevated inflammatory signaling. They then show that inhibiting Mf EGFR activation can lead to elevated STAT6 activation, therefore promoting the production of antiinflammatory mediators, and EGFR ligands (Zhao G et al., 2016). Elevated levels of HB-EGF for instance can then contribute to immorto-min colonic epithelial (IMCEras) tumor cell proliferation, and epithelial to mesenchymal transition (EMT), ultimately increasing tumor burden (Zhao G et al., 2016).

The 2 most recent studies of Mf EGFR have examined its role in CVD. In the first, Mf EGFR has been shown to promote atherosclerosis through varied mechanisms, the full extent of which is unknown (Zeboudj et al., 2018). In the context of elevated oxidized low density lipoprotein (oxLDL), Mf EGFR regulates the expression of a scavenger receptor, cluster of differentiation (CD) 36, allowing Mf to engulf oxidized cholesterol (Zeboudj et al., 2018). As a result, myl EGFR deletion leads to reduced CD36. Heightened endocytosis of oxLDL can result to greater inflammation in the vessel wall, resulting in more advanced atherosclerotic lesions (Zeboudj et al., 2018). The mechanisms through which EGFR regulates the expression of scavenger receptors is currently unknown, and whether this will have an impact in other disease contexts where Mf endocytic function is critical is currently unclear.

The most recent study examining Mf EGFR sheds the most light on the multifaceted roles of EGFR, and is the first to examine how EGFR regulates function of Mf differing in origin (Hoyer et al., 2019). Specifically, this study highlights that alveolar Mf, which are maintained primarily through self-renewal, can exhibit high expression of EGFR during stress, leading to the production and regulation of inflammatory cytokines (Hoyer et al., 2019). Notably, in the exact same stress environment, interstitial Mf, which derive from Mon differentiation, exhibit lower levels of EGFR, and EGFR is dispensable for regulating interstitial Mf inflammatory mediators (Hoyer et al., 2019). These findings highlight the importance of Mf EGFR signaling, but further point to its complexity, especially when considering how differing origin can contribute to Mf gene expression and function (Hoyer et al., 2019).

### **1.5 Summary, Thesis Key Questions, and Hypothesis**

HF is a global public health crisis and economic burden (Virani et al., 2021). As such, there is an enormous interest to identify novel therapeutic angles (Mascolo et al., 2022). Inflammation has long been associated with HF, and recently, clinical trials targeting inflammation have had moderate success, leaving a desire to explore the full extent of how inflammation can contribute to cardiac physiology and HF development (Mascolo et al., 2022; Swirski et al., 2018). The most abundant, and complex leukocyte in the heart is the Mf (Tucker et al., 2020). Recently, cardiac Mf have been shown to be important in stages of cardiac development, heart homeostasis, and HF development following MI (Lavine et al., 2018). While these studies have pinpointed Mf roles in the heart, exactly how Mf function to yield these outcomes is not fully understood. EGFR is a growth factor receptor, critical to a number of biological processes (Holbro et al.,

2004). EGFR has been shown to be important for Mf function, however, the literature surrounding this topic suggests that how Mf EGFR contributes to Mf function is often complex, and context dependent (Srivatsa et al., 2017; Lu et al., 2014; Hardbower et al., 2017; Zhao G et al., 2016; Zeboudj et al., 2018; Hardbower et al., 2016; Hoyer et al., 2019). This then leaves many unanswered questions, especially when we consider cardiac physiology, and HF development subsequent to ischemic attack. For one, how does EGFR shape cardiac Mf dynamics, function, and global gene expression? Does this have any implications for general cardiac physiology? Additionally, in response to MI - where the needs of macrophages become varied, ranging from debris clearance, repair induction, to stabilizing the infarct microenvironment, what roles do Mf EGFR play? and how? Considering the preliminary evidence, in response to these questions, we *hypothesized* that macrophage EGFR would have protective roles in cardiac physiology, and reduce the severity of HF outcomes. The studies outlined below will carefully consider these knowledge gaps and provide findings to support that myl/Mf EGFR is critical to cardiac homeostasis and protects the infarcted heart during repair.

## CHAPTER 2

### EXPANDED MATERIALS AND METHODS

#### 2.1 Animal Protocols

All experiments requiring mice paid attention to the National Institutes of Health (NIH) Guide for the Care and Use of Laboratory Animals and were approved by the Institutional Animal Care and Use Committee (IACUC) at Temple University. The project took advantage of the B6.129s6-Egfr<sup>tm1Dwt</sup>/Mmnc, ID 031765-UNC mouse, initially donated by David Threadgill, Ph.D., North Carolina State University. The mice were obtained from the Mutant Mouse Regional Resource Center (MMRRC), an NIH-funded strain repository. They harbor a conditional allele of Egfr with exon 3 flanked by two loxP sites (EGFR<sup>f/f</sup>); deletion results in early termination of translation (Lee et al., 2009). To generate EGFR deletion specifically in myeloid cells, EGFR<sup>f/f</sup> mice were crossbred with homozygous LysM cre transgenic mice, and will be denoted EGFRmylKO for brevity (Clausen et al., 1999). EGFRmylKO mice were bred and maintained at homozygosity (Figure 7). LysMcre mice were secured from Jackson Laboratory (B6.129P2-Lyz2<sup>tm1(cre)</sup>If0/J, Stock No: 004781). The study featured both male and female 12 - 16 week old EGFRmylKO, LysM Cre, and EGFR<sup>f/f</sup> controls, unless otherwise stated. Individual replicates are represented by bullets in bar graphs, and/or are indicated in figure legends.

#### 2.2 Mouse Genotyping

Mouse genotypes were assessed with agarose gel separation of polymerase chain reaction (PCR) products using mouse tail clippings. At roughly 3 weeks of age, about 0.5

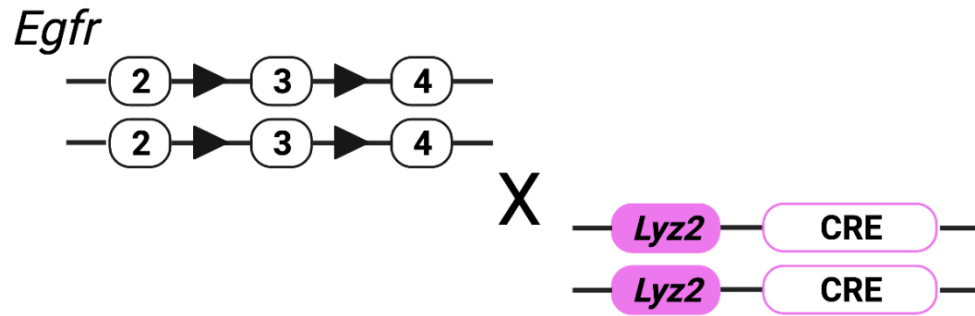


**Figure 7. Generation of Myeloid-Cell Specific EGFR Knockout (KO) Mouse Model.** Schematic showing generation of myeloid-specific EGFR knockout mice (EGFR<sup>mylKO</sup>). Homozygous LysM-Cre transgenic mice (LysM Cre) were crossed to mice carrying a conditional allele of *Egfr* with exon 3 flanked by two loxP sites (EGFR<sup>f/f</sup>).

cm of tail was clipped and digested in 50 ul of DirectPCR Lysis Reagent (Viagen Biotech, Los Angeles, CA) at 95°C for 20 min. After this, the tails then received an addition of 50 ul of DirectPCR Lysis Reagent, supplemented with 0.6 mg/ml of proteinase K (VWR, Solon, OH). The tails in solution were then kept at 55°C overnight (O/N). The next day, tail solutions were heated at 95°C for 10 min, and after robust vortex/centrifugation, tail DNA was used for PCR. PCR primers that were used to detect floxed *Egfr* and *Cre* are provided in Table 1. PCR was completed at the same time, with conditions set at 30 cycles of 94°C for 30 sec, 56°C for 25 sec, and 72°C for 60 secs. Following PCR, products were subject to agarose gel (2% in 1X Tris-acetate-Ethylenediaminetetraacetic acid (EDTA), Thermo Scientific, Wilmington, DE) and distinguished based on size: homozygous EGFR<sup>f/f</sup> (348 bp), WT EGFR (253 bp), *Cre* (565-585 bp).

**Table 1.** Primer Sequences for Mouse Genotyping

| <i>Name</i> | <i>Sequence</i>          |                          |
|-------------|--------------------------|--------------------------|
|             | <b>Forward (5' - 3')</b> | <b>Reverse (5' - 3')</b> |
| <i>Lox3</i> | CTTTGGAGAACCTGCAGATC     | CTGCTACTGGCTCAAGTTTC     |
| <i>Cre</i>  | GGCGTTTTCTGAGCATACT      | CTACACCAGAGACGGAAATCCA   |

### **2.3 Reverse Transcription – quantitative Polymerase Chain Reaction (RT-qPCR)**

Total RNA was extracted from a variety of samples: frozen or fresh quarter heart tissue, as well as frozen or fresh cell pellets/dishes. RNA was extracted using the PureLink RNA mini kit (Invitrogen, Carlsbad, CA) according to the manufacturer's instructions. The RNA was tested for quality and concentration with a Nanodrop 2000 (Thermo Scientific, Wilmington, DE). Following this quantification, 500 ng (cells) or 1000 ng (tissue) of RNA was converted to complementary DNA (cDNA) using the High Capacity cDNA Reverse Transcription kit (Applied Biosystems, Waltham, MA). A normalized amount of cDNA (25 ng) was subject to RT-qPCR in triplicate with the Powerup Sybr Select Master Mix (Applied Biosystems, Waltham, MA). All of the gene expression was normalized to an internal control, glyceraldehyde-3-phosphate dehydrogenase (GAPDH), and analyzed with the Applied Biosystems Comparative CT Method ( $2^{-\Delta\Delta CT}$ ). All of the primers used in RT-qPCR are listed in Table 2.

### **2.4 Tissue Histology**

All mouse hearts were perfused with saline, cutout, and fixed (whole heart) in 4% paraformaldehyde (PFA) in phosphate-buffered saline (PBS). 72 hr following fixation, hearts were thoroughly rinsed in PBS, and dehydrated with the Microm STP120 tissue processor. Hearts were embedded in paraffin with the HistoStar apparatus, and a Microm

**Table 2.** Primer Sequences for RT-qPCR

| <i>Name</i>      | <i>Sequence</i>          |                           |
|------------------|--------------------------|---------------------------|
|                  | <b>Forward (5' - 3')</b> | <b>Reverse (5' - 3')</b>  |
| <i>Egfr</i>      | GGAGAGAATCCCTTTGGAGAAC   | CCAGTTCTGTTTGTCCCATAGT    |
| <i>Cre</i>       | CAGGTTTCGTTCACTCATGGAA   | TCCTGGCAATTTTCGGCTATAC    |
| <i>Acta1</i>     | CCCAAAGCTAACCGGGAGAAG    | CCAGAATCCAACACGATGCC      |
| <i>Nppb</i>      | GAGGTCACTCCTATCCTCTGG    | GCCATTTCCCTCCGACTTTTCTC   |
| <i>Myh7</i>      | ACTGTCAACACTAAGAGGGTC    | TTGGATGATTTGATCTTCCAG     |
| <i>Col1a1</i>    | GAAACCCGAGGTATGCTTGA     | GGGTCCCTCGACTCCTACAT      |
| <i>Igfbp5</i>    | CCTTGGTGTCTCCCATCTAATC   | CTGTGACTTGAAGTACCTCAT     |
| <i>Igfbp7</i>    | GTAAGGAGGACGCTGGAGAGT    | CTGGCTGTAATAAAGTGTTAGTGG  |
| <i>Igf1</i>      | TGGATGCTCTTCAGTTCGTG     | GTCTTGGGCATGTCAGTGTG      |
| <i>Igf2</i>      | CCCTCAGCAAGTGCCTAAAG     | TTAGGGTGCCTCGAGATGTT      |
| <i>Cd36</i>      | TCGGATCTGAAATCGACCTT     | CACAGGCTTTCCTTCTTTGC      |
| <i>Fabp4</i>     | ACACCGAGATTTCCTTCAAAGT   | CCATCTAGGGTTATGATGCTCTTCA |
| <i>Cx43/Gjal</i> | CCATCCAAAGACTGCGGAT      | GTAATTGCGGCACGAGGAA       |
| <i>Timp4</i>     | GCAAAGACCCTGCTGACACT     | GGGCTCAATGTAGTTGCACA      |
| <i>Cxcl12</i>    | AGAGCCAACGTCAAGCATCT     | TAATTTCCGGTCAATGCACA      |
| <i>Angptl4</i>   | GTTTGCAGACTCAGCTCAAGG    | CCAAGAGGTCTATCTGGCTCTG    |
| <i>Ccr2</i>      | TGCCATCATAAAGGAGCCATAC   | GTGAATCCAATGCCCTCTTCT     |
| <i>Tim4</i>      | TTTGCCTTGTCATTACCTCT     | TGACTTCCTGGAGATGATTC      |
| <i>Cx3cr1</i>    | GAGAGATGGCTCAGTGGTTAAG   | CACAGGAACAGGGAGCTATTT     |
| <i>Erbp2</i>     | ATTTGCTGGAGAAGGGAGAAC    | GCGACATTCGGAGTCAATCA      |
| <i>Erbp3</i>     | CAGTATGTCCTGGGACTCTAAAC  | GACCACCTCACACTTCTCATAG    |
| <i>Gapdh</i>     | AACAGCAACTCCCACTCTTC     | CCTGTTGCTGTAGCCGTATT      |
| <i>Lyz2</i>      | AATGGCTGGCTACTATGGAGTCA  | TGCTCTCGTGCTGAGCTAAACA    |
| <i>Arg1</i>      | AAGAAAAGGCCGATTCACCT     | CACCTCCTCTGCTGTCTTCC      |
| <i>Il10</i>      | CCAAGCCTTATCGGAAATGA     | TCACTCTTCACCTGCTCCAC      |
| <i>Cd206</i>     | CACAAAGCCATGCTGTAGTA     | GTGAAGGTGGATAGAGTGGA      |
| <i>Vegfa</i>     | GAGGATGTCCTCACTCGGATG    | GTCGTGTTTCTGGAAGTGAGCAA   |
| <i>Fgf2</i>      | CACCAGGCCACTTCAAGGA      | GATGGATGCGCAGGAAGAA       |

HM was used to make sections at 5-micron thickness that were placed onto charged microscope slides (Globe Scientific, Mahwah, NJ). Attached heart sections were then deparaffinized in xylene (15 min) and ethanol (100,90,80, 70%, 5 min each) before any staining. For analysis of cell size and cell cross-sectional areas, hearts were stained O/N at 4°C with Wheat Germ Agglutinin (WGA, 1:250, Vector Labs, San Francisco, CA), then rinsed (3x PBS), and counterstained with NucBlue Fixed Cell ReadyProbes (ThermoFisher, Fair Lawn, NJ) for 10 min at room temperature (RT). Next, to assess capillary density within the left ventricle (LV), hearts were stained O/N at 4°C with isolectin B4 (Lectin, 1:250, Vector Labs, San Francisco, CA), then washed as described above, and similarly counterstained with NucBlue. To assess cardiac cell death, sections were subjected to terminal deoxynucleotidyl transferase (TdT)-mediated dUTP- nick end labeling (TUNEL) via an *In Situ* Cell Death Detection Kit, TMR Red (Sigma-Aldrich, St. Louis, MO). After treating sections with proteinase K, hearts were incubated with TMR-dUTP for 1 hr at 37°C, and counterstained with troponin I (TNNI, 1:100, Cell Signaling, Danvers, MA) O/N at 4°C. Donkey anti-Rabbit ReadyProbes Secondary Antibody Alexa Fluor 488 (1:250, ThermoFisher, Fair Lawn, NJ) was then used against TNNI for visualization. Nuclei were identified after NucBlue Fixed Cell ReadyProbes staining, similarly as described above. Neutrophil density was determined via myeloperoxidase (MPO) staining. After antigen retrieval for 1 hr at 95 °C (Vector Labs, San Francisco, CA), hearts were subject to MPO (15 ug/ml, R&D Systems, Minneapolis, MN) O/N at 4°C. Donkey anti-Goat ReadyProbes Secondary Antibody Alexa Fluor 555 (1:250, ThermoFisher, Fair Lawn, NJ) was then used against MPO for visualization. Nuclei were determined after staining with NucBlue Fixed Cell ReadyProbes as described above. All

slides subject to immunofluorescence were preserved with 1-2 drops of ProLong Gold Antifade Mountant (ThermoFisher, Fair Lawn, NJ).

To determine fibrosis and infarct size, heart sections were stained with Masson's trichrome (Sigma-Aldrich, St. Louis, MO). Here, sections were kept in Bouins fluid O/N at RT. After thorough washing, sections were then incubated in Hematoxylin-Eosin, followed by Biebrich Scarlet-Acid Fuchsin for 5 mins, with washing in between. Tissue slides were then transferred to phosphotungstic-phosphomolybdic acid, and stained with Aniline Blue. Additional tissue sections were stained with Harris modified Hematoxylin-Eosin to determine cell and tissue morphology (Sigma-Aldrich, St. Louis, MO). Immunohistochemistry slides were preserved with 1-2 drops of Permount Mounting Media (ThermoFisher, Fair Lawn, NJ).

Stained heart slides were then analyzed with microscopy, using the Nikon Eclipse NiE or TiE microscope at the necessary magnification (x) 0.8, 1, 20 or 40. The Nikon NIS-Elements software was required to record and analyze images. Cell size was identified after tracing and averaging the area of 80-100 cardiomyocytes over 8-10 individual images from each LV. The density of capillaries was estimated as lectin positive capillaries over tissue area in 8-10 individual images from each LV. Cell death was determined to be the number of TUNEL, NucBlue, TNNI, triple positive cells over the total number of NucBlue, TNNI double positive cells in 8-10 images in the infarct zone and remaining area of each LV. MPO positive neutrophils were determined as MPO/DAPI double positive cells in 8-10 images over the infarct zone and remote area. To determine infarct lengths after injury, the average percent of collagen scar length was taken as a percentage over total LV length in 3 images of each LV.

## 2.5 Primary Cell Isolation & Staining for Flow Cytometry

Cells were isolated from multiple organs from each mouse for analysis. Cells isolated from the heart, spleen, bone marrow, and blood were subject to flow cytometry. In the heart, non-cardiomyocyte cells were enriched after both manual and enzymatic digestion. After PBS infusion, hearts were cut into 1 mm<sup>3</sup> pieces and placed into Roswell Park Memorial Institute 1640 Media (RPMI) (Cellgro Corning, Corning, NY) containing 450 U collagenase II (Worthington Biochemical Lakewood, NJ), and 60 U hyaluronidase (Sigma-Aldrich, St. Louis, MO) for every ml. About 7 mls of this digestion buffer was used for every 120 mg of tissue. After 1 hr in a rocking 37°C water bath, cell suspensions were collected and strained through a 40-µm strainer (Greiner Bio-One, Monroe, NC) primed with PBS. Red blood cells (RBCs) were then lysed at 37°C for 5 min with Ammonium Chloride Potassium (ACK) Lysis Buffer (ThermoFisher, Fair Lawn, NJ), washed, and separated at 1000 rpm for 5 min at 4°C. Cells were then counted using Trypan Blue Solution (ThermoFisher, Fair Lawn, NJ) to check viability.

Spleens were carefully excised out, rinsed in PBS, and digested manually through mashing with syringes and rinsing over 40-µm strainers. Spleen leukocytes were then pelleted at 1000 rpm for 5 min at 4°C. Similarly, RBCs were lysed as described above, and the remaining cell pellet was separated and counted as described above. To isolate bone marrow leukocytes, femur and tibia bones were cleared of all skin and muscle, and flushed with Hanks Buffered Salt Solution (HBSS) using a 27 G needle (BD, Franklin Lakes, NJ). Bone marrow pellets were then resuspended into single cell suspensions (18 G needle, BD, Franklin Lakes, NJ), and leukocytes were spun at 1000 rpm for 5 min at 4°C. RBCs were again lysed as described above, and the remaining cell pellet was

washed and counted as described above. To collect blood, syringes were coated with heparin, and after snipping the aorta, blood was collected and placed in a tube containing 10% 0.5 M EDTA. Here, RBCs were lysed with 10X blood volume using the protocol described above, and the remaining cell pellet was separated and counted as described above.

For flow cytometry analysis, at least  $1.0 \times 10^6$  live cells were stained in FACs buffer (10% fetal bovine serum (FBS, Gemini Bio-Products) in PBS) with the addition of a mixture of antibodies for 1 hr at 4°C or 15 min at RT. If intracellular staining was necessary, cells were treated for 20 min at 4°C with a fixation/permeabilization buffer (Cytofix/Cytoperm Fixation/ Permeabilization Kit, BD, Franklin Lakes, NJ). All antibodies are listed in Table 3. For each experiment, there was an unstained control of each mouse/organ, and single-color compensations using Ultracomp eBeads (ThermoFisher, Fair Lawn, NJ) and ArC Amine Reactive Compensation Bead Kit (ThermoFisher, Fair Lawn, NJ) depending on what was necessary. To determine antibody specificity, cells from the spleen were subject to isotype controls of all fluorophore conjugated antibodies, all listed in Table 4. After staining was complete, data from the cell pellets resuspended in PBS were acquired on an LSRII flow cytometer and analyzed using FlowJo software (Tree Star Inc.). Cell populations were generally regarded as a percent of the total number of leukocytes, unless specified.

## **2.6 Isolation of Cardiac Cluster of Differentiation (CD)11b Cells**

Non-cardiomyocyte cells were isolated from roughly 500-700 mg of combined heart tissue (here, 3-6 hearts were combined for each replicate) as described above. After counting with trypan blue, cells were placed in chilled, sterile PBS, and purified with

**Table 3.** Conjugated Antibodies for Flow Cytometry

| <i>Antibody</i>  | <i>Fluorophore</i> | <i>Manufacture</i>       | <i>Concentration</i> |
|------------------|--------------------|--------------------------|----------------------|
| <i>CD45</i>      | BUV395             | BD, Franklin Lakes, NJ   | 1:100                |
| <i>Ly6G</i>      | BV421              | BD, Franklin Lakes, NJ   | 1:100                |
| <i>CD117</i>     | APC-H7             | BD, Franklin Lakes, NJ   | 1:50                 |
| <i>CD11b</i>     | BV650              | BD, Franklin Lakes, NJ   | 1:50                 |
| <i>CD68</i>      | PE                 | BioLegend, San Diego, CA | 1:100                |
| <i>Ly6C</i>      | PE-Cy7             | BioLegend, San Diego, CA | 1:500                |
| <i>TIM4</i>      | PE-Cy7             | BioLegend, San Diego, CA | 1:30                 |
| <i>CCR2</i>      | FITC               | BioLegend, San Diego, CA | 1:100                |
| <i>CD64</i>      | AlexaFluor647      | BioLegend, San Diego, CA | 1:100                |
| <i>MHC-II</i>    | PE                 | BioLegend, San Diego, CA | 1:100                |
| <i>F4/80</i>     | AlexaFluor647      | Invitrogen, Carlsbad, CA | 1:100                |
| <i>LIVE/DEAD</i> | Aqua               | Invitrogen, Carlsbad, CA | 1:40                 |

**Table 4.** Flow Cytometry Isotype Control Antibodies

| <i>Antibody</i>    | <i>Isotope</i>  | <i>Manufacture</i>          | <i>Concentration</i> |
|--------------------|-----------------|-----------------------------|----------------------|
| <i>rat IgG2b</i>   | BUV395 κ        | BD, Franklin Lakes, NJ      | 1:100                |
| <i>rat IgG2a</i>   | BV421 κ         | BD, Franklin Lakes, NJ      | 1:100                |
| <i>rat IgG2b</i>   | APC-H7 κ        | BD, Franklin Lakes, NJ      | 1:50                 |
| <i>rat IgG2b</i>   | BV650 κ         | BD, Franklin Lakes, NJ      | 1:50                 |
| <i>rat IgG2a</i>   | PE κ            | BD, Franklin Lakes, NJ      | 1:100                |
| <i>rat IgG2c</i>   | PE-Cy7 κ        | BioLegend, San Diego, CA    | 1:500                |
| <i>rat IgG2a</i>   | PE-Cy7 κ        | BD, Franklin Lakes, NJ      | 1:30                 |
| <i>rat IgG2b</i>   | FITC κ          | BD, Franklin Lakes, NJ      | 1:100                |
| <i>mouse IgG1</i>  | AlexaFluor647κ  | BD, Franklin Lakes, NJ      | 1:100                |
| <i>mouse IgG2a</i> | PE κ            | BD, Franklin Lakes, NJ      | 1:100                |
| <i>rat IgG2a</i>   | AlexaFluor647 κ | ThermoFisher, Fair Lawn, NJ | 1:100                |

Debris Removal Solution (Miltenyi Biotec, Auburn, CA) according to manufacture instructions. Debris was thrown out, and the remaining cells underwent RBC lysis as described above. After washing with PBS, the cells were transferred to a degassed, chilled, solution of PBS containing 2% bovine serum albumin (BSA) and 0.5 mM EDTA (isolation buffer). The CD11b Microbead Cocktail (Miltenyi Biotec, Auburn, CA) was then added to cell suspensions, paying attention to manufacture protocols. Here, after 15 min at 4°C, cells were washed with isolation buffer and passed through an MS column in a magnetic separator (Miltenyi Biotec, Auburn, CA). CD11b cells were held in the column, and then carefully pushed out. Cells were counted with trypan blue and used for further applications. Adequate debris removal and CD11b concentration were verified with flow cytometry using CD11b-BV650 (1:100, BD, Franklin Lakes, NJ), CD45-BUV395 (1:100, BD, Franklin Lakes, NJ), and LIVE/DEAD Fixable Aqua Dead Cell Stain Kit (1:40, Invitrogen, Carlsbad, CA).

## **2.7 Whole Transcriptome Analysis**

Immediately following isolation, cardiac CD11b cells from EGFR<sup>mylKO</sup> vs EGFR<sup>f/f</sup> control were subject to RNA isolation and quantification as described above. Total RNA samples were submitted for transcriptomic analysis as a fee-for-service through the Fox Chase Cancer Center (Philadelphia, PA) using the NextSeq2000 platform (Illumina, San Diego, CA). The Bioanalyzer (Agilent Technologies, Santa Clara, CA), and Qubit (Invitrogen, Carlsbad, CA) were first used to identify RNA quality, and verify concentrations. Then, 200 ng of samples with RNA integrity number (RIN) over 8 were used for the mRNA library, which required the NEBNext Ultra II Directional RNA Library Prep Kit, Nextseq 2000 R2 100 cycle reagent (Illumina, San

Diego, CA). Here, mRNAs were enriched two times using the poly-T based RNA purification beads, and were then fragmented at 94°C (8 min) by the divalent cation methodology. 1<sup>st</sup> strand cDNA was synthesized with SuperscriptII and random primers at 42°C (15 min), followed by 2<sup>nd</sup> strand synthesis at 16°C (60 min). In 2<sup>nd</sup> strand synthesis, dUTP was used to replace dTTP to quench the 2<sup>nd</sup> strand during amplification. A nucleotide ('A') was then added to the 3' ends of the blunt fragments at 37°C (30 min), then both adapters with illuminaP5, P7 sequences, and indices were ligated to the cDNA fragment at 30°C (10 min). Samples were then subject to AMPure bead purification (Beckman Coulter, Pasadena, CA), and subject to PCR to enrich fragments, with conditions of 15 cycles at 98°C (10 sec), at 60°C (30 sec), and 72°C (30 sec). After additional purification using AMPure beads, libraries were assessed for quality and quantity with the bioanalyzer and Qubit. Libraries were then pooled and added to the sequencer. Single end reads at 65bp were generated prior to bioinformatics analyses using the Cufflink software (Trapnell Lab) at the Illumina server. Genes with absolute value  $\log_2[\text{fold change}] > 1.5$  and a false discovery rate (FDR)  $< 0.05$  were identified as significantly differentially expressed between the two groups. To analyze the data set, functional annotation, networks, and upstream regulator analyses were performed in the Ingenuity Pathway Analysis software (Ingenuity Systems, Redwood City, CA).

## **2.8 Antibody Array Analysis**

Using a custom c-series mouse protein array kit (RayBiotech, Peachtree Corners, GA), samples were lysed in a proprietary lysis buffer reagent supplemented with 1X HALT protease inhibitor cocktail (ThermoFisher, Fair Lawn, NJ). After maximum speed centrifugation, sample supernatants were collected and assayed for protein concentration

using the Pierce 660 nm Protein Assay Reagent (ThermoFisher, Fair Lawn, NJ). Normalized protein concentrations were diluted in kit supplied blocking buffer, and were applied to membranes with capture antibodies of interest (IGF1, IGF2, Igfbp1, 2, 3, 5, 6, 7). After sample incubation, the kit provided biotinylated antibody cocktail was applied, followed by streptavidin labeling. The chemiluminescence signals were then recorded using an iBright 1500 Imaging System (Invitrogen, Carlsbad, CA). Densitometry was then used to quantify protein using kit supported software (RayBiotech, Peachtree Corners, GA).

## **2.9 Neonatal Rat Ventricular Myocyte (NRVM) Isolation**

Primary neonatal rat ventricular myocytes (NRVM) were isolated from 1 day old Sprague Dawley rat pups (Harlan Laboratories, Indianapolis, IN). Hearts were excised and placed in sterile ADS solution (116 mM NaCl, 20 mM HEPES, 80 mM Na<sub>2</sub>HPO<sub>4</sub>, 56 mM glucose, 5.4 mM KCl, 80 mM MgSO<sub>4</sub>; pH 7.4). Hearts were cleaned of blood and connective tissue, and were then minced for enzymatic digestion. 10-12 hearts were combined and processed 4-5 times in a total of 70 mls of digestion buffer (ADS supplemented with 17640 U collagenase II (Worthington Biochemical Lakewood, NJ), and 42 mg pancreatin (Sigma-Aldrich, St. Louis, MO)). Cells were collected and plated to allow fibroblasts to adhere. 2 hours later, NRVM were collected and plated in HAMs F-10 Nutrient Mixture (ThermoFisher, Fair Lawn, NJ) with the addition of 10% horse serum, 5% FBS, and 1% penicillin/streptomycin/amphotericin B (PSF) (Gemini Bio-Products). Cells were kept at 37°C in a humidified incubator with 5% CO<sub>2</sub>. Where appropriate, NRVM were then kept in HAMs F-10 growth medium without serum or FBS.

## **2.10 Isolation and Culture of Bone Marrow Derived Macrophages**

Bone marrow derived mf (BMDM) came from tibia and femur leukocytes that were isolated as described above, except here, using sterile tools and conditions. Isolated and strained cells were subsequently resuspended in RPMI that had 10% FBS, 1% penicillin/streptomycin/amphotericin B (PSF, Gemini Bio-Products), and 20% conditioned media from a culture of L929 fibroblasts (BMDM media) (Weischenfeldt et al., 2008). Cells were plated under sterile conditions, and mononuclear phagocytes were given time to adhere in a humidified atmosphere of 5% CO<sub>2</sub> at 37°C. Adherent monocytes were then cultured for a total of 5 days, and on day 3, BMDM media was refreshed. For culturing, 1 ml of media was added for every 1.0 x 10<sup>6</sup> cells. Based on experimental needs, leukocytes were initially seeded at a density of 3.0 x 10<sup>6</sup> in 6 well dishes, 6.0 x 10<sup>6</sup> in 60 mm dishes, or 10.0 x 10<sup>6</sup> in 100 mm dishes. Mf were confirmed by flow cytometric analysis of F4/80 expression.

## **2.11 L-cell clone 929 Culture**

L929 fibroblast cells were kept in culture in Minimum Essential Medium (MEM, Cellgro Corning, Corning NY) with the addition of 10% FBS and 1% PSF. Cells were grown in a humidified atmosphere of 5% CO<sub>2</sub> at 37 °C. L929 cells were seeded using a density of 5.0 x 10<sup>6</sup> cells in a T175 cell culture flask, and allowed to grow until they reached 75% confluency (20 x 10<sup>6</sup>). At confluency, media was taken off the cells and next sterile filtered to be used for deriving mf from bones.

## **2.12 Bone Marrow Derived Macrophage Polarization**

On day 6, BMDMs grown in 6 well dishes or 60/100 mm cell culture plates were washed with PBS that was warmed. Cells were then placed in BMDM media with the

addition of 10 ng/ml of recombinant IL-4 (BioLegend, San Diego, CA) distributed in 0.5% BSA in PBS. BMDMs were cultured in IL-4 for 0-24 hours to induce polarization (Hardbower et al., 2017). Specific time points will be highlighted in figure legends. Polarized mf were confirmed by expression of CD206, and Arginase 1 (Viola et al, 2019; Ying et al., 2013).

### **2.13 Conditioned Media Assays**

BMDM were isolated and cultured as described above. To collect naïve, unpolarized BMDM conditioned media, on day 6, control BMDM cultures were placed in 5% FBS, and 1% PSF supplemented RPMI, and kept for 48 hours. After which, media was collected and stored at -20 °C for future use (24296981 – Engstrom et al., 2014; 27507810 – Zhao et al., 2016). To culture NRVMs with conditioned media, Day 2 NRVM were placed in HAMs F-10 free of serum for 24 hours. After which, NRVM were then incubated with conditioned media vehicle, or conditioned media from control BMDM conditioned media for 2 hours (Evdokimova et al., 2012).

### **2.14 Protein Extraction and Immunoblot Analysis**

Heart tissue or cells in culture were perfused/washed with PBS and flash frozen in liquid nitrogen and -80°C. Both heart tissue, and/or cells were lysed in RIPA buffer (1 M Tris pH 7.4, 10% NP-40, 10% sodium deoxycholate, 1 M sodium chloride, 0.5 M EDTA pH 8, 0.5 M sodium fluoride) with 1X HALT protease inhibitor cocktail (ThermoFisher, Fair Lawn, NJ) and phosphatase inhibitor cocktail set IV (Calbiochem, San Diego, CA). Protein concentrations were quantified as described above. Normalized concentrations (30 - 100 µg) of sample lysates were subjected to SDS-polyacrylamide gel electrophoresis (8-10% gels), and transferred onto Immobilon-PSQ polyvinylidene

fluoride 0.2  $\mu\text{m}$  pore membranes (Millipore, Burlington, MA). To limit non-specific binding, membranes were placed in blocking buffer (Rockland, Pottstown, PA), and then subjected to antibodies of interest. All primary antibodies used are provided in Table 5. After washing western blot membranes with TBS-T, they were subjected to secondary antibody at RT for 1 hr in the dark (1:15000, IRDye680 Donkey anti-rabbit IgG, or IRDye800 Goat anti-mouse IgG (LI-COR Biosciences, Lincoln, NE). Membranes were then visualized on the LI-COR Biosciences Odyssey System. Protein levels were quantified using automated densitometry in the ImageStudio software.

**Table 5.** Immunoblot Primary Antibodies

| <i>Antibody</i>           | <i>Manufacture</i>                       | <i>Concentration</i> |
|---------------------------|--|----------------------|
| <i>EGFR</i>               | Cell Signaling Technologies, Danvers, MA | 1:1000               |
| <i>STAT3</i>              | Cell Signaling Technologies, Danvers, MA | 1:1000               |
| <i>pSTAT3 Y705</i>        | Cell Signaling Technologies, Danvers, MA | 1:500                |
| <i>AKT</i>                | Cell Signaling Technologies, Danvers, MA | 1:1000               |
| <i>pAKT S473</i>          | Cell Signaling Technologies, Danvers, MA | 1:1000               |
| <i>ERK1/2</i>             | Cell Signaling Technologies, Danvers, MA | 1:1000               |
| <i>pERK 1/2 T202/Y204</i> | Cell Signaling Technologies, Danvers, MA | 1:1000               |
| <i>B Actin</i>            | Cell Signaling Technologies, Danvers, MA | 1:1000               |
| <i>B Tubulin</i>          | Cell Signaling Technologies, Danvers, MA | 1:1000               |
| <i>GAPDH</i>              | Cell Signaling Technologies, Danvers, MA | 1:1000               |

## 2.15 Mouse Model of Non-Reperfused Myocardial Infarction

Myocardial infarction was surgically induced in mice, after they were anesthetized with 2% isoflurane inhalation (Gao et al., 2010). In detail, a small incision into the skin (1.2 cm) was made over the left chest, followed by a purse suture, allowing the pectoral muscles to be exposed, dissected, and retracted. The 4<sup>th</sup> intercostal space was then apparent, and a tiny hole was made in order to gently free the heart out. Once the left

main descending coronary artery (LCA) was identified, it was sutured and ligated about 3 mm from its start using a 6-0 silk suture. After ligation, the heart was returned into the intra-thoracic space, and the chest was closed back up. Sham operated mice received similar treatment, except here, the LCA was left not occluded.

### **2.16 Echocardiography**

The VisualSonic Vevo 2100 Imaging System (FUJIFILM, Toronto, ON) was used to track cardiac function in EGFRmylKO and control mice. Mouse hair was removed from the chest with Nair prior to echocardiograms. All mice were sedated with 2-3% isoflurane (Patterson Veterinary, Greeley, CO) which allowed the heart rate (HR) to be maintained at 450 – 550 beats per minute (bpm). To capture echocardiograms, long and short axis orientation images of the LV were taken in B and M mode using the MS400 (30-MHz centerline frequency) probe. Parameters of cardiac function and structure were measured using M mode images. These included the diastolic and systolic internal diameters of the LV (ID d, s), as well as the posterior and anterior LV wall thickness (PW, AW d,s), and volumes (V d,s). The stroke volume (SV) was calculated as the difference between diastolic and systolic end volumes. Additionally, ejection fraction (EF) was calculated as 100 times the SV/Vd. Fractional shortening (FS) was achieved by taking the percentage of the difference in internal diameters between diastole and systole, over the diastolic diameter. Additionally, the cardiac output (CO) was calculated as the SV multiplied by HR.

### **2.17 Mitochondrial Bioenergetics Analysis**

Naïve and polarized BMDM were subject to analysis of oxygen consumption rate using the Mito Stress Test Kit (Seahorse Biosciences, North Billerica, MA) according to

manufacturer's instructions. BMDM were first detached from cell culture plates using Accutase (Millipore, Burlington, MA). They were then seeded at  $1.5 \times 10^5$  cells in an XF96 extracellular flux analyzer 96-well plate with XF media pH 7.4 supplemented with 10 mM glucose and 1 mM sodium pyruvate. Cells were loaded into the analyzer, and basal OCR was measured. Following this,  $1\mu\text{g/ml}$  of oligomycin was injected to inhibit the ATP-linked respiration. Next,  $1\mu\text{M}$  of FCCP was injected to measure maximal respiration. Lastly,  $1/20\mu\text{M}$  of rotenone/antimycin A was injected to inhibit all mitochondrial respiration. All data was analyzed using the Wave software.

## **2.18 Statistical Analysis**

All statistical analysis was carried out using GraphPad Prism 8.4.0 software (GraphPad Software Inc., San Diego, CA). All data graphs were created after plotting the mean  $\pm$  standard error of the mean (SEM) from at least 3 individual samples per group. Statistical comparisons were made by using two-tailed unpaired t tests for two groups, and ordinary one-way ANOVA with Tukey's multiple comparisons for 3 or more groups at a single time point. Two-way ANOVA with Bonferroni's multiple comparisons test was for when comparing two or more groups during time course experiments. All differences were considered significant at  $P < 0.05$ .

## CHAPTER 3

### MYELOID SPECIFIC EGFR REGULATES CARDIAC HOMEOSTASIS AND PROTECTS THE INFARCTED HEART DURING REPAIR

#### 3.1 Myeloid-Cell Specific EGFR Knockout Mice Show Significantly Reduced EGFR Expression in Cardiac Myeloid Cells and Bone Marrow Derived Macrophages

To investigate how mf EGFR contributes to cardiac physiology and HF development, we generated a mouse model of mf-specific EGFR deletion using LysM Cre-mediated recombination. In this model, the cre recombinase is inserted in the first coding ATG of *Lyz2*; this results in the loss of endogenous *Lyz2* expression and function, for the replacement of cre (Clausen et al., 1999). The LysM Cre transgene then allows for genetic deletion in cells of myelomonocytic origin, specifically in monocytes, macrophages and granulocytes (Abram et al., 2014; Shi et al., 2019). This is because *Lyz2* expression is not unique to mf, though, as discussed in chapter 1.4.5, this is a common limitation in all myeloid and mf targeting cre systems (Abram et al., 2014; Shi et al., 2019).

Homozygous LysM Cre transgenic mice were crossbred with mice expressing loxP-flanked alleles of EGFR (Figure 7). We first confirmed mf derivation from BM mon; about 90% of BMDM were double positive for CD11b and F4/80, indicating successful differentiation (Figure 8a) (Ma et al., 2018). Using BMDM, we then checked for, and observed a significant induction of Cre in EGFRmylKO and LysM Cre in comparison to EGFR<sup>f/f</sup> controls (Figure 8b). We then assayed BMDM for EGFR gene expression and protein level to confirm successful deletion. EGFRmylKO BMDM exhibited about 80-90% reduction in *Egfr* transcript level when compared to EGFR<sup>f/f</sup>

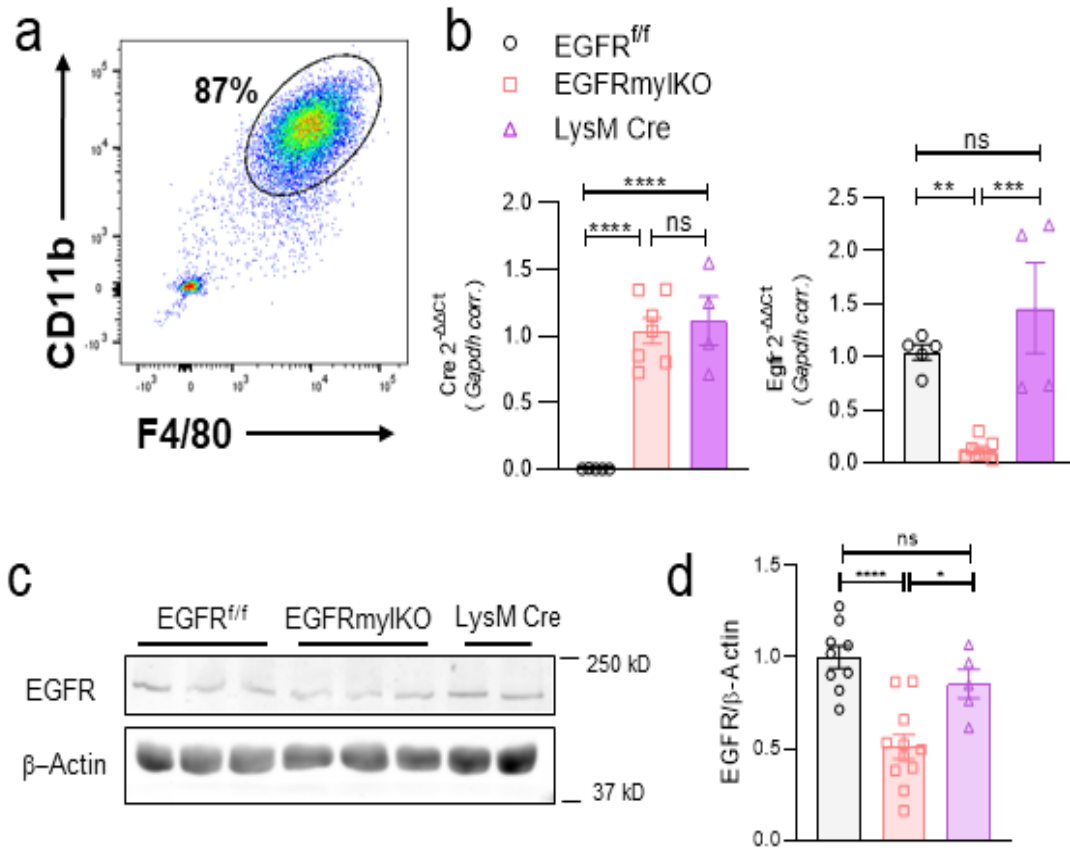


**Figure 8. Myeloid-Cell Specific EGFR Deletion Results in Significant Reduction in EGFR Gene Expression and Protein Level in Bone Marrow Derived Mf (BMDM).**  
 a) BMDM were subject to flow cytometry to verify mf derivation using CD11b, and F4/80. b) RT-qPCR was used to measure *Cre* expression and *Egfr* expression in bmdm from EGFRmylKO, versus EGFR<sup>fl/fl</sup> and LysM Cre controls, normalized to Gapdh. N = 4-11, represented in histogram by individual bullets. \*\*P<0.01, \*\*\*P<0.001, ns, not significant using one-way ANOVA with Tukey's multiple comparisons test. c) Representative immunoblot showing EGFR and β-Actin protein in bmdm from EGFRmylKO, EGFR<sup>fl/fl</sup>, and LysM Cre controls. d) EGFR expression normalized to β-Actin. N = 4-11, represented in histogram by individual bullets. \*P<0.05, \*\*\*\*P<0.0001, ns not significant using one-way ANOVA with Tukey's multiple comparisons test.

control, and was even further reduced when compared to LysM Cre transgenic controls (Figure 8b). Immunoblot analyses of protein levels of the receptor revealed that in BMDM, EGFR is significantly reduced by about 50 - 60% (Figure 8c-d).

Due to the divergent and complex ontogeny of cardiac mf, we wondered if LysM Cre mediated recombination would similarly lead to a significant reduction in EGFR in cardiac myeloid cells (Williams et al., 2018). Recently, however, the use of a LysM specific fluorescent reporter revealed LysM tracing and targeting of almost 90% of cardiac mf (Nicolas-Avila et al., 2020). To verify *Lyz2* and *Egfr* expression, we isolated cardiac non-myocyte cells, and concentrated Cd11b expressing myeloid cells. We assessed mf density, finding on average, the cell isolates contained about 85 - 90% CD45/CD11b/CD64 triple positive mf (Figure 9a). In EGFR<sup>f/f</sup> control animals, cardiac CD11b isolates expressed *Lyz2* and *Egfr* (Figure 9b-c). LysM Cre transgenics and EGFRmylKO showed no expression of *Lyz2* (Figure 9b-c). However, only EGFRmylKO exhibited a significant reduction in *Egfr* gene expression (Figure 9b-c).

The EGFR signaling network relies on the formation of not only receptor homodimers, but also heterodimers with other ErbB receptors to initiate major canonical pathways (Holbro et al., 2004). Other ErbB family members have been shown to be expressed in CD11b myeloid cells, so we wondered if the reduction in EGFR would result in compensatory changes in other ErbB family receptors (Yin et al., 2021). In BMDM, though EGFRmylKO had significantly reduced EGFR gene expression and protein level, ErbB 2 and ErbB3 gene expression were not significantly altered (Figure 10a). ErbB 4 was not detected in BMDM from either group (Figure 10a). We next assessed the activation of canonical pathways downstream of EGFR to understand how

its deletion impacted growth factor signaling. We subject BMDM from EGFRmylKO and controls to immunoblot analyses, finding no significant changes in ERK1/2, or AKT phosphorylation when normalized to total protein (Figure 11a-b). Together, these findings indicate successful generation of myeloid EGFR knockout, with major EGFR signaling partners remaining intact.

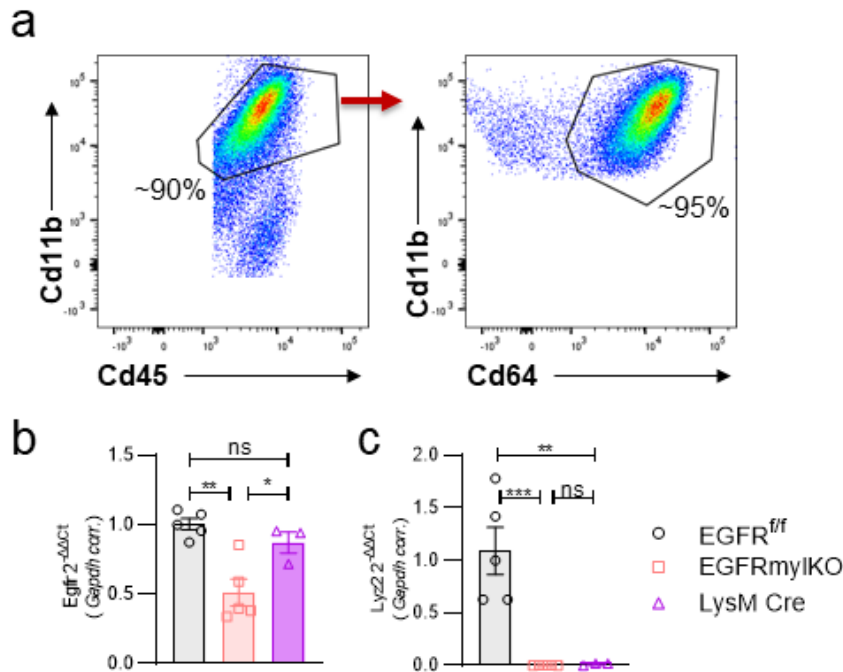


**Figure 9. Myeloid-Cell Specific EGFR Deletion Results in Significant Reduction in EGFR Gene Expression in Cardiac Myeloid Cells.** a) Cardiac non-myocytes were subject to CD11b cell column isolation. CD11b<sup>+</sup> cells were subject to flow cytometry to verify and estimate cardiac mf concentration in isolates from EGFR<sup>fl/fl</sup> versus EGFRmylKO hearts using CD45, CD11b, and CD64. b) RT-qPCR was used to measure *Egfr* and c) *Lyz 2* expression in cardiac CD11b<sup>+</sup> non-myocyte cells from EGFRmylKO, versus EGFR<sup>fl/fl</sup> and LysM Cre controls, normalized to *Gapdh*. N = 3-5, represented in histogram by individual bullets. \*P<0.05, \*\*P<0.01, \*\*\*P<0.001, ns, not significant using one-way ANOVA with Tukey's multiple comparisons test.

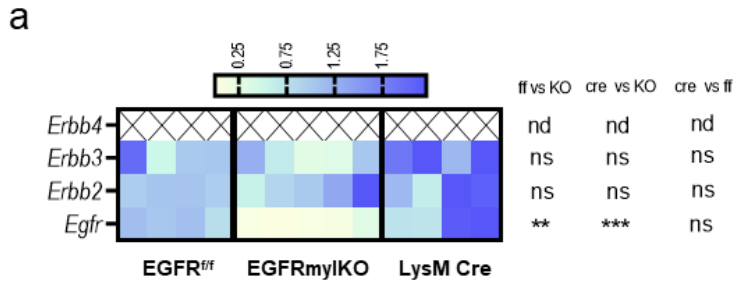


**Figure 10. Myeloid-Cell Specific EGFR Deletion does not Result in Compensatory Changes in the ErbB2-4 Family.** a) RT-qPCR was used to measure *Egfr* and *ErbB 2 - 4* in bmdm from EGFRmylKO, versus EGFR<sup>fl/fl</sup> and LysM Cre controls, normalized to *Gapdh*. nd = not detected. N = 4-5, represented in heatmap by individual boxes. \*\*P<0.01, \*\*\*P<0.001, ns, not significant using one-way ANOVA with Tukey's multiple comparisons test.

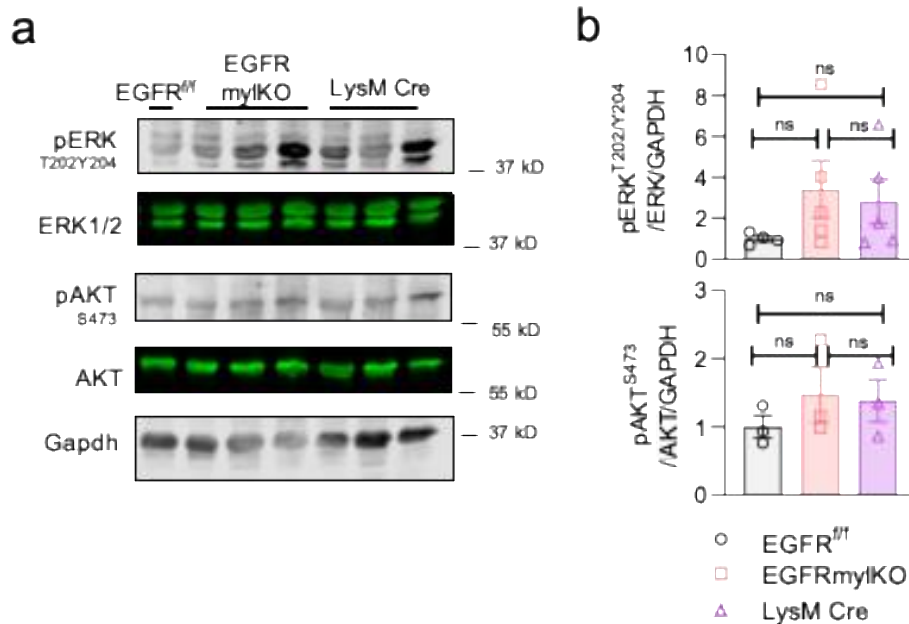


**Figure 11. Myeloid-Cell Specific EGFR Deletion does not Alter Canonical EGFR Signaling.** a) Representative immunoblot showing levels of total ERK 1/2, pERK 1/2 at threonine 202/tyrosine 204, total AKT, pAKT at serine 473, and  $\beta$ -Actin in bmdmf from EGFRmylKO, EGFR<sup>fl/fl</sup>, and LysM Cre controls. b) Total and phospho protein levels normalized to  $\beta$ -Actin. N = 3-5, represented in histogram by individual bullets. ns not significant using one-way ANOVA with Tukey's multiple comparisons test.

### 3.2 Myeloid-Cell Specific EGFR Maintains Cardiac Homeostasis During Normal Physiology

Since cardiac mf can regulate cardiac development, homeostasis, and physiology, and EGFR activity and function has been shown to be important for cardiac integrity, we sought to determine whether myeloid EGFR deletion would result in any phenotypic alterations during normal physiology (Barrick et al., 2009; Lavine et al., 2018). We assessed global cardiac morphology with WGA and H&E, finding a significant increase in cm cell area in EGFRmylKO hearts relative to controls (Figure 12a-b). This increase in cell size did not lead to significant changes in heart tissue weight when normalized to body weight (Figure 12c). Further assessment of H&E stained hearts at 1 or 10X revealed that EGFRmylKO had no other gross morphological changes or cellular changes (Figure 12d).

We next wondered if the increase in cm size was accompanied with any fetal, fibrotic, or inflammatory gene changes, reminiscent of myocardial stress. We observed in EGFRmylKO hearts, relative to either control, elevated transcripts of *Acta1*, *Nppb*, and *Myh7* (Figure 13a). Neither *Tnf* or *Il1b* were significantly upregulated in EGFRmylKO hearts compared to controls (Figure 13b). Interestingly, we observed elevated transcripts of *Colla1*, especially in comparison to LysM Cre controls (Figure 13b). Cardiac function is tightly coupled to cardiac structure, and hypertrophy can be associated with either preserved or altered cardiac function (Nakamura et al., 2018). Thus, we assessed whether elevated fetal gene transcripts and cm area were accompanied by changes in cardiac contractile function. We performed serial echocardiographic assessment of EGFRmylKO and control animals monthly from 3 to 8 months of age. Representative m-mode

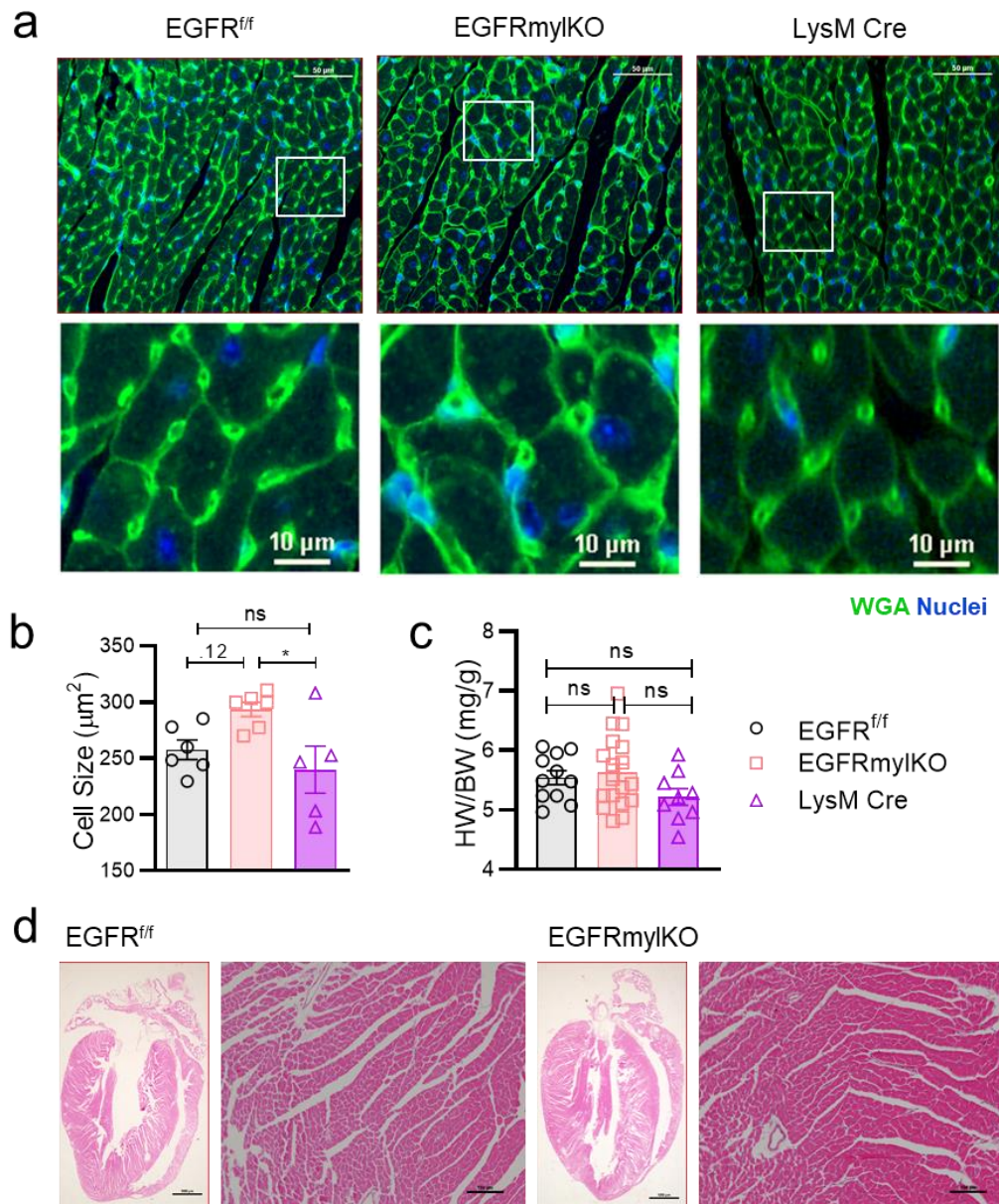


**Figure 12. Myeloid-Cell Specific EGFR Deletion Results in Increased Cardiomyocyte Size in the Left Ventricle, with No Change in Total Tissue Weight.**

a) Cardiomyocyte size was assessed in LVs of 12-16-week-old EGFR<sup>mylKO</sup> and control mice after WGA staining. Panels shown are representative regions of interest (ROI) from 20X magnification of the LV from each group, scale bar denotes 50 (upper) 10 (lower) μm. b) Quantification of cardiomyocyte size is shown in the histogram. N = 5-6, represented by individual bullets in the histogram. \*P<0.05, ns not significant, one-way ANOVA with Tukey's multiple comparisons test. c) Heart weights were normalized to body weights in 12-16 week old EGFR<sup>mylKO</sup> and control mice. ns not significant, one-way ANOVA with Tukey's multiple comparisons test. d) Panels shown are representative regions of interest from 1 (left) and 10 (right) X magnification H & E images of the LV from EGFR<sup>mylKO</sup> and EGFR<sup>f/f</sup> control. Scale bar denotes 1000 (left) 100 (right) μm.

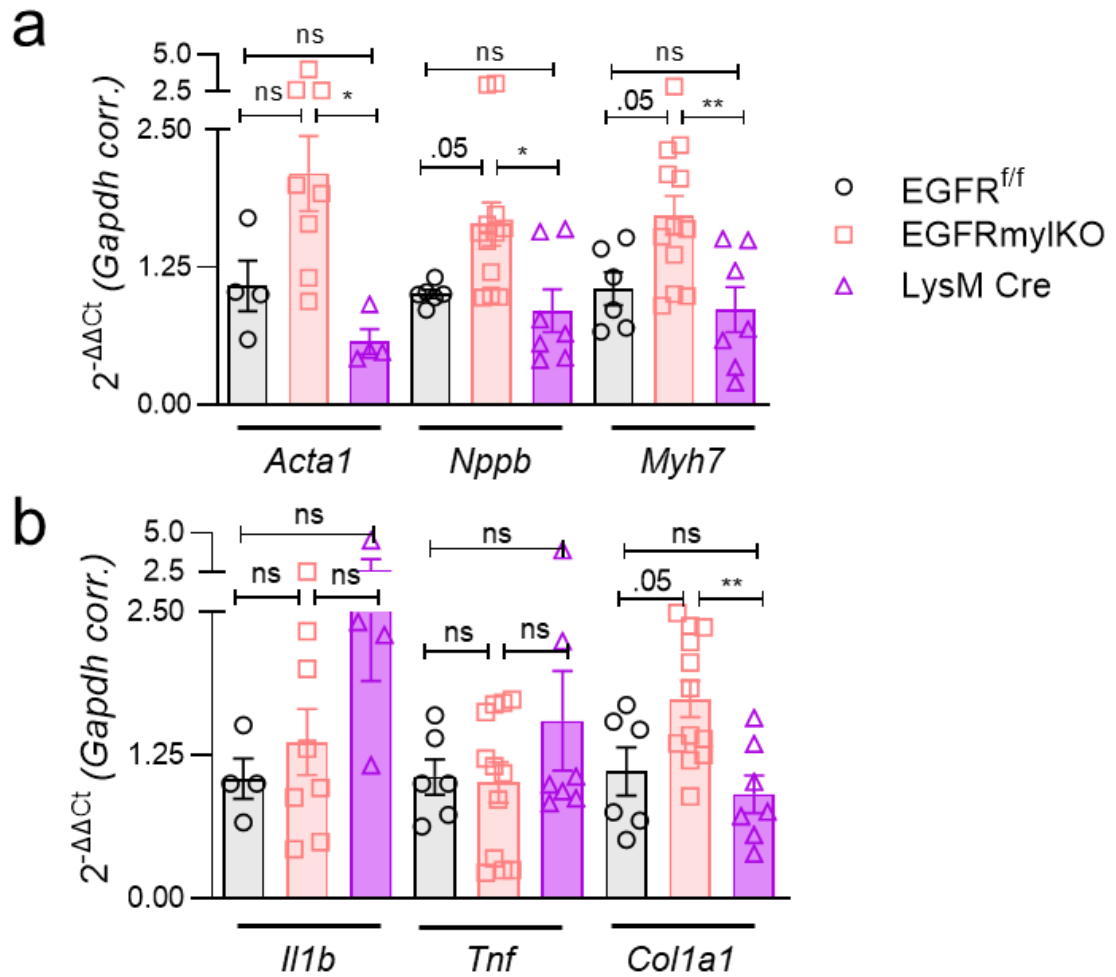


**Figure 13. Myeloid-Cell Specific EGFR Deletion Leads to Elevated Levels of Fetal Gene Transcripts in the Left Ventricle.** RT-qPCR was used to measure the expression of a) *Acta1*, *Nppb*, and *Myh7* and b) *Il1b*, *Tnf*, and *Col1a1*, in left ventricles (LV) of 12-16-week-old EGFRmylKO mice and controls, normalized to *Gapdh*. N = 4-12, represented by individual bullets in histogram. \*P<0.05, \*\*P<0.01, ns, not significant using one-way ANOVA with Tukey's multiple comparisons test.

echocardiograms revealed cardiac function and morphology (Figure 14a). Over this 6 month course, cardiac functional parameters in control mice did not significantly change, consistent with previous findings (Figure 14A-B) (Bai et al., 2019). Similarly, in EGFRmylKO animals, we observed preserved cardiac function in hearts over this timecourse (Figure 14a-b). Table 6 details all echocardiography parameters from the studied mice. Altogether, these findings may suggest a minor role for myeloid EGFR in preserving cardiac homeostasis, specifically through its regulation of cm structural integrity and fetal gene expression.

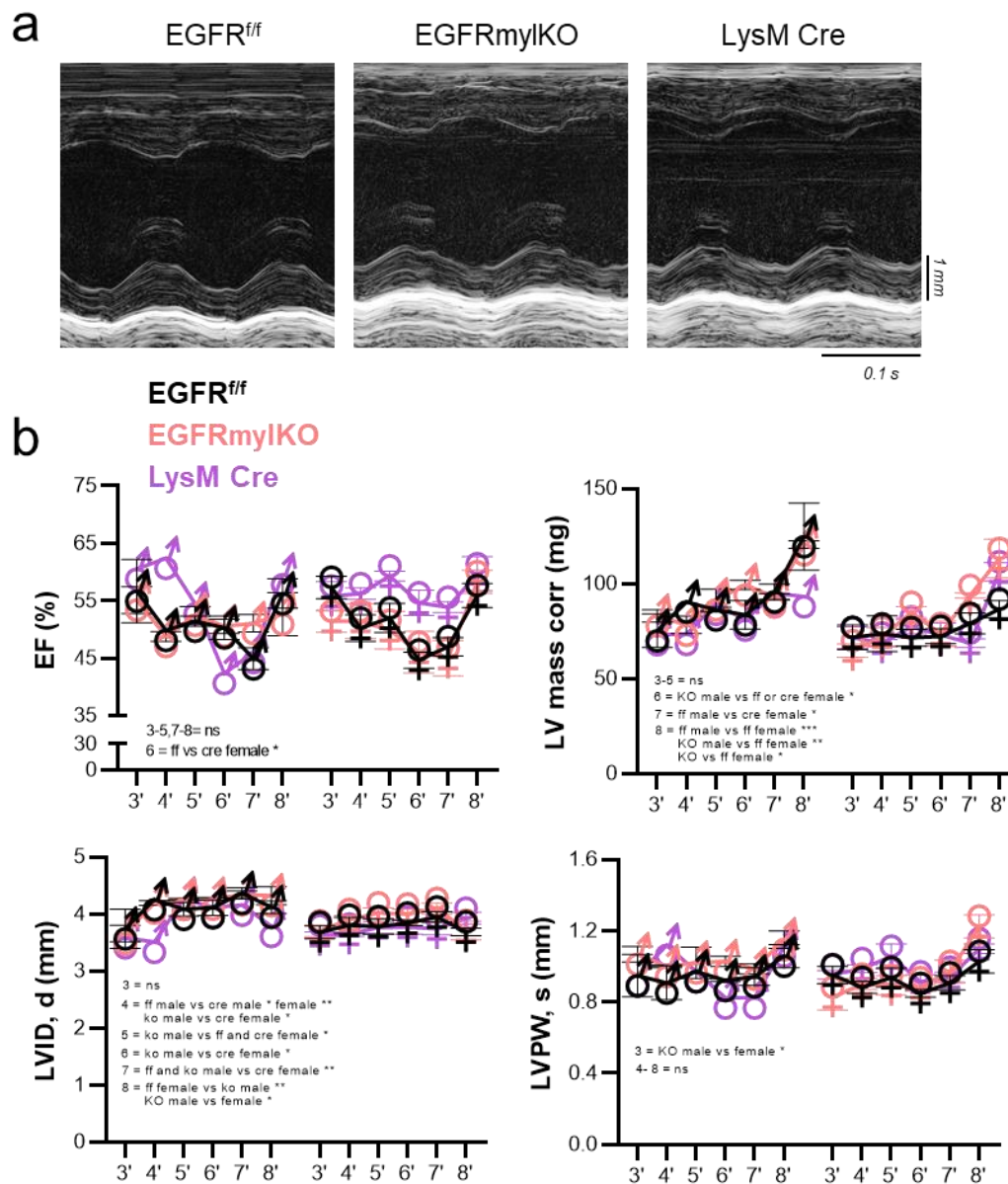


**Figure 14. Myeloid-Cell Specific EGFR Deletion does not Result in Altered Cardiac Function During Normal Adulthood.** a) Representative m-mode echocardiograms of EGFRmylKO and control hearts at 12 weeks of age. Upper scale depicts 1 mm. Bottom scale depicts 0.1 seconds. b) EF, LVIDd, LVPWs, and LV mass corr of EGFRmylKO and control mice were analyzed monthly after echo at 3 - 8 months of age (x axis) using the VisualSonics Vevo software N = 5-8 per group. Left symbols male, right symbols female. \*P<0.05, \*\*P<0.01, \*\*\*P<0.001 ns, not significant, with two-way ANOVA with Bonferonni's multiple comparisons test.

**Table 6.** All Echocardiographic Parameters for Aged Mice

| 3 MONTH        | <b>Egfr f/f</b> |               |             |               | <b>EGFRmylKO</b> |               |             |               | <b>Lys M Cre</b> |               |             |               |
|----------------|-----------------|---------------|-------------|---------------|------------------|---------------|-------------|---------------|------------------|---------------|-------------|---------------|
|                | MALE            |               | FEMALE      |               | MALE             |               | FEMALE      |               | MALE             |               | FEMALE      |               |
|                | AVG             | SEM           | AVG         | SEM           | AVG              | SEM           | AVG         | SEM           | AVG              | SEM           | AVG         | SEM           |
| HR             | 450.54          | 14.22         | 435.71      | 7.14          | 474.87           | 10.48         | 480.98      | 5.71          | 451.54           | 26.78         | 475.65      | 2.29          |
| Vol s          | 28.55           | 4.94          | 24.29       | 1.74          | 26.43            | 1.19          | 30.12       | 1.28          | 25.22            | 1.78          | 26.90       | 0.76          |
| Vol d          | 62.60           | 7.50          | 55.93       | 2.80          | 58.25            | 1.83          | 65.05       | 1.93          | 61.83            | 3.05          | 60.84       | 0.31          |
| SV             | 34.05           | 2.56          | 31.64       | 1.11          | 31.82            | 0.85          | 34.92       | 0.95          | 36.62            | 1.27          | 33.93       | 0.83          |
| EF             | 56.70           | 3.16          | 57.34       | 0.88          | 54.77            | 0.84          | 54.08       | 1.10          | 59.27            | 0.90          | 55.83       | 1.26          |
| FS             | 29.40           | 2.05          | 29.51       | 0.54          | 27.88            | 0.53          | 27.54       | 0.68          | 30.91            | 0.55          | 28.66       | 0.85          |
| CO             | 15.12           | 0.73          | 13.76       | 0.50          | 15.11            | 0.54          | 16.33       | 0.38          | 16.45            | 0.42          | 16.13       | 0.35          |
| LV Mass        | 94.14           | 6.39          | 89.69       | 3.66          | 102.84           | 1.53          | 107.38      | 2.53          | 91.57            | 0.07          | 89.49       | 3.55          |
| LV Mass Cor    | 75.31           | 5.11          | 71.76       | 2.93          | 82.27            | 1.22          | 85.90       | 2.03          | 73.26            | 0.06          | 71.59       | 2.84          |
| LVID;d         | 3.74            | 0.20          | 3.68        | 0.05          | 3.62             | 0.05          | 3.76        | 0.06          | 3.72             | 0.09          | 3.63        | 0.03          |
| LVID;s         | 2.83            | 0.22          | 2.72        | 0.07          | 2.69             | 0.04          | 2.86        | 0.09          | 2.73             | 0.11          | 2.68        | 0.07          |
| LVPW;d         | 0.75            | 0.05          | 0.76        | 0.02          | 0.81             | 0.03          | 0.84        | 0.02          | 0.80             | 0.00          | 0.74        | 0.02          |
| LVPW;s         | 0.95            | 0.07          | 0.95        | 0.02          | 1.07             | 0.02          | 1.07        | 0.04          | 0.95             | 0.00          | 0.95        | 0.01          |
| <b>4 MONTH</b> | <b>MALE</b>     | <b>FEMALE</b> | <b>MALE</b> | <b>FEMALE</b> | <b>MALE</b>      | <b>FEMALE</b> | <b>MALE</b> | <b>FEMALE</b> | <b>MALE</b>      | <b>FEMALE</b> | <b>MALE</b> | <b>FEMALE</b> |
|                | AVG             | SEM           | AVG         | SEM           | AVG              | SEM           | AVG         | SEM           | AVG              | SEM           | AVG         | SEM           |
| HR             | 462.41          | 7.53          | 457.68      | 6.67          | 444.61           | 11.29         | 456.23      | 10.72         | 465.82           | 21.91         | 488.40      | 3.59          |
| Vol s          | 44.77           | 1.57          | 34.70       | 2.23          | 43.49            | 2.05          | 43.09       | 2.27          | 17.93            | 1.09          | 27.10       | 0.57          |
| Vol d          | 89.36           | 2.10          | 68.93       | 3.17          | 81.48            | 2.33          | 81.76       | 2.10          | 49.68            | 1.42          | 61.96       | 1.02          |
| SV             | 44.58           | 1.34          | 34.23       | 1.14          | 37.99            | 0.56          | 38.67       | 0.38          | 31.75            | 0.33          | 34.86       | 0.64          |
| EF             | 49.91           | 1.19          | 50.26       | 1.03          | 46.91            | 1.00          | 47.50       | 1.74          | 63.95            | 1.09          | 56.27       | 0.50          |
| FS             | 25.21           | 0.72          | 25.21       | 0.61          | 23.30            | 0.57          | 23.64       | 1.06          | 34.00            | 0.77          | 28.89       | 0.33          |
| CO             | 20.62           | 0.63          | 15.64       | 0.54          | 16.97            | 0.67          | 17.30       | 0.49          | 14.77            | 0.54          | 17.02       | 0.35          |
| LV Mass        | 112.98          | 5.26          | 92.02       | 5.27          | 100.20           | 2.30          | 108.01      | 3.70          | 90.74            | 0.68          | 86.03       | 1.10          |
| LV Mass Cor    | 90.38           | 4.21          | 73.62       | 4.22          | 80.16            | 1.84          | 86.41       | 2.96          | 72.59            | 0.54          | 68.82       | 0.88          |
| LVID;d         | 4.25            | 0.06          | 3.80        | 0.06          | 4.27             | 0.04          | 4.20        | 0.04          | 3.52             | 0.01          | 3.65        | 0.02          |
| LVID;s         | 3.36            | 0.04          | 2.97        | 0.07          | 3.34             | 0.07          | 3.27        | 0.08          | 2.33             | 0.04          | 2.78        | 0.02          |
| LVPW;d         | 0.73            | 0.05          | 0.73        | 0.02          | 0.71             | 0.01          | 0.77        | 0.04          | 0.80             | 0.04          | 0.81        | 0.03          |
| LVPW;s         | 0.91            | 0.05          | 0.88        | 0.02          | 0.98             | 0.01          | 0.99        | 0.02          | 1.11             | 0.01          | 0.99        | 0.01          |
| <b>5 MONTH</b> | <b>MALE</b>     | <b>FEMALE</b> | <b>MALE</b> | <b>FEMALE</b> | <b>MALE</b>      | <b>FEMALE</b> | <b>MALE</b> | <b>FEMALE</b> | <b>MALE</b>      | <b>FEMALE</b> | <b>MALE</b> | <b>FEMALE</b> |
|                | AVG             | SEM           | AVG         | SEM           | AVG              | SEM           | AVG         | SEM           | AVG              | SEM           | AVG         | SEM           |
| HR             | 450.67          | 3.45          | 470.31      | 6.67          | 477.56           | 7.36          | 493.39      | 14.07         | 457.73           | 11.85         | 475.55      | 8.55          |
| Vol s          | 38.53           | 0.40          | 32.56       | 1.92          | 41.17            | 1.09          | 42.83       | 2.41          | 34.69            | 2.43          | 26.46       | 0.82          |
| Vol d          | 79.32           | 0.89          | 66.85       | 2.36          | 86.57            | 1.17          | 86.17       | 2.32          | 78.79            | 3.59          | 65.14       | 2.01          |
| SV             | 40.79           | 0.73          | 34.29       | 0.51          | 45.40            | 0.16          | 43.34       | 0.85          | 44.10            | 1.15          | 38.68       | 1.27          |
| EF             | 51.46           | 0.50          | 52.02       | 1.14          | 52.51            | 0.65          | 50.31       | 1.88          | 56.07            | 1.09          | 59.33       | 0.42          |
| FS             | 26.01           | 0.32          | 26.30       | 0.68          | 26.78            | 0.40          | 25.44       | 1.13          | 28.98            | 0.69          | 31.02       | 0.30          |
| CO             | 18.38           | 0.22          | 16.11       | 0.28          | 21.68            | 0.27          | 20.33       | 0.46          | 20.16            | 0.01          | 18.35       | 0.61          |
| LV Mass        | 107.91          | 0.87          | 89.42       | 2.46          | 114.54           | 2.97          | 113.25      | 2.12          | 115.83           | 3.07          | 96.62       | 2.32          |
| LV Mass Cor    | 86.33           | 0.69          | 71.54       | 1.97          | 91.63            | 2.38          | 90.60       | 1.69          | 92.67            | 2.45          | 77.30       | 1.86          |
| LVID;d         | 4.08            | 0.07          | 3.78        | 0.06          | 4.26             | 0.01          | 4.25        | 0.05          | 4.11             | 0.11          | 3.76        | 0.05          |
| LVID;s         | 3.41            | 0.04          | 3.02        | 0.07          | 3.34             | 0.06          | 3.39        | 0.11          | 3.12             | 0.10          | 2.68        | 0.03          |
| LVPW;d         | 0.81            | 0.04          | 0.74        | 0.02          | 0.80             | 0.01          | 0.78        | 0.01          | 0.79             | 0.08          | 0.78        | 0.01          |
| LVPW;s         | 0.97            | 0.02          | 0.94        | 0.02          | 1.02             | 0.04          | 0.99        | 0.03          | 1.05             | 0.05          | 1.06        | 0.04          |
| <b>6 MONTH</b> | <b>MALE</b>     | <b>FEMALE</b> | <b>MALE</b> | <b>FEMALE</b> | <b>MALE</b>      | <b>FEMALE</b> | <b>MALE</b> | <b>FEMALE</b> | <b>MALE</b>      | <b>FEMALE</b> | <b>MALE</b> | <b>FEMALE</b> |
|                | AVG             | SEM           | AVG         | SEM           | AVG              | SEM           | AVG         | SEM           | AVG              | SEM           | AVG         | SEM           |
| HR             | 504.91          | 15.25         | 474.15      | 5.85          | 540.34           | 7.31          | 473.06      | 9.60          | 507.05           | 5.98          | 503.37      | 7.01          |
| Vol s          | 38.34           | 1.17          | 37.49       | 0.46          | 41.03            | 1.29          | 40.69       | 2.57          | 45.09            | 1.37          | 30.00       | 2.08          |
| Vol d          | 77.70           | 4.01          | 67.82       | 0.11          | 82.87            | 2.00          | 79.14       | 1.97          | 79.97            | 1.23          | 65.43       | 3.27          |
| SV             | 39.37           | 2.85          | 30.34       | 0.41          | 41.84            | 0.86          | 38.45       | 0.63          | 34.88            | 0.14          | 35.43       | 1.26          |
| EF             | 50.31           | 1.17          | 44.70       | 0.63          | 50.57            | 0.53          | 48.33       | 2.09          | 43.64            | 0.85          | 54.68       | 1.10          |
| FS             | 25.33           | 0.76          | 21.85       | 0.37          | 25.52            | 0.31          | 24.16       | 1.23          | 21.34            | 0.49          | 27.94       | 0.69          |
| CO             | 19.78           | 1.42          | 14.42       | 0.35          | 22.58            | 0.44          | 20.30       | 0.61          | 17.68            | 0.14          | 17.73       | 0.38          |
| LV Mass        | 104.51          | 5.43          | 90.41       | 2.22          | 124.12           | 1.30          | 120.12      | 4.67          | 103.71           | 1.83          | 91.44       | 3.79          |
| LV Mass Cor    | 83.61           | 4.34          | 72.33       | 1.77          | 99.30            | 1.04          | 96.10       | 3.74          | 82.97            | 1.46          | 73.15       | 3.03          |
| LVID;d         | 4.11            | 0.08          | 3.84        | 0.02          | 4.27             | 0.01          | 4.19        | 0.05          | 4.04             | 0.05          | 3.77        | 0.06          |
| LVID;s         | 3.21            | 0.04          | 3.15        | 0.02          | 3.32             | 0.01          | 3.28        | 0.08          | 3.41             | 0.04          | 2.84        | 0.06          |
| LVPW;d         | 0.76            | 0.04          | 0.68        | 0.02          | 0.78             | 0.02          | 0.79        | 0.03          | 0.75             | 0.02          | 0.70        | 0.02          |

|                |             |            |               |            |             |            |               |            |             |            |               |            |
|----------------|-------------|------------|---------------|------------|-------------|------------|---------------|------------|-------------|------------|---------------|------------|
| LVPW;s         | 0.92        | 0.00       | 0.85          | 0.01       | 1.03        | 0.01       | 1.00          | 0.01       | 0.84        | 0.01       | 0.91          | 0.02       |
| <b>7 MONTH</b> | <b>MALE</b> |            | <b>FEMALE</b> |            | <b>MALE</b> |            | <b>FEMALE</b> |            | <b>MALE</b> |            | <b>FEMALE</b> |            |
|                | <b>AVG</b>  | <b>SEM</b> | <b>AVG</b>    | <b>SEM</b> | <b>AVG</b>  | <b>SEM</b> | <b>AVG</b>    | <b>SEM</b> | <b>AVG</b>  | <b>SEM</b> | <b>AVG</b>    | <b>SEM</b> |
| HR             | 451.53      | 3.54       | 486.47        | 2.31       | 501.70      | 3.18       | 469.63        | 5.31       | 507.28      | 0.00       | 503.49        | 3.96       |
| Vol s          | 49.62       | 2.53       | 36.45         | 2.01       | 42.85       | 0.28       | 45.68         | 3.04       | 43.26       | 0.00       | 29.69         | 1.10       |
| Vol d          | 90.06       | 3.69       | 68.28         | 2.88       | 87.82       | 1.05       | 88.93         | 3.02       | 80.19       | 0.00       | 64.27         | 1.90       |
| SV             | 40.44       | 1.69       | 31.84         | 1.01       | 44.97       | 1.07       | 43.25         | 0.66       | 36.93       | 0.00       | 34.58         | 0.83       |
| EF             | 44.96       | 1.11       | 47.03         | 0.72       | 51.11       | 0.66       | 48.66         | 1.78       | 46.06       | 0.00       | 53.90         | 0.46       |
| FS             | 22.22       | 0.66       | 23.20         | 0.41       | 25.92       | 0.42       | 24.47         | 1.02       | 22.74       | 0.00       | 27.39         | 0.28       |
| CO             | 18.29       | 0.90       | 15.48         | 0.48       | 22.59       | 0.67       | 21.68         | 0.47       | 18.73       | 0.00       | 17.38         | 0.29       |
| LV Mass        | 119.67      | 2.95       | 98.82         | 3.07       | 116.44      | 0.84       | 118.06        | 0.92       | 118.69      | 0.00       | 85.88         | 1.39       |
| LV Mass Cor    | 95.73       | 2.36       | 79.05         | 2.46       | 93.15       | 0.67       | 94.45         | 0.74       | 94.95       | 0.00       | 68.70         | 1.11       |
| LVID;d         | 4.36        | 0.06       | 3.95          | 0.04       | 4.34        | 0.03       | 4.32          | 0.06       | 4.16        | 0.00       | 3.74          | 0.05       |
| LVID;s         | 3.48        | 0.11       | 3.15          | 0.05       | 3.27        | 0.02       | 3.34          | 0.11       | 3.44        | 0.00       | 2.83          | 0.05       |
| LVPW;d         | 0.73        | 0.04       | 0.65          | 0.01       | 0.73        | 0.00       | 0.73          | 0.02       | 0.68        | 0.00       | 0.73          | 0.01       |
| LVPW;s         | 0.94        | 0.03       | 0.91          | 0.02       | 0.99        | 0.01       | 0.99          | 0.04       | 0.82        | 0.00       | 0.94          | 0.01       |
| <b>8 MONTH</b> | <b>MALE</b> |            | <b>FEMALE</b> |            | <b>MALE</b> |            | <b>FEMALE</b> |            | <b>MALE</b> |            | <b>FEMALE</b> |            |
|                | <b>AVG</b>  | <b>SEM</b> | <b>AVG</b>    | <b>SEM</b> | <b>AVG</b>  | <b>SEM</b> | <b>AVG</b>    | <b>SEM</b> | <b>AVG</b>  | <b>SEM</b> | <b>AVG</b>    | <b>SEM</b> |
| HR             | 521.26      | 6.63       | 469.08        | 4.23       | 523.95      | 4.21       | 480.11        | 7.51       | 505.70      | 0.00       | 478.65        | 4.35       |
| Vol s          | 36.52       | 0.86       | 28.35         | 0.82       | 43.03       | 1.67       | 37.96         | 1.61       | 27.75       | 0.00       | 28.09         | 1.76       |
| Vol d          | 84.17       | 3.95       | 64.34         | 1.27       | 91.14       | 2.35       | 83.94         | 3.17       | 68.74       | 0.00       | 69.16         | 2.80       |
| SV             | 47.65       | 3.40       | 35.99         | 0.91       | 48.11       | 2.19       | 45.98         | 1.96       | 40.98       | 0.00       | 41.07         | 1.47       |
| EF             | 56.27       | 1.47       | 55.95         | 0.94       | 52.69       | 1.62       | 55.40         | 1.15       | 59.59       | 0.00       | 59.72         | 1.48       |
| FS             | 29.25       | 1.03       | 28.79         | 0.63       | 27.03       | 1.03       | 28.76         | 0.78       | 31.33       | 0.00       | 31.44         | 1.02       |
| CO             | 24.70       | 1.42       | 16.93         | 0.55       | 25.13       | 1.01       | 23.38         | 1.21       | 20.73       | 0.00       | 19.64         | 0.69       |
| LV Mass        | 155.95      | 12.74      | 108.30        | 2.50       | 150.73      | 1.11       | 143.80        | 7.32       | 116.55      | 0.00       | 132.84        | 2.99       |
| LV Mass Cor    | 124.76      | 10.19      | 86.64         | 2.00       | 120.58      | 0.89       | 115.04        | 5.85       | 93.24       | 0.00       | 106.27        | 2.39       |
| LVID;d         | 4.12        | 0.06       | 3.69          | 0.03       | 4.32        | 0.07       | 4.13          | 0.10       | 3.79        | 0.00       | 3.93          | 0.05       |
| LVID;s         | 3.23        | 0.03       | 2.84          | 0.06       | 3.38        | 0.06       | 3.12          | 0.05       | 2.90        | 0.00       | 2.84          | 0.08       |
| LVPW;d         | 0.93        | 0.01       | 0.88          | 0.02       | 0.85        | 0.03       | 0.89          | 0.04       | 0.84        | 0.00       | 0.82          | 0.01       |
| LVPW;s         | 1.06        | 0.04       | 1.03          | 0.03       | 1.15        | 0.02       | 1.17          | 0.04       | 1.11        | 0.00       | 1.10          | 0.01       |

### 3.3 Myeloid-Cell Specific EGFR Deletion Does not Shift Resident Cardiac Macrophage Subsets in the Steady State Heart

Since we observed larger CM areas and stress associated fetal gene transcripts in EGFRmylKO hearts, we wondered how deletion of myeloid specific EGFR resulted in these outcomes. The resting heart contains 4 major mf types, which can be maintained through self renewal, or monocyte replacement (Dick et al., 2019; Dick et al., 2022). As EGFR is a potent regulator of cell survival and proliferation, we wondered if the loss of myeloid expressed EGFR led to a disruption in the normal distribution and maintenance of steady state cardiac mf, ultimately leading to this loss in CM integrity (Wee et al., 2017). We isolated non-CM from heart tissue, and by flow cytometric analyses, quantified levels of steady state immune cells. We stratified cardiac leukocytes for

CD11b and CD64 expression; on average 28-30% of cells were cardiac mf, unchanged in EGFRmylKO hearts (Figure 15a-b) (Zaman et al., 2021; Dick et al., 2019). We then wanted to assess if cardiac mf in EGFRmylKO exhibited a unique distribution. We analyzed mf for their expression of Tim4, MHC-II, and CCR2 to characterize TRM subtypes in basal hearts. MHC-II expression was observed in a large percentage of cardiac mf across all groups (Figure 15c-d). Most MHC-II mf exhibited little to no expression of CCR2, distinguishing them from CCR2+ mf, which were present in the tissue at low densities (Figure 15c). EGFRmylKO hearts exhibited similar levels of CCR2 and MHC-II mf relative to controls (Figure 15c-d). Tim4+ mf were the next most abundant mf type in basal hearts, with no significant changes observed in EGFRmylKO hearts (Figure 15d-e). Analyses of Tim4 vs CCR2 revealed virtually no overlap, confirming their distinct origin; this remained unchanged in EGFRmylKO hearts. The relative distribution of cardiac mf subtypes was further confirmed by gene expression analyses of common TRM markers including *Cx3cr1*, *Tim4*, and *Ccr2*, where no significant differences were observed in EGFRmylKO compared to control (Figure 16a) (Hulsmans et al., 2017). Together, these data suggest that major cardiac mf subsets are maintained even in the absence of myeloid EGFR during normal physiology.

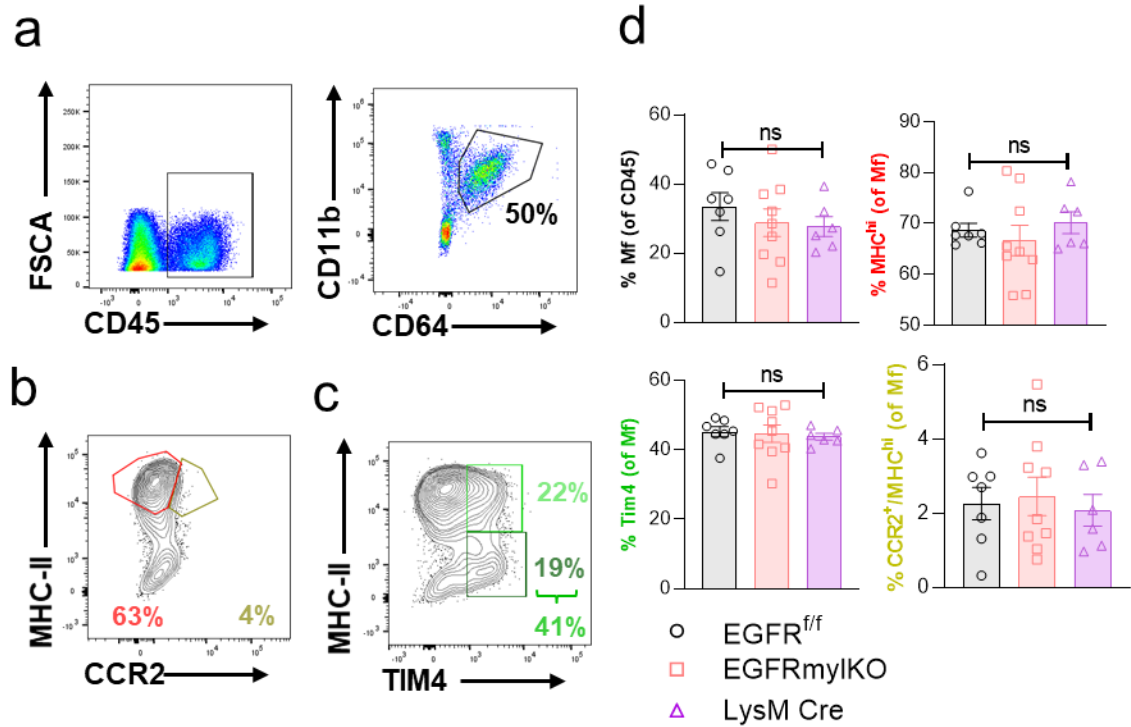


**Figure 15. Myeloid-Cell Specific EGFR Deletion does not Significantly Influence Resident Macrophage Subtypes in the Heart.** a) Panels show representative flow cytometry plots from EGFRmylKO, showing CD45 leukocytes, which were further evaluated for CD11b and CD64 to identify Mf. b) Panels show Mf which were further evaluated for their expression of CCR2 vs MHC-II, c) MHC-II vs TIM4. d) Accompanying histograms detail respective cell percentages. N = 6-9 per group, ns, not significant, with one-way ANOVA with Tukey's multiple comparisons test.

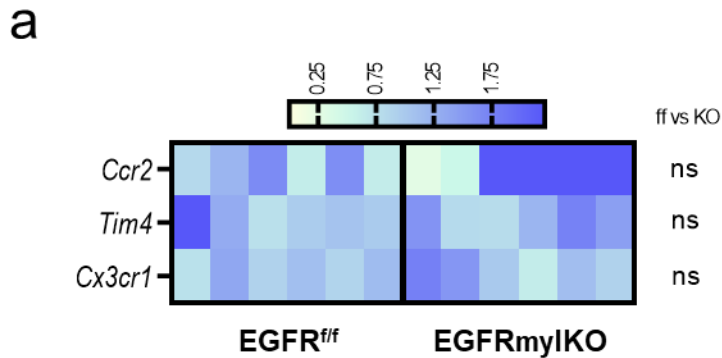


**Figure 16. Cardiac CD11b<sup>+</sup> Cells in EGFR<sup>mylKO</sup> Exhibit Unaltered Transcripts of Resident Macrophage Markers.** a) RT-qPCR was used to measure *Tim4*, *Cx3cr1*, and *Ccr2* in cardiac CD11b<sup>+</sup> non-myocyte cells from EGFR<sup>mylKO</sup>, versus EGFR<sup>ff</sup> controls, normalized to *Gapdh*. N = 6, represented in heatmap by individual boxes. Ns, not significant using students unpaired t-test.

### 3.4 Myeloid-Cell Specific EGFR Deletion Significantly Shapes the Cardiac CD11b<sup>+</sup> Transcriptome in the Steady State Heart

In recent years, TRM have been shown to influence basal cardiac homeostasis through a number of mechanisms (Dick et al., 2019; Hulsmans et al., 2017; Nicolas-Avila et al., 2020). Since EGFR<sup>mylKO</sup> hearts exhibited signs of stress, we sought to investigate global transcriptional changes in EGFR<sup>ff</sup> control and EGFR knockout cardiac myeloid cells. We isolated non-CM and concentrated them by CD11b (Figure 17a). We then subject control and EGFR<sup>mylKO</sup> cardiac CD11b<sup>+</sup> cells to bulk RNA sequencing (RNAseq); after identifying those with a false discovery rate (FDR) of 0.05 or less, and an absolute value log<sub>2</sub> fold change of 1.5 or greater, 763 transcripts were considered differentially expressed. Of these 763 differentially expressed genes, 612 were downregulated, and 151 were upregulated in EGFR<sup>mylKO</sup> cells (Figure 17b). *Lyz2* and *Egfr* were among the top most significantly differentially expressed genes (Figure 17b).

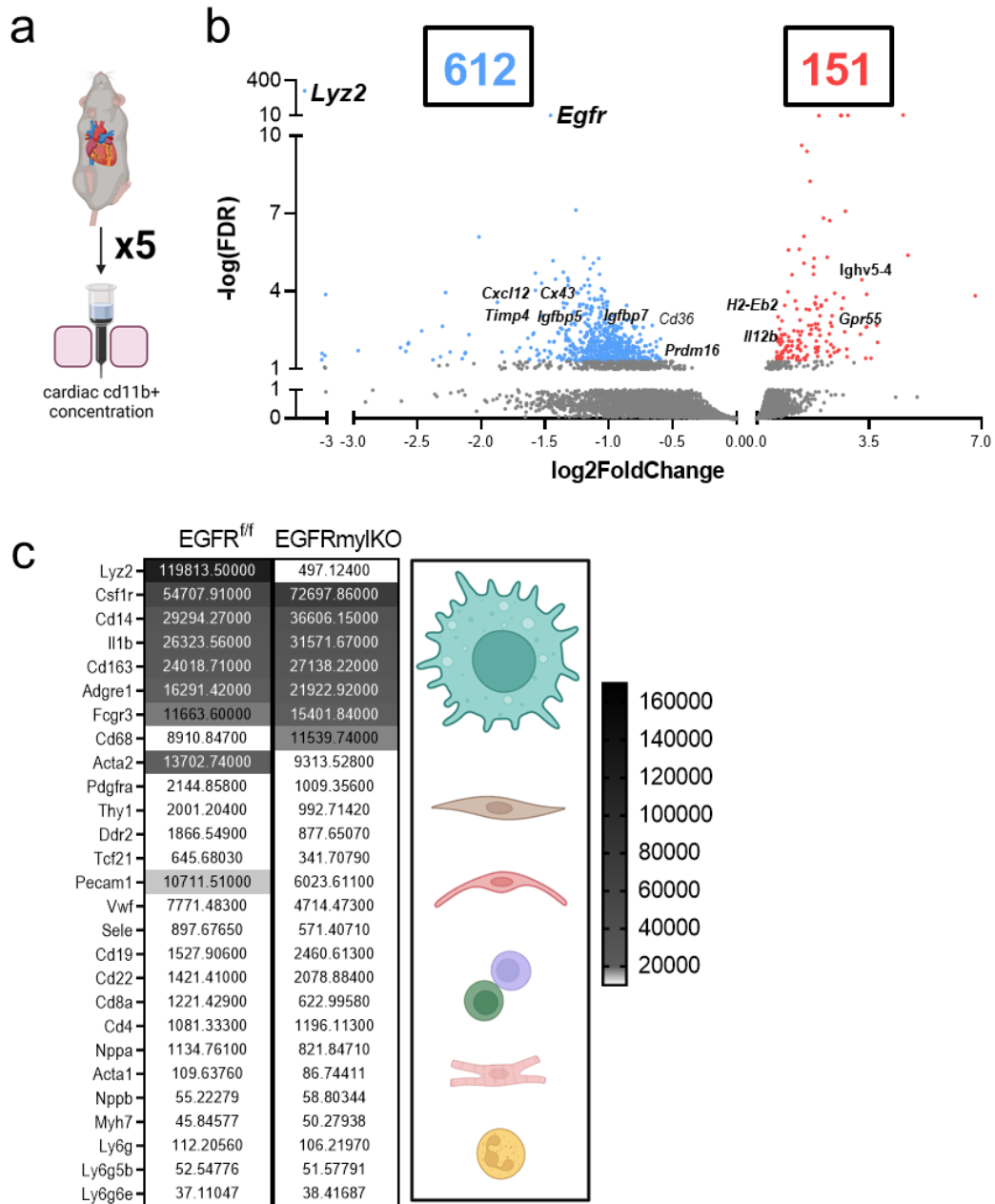


**Figure 17. Cardiac CD11b<sup>+</sup> Cells in EGFR<sup>mylKO</sup> Hearts Show Significant Differential Gene Expression Compared to Control.** a) Schematic depicting experimental setup for whole transcriptome analysis. 5-7 hearts were combined to generate individual biological replicates, with a total N = 3/group. b) Volcano plot of differentially expressed RNA transcripts highlighting the number of genes increased and decreased in expression out of total transcripts analyzed. Transcripts were only considered significantly differentially expressed at cutoffs: fold change absolute value (>1.5) and false discovery rate (< 0.05). Significant transcripts are coded in blue (downregulated) or red (upregulated). c) Average expression of cardiac cell types rank ordered from RNAseq dataset from high to low, mf, CF, endo, lymphocyte, CM, neutrophil. Average transcript expression is listed within graph.

To verify the cell makeup of our RNAseq samples, we rank ordered cardiac cell markers, finding cardiac mf to be enriched in our cell isolates (Figure 17c).

To understand how these differentially expressed transcripts could be linked to changes in cardiac structure and physiology, we first processed the dataset through Ingenuity Pathway Analysis (IPA). IPA grouped significantly differentially expressed genes into known pathways and biological functions (Figure 18a). Interestingly, several genes were clustered in pathways related to “communication between innate and adaptive immune cells” and “IL15 signaling”. Specific targets assigned to these pathways that were differentially altered included T and B cell activating cytokines, complement pathway genes, and immunoglobulin heavy and kappa variable genes many which have predicted roles in antigen binding, activation of complement, activation of the immune response, and phagocytosis (Figure 18b) (Fuchs et al., 2018; Luck et al., 2019).

Beyond IPA, RNAseq results were cross-referenced to previous findings that detail cardiac mf genes involved in homeostasis, and genes identified in resident mf populations. In this regard, we identified reduced expression of *Cx43* in EGFRmylKO cells, which was validated against both control groups (Figure 19a). Cardiac mf *Cx43* has been shown to facilitate mf and cm coupling, and its loss in cardiac mf has been shown to delay AV conduction, resulting in mild abnormalities in either cardiac chambers (Hulsmans et al., 2017). Next, we observed differential expression in *Cd36* and *Fabp4* in EGFRmylKO RNAseq results, both of which have been shown to be uniquely upregulated in resident cardiac mf (Dick et al., 2019). RT-qPCR validation of these targets in additional EGFRmylKO cells revealed significant downregulation in only *Cd36* expression (Figure 19a). Cardiac stress is known to amplify mf subtype and diversify mf

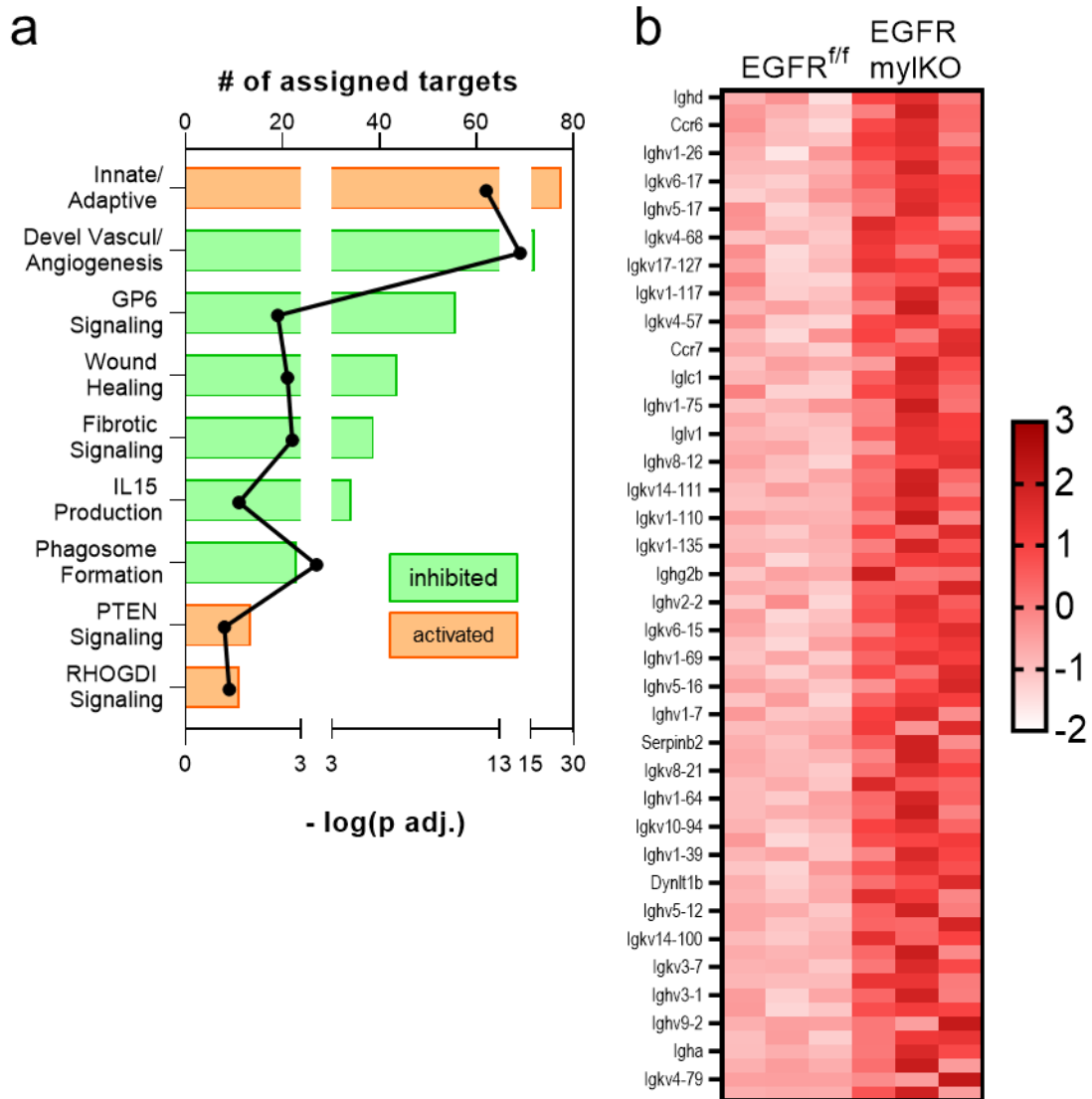


**Figure 18. IPA Revealed Relevant Pathways Altered in Cardiac CD11b<sup>+</sup> Cells in EGFRmylKO Hearts Compared to Control.** a) IPA analysis grouped genes into most inhibited/activated signaling pathways altered in EGFRmylKO versus control. Line graph depicts number of targets assigned to pathway, see upper x axis. Bar graphs depict level of significance, see lower x axis. Inhibited pathways are shown by green bars, activated pathways are shown by orange bars. b) Heat maps detail significant changes in EGFRmylKO, versus EGFR<sup>f/f</sup> CD11b<sup>+</sup> for genes related to “innate/adaptive immunity” and “IL15 signaling”.

gene expression (Dick et al., 2019). We observed elevated transcripts in EGFRmylKO cells shown to be specifically upregulated in cardiac myeloid cells under pathological conditions (Figure 19b) (Dick et al., 2019). Altogether, these findings point to EGFR as a critical regulator of cardiac myeloid gene expression, and hint at elevated levels of stress within hearts deficient in myeloid EGFR.

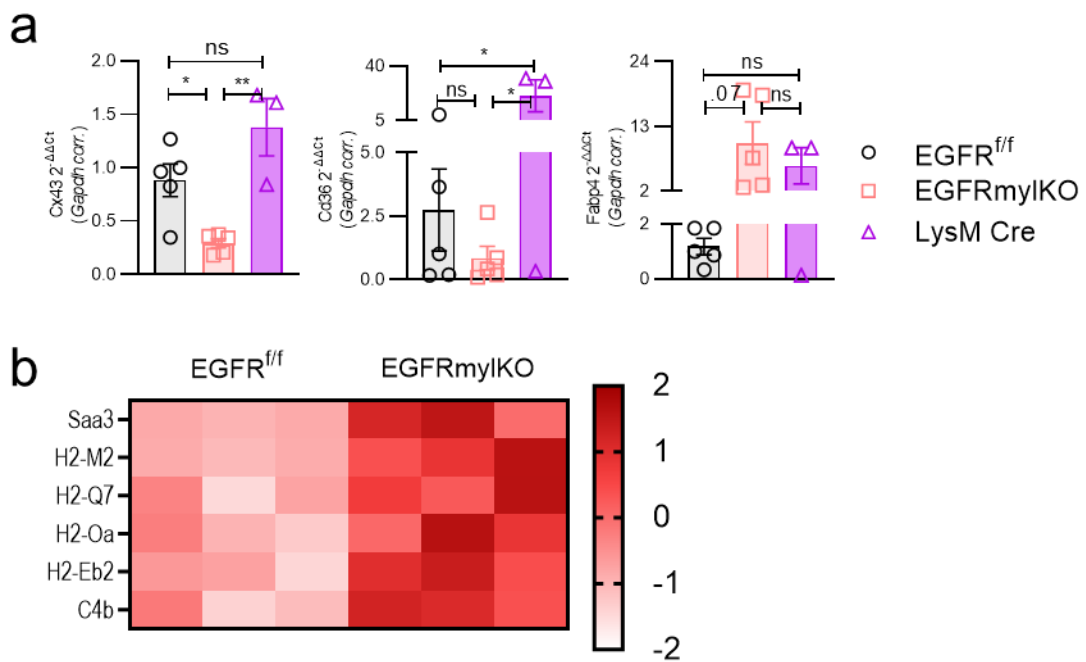


**Figure 19. EGFRmylKO Cardiac CD11b<sup>+</sup> Cells Differentially Express Transcripts Associated with Resident and Injured Mf Subtypes.** a) To validate RNA-seq results, RT-qPCR was used to measure *Cx43*, *Cd36*, *Fabp4*, and *Gapdh* in cardiac CD11b<sup>+</sup> cells from EGFRmylKO, versus EGFR<sup>f/f</sup> and LysM Cre hearts. N = 3-5 per group from 5-7 pooled hearts/replicate, \*\*P<0.01, \*\*\*P<0.001, ns, not significant using one-way ANOVA with Tukey's multiple comparisons test. b) Heat maps detail significant changes in EGFRmylKO, versus EGFR<sup>f/f</sup> CD11b<sup>+</sup> for genes previously identified to be upregulated in cardiac myeloid cells under stress.

### **3.5 Myeloid-Cell Specific EGFR Regulates CD11b<sup>+</sup> IGFBP Expression and is Associated with Elevated Growth Factor Signaling in the Heart**

To understand what differentially expressed genes from the transcriptomics dataset might be directly involved in cardiac hypertrophy, we further considered recent findings linking cardiac resident mf IGF and IGF binding protein (IGFBP) to hypertrophic growth (Zaman et al., 2021; De Ponti et al., 2021; Wong et al., 2021). While we observed no changes in *Igf1* or *Igfbp3, 4* expression, EGFRmylKO cardiac cd11b cells had significantly reduced transcript levels of *Igfbp5* and *Igfbp7* in comparison to EGFR<sup>f/f</sup> controls (Figure 20a-b). Lys M Cre transgenic cells had significantly elevated levels of *Igfbp4* (Figure 20b). EGFRmylKO cells still maintained reduced transcript levels of all *Igfbps* analyzed in comparison to Lys M Cre controls (Figure 20b).

IGFBPs are a family of secreted proteins which regulate cell signaling through a variety of mechanisms (Allard et al., 2018; Ito et al., 1993). IGFBPs are capable of binding, and thus limiting the bioavailability of IGFs (Allard et al., 2018). However, they also bind cell surface receptors like the IGF1 receptor (IGF1R) and TNFR1 (Evdokimova et al., 2012; Hwang et al., 2011). When IGFBPs bind these receptors, they reduce growth factor or cytokine signaling (Evdokimova et al., 2012; Hwang et al., 2011). Thus, we wondered if reduced expression of IGFBP 5 and 7 in EGFRmylKO myeloid cells would result in enhanced growth factor or hypertrophic signaling in hearts. As AKT, and ERK1/2, are downstream of IGF1R and TNFR1, we assessed their activation in hearts from EGFRmylKO and controls (Riedemann et al., 2006; Heineke et al., 2006; Chen et al., 2002). We observed enhanced phosphorylation of ERK in EGFRmylKO LV relative

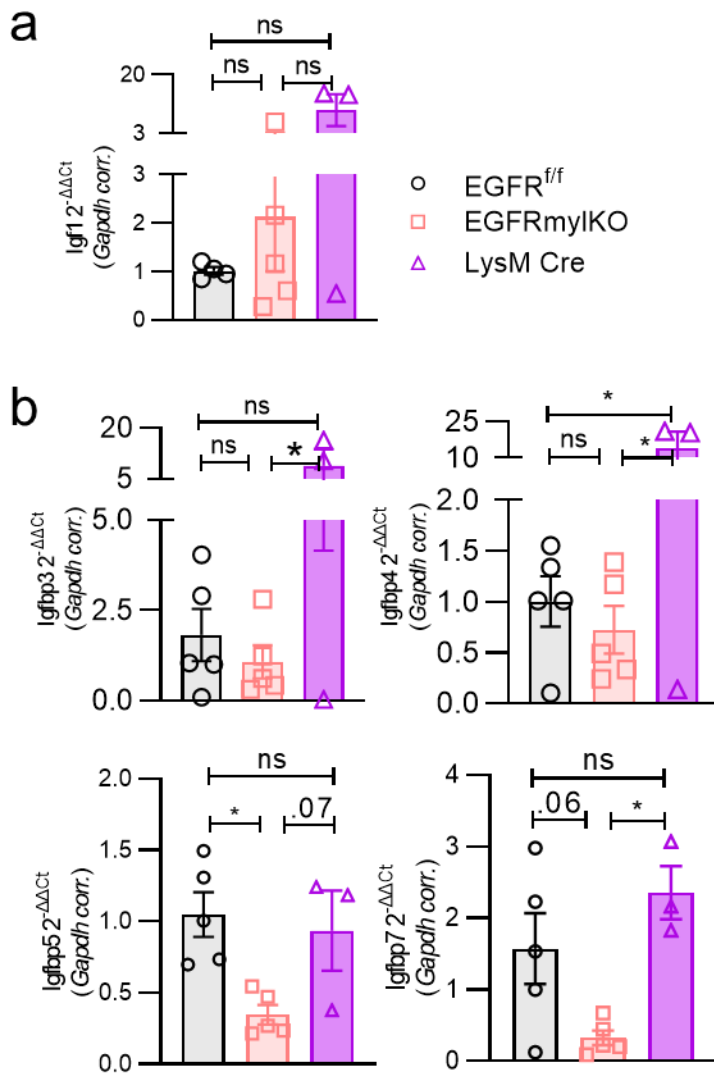


**Figure 20. Cardiac CD11b<sup>+</sup> Cells in EGFRmylKO Hearts Show Differential Expression of Igfbp5/7 Relative to Controls.** a) RT-qPCR was used to measure *Igf1*, b) *Igfbp3*, *Igfbp4*, *Igfbp5*, *Igfbp7* and *Gapdh* in cardiac CD11b<sup>+</sup> cells from EGFRmylKO, versus EGFR<sup>f/f</sup> and LysM Cre hearts. N = 3-5 per group from 5-7 pooled hearts/replicate, \*P<0.05, \*\*P<0.01, ns, not significant using one-way ANOVA with Tukey's multiple comparisons test.

to control, though not AKT (Figure 21a-b). In total, these findings may suggest novel mechanisms through which mf EGFR may contribute to cm homeostasis.

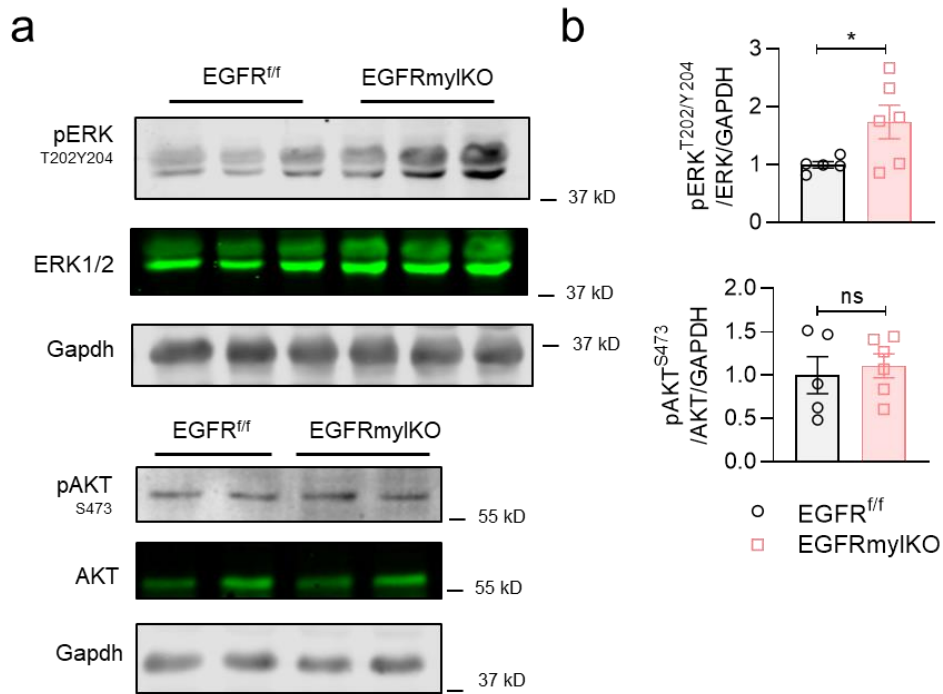


**Figure 21. EGFRmylKO Hearts Exhibit Elevated Growth Factor Receptor Activation Relative to Control.** a) Representative immunoblot showing levels of total AKT, pAKT at serine 473, total ERK 1/2, pERK 1/2 at threonine 202/tyrosine 204, pMEK1/2 at serine 217 221 and Gapdh in total heart lysate from EGFRmylKO, and EGFR<sup>f/f</sup> controls. b) Total and phospho protein levels normalized to loading control. N = 5-6, represented in histogram by individual bullets. \*P<0.05, ns not significant using students unpaired t-test.

### **3.6 Impact of Myeloid-Cell Specific EGFR on Cardiac Structural Integrity During Ageing**

With age, the normal heart experiences cellular and molecular changes, which lead to structural remodeling and decreased cardiac function (Nakou et al., 2016). Additionally, aging hearts also experience elevated inflammation (Hulsmans et al., 2018). In detail, we know that by 18 months of age, hearts experience an expansion in cardiac mf, and enhanced BM hematopoiesis (Hulsmans et al., 2018). Since young EGFRmylKO had alterations in cardiac mf gene expression, coupled with elevated hypertrophy and stress in hearts, we wondered if over time this would further aggravate cardiac aging. To that end, we aged EGFRmylKO and controls to 18 months, where we tracked cardiac function at 10, 12, 15 and 18 months. We assessed body weights at each of these time points. Here, all mice had comparable body weight, when separated by sex (Figure 22a). Representative images of m-mode 2D echocardiography show cardiac function and structure in female mice (Figure 22b). By 15 months, all animals exhibited a significant, though modest decrease in cardiac function, as shown by EF, and FS when compared to their cardiac function at 3 months of age (Figure 22c, Figure 14b). Additionally, by this time point, total LV mass in all groups were elevated (Figure 22a-c). Increased LV mass was also accompanied with increased LV diameters at both systole and diastole (Figure 22c). Echocardiography analyses did not resolve any differences in wall thickness (Figure 22c). There were no significant changes in LV posterior wall thickness during systole across either group (Figure 22c). Table 7 details all echo parameters from aged mice. Altogether, these reports may hint at a role for myeloid expressed EGFR in maintaining cardiac integrity with age.

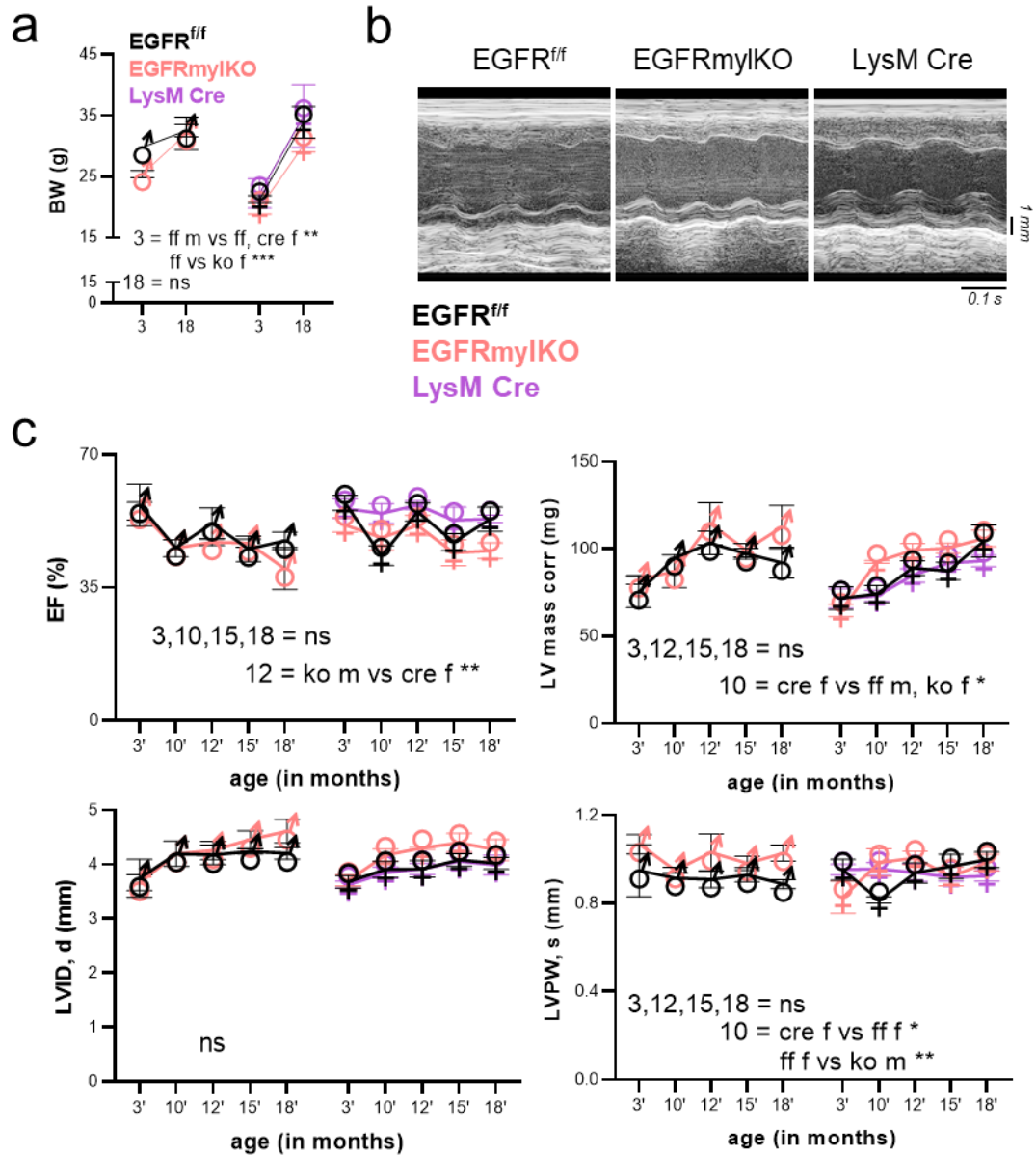


**Figure 22. Impact of Myeloid-Cell Specific on Cardiac Structural Integrity During Ageing.** a) Body weight of male and female EGFRmylKO mice and controls at 3 and 18 months of age (n = 5-8/group) \*\*P<0.01, \*\*\*P<0.001 ns, not significant, with one-way ANOVA with Tukey's multiple comparisons test. b) Representative m-mode echocardiograms EGFRmylKO and control hearts at 18 months of age. c) EF, LVIDd, LVPWs, and LV mass corr of EGFRmylKO and control mice were analyzed after echo using the VisualSonic Vevo software N = 5-8 per group. \*P<0.05, ns, not significant, with two-way ANOVA with Bonferonni's multiple comparisons test.

**Table 7.** 10-15 mo Echo Parameters

| 10 MONTH        | Egfr f/f    |            |               |            | EGFRmylKO   |            |               |            | Lys M Cre   |            |               |            |
|-----------------|-------------|------------|---------------|------------|-------------|------------|---------------|------------|-------------|------------|---------------|------------|
|                 | MALE        |            | FEMALE        |            | MALE        |            | FEMALE        |            | MALE        |            | FEMALE        |            |
|                 | AVG         | SEM        | AVG           | SEM        | AVG         | SEM        | AVG           | SEM        | AVG         | SEM        | AVG           | SEM        |
| HR              | 451.96      | 7.43       | 468.23        | 5.40       | 472.04      | 4.89       | 472.00        | 6.15       | 488.46      | 0.00       | 460.52        | 7.10       |
| Vol s           | 48.41       | 1.91       | 42.01         | 2.47       | 45.96       | 2.66       | 41.57         | 2.91       | 41.71       | 0.00       | 29.74         | 1.30       |
| Vol d           | 88.72       | 3.17       | 73.66         | 3.61       | 83.55       | 3.31       | 79.73         | 2.89       | 87.33       | 0.00       | 65.09         | 1.34       |
| SV              | 40.31       | 1.29       | 31.65         | 1.51       | 37.59       | 0.72       | 38.16         | 0.78       | 45.62       | 0.00       | 35.34         | 0.58       |
| EF              | 45.48       | 0.29       | 43.41         | 1.15       | 45.38       | 0.97       | 48.16         | 1.90       | 52.27       | 0.00       | 54.52         | 1.30       |
| FS              | 22.50       | 0.15       | 21.22         | 0.64       | 22.41       | 0.54       | 24.06         | 1.12       | 26.63       | 0.00       | 27.86         | 0.85       |
| CO              | 18.28       | 0.89       | 14.94         | 0.85       | 17.76       | 0.43       | 18.00         | 0.34       | 22.29       | 0.00       | 16.25         | 0.25       |
| LV Mass         | 118.56      | 2.75       | 92.74         | 2.71       | 108.99      | 5.07       | 115.72        | 0.48       | 88.74       | 0.00       | 91.53         | 1.96       |
| LV Mass Cor     | 94.85       | 2.20       | 74.19         | 2.17       | 87.20       | 4.05       | 92.57         | 0.38       | 70.99       | 0.00       | 73.23         | 1.57       |
| LVID;d          | 4.20        | 0.02       | 3.90          | 0.07       | 4.20        | 0.10       | 4.17          | 0.07       | 4.12        | 0.00       | 3.84          | 0.05       |
| LVID;s          | 3.55        | 0.08       | 3.24          | 0.08       | 3.32        | 0.07       | 3.27          | 0.09       | 3.25        | 0.00       | 2.88          | 0.08       |
| LVPW;d          | 0.80        | 0.01       | 0.70          | 0.01       | 0.73        | 0.01       | 0.73          | 0.01       | 0.68        | 0.00       | 0.71          | 0.02       |
| LVPW;s          | 0.92        | 0.02       | 0.82          | 0.01       | 0.95        | 0.01       | 0.99          | 0.04       | 0.91        | 0.00       | 0.96          | 0.01       |
| <b>12 MONTH</b> | <b>MALE</b> |            | <b>FEMALE</b> |            | <b>MALE</b> |            | <b>FEMALE</b> |            | <b>MALE</b> |            | <b>FEMALE</b> |            |
|                 | <b>AVG</b>  | <b>SEM</b> | <b>AVG</b>    | <b>SEM</b> | <b>AVG</b>  | <b>SEM</b> | <b>AVG</b>    | <b>SEM</b> | <b>AVG</b>  | <b>SEM</b> | <b>AVG</b>    | <b>SEM</b> |
| HR              | 471.21      | 8.47       | 437.76        | 5.02       | 476.80      | 8.91       | 448.36        | 11.80      | 458.24      | 0.00       | 456.23        | 3.13       |
| Vol s           | 42.69       | 3.90       | 33.05         | 1.90       | 45.90       | 1.15       | 40.96         | 2.66       | 28.03       | 0.00       | 29.88         | 0.78       |
| Vol d           | 87.95       | 4.12       | 72.03         | 3.13       | 86.82       | 2.74       | 83.64         | 2.97       | 65.53       | 0.00       | 69.07         | 1.74       |
| SV              | 45.27       | 1.46       | 38.98         | 1.31       | 40.91       | 1.60       | 42.68         | 0.35       | 37.50       | 0.00       | 39.20         | 1.13       |
| EF              | 51.92       | 2.34       | 54.92         | 1.06       | 46.99       | 0.38       | 51.37         | 1.56       | 57.23       | 0.00       | 56.70         | 0.57       |
| FS              | 26.52       | 1.45       | 28.22         | 0.67       | 23.39       | 0.25       | 26.07         | 0.97       | 29.56       | 0.00       | 29.29         | 0.38       |
| CO              | 21.27       | 0.38       | 17.12         | 0.65       | 19.50       | 0.83       | 19.13         | 0.51       | 17.19       | 0.00       | 17.87         | 0.50       |
| LV Mass         | 129.18      | 4.84       | 111.33        | 2.32       | 143.06      | 6.50       | 123.90        | 2.91       | 118.86      | 0.00       | 105.91        | 2.45       |
| LV Mass Cor     | 103.34      | 3.87       | 89.06         | 1.85       | 114.45      | 5.20       | 99.12         | 2.33       | 95.09       | 0.00       | 84.73         | 1.96       |
| LVID;d          | 4.18        | 0.10       | 3.92          | 0.07       | 4.26        | 0.07       | 4.30          | 0.01       | 3.86        | 0.00       | 3.92          | 0.05       |
| LVID;s          | 3.33        | 0.13       | 3.16          | 0.08       | 3.49        | 0.03       | 3.37          | 0.04       | 2.94        | 0.00       | 3.01          | 0.05       |
| LVPW;d          | 0.80        | 0.01       | 0.80          | 0.01       | 0.86        | 0.02       | 0.80          | 0.00       | 0.80        | 0.00       | 0.76          | 0.01       |
| LVPW;s          | 0.91        | 0.02       | 0.94          | 0.02       | 1.03        | 0.04       | 1.01          | 0.02       | 0.89        | 0.00       | 0.94          | 0.02       |
| <b>15 MONTH</b> | <b>MALE</b> |            | <b>FEMALE</b> |            | <b>MALE</b> |            | <b>FEMALE</b> |            | <b>MALE</b> |            | <b>FEMALE</b> |            |
|                 | <b>AVG</b>  | <b>SEM</b> | <b>AVG</b>    | <b>SEM</b> | <b>AVG</b>  | <b>SEM</b> | <b>AVG</b>    | <b>SEM</b> | <b>AVG</b>  | <b>SEM</b> | <b>AVG</b>    | <b>SEM</b> |
| HR              | 436.41      | 6.81       | 487.60        | 4.77       | 427.42      | 5.21       | 461.46        | 18.46      | 514.38      | 0.00       | 417.31        | 8.19       |
| Vol s           | 44.19       | 2.47       | 41.59         | 1.74       | 50.76       | 1.52       | 49.86         | 3.07       | 37.01       | 0.00       | 34.88         | 2.55       |
| Vol d           | 80.36       | 2.23       | 77.71         | 1.95       | 95.10       | 2.28       | 88.78         | 2.59       | 68.89       | 0.00       | 72.52         | 2.94       |

|             |        |      |        |      |        |      |        |      |       |      |        |      |
|-------------|--------|------|--------|------|--------|------|--------|------|-------|------|--------|------|
| SV          | 36.17  | 1.15 | 36.12  | 0.21 | 44.35  | 0.86 | 38.92  | 0.80 | 31.88 | 0.00 | 37.64  | 0.54 |
| EF          | 45.19  | 1.94 | 46.97  | 1.01 | 46.72  | 0.45 | 44.14  | 1.98 | 46.28 | 0.00 | 52.72  | 1.73 |
| FS          | 22.28  | 1.15 | 23.33  | 0.60 | 23.29  | 0.26 | 21.76  | 1.14 | 22.75 | 0.00 | 26.87  | 1.10 |
| CO          | 15.81  | 0.67 | 17.62  | 0.26 | 18.93  | 0.23 | 18.01  | 0.99 | 16.40 | 0.00 | 15.72  | 0.41 |
| LV Mass     | 121.52 | 2.21 | 109.10 | 2.78 | 124.09 | 2.13 | 125.55 | 2.09 | 97.24 | 0.00 | 114.85 | 2.21 |
| LV Mass Cor | 97.21  | 1.77 | 87.28  | 2.23 | 99.27  | 1.70 | 100.44 | 1.67 | 77.80 | 0.00 | 91.88  | 1.77 |
| LVID;d      | 4.24   | 0.03 | 4.08   | 0.05 | 4.46   | 0.07 | 4.40   | 0.10 | 3.97  | 0.00 | 4.06   | 0.07 |
| LVID;s      | 3.57   | 0.04 | 3.34   | 0.06 | 3.62   | 0.05 | 3.61   | 0.09 | 3.29  | 0.00 | 3.14   | 0.07 |
| LVPW;d      | 0.80   | 0.01 | 0.77   | 0.02 | 0.81   | 0.03 | 0.75   | 0.02 | 0.78  | 0.00 | 0.74   | 0.02 |
| LVPW;s      | 0.93   | 0.02 | 0.97   | 0.02 | 1.08   | 0.04 | 0.92   | 0.02 | 0.91  | 0.00 | 0.92   | 0.01 |

### 3.7 Myeloid-Cell Specific EGFR Deletion Aggravates Cardiac Dysfunction

#### Following Ischemic Injury

In addition to regulating cardiac homeostasis, mf are vital to the post injury response (Ma et al., 2018). In this case, both resident mf and mon derived mf are important for adequate injury resolution (Ma et al., 2018; Bajpai et al., 2019; Sager et al., 2016). From RNAseq analysis, IPA clustered several transcripts to wound healing, phagosome formation, and vasculogenesis pathways, which were downregulated or inhibited in EGFRmylKO cardiac myeloid cells (Figure 18a). Thus, we wondered how EGFRmylKO hearts would respond to ischemic injury. We subjected EGFRmylKO and control mice to permanent LAD ligation to induce an MI (Gao et al., 2010). We first tracked injury survival across multiple cohorts. We observed that in response to MI, EGFRmylKO experienced 20-30% mortality, which was not significantly different from either control lines (Figure 23a). Next, to understand how EGFRmylKO mice progressed to HF relative to controls, we analyzed cardiac function via 2D echocardiography weekly following MI (Figure 24a-b). Here, we observed a hastened decline in cardiac function in EGFRmylKO mice, when compared to either control group, indicated by significant

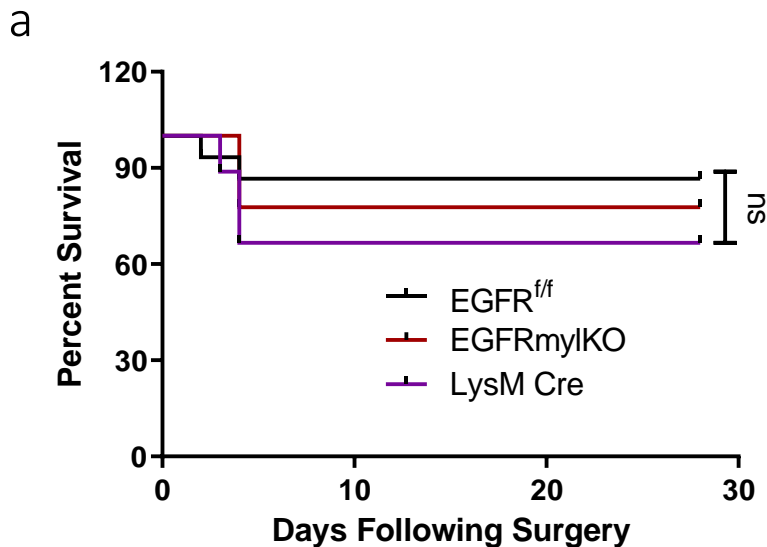


**Figure 23. Loss of Myeloid-Cell Specific EGFR Does not Significantly Impact Survival Following Ischemic Injury.** Post MI survival is plotted using Kaplan-Meier strategy, with median survival at X days following injury. Survival rate is shown as a percent change of the starting number of mice/group. N = 7-12/group. ns, not significant.

changes in ventricular EF and FS (Figure 24c). Cardiac dysfunction was maintained in EGFRmylKO mice for up to 4 weeks, where it was significantly decreased when compared to the LysM Cre controls (Figure 24c). Additionally, the loss of function in response to injury relative to baseline, was far greater in EGFRmylKO hearts (Figure 24d). Echocardiography analyses also revealed signs of grave cardiac remodeling in EGFRmylKO hearts (Figure 24b-c). Infarcted animals exhibited severe cardiac dilation, in comparison to sham operated animals as indicated by enhanced LVID (Figure 24b-c). Though this was slightly higher in EGFRmylKO hearts, the difference did not reach statistical significance (Figure 24b-c). Table 8 details all echo parameters in sham or infarcted animals. In conclusion, these data suggest that myeloid cell-expressed EGFR protects the injured heart from cardiac dysfunction.

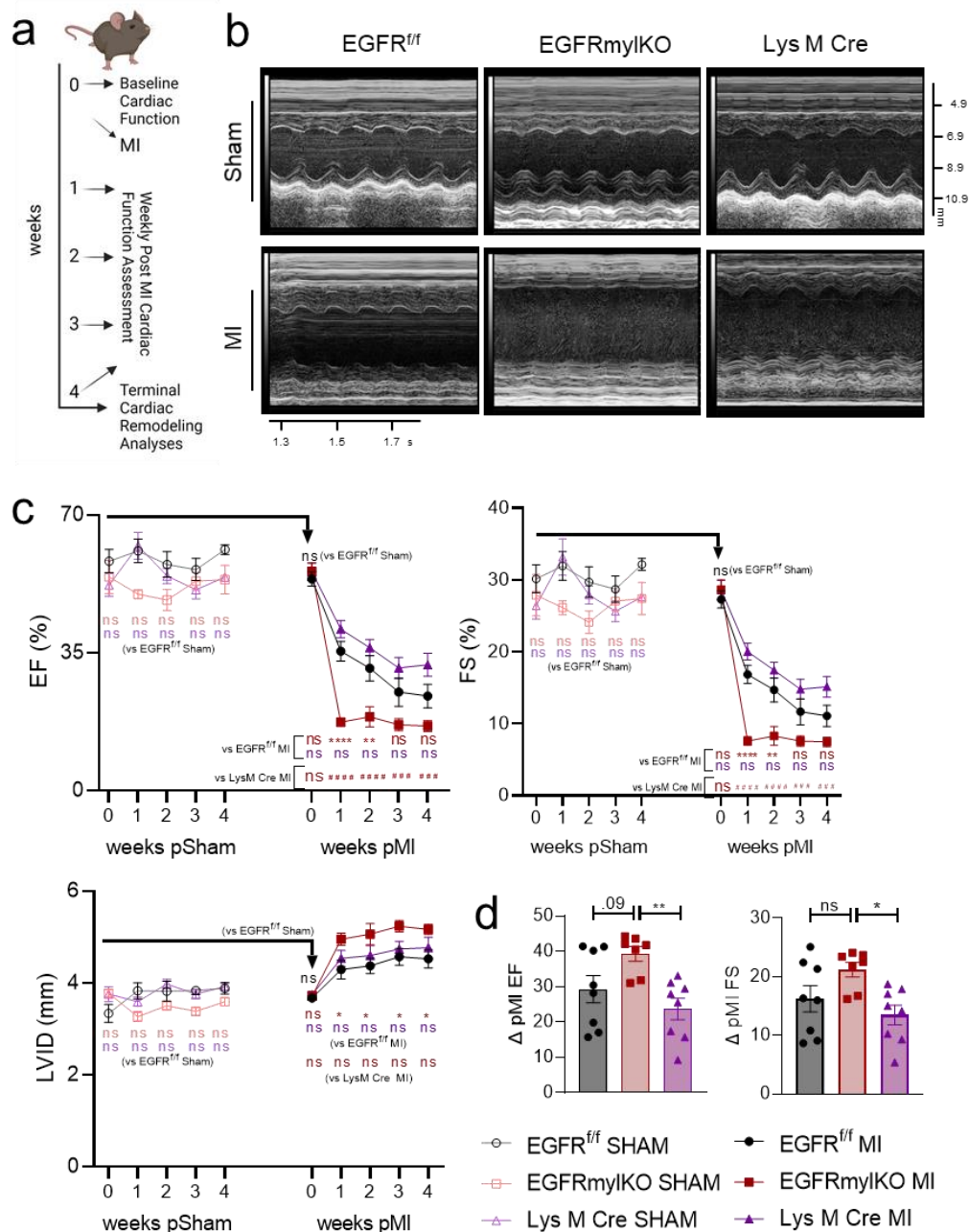


**Figure 24. Loss of Myeloid-Cell Specific EGFR Results in Rapid Decline in Cardiac Function Following Ischemic Injury.** a) Schematic depicting experimental timeline b) Representative m-mode echocardiograms of EGFRmylKO and control hearts 1 week following sham or MI. c) EF, FS, and LVIDd of EGFRmylKO and control mice were analyzed after echo using the VisualSonics Vevo software and reported prior to, and 1-4 weeks after surgery. N = 5-6 (sham) 7-8 (MI) per group. \*P<0.05, \*\*P<0.01, \*\*\*P<0.001, ns, not significant, with two-way ANOVA with Bonferonni's multiple comparisons test. d) Difference in post MI 4wk EF and FS from baseline values plotted for EGFRmylKO and controls. \*P<0.05, \*\*P<0.01, ns, not significant, with one-way ANOVA with Tukey's multiple comparisons test.

**Table 8. Sham & MI Echo Parameters**

| Baseline | SHAM        |       |               |       |              |       | MI          |       |               |       |              |       |
|----------|-------------|-------|---------------|-------|--------------|-------|-------------|-------|---------------|-------|--------------|-------|
|          | EGFRf/f (5) |       | EGFRmylKO (5) |       | LysM Cre (6) |       | EGFRf/f (8) |       | EGFRmylKO (7) |       | LysM Cre (8) |       |
|          | AVG         | SEM   | AVG           | SEM   | AVG          | SEM   | AVG         | SEM   | AVG           | SEM   | AVG          | SEM   |
| HR       | 465.44      | 15.16 | 454.48        | 13.15 | 488.56       | 7.20  | 454.63      | 12.99 | 468.20        | 8.30  | 458.14       | 10.03 |
| SV       | 29.16       | 2.95  | 33.67         | 3.12  | 32.07        | 3.04  | 31.57       | 1.52  | 35.64         | 2.18  | 34.67        | 1.67  |
| EF       | 58.29       | 2.94  | 54.27         | 4.26  | 52.22        | 2.94  | 53.77       | 1.84  | 55.70         | 2.14  | 55.62        | 2.18  |
| FS       | 30.17       | 1.94  | 27.89         | 2.90  | 26.43        | 1.86  | 27.29       | 1.19  | 28.64         | 1.34  | 28.60        | 1.40  |
| CO       | 13.52       | 1.31  | 15.21         | 1.17  | 15.66        | 1.51  | 14.27       | 0.50  | 16.62         | 0.96  | 15.87        | 0.82  |
| LV Mass  | 76.64       | 8.16  | 94.72         | 3.79  | 99.37        | 4.97  | 85.23       | 3.69  | 99.88         | 3.45  | 94.83        | 3.81  |
| LVAW;s   | 1.08        | 0.08  | 1.04          | 0.04  | 1.12         | 0.05  | 0.97        | 0.05  | 1.14          | 0.03  | 0.99         | 0.05  |
| LVAW;d   | 0.65        | 0.09  | 0.63          | 0.04  | 0.72         | 0.04  | 0.68        | 0.02  | 0.69          | 0.03  | 0.68         | 0.01  |
| LVID;d   | 3.34        | 0.19  | 3.78          | 0.08  | 3.76         | 0.16  | 3.67        | 0.05  | 3.71          | 0.08  | 3.74         | 0.08  |
| LVID;s   | 2.54        | 0.20  | 2.94          | 0.14  | 2.92         | 0.14  | 2.87        | 0.11  | 2.93          | 0.09  | 2.80         | 0.09  |
| LVPW;d   | 0.85        | 0.05  | 0.84          | 0.03  | 0.76         | 0.05  | 0.73        | 0.03  | 0.84          | 0.03  | 0.79         | 0.05  |
| LVPW;s   | 0.98        | 0.04  | 1.05          | 0.03  | 0.98         | 0.05  | 0.90        | 0.04  | 0.97          | 0.04  | 1.00         | 0.05  |
| 1wk      | EGFRf/f (5) |       | EGFRmylKO (5) |       | LysM Cre (6) |       | EGFRf/f (8) |       | EGFRmylKO (7) |       | LysM Cre (8) |       |
| HR       | 497.84      | 10.19 | 475.45        | 8.60  | 473.00       | 6.76  | 473.77      | 9.71  | 492.52        | 12.42 | 481.33       | 9.52  |
| SV       | 28.75       | 1.16  | 32.05         | 2.35  | 33.88        | 2.60  | 28.54       | 2.61  | 20.06         | 0.92  | 38.38        | 2.42  |
| EF       | 60.90       | 2.99  | 49.90         | 1.10  | 62.21        | 3.43  | 35.43       | 2.48  | 16.78         | 1.31  | 41.01        | 2.20  |
| FS       | 31.94       | 1.98  | 24.89         | 0.66  | 33.19        | 2.53  | 16.87       | 1.29  | 7.59          | 0.60  | 20.03        | 1.18  |
| CO       | 14.27       | 0.40  | 15.31         | 1.34  | 16.09        | 1.40  | 13.54       | 1.26  | 9.86          | 0.44  | 18.35        | 0.89  |
| LV Mass  | 81.63       | 9.65  | 106.72        | 7.86  | 103.78       | 4.29  | 104.18      | 6.61  | 121.48        | 8.54  | 125.38       | 8.89  |
| LVAW;s   | 1.08        | 0.09  | 1.04          | 0.01  | 1.22         | 0.06  | 0.84        | 0.04  | 0.73          | 0.03  | 0.95         | 0.06  |
| LVAW;d   | 0.70        | 0.06  | 0.69          | 0.03  | 0.77         | 0.05  | 0.68        | 0.02  | 0.60          | 0.02  | 0.69         | 0.02  |
| LVID;d   | 3.27        | 0.11  | 3.83          | 0.17  | 3.59         | 0.10  | 4.29        | 0.20  | 4.95          | 0.13  | 4.54         | 0.17  |
| LVID;s   | 2.41        | 0.11  | 2.93          | 0.14  | 2.60         | 0.10  | 3.62        | 0.19  | 4.61          | 0.18  | 3.57         | 0.19  |
| LVPW;d   | 0.78        | 0.05  | 0.88          | 0.04  | 0.83         | 0.03  | 0.66        | 0.05  | 0.61          | 0.03  | 0.73         | 0.03  |
| LVPW;s   | 1.02        | 0.04  | 1.00          | 0.04  | 1.09         | 0.06  | 0.76        | 0.05  | 0.66          | 0.02  | 0.89         | 0.06  |
| 2wk      | EGFRf/f (5) |       | EGFRmylKO (5) |       | LysM Cre (6) |       | EGFRf/f (8) |       | EGFRmylKO (7) |       | LysM Cre (8) |       |
| HR       | 482.65      | 14.41 | 464.39        | 12.12 | 464.43       | 15.07 | 468.13      | 9.35  | 431.93        | 9.85  | 452.58       | 14.89 |
| SV       | 30.81       | 1.26  | 32.83         | 1.82  | 37.31        | 2.58  | 28.70       | 3.85  | 21.41         | 2.39  | 36.43        | 3.65  |
| EF       | 57.47       | 3.24  | 48.43         | 2.68  | 54.52        | 1.93  | 31.07       | 3.21  | 18.73         | 2.57  | 36.30        | 2.10  |
| FS       | 29.71       | 2.10  | 24.12         | 1.57  | 27.90        | 1.24  | 14.69       | 1.68  | 8.30          | 1.32  | 17.44        | 1.12  |
| CO       | 14.83       | 0.53  | 15.34         | 1.22  | 17.43        | 1.52  | 13.27       | 1.67  | 9.17          | 1.01  | 16.57        | 1.87  |
| LV Mass  | 84.58       | 8.31  | 92.20         | 4.29  | 101.21       | 2.67  | 108.59      | 5.28  | 131.28        | 11.72 | 124.92       | 11.96 |
| LVAW;s   | 1.04        | 0.05  | 0.96          | 0.03  | 1.02         | 0.04  | 0.83        | 0.05  | 0.75          | 0.05  | 0.91         | 0.05  |
| LVAW;d   | 0.68        | 0.06  | 0.64          | 0.02  | 0.73         | 0.03  | 0.63        | 0.04  | 0.63          | 0.04  | 0.67         | 0.02  |

|        |      |      |      |      |      |      |      |      |      |      |      |      |
|--------|------|------|------|------|------|------|------|------|------|------|------|------|
| LVID;d | 3.50 | 0.09 | 3.82 | 0.21 | 3.98 | 0.11 | 4.37 | 0.17 | 5.06 | 0.23 | 4.60 | 0.21 |
| LVID;s | 2.58 | 0.17 | 3.12 | 0.23 | 3.04 | 0.11 | 3.85 | 0.14 | 4.76 | 0.24 | 3.79 | 0.21 |
| LVPW;d | 0.84 | 0.04 | 0.74 | 0.08 | 0.73 | 0.01 | 0.71 | 0.07 | 0.64 | 0.03 | 0.62 | 0.04 |
| LVPW;s | 1.05 | 0.05 | 0.94 | 0.08 | 0.94 | 0.04 | 0.83 | 0.06 | 0.67 | 0.04 | 0.75 | 0.02 |

| 3wk     | EGFRf/f (5) |       | EGFRmylKO (5) |       | LysM Cre (6) |       | EGFRf/f (8) |      | EGFRmylKO (7) |       | LysM Cre (8) |       |
|---------|-------------|-------|---------------|-------|--------------|-------|-------------|------|---------------|-------|--------------|-------|
| HR      | 481.89      | 18.95 | 509.72        | 21.97 | 472.95       | 12.76 | 480.70      | 5.59 | 499.51        | 19.21 | 496.53       | 13.15 |
| SV      | 27.85       | 2.03  | 36.11         | 1.54  | 32.77        | 1.76  | 24.58       | 4.01 | 22.09         | 2.44  | 32.17        | 1.38  |
| EF      | 56.16       | 2.83  | 53.21         | 2.22  | 51.02        | 2.32  | 25.01       | 3.58 | 16.70         | 1.56  | 31.14        | 2.69  |
| FS      | 28.73       | 1.85  | 27.08         | 1.37  | 25.66        | 1.43  | 11.66       | 1.80 | 7.59          | 0.74  | 14.80        | 1.38  |
| CO      | 13.34       | 0.86  | 18.46         | 1.42  | 15.44        | 0.71  | 11.78       | 1.88 | 10.88         | 1.11  | 15.97        | 0.88  |
| LV Mass | 79.95       | 9.49  | 93.84         | 3.60  | 102.71       | 7.43  | 113.52      | 8.45 | 135.94        | 8.25  | 132.41       | 10.92 |
| LVAW;s  | 1.03        | 0.05  | 0.99          | 0.03  | 1.08         | 0.05  | 0.82        | 0.07 | 0.76          | 0.05  | 0.86         | 0.04  |
| LVAW;d  | 0.68        | 0.08  | 0.64          | 0.02  | 0.76         | 0.05  | 0.66        | 0.05 | 0.57          | 0.03  | 0.69         | 0.01  |
| LVID;d  | 3.38        | 0.08  | 3.83          | 0.09  | 3.76         | 0.11  | 4.57        | 0.18 | 5.24          | 0.13  | 4.74         | 0.17  |
| LVID;s  | 2.54        | 0.11  | 2.95          | 0.15  | 2.89         | 0.11  | 3.98        | 0.16 | 4.84          | 0.15  | 4.02         | 0.18  |
| LVPW;d  | 0.76        | 0.02  | 0.77          | 0.03  | 0.79         | 0.04  | 0.60        | 0.03 | 0.68          | 0.03  | 0.66         | 0.04  |
| LVPW;s  | 1.01        | 0.04  | 0.97          | 0.04  | 0.98         | 0.04  | 0.72        | 0.03 | 0.77          | 0.03  | 0.74         | 0.04  |

| 4wk     | EGFRf/f (5) |      | EGFRmylKO (5) |       | LysM Cre (6) |       | EGFRf/f (8) |       | EGFRmylKO (7) |      | LysM Cre (8) |       |
|---------|-------------|------|---------------|-------|--------------|-------|-------------|-------|---------------|------|--------------|-------|
| HR      | 496.40      | 6.09 | 519.30        | 22.42 | 460.56       | 13.39 | 482.80      | 15.43 | 510.23        | 9.25 | 462.61       | 7.41  |
| SV      | 33.05       | 1.40 | 35.01         | 0.79  | 34.61        | 1.23  | 23.01       | 3.34  | 21.32         | 1.98 | 30.45        | 1.32  |
| EF      | 61.23       | 1.22 | 53.61         | 3.62  | 54.24        | 0.73  | 23.99       | 3.01  | 16.40         | 1.39 | 31.95        | 2.91  |
| FS      | 32.17       | 0.84 | 27.42         | 2.25  | 27.61        | 0.47  | 11.08       | 1.47  | 7.45          | 0.66 | 15.14        | 1.46  |
| CO      | 16.38       | 0.55 | 18.12         | 0.47  | 15.96        | 0.84  | 11.21       | 1.69  | 10.89         | 1.06 | 14.09        | 0.65  |
| LV Mass | 88.22       | 4.27 | 95.62         | 8.92  | 104.21       | 4.39  | 131.71      | 14.39 | 144.47        | 6.84 | 137.26       | 17.06 |
| LVAW;s  | 1.19        | 0.02 | 1.05          | 0.03  | 1.15         | 0.04  | 0.89        | 0.05  | 0.82          | 0.05 | 0.97         | 0.06  |
| LVAW;d  | 0.73        | 0.03 | 0.65          | 0.05  | 0.76         | 0.03  | 0.72        | 0.04  | 0.64          | 0.04 | 0.75         | 0.04  |
| LVID;d  | 3.59        | 0.08 | 3.88          | 0.12  | 3.92         | 0.08  | 4.53        | 0.20  | 5.17          | 0.11 | 4.77         | 0.23  |
| LVID;s  | 2.49        | 0.08 | 2.96          | 0.15  | 2.95         | 0.05  | 4.02        | 0.22  | 4.75          | 0.09 | 4.01         | 0.27  |
| LVPW;d  | 0.75        | 0.04 | 0.71          | 0.04  | 0.75         | 0.02  | 0.59        | 0.05  | 0.63          | 0.03 | 0.66         | 0.06  |
| LVPW;s  | 1.04        | 0.04 | 0.97          | 0.04  | 0.95         | 0.04  | 0.68        | 0.04  | 0.65          | 0.03 | 0.81         | 0.06  |

### 3.8 Myeloid-Cell Specific EGFR Limits Adverse Cardiac Remodeling Following Ischemic Injury

Excessive and adverse cardiac remodeling after injury can increase HF severity, and in patients, is associated with poor prognosis (van der Laan et al., 2012; Burchfield et al., 2013). Post MI cardiac mf are critical to the remodeling myocardium, as they function in numerous wound healing processes (Peet et al., 2020). Since EGFRmylKO experienced severe cardiac dysfunction following injury, we assessed hearts for parameters of cardiac remodeling. We initially sought to assess the level of ischemic injury, and found similar infarct lengths relative to total LV length across all groups (Figure 25a-b). Analyses of total collagen in the ischemic border zone indicated enhanced fibrotic remodeling near the infarct, which was unchanged by myeloid cell-specific EGFR deletion (Figure 25c-d). Compared to sham animals, no significant changes in interstitial fibrosis were observed in the remote zones of all infarcted animals (Figure 25c-d). We next assessed hypertrophic remodeling at the cellular level by WGA. When compared to either the EGFR<sup>f/f</sup> or LysM Cre control group, EGFRmylKO hearts had elevated cell size (Figure 26a-b). Post MI cardiac hypertrophy was further confirmed by gravimetrics and gene expression analysis where EGFRmylKO had larger heart weights (Figure 26c-d). Expression of *Acta1* was also elevated in EGFRmylKO ventricles when compared to control (Figure 26e). We next stained hearts for isolectin, to assess capillary formation following the infarct. When compared to either control group, EGFRmylKO hearts had significantly fewer capillaries (Figure 27a-b). These data were also accompanied with decreased expression of *Il10* in post MI EGFRmylKO ventricles when

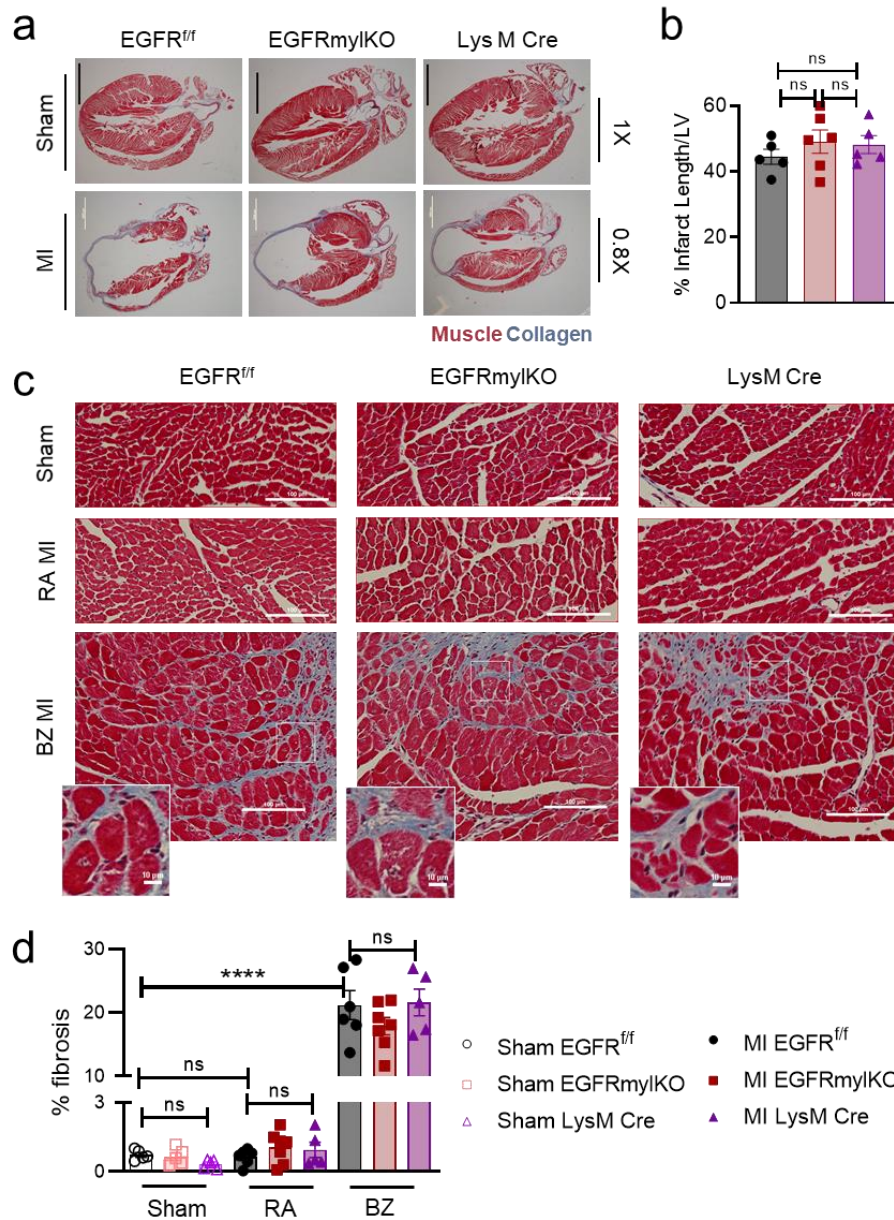


**Figure 25. Loss of Myeloid-Cell Specific EGFR does not Alter Cardiac Fibrosis Following Ischemia.** a) Representative 0.8X and 1X panels of MTC stained LV 4 weeks following sham or MI in EGFR<sup>mylKO</sup> versus EGFR<sup>f/f</sup> and Lys M Cre controls. Scale bar denotes 2 mm (0.8X) and 1 mm (1X). b) Infarct length was assessed as a percentage of the total LV length. N = 5-6 (sham) 7-8 (MI), represented by individual bullets in the histogram. ns, not significant using one-way ANOVA with Tukey's multiple comparisons test. c) Representative 20X panels of MTC stained LV 4 weeks following sham or MI in EGFR<sup>mylKO</sup> versus EGFR<sup>f/f</sup> and Lys M Cre controls. Scale bar denotes scale bar denotes 100  $\mu$ m. d) Fibrosis was assessed as a percentage of the total LV area in sham, and both remote (RA) and infarct border zone (BZ) regions. N = 5-6 (sham), 7-8 (MI) represented by individual bullets in histogram. \*\*\*P<0.001, ns, not significant using one-way ANOVA with Tukey's multiple comparisons test.

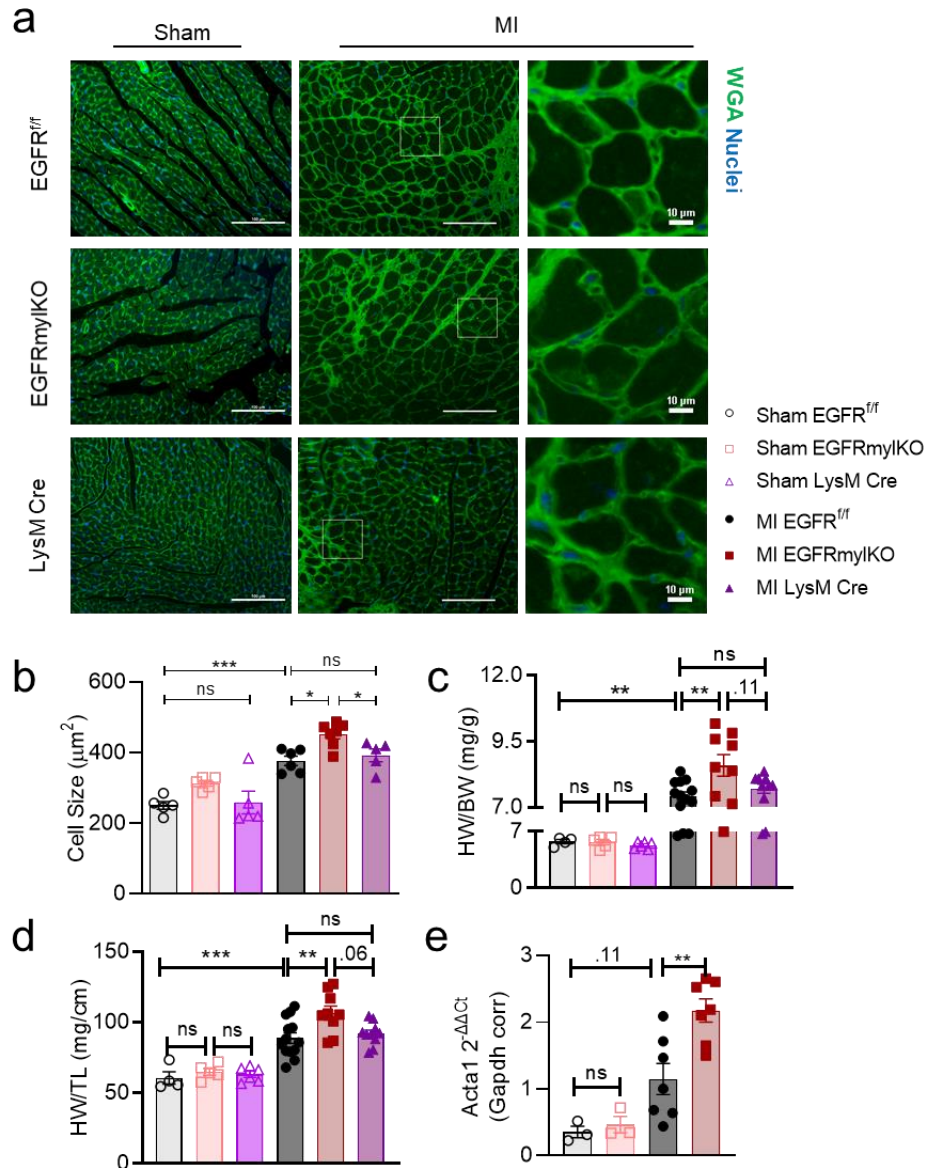


**Figure 26. Loss of Myeloid-Cell Specific EGFR Aggravates Pathological Hypertrophy Following Ischemia.** a) Panels show representative regions of interest from 20X magnification of WGA stained hearts 4 weeks following sham or MI in EGFR<sup>myfKO</sup> versus EGFR<sup>f/f</sup> and Lys M Cre controls. b) Histogram shows quantification of cardiomyocyte cell size. N = 4-8, represented by individual bullets in the histogram. \*P<0.05, \*\*\*P<0.001, \*\*P<0.001 using one-way ANOVA with Tukey's multiple comparisons test. Heart weights from EGFR<sup>myfKO</sup> versus EGFR<sup>f/f</sup> and Lys M Cre controls were normalized to c) body weights or d) tibia lengths 4 weeks following sham or MI. N = 4-12, represented by individual bullets in the histogram. \*\*P<0.01, \*\*\*P<0.001 one-way ANOVA with Tukey's multiple comparisons test. e) RT-qPCR was used to measure the expression of *Act1*, and *Gapdh* in the LV of EGFR<sup>myfKO</sup> mice vs EGFR<sup>f/f</sup> 7 days post MI, normalized to *Gapdh*. N = 3 sham, 7-8 MI, represented by individual bullets in the histogram. \*\*P<0.01, ns not significant, using one-way ANOVA with Tukey's multiple comparisons test.

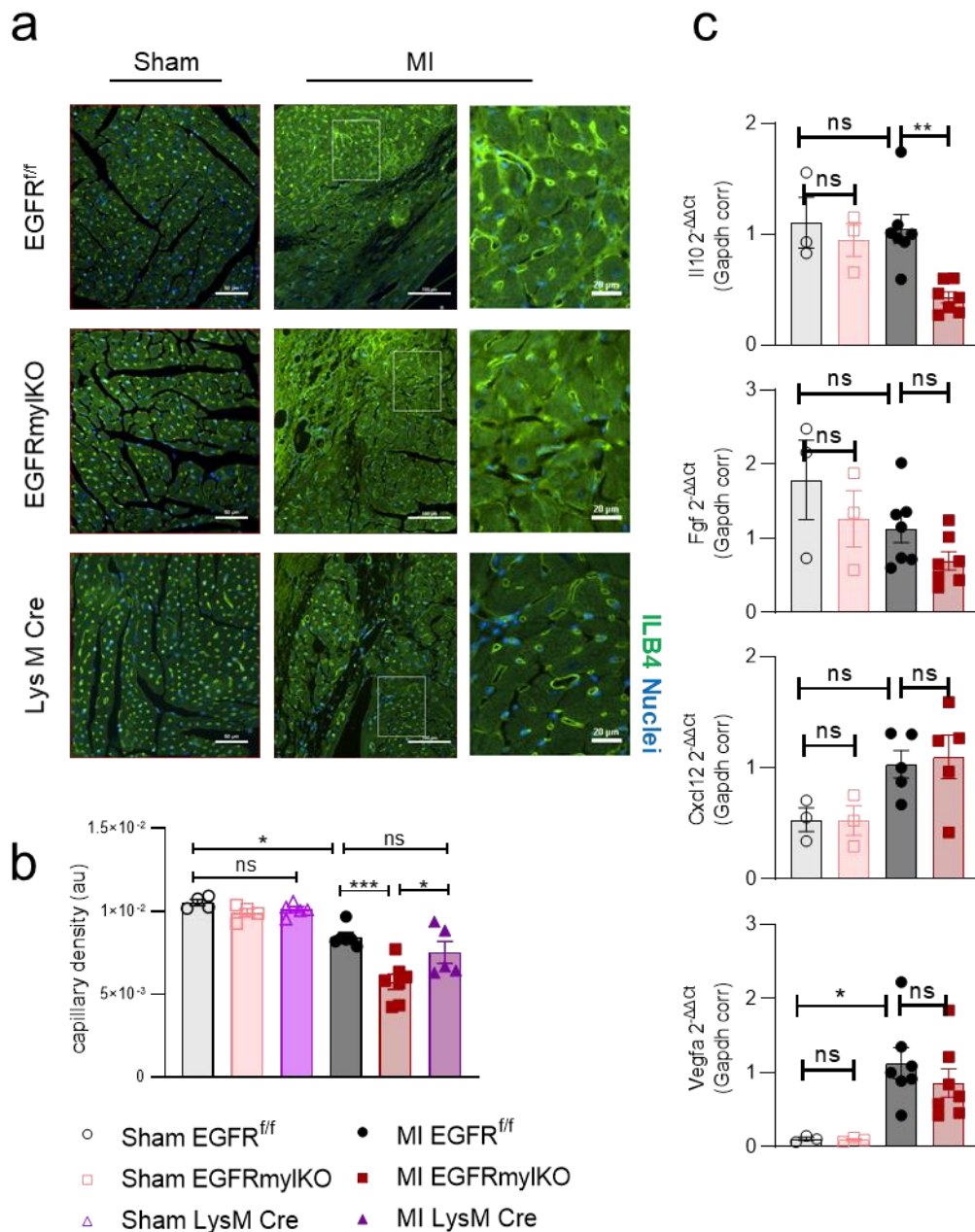


**Figure 27. Loss of Myeloid-Cell Specific EGFR Limits Angiogenic Repair Following Ischemia.** a) Panels show representative regions of interest from 20X magnification of isolectin B4 (ILB4) stained hearts 4 weeks following sham or MI in EGFR<sup>mylKO</sup> versus EGFR<sup>f/f</sup> and Lys M Cre controls. b) Histogram shows quantification of lectin-stained capillary density. N = 5-8, represented by individual bullets in the histogram. \*\*\*P<0.001, \*\*P<0.01, ns, not significant using one-way ANOVA with Tukey's multiple comparisons test. c) RT-qPCR was used to measure the expression of *Il10*, *Fgf*, *Cxcl12*, and *Vegfa*, and *Gapdh* in the LV of EGFR<sup>mylKO</sup> mice vs EGFR<sup>f/f</sup> 7 days post MI, normalized to *Gapdh*. N = 3 sham, 5-8 MI, represented by individual bullets in the histogram. \*\*P<0.01, \*P<0.05, using one-way ANOVA with Tukey's multiple comparisons test.

compared to control (Figure 27c). Levels of *Cxcl12*, *Vegf* and *Fgf* in EGFRmylKO hearts were not significantly changed (Figure 27c). Together, these findings provide evidence to suggest a role for myeloid cell-specific EGFR in limiting adverse remodeling following cardiac injury.

### **3.9 Myeloid-Cell Specific EGFR Regulates the Post Ischemic Inflammatory Response**

Myeloid and mf EGFR has been shown to differentially regulate inflammatory outcomes in varying disease stages and contexts (Hoyer et al., 2019; Hardbower et al., 2016). In response to cardiac injury, a multiphasic inflammatory response ensues, and is necessary for the healing heart (Prabhu et al., 2016). As EGFRmylKO hearts experience greater dysfunction and adverse remodeling, we wondered how myeloid EGFR might contribute to the post-MI inflammatory response. We first sought to understand how much cell death occurred within the first 24 hours of ischemia. To this end, a second cohort of animals were subject to MI, and 24 hours after, we analyzed TUNEL positive nuclei. Here, we observed 20-30% TUNEL-positive nuclei within troponin-stained cells, indicating a severe level of CM death (Figure 28a-b). This was unchanged in EGFRmylKO hearts, and in either group, was not observed in areas remote to the infarct (Figure 28a-b).

As the earliest response to injury, neutrophils exit the circulation and infiltrate the infarcted heart (Prabhu et al., 2016). We quantified neutrophil density by myeloperoxidase (MPO) staining within infarcted hearts at 24 hours post-MI (Figure 29a-b). We observed little to no neutrophils in remote areas, however, infarct regions in all

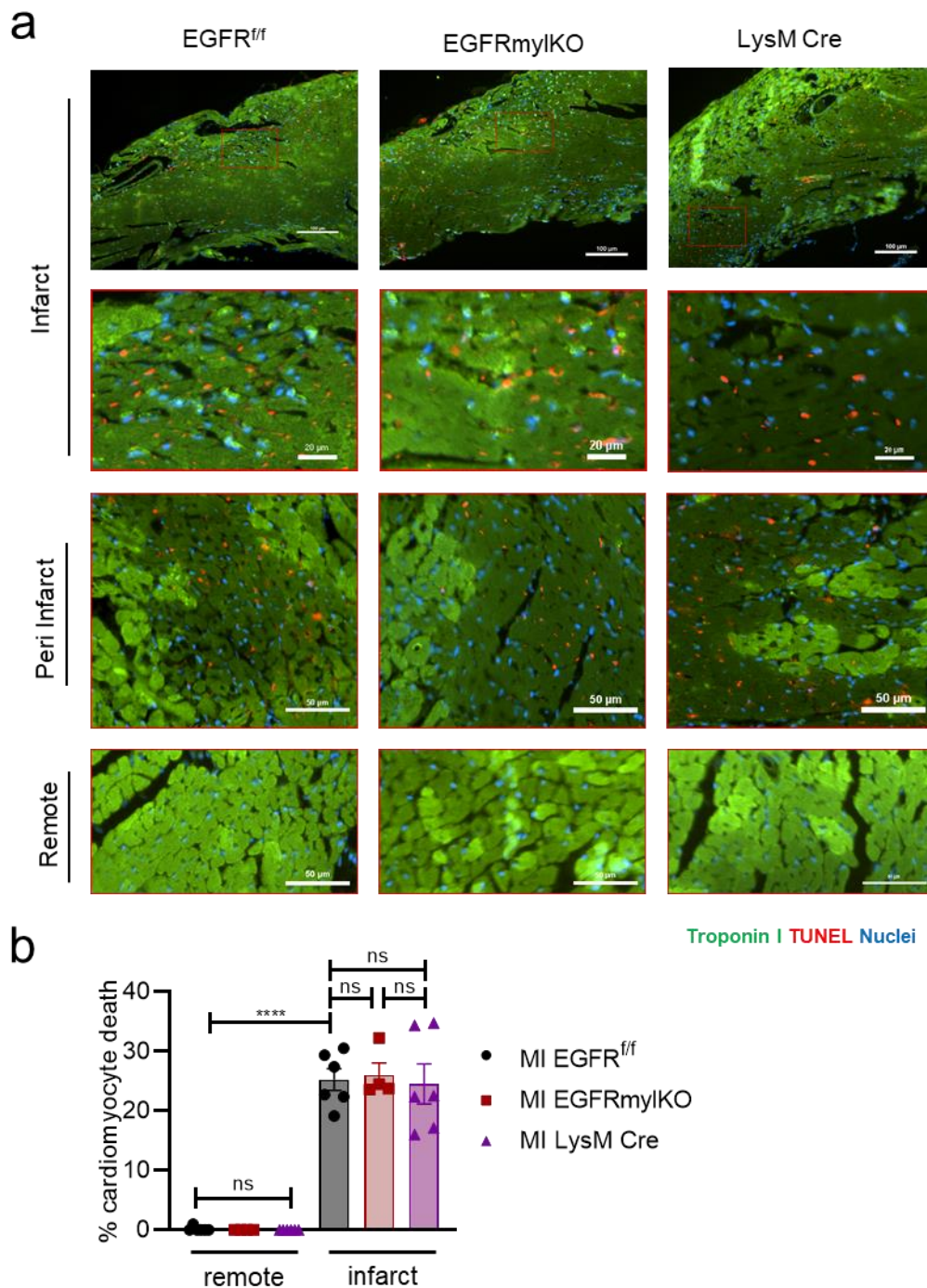


**Figure 28. Early Following Ischemia, EGFRmylKO Hearts Exhibit Similar Loss of Cardiomyocytes.** Panels are representative images of TUNEL, DAPI, and troponin I (TnI) stained hearts 24 hours post MI in EGFRmylKO versus EGFR<sup>f/f</sup> and Lys M Cre controls in a) infarct, peri infarct, and remote area, regions of interest from 20X magnification. b) Accompanying histogram details TUNEL, TnI, and DAPI positive cells over total TnI, DAPI positive cells in the remote and infarcted LV. N = 4-6, represented by individual bullets in the histogram. \*\*\*\*P<0.0001, ns, not significant using one-way ANOVA with Tukey's multiple comparisons test.

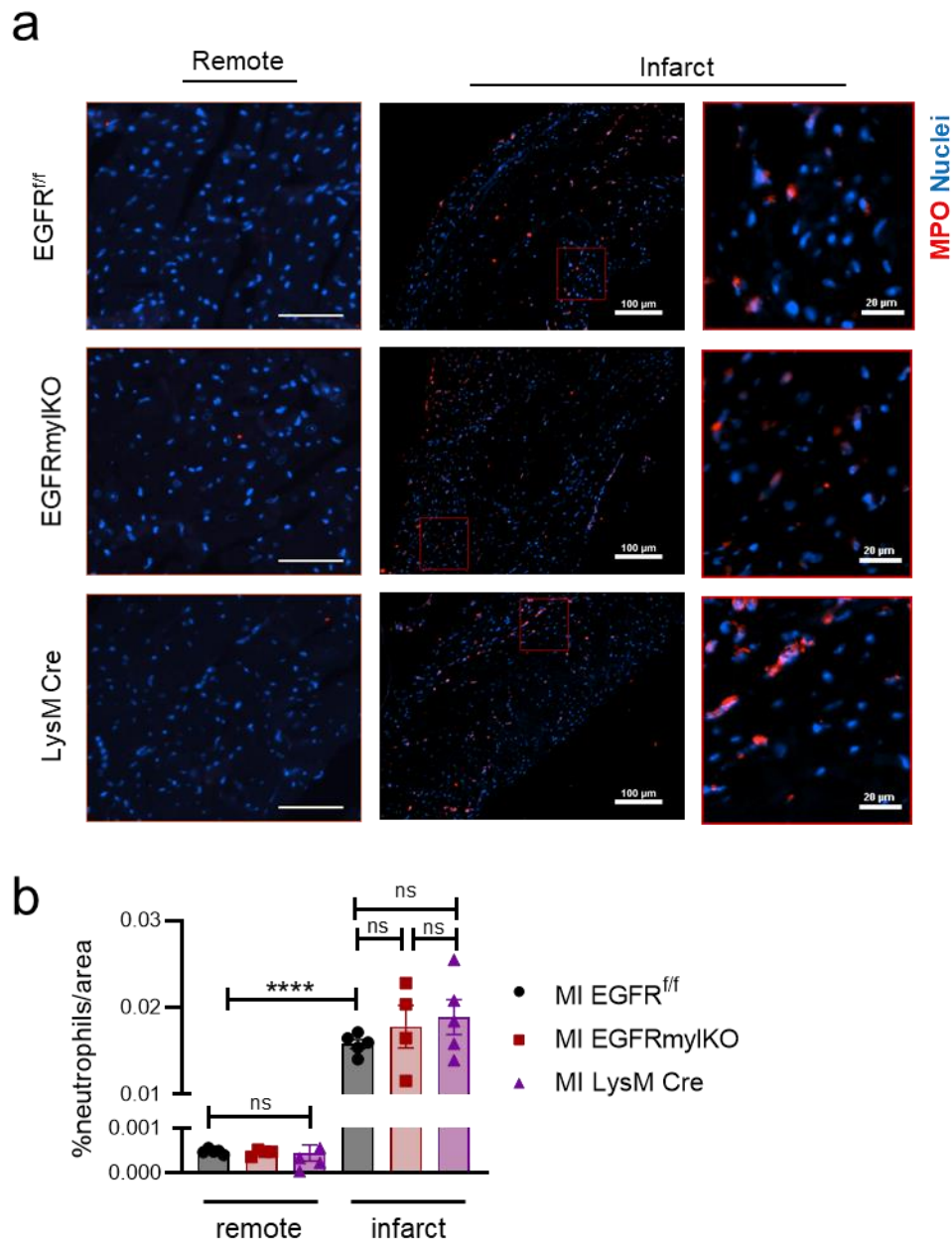


**Figure 29. Early Following Ischemia, EGFRmylKO Hearts Exhibit Similar Neutrophil Densities.** Panels are representative images of MPO, and DAPI stained hearts 24 hours post MI in EGFRmylKO versus EGFR<sup>f/f</sup> and Lys M Cre controls in a) infarct and remote areas, from regions of interest at 20X magnification. b) Accompanying histogram details MPO and DAPI positive cells over total DAPI positive cells in the remote and infarcted LV. N = 4-6, represented by individual bullets in the histogram. \*\*\*\*P<0.0001, ns, not significant using one-way ANOVA with Tukey's multiple comparisons test.

mice exhibited significantly higher neutrophil density (Figure 29a-b). This was accompanied by comparable levels of Ly6G positive neutrophils in circulation for all groups (Figure 30a,c). The completion of the initial inflammatory phase includes an expansion in proinflammatory macrophages, so we assessed levels of inflammatory monocytes in the blood at this earliest time point (Prabhu et al., 2016). We did not observe a difference in Ly6C and CCR2 double positive inflammatory mon in EGFRmylKO blood at 24 hours post MI (Figure 30b-c).

Inflammatory monocytes and mf peak around 3-4 days following MI, so we analyzed a 3rd cohort of animals at 4 days post MI (Prabhu et al., 2016). By flow cytometry, we investigated inflammatory dynamics within these hearts. We identified elevated CD45+ leukocytes in all infarcted hearts, relative to sham (Figure 31D). Similarly, neutrophil levels were much greater in infarcted hearts relative to sham, though they were similar across all groups (Figure 31a-b,d). Next, when we quantified total mf levels, we observed no difference in EGFRmylKO hearts (Figure 31a-b,d). However, we stratified mf by Ly6C and CCR2 to understand the distribution of inflammatory mf in the tissue (Figure 31a-d). Here, we observed in EGFRmylKO hearts elevated inflammatory mon-derived mf relative to EGFR<sup>ff</sup> controls (Figure 31c,e). Since this time point also marks the beginning of the proliferation and resolution phase, we wondered what the distribution of pro resolving mf were in hearts, so we analyzed mf for low expression of Ly6C (Fu et al., 2017). We identified at 4 days post MI that EGFRmylKO exhibited a higher ratio of Ly6C high relative to Ly6C low mf in comparison to either control (Figure 31e). To understand if this persisted into the repair phase, we injured an additional cohort of mice and characterized myeloid inflammation at 7 days post MI. Here, we also

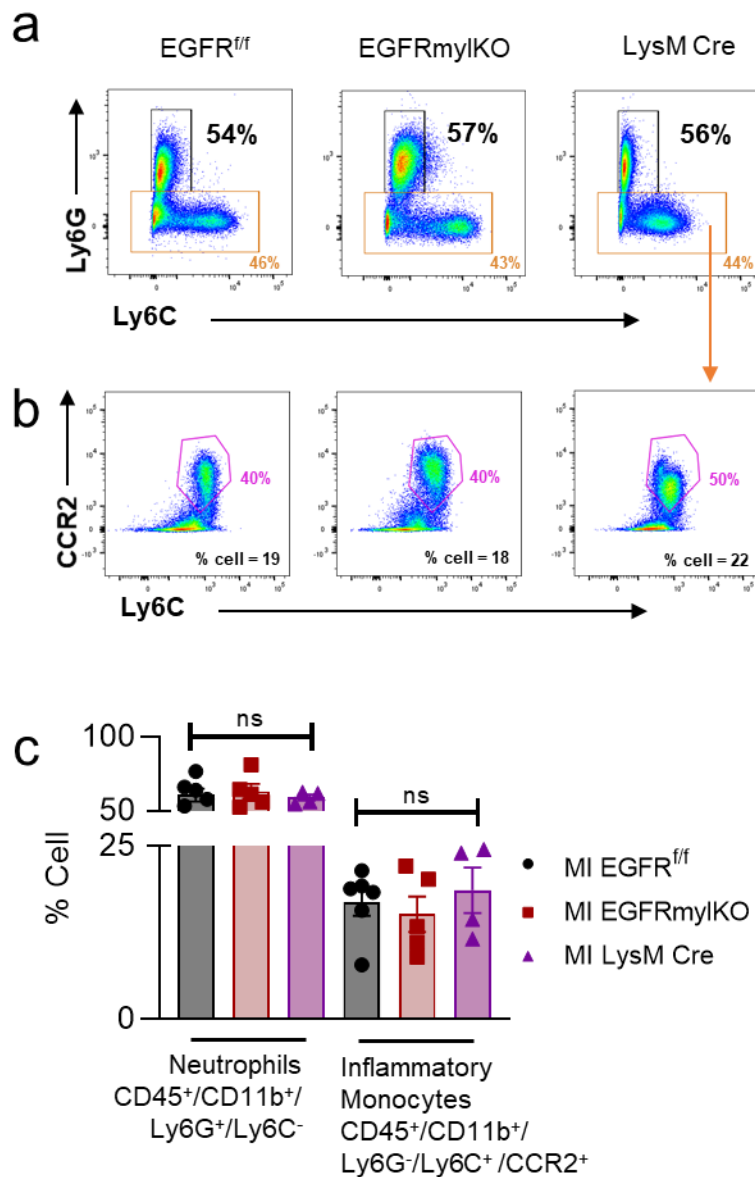


**Figure 30. Early Following Ischemia, Myeloid-Cell Specific EGFR does not Significantly Impact Myeloid Mobilization.** Representative flow cytometry plots showing CD45<sup>+</sup> CD11b<sup>+</sup> cells which were stratified for a) Ly6G vs Ly6C b) Ly6G<sup>-</sup> cells were stratified for Ly6C and CCR2 in the blood 24 hr following MI in EGFRmylKO versus EGFR<sup>f/f</sup> and Lys M Cre controls. Accompanying histogram details flow cytometry gated cell populations: c) neutrophils, and inflammatory monocytes. N = 4-6, represented by individual bullets in histogram. ns, not significant using one-way ANOVA with Tukey's multiple comparisons test.

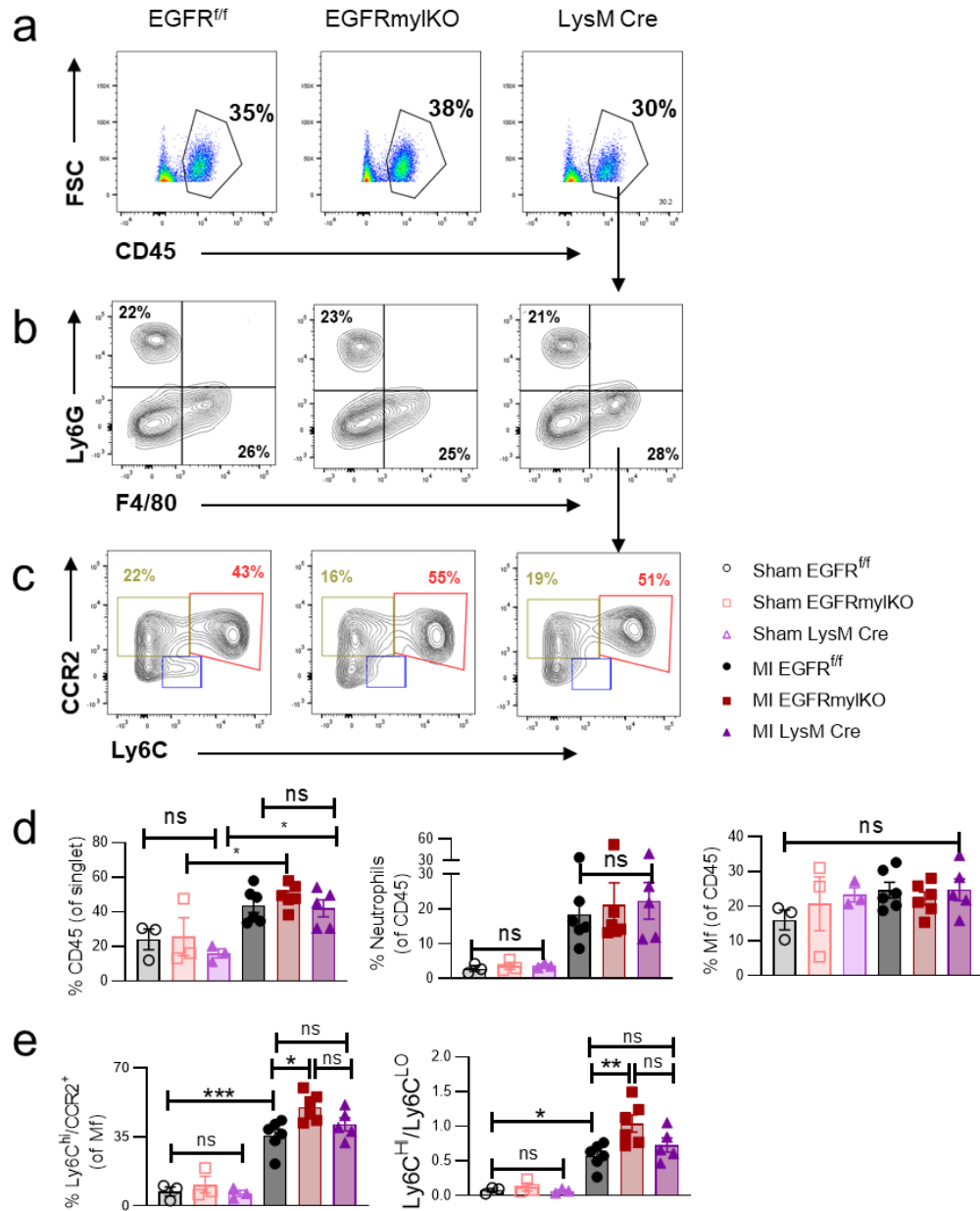


**Figure 31. During the Peak of Acute Inflammation, EGFRmylKO have enhanced Inflammatory Mfs.** Representative flow cytometry plots showing a) live, CD45<sup>+</sup>, b) F4/80<sup>+</sup>, Ly6G<sup>+</sup>, c) Ly6C<sup>+</sup>, CCR2<sup>+</sup>, in the heart 4 days following MI in EGFRmylKO versus EGFR<sup>fl/fl</sup> and Lys M Cre controls. d) Accompanying histogram details flow cytometry gated cell populations: total neutrophils and macrophages (% Mf) at sham, and 4 days pMI. N = 3-8, represented by individual bullets in histogram. ns, not significant using one-way ANOVA with Tukey's multiple comparisons test. e) Ly6C<sup>hi</sup> (percent of mf) and ratio of ly6c hi vs lo Mf were plotted in EGFRmylKO versus EGFR<sup>fl/fl</sup> and Lys M Cre controls at sham, and 4 days pMI. N = 3-8, represented by individual bullets in histogram. ns, not significant using one-way ANOVA with Tukey's multiple comparisons test. \*P<0.05, \*\*P<0.01 ns, not significant using one-way ANOVA with Tukey's multiple comparisons test.

assessed total leukocyte, neutrophil, and mf density, and observed similar myeloid profiles in EGFRmylKO compared to controls (Figure 32a-d). When we further stratified mf for their expression of Ly6C and CCR2, we identified a greater number of inflammatory mf in EGFRmylKO hearts relative to either control group (Figure 32e). This ultimately resulted in a significant increase in the proportion of inflammatory mf in comparison to reparative subsets (Figure 32e). Next, we wondered how TRM in EGFRmylKO and control hearts responded to the injury. Around 7 days post MI, TRM levels begin to rise through proliferation, to account for those lost in the injury (Dick et al., 2019). We analyzed cardiac myeloid cells for their expression of Tim4 to understand if the deletion of myeloid EGFR would impact TRM replenishment. We identified no significant differences in Tim4/CD11b double positive cells in EGFRmylKO hearts at 7 days post MI compared to either control (Figure 33a-b).

Recently, myeloid specific deletion in EGFR was linked to altered lymphocyte inflammatory responses in pathological settings, thus, we assayed for levels of B and T lymphocytes in hearts 7 days following MI (Hardbower et al., 2016). We observed no differences in total CD3-positive T cells in EGFRmylKO hearts compared to controls (Figure 34a-c). Interestingly, in some EGFRmylKO hearts, CD19-positive B cells were slightly elevated relative to either control group, though this difference was not statistically significant (Figure 34a,c).

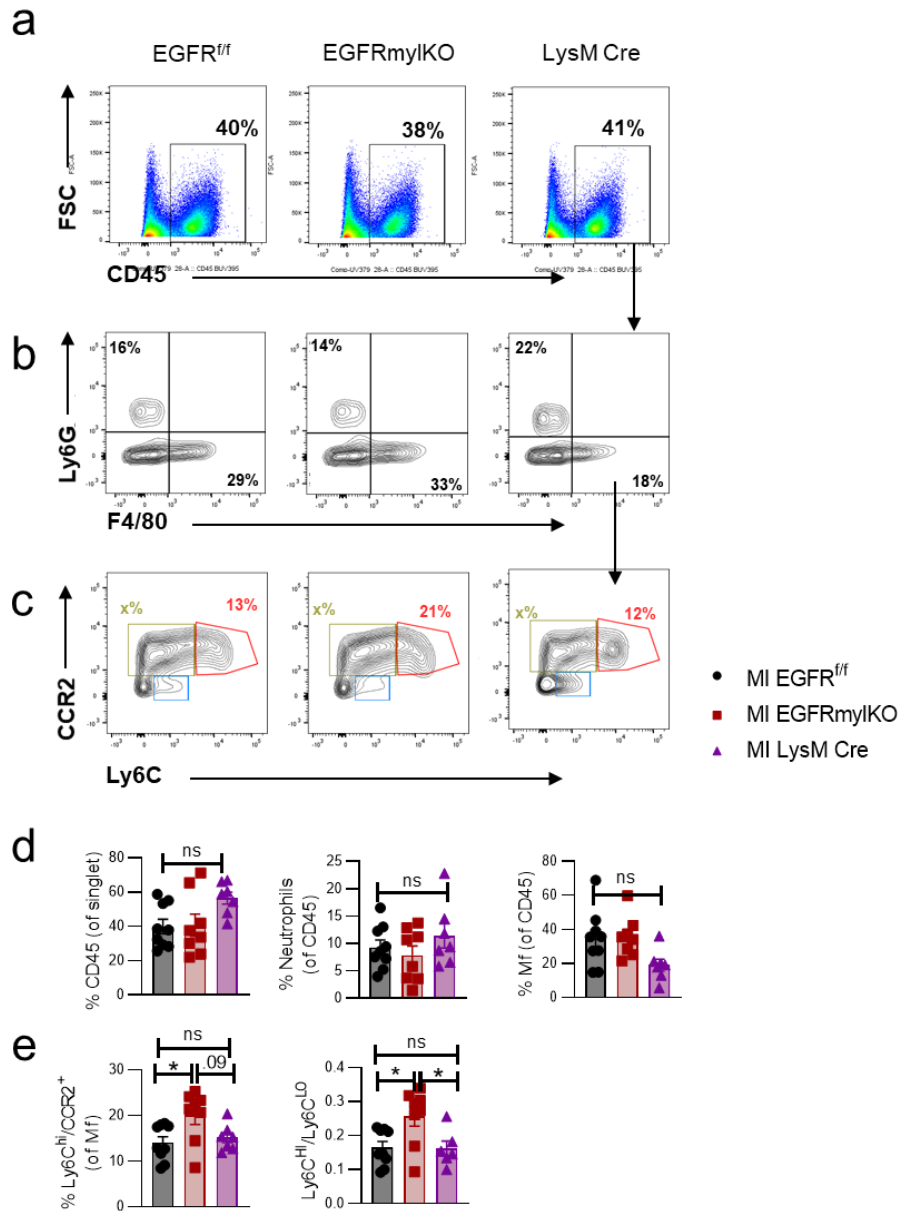


**Figure 32. During Repair & Resolution, EGFRmylKO Hearts Exhibit Reduced Reparative Macrophage Subsets.** Representative flow cytometry plots showing a) live, CD45<sup>+</sup>, b) F4/80<sup>+</sup>, Ly6G<sup>+</sup>, c) Ly6C<sup>+</sup>, CCR2<sup>+</sup>, in the heart 7 days following MI in EGFRmylKO versus EGFR<sup>f/f</sup> and Lys M Cre controls. d) Accompanying histogram details flow cytometry gated cell populations: total leukocytes (% CD45), neutrophils (% NTP), and macrophages (% Mf) at sham, and 7 days pMI. N = 3-8, represented by individual bullets in histogram. ns, not significant using one-way ANOVA with Tukey's multiple comparisons test. e) Ly6C<sup>hi</sup> (percent of mf) and ratio of ly6c hi vs lo Mf were plotted in EGFRmylKO versus EGFR<sup>f/f</sup> and Lys M Cre controls at sham, and 7 days pMI. N = 3-8, represented by individual bullets in histogram. ns, not significant using one-way ANOVA with Tukey's multiple comparisons test. \*P<0.05, \*\*P<0.01 ns, not significant using one-way ANOVA with Tukey's multiple comparisons test.

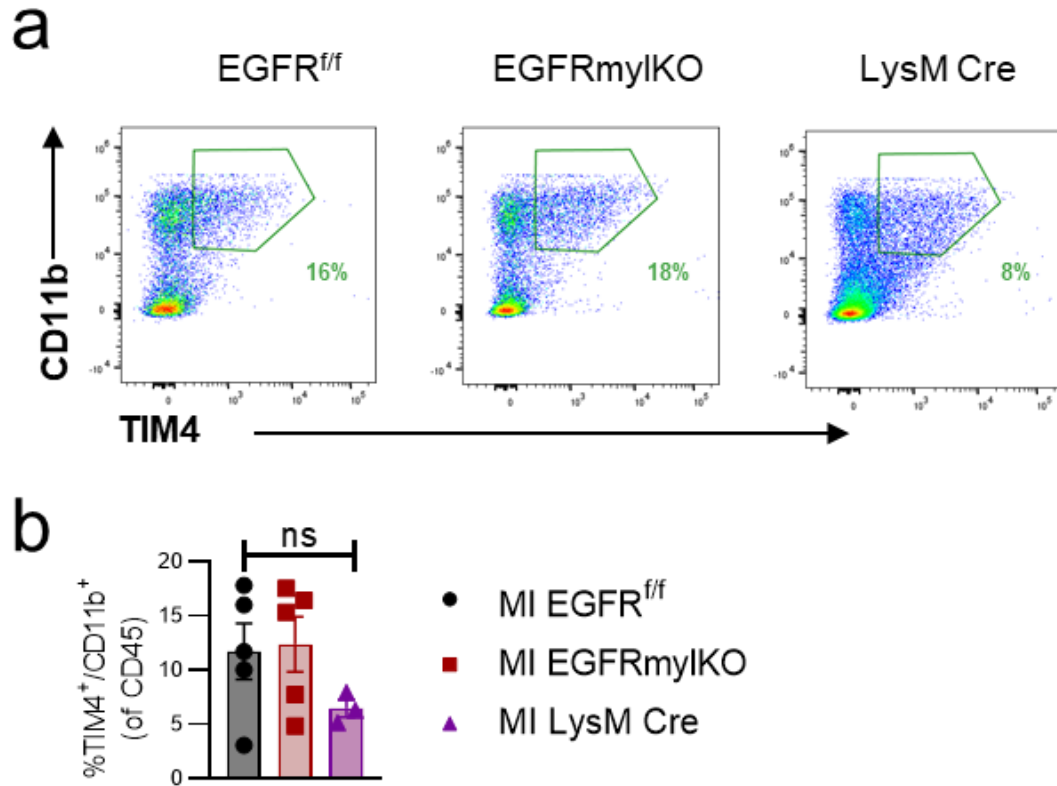


**Figure 33. Deletion of Myeloid-Specific EGFR does not Impact TRM Replenishment 7d pMI.** Representative flow cytometry plots showing live, CD45<sup>+</sup> cells which were stratified for a) CD11b<sup>+</sup> vs TIM4<sup>+</sup> cells in the heart 7 days following MI in EGFRmylKO versus EGFR<sup>f/f</sup> and Lys M Cre controls. b) Accompanying histogram details flow cytometry gated cell populations, and the ratio of live/dead cells. N = 3-5, represented by individual bullets in histogram. \*P<0.05, ns, not significant using one-way ANOVA with Tukey's multiple comparisons test.

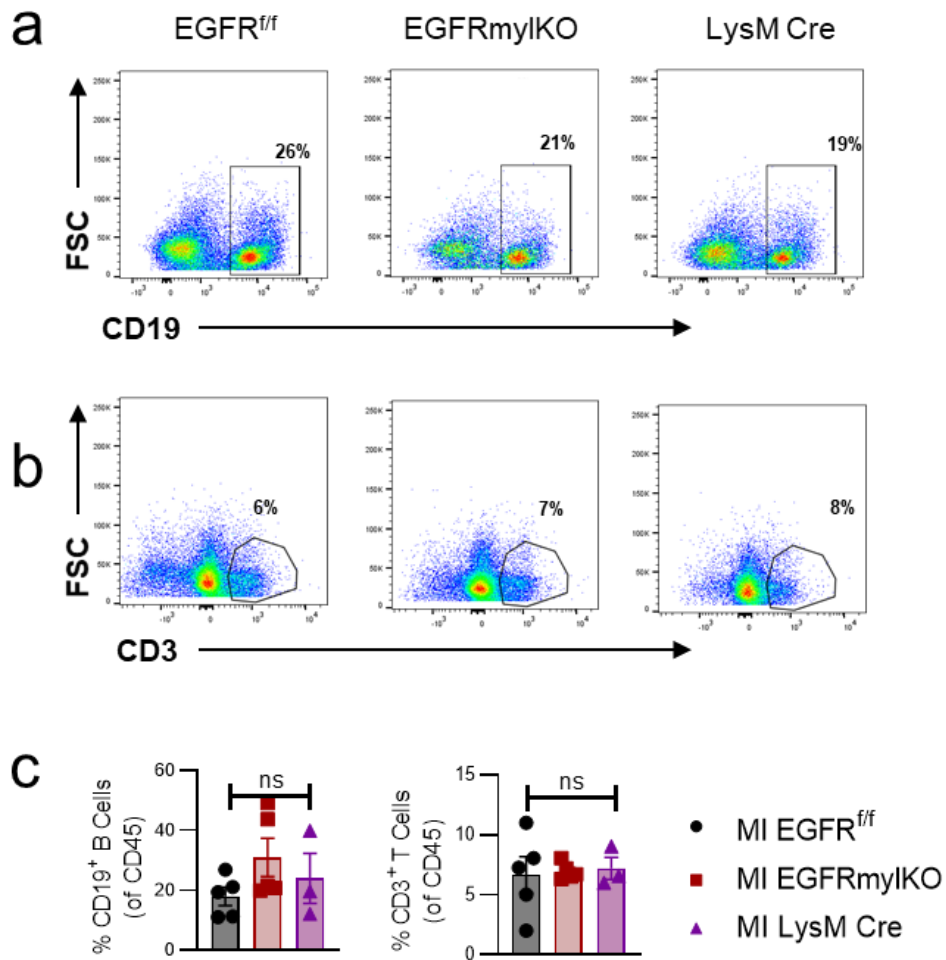


**Figure 34. Deletion of Myeloid-Specific EGFR does not Significantly Impact Lymphocyte Density 7d pMI.** Representative flow cytometry plots showing live, CD45<sup>+</sup> Ly6G<sup>-</sup> F4/80<sup>-</sup> cells which were gated for a) CD19<sup>+</sup>, or b) CD3<sup>+</sup> cells in the heart 7 days following MI in EGFRmylKO versus EGFR<sup>f/f</sup> and Lys M Cre controls. c) Accompanying histogram details flow cytometry gated cell populations. N = 3-5, represented by individual bullets in histogram. \*P<0.05, ns, not significant using one-way ANOVA with Tukey's multiple comparisons test.

In response to an MI, elevated hematopoiesis in the BM and spleen provide a major source of leukocytes to mediate the inflammatory response (Ma et al., 2018). Since EGFRmylKO hearts exhibited more recruited, inflammatory, mon-derived mf, we sought to understand if BM and spleen compartments had elevated inflammatory leukocytes. In total, MI did not significantly change leukocyte or neutrophil levels in the BM at 4 or 7 days (Figure 35a-e). We then looked to characterize CCR2 and Ly6C positive cells in the BM. At 4 days post MI, though they were elevated in MI relative to sham, we observed no differences in these inflammatory cells in EGFRmylKO animals in comparison to controls (Figure 35a-d). By 7 days post MI, this population was not significantly different from sham animals (Figure 35e).

In addition to these findings, we initially observed that control animals had significantly larger spleens, normalized to body weight 7 days post MI (Figure 36a). Following injury, an increase in spleen weight can be indicative of an increase in myelopoiesis (Leuschner et al., 2012; Halade et al., 2018; Loukov et al., 2016). Thus, we similarly assessed levels of inflammation within the spleen in EGFRmylKO animals and controls post MI. We first assessed Il1b transcripts at each timepoint, finding no significant changes in EGFRmylKO spleens (Figure 36b). We then characterized immune cell dynamics. At 4 days post-MI, we identified reduced levels of leukocytes and neutrophils in infarcted spleens, relative to sham (Figure 37a-d). Interestingly, levels of inflammatory CCR2/Ly6C cells were unchanged in sham or infarcted hearts in either control, though in EGFRmylKO spleens, they were significantly reduced post-MI (Figure 37e). By 7 days post-MI, these differences were no longer observed (Figure 37e).

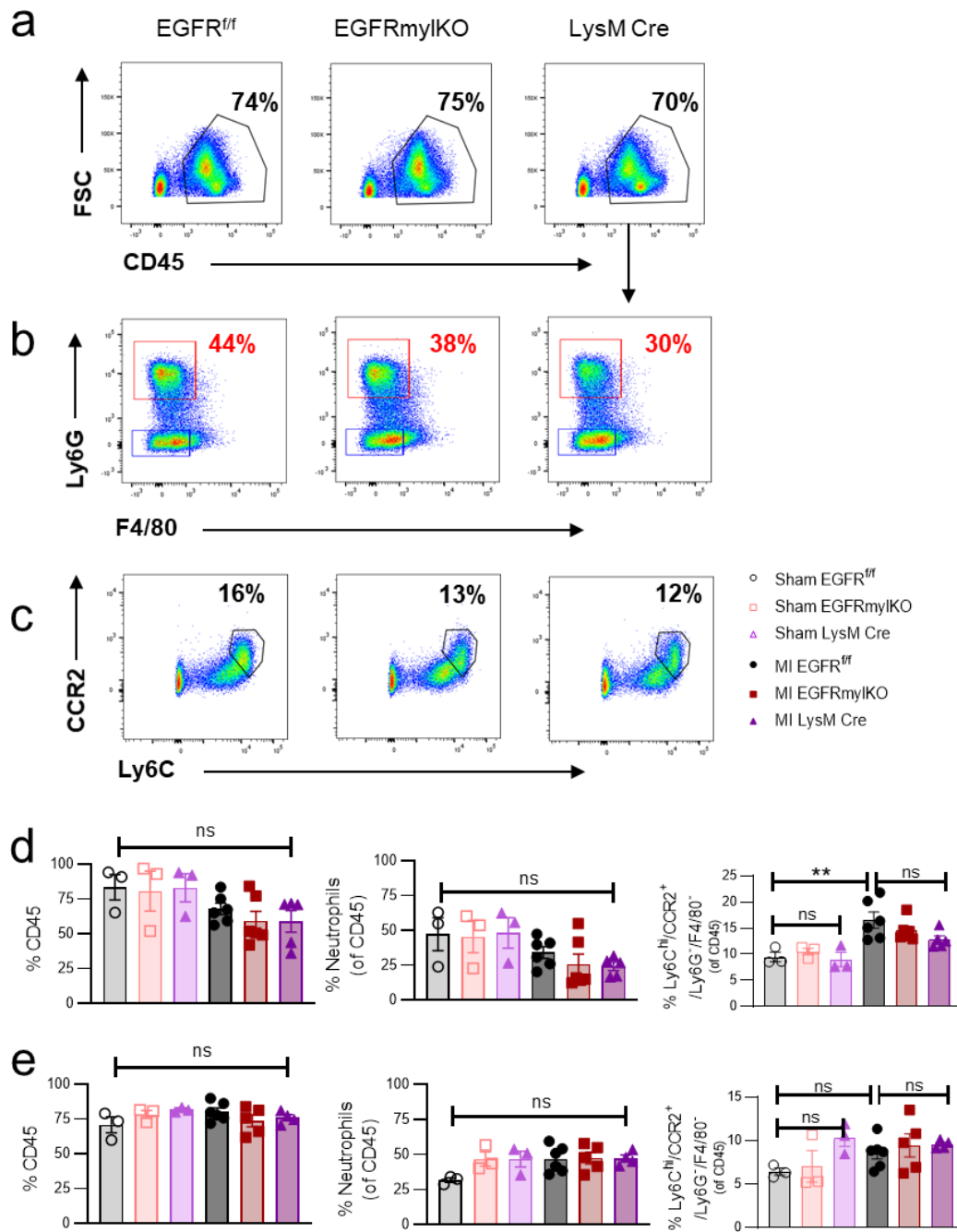


**Figure 35. Following MI, Myeloid-Cell Specific EGFR does not Significantly Impact Leukocyte Density in BM.** Representative flow cytometry plots showing a) live, CD45<sup>+</sup>, b) Ly6G<sup>+</sup>, F4/80<sup>+</sup>, and c) Ly6C<sup>+</sup>, vs CCR2<sup>+</sup>, in the BM following MI in EGFRmylKO versus EGFR<sup>f/f</sup> and Lys M Cre controls. Accompanying histogram details flow cytometry gated cell populations: total leukocytes (% CD45), neutrophils, and inflammatory recruited cells at d) 4, and e) 7 days post sham or MI. N = 3-8, represented by individual bullets in histogram. ns, not significant using one-way ANOVA with Tukey's multiple comparisons test.

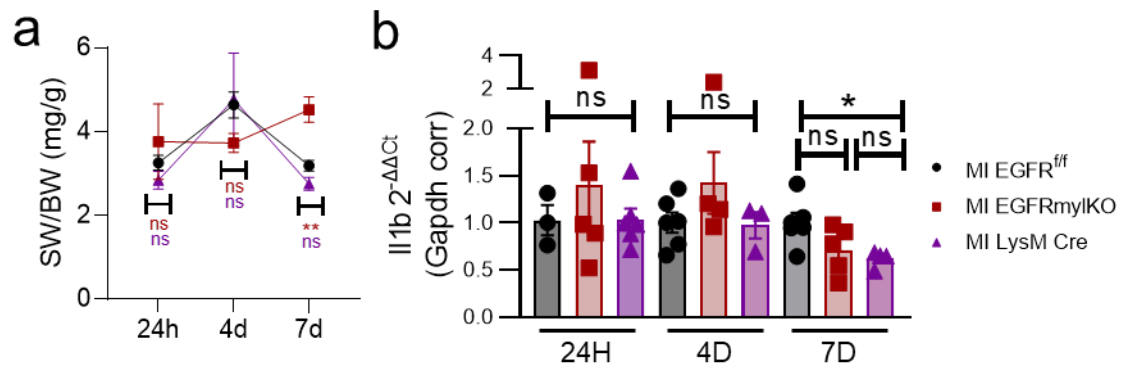


**Figure 36. Following MI, Myeloid-Cell Specific EGFR May Influence Inflammation in the Spleen.** a) Spleen weights from EGFR<sup>mylKO</sup> versus EGFR<sup>f/f</sup> and Lys M Cre controls were normalized to body weights at 24 hr, 4 or 7 days post MI. N = 5-12, \*\*P<0.01, \*\*\*\*P<0.0001 one-way ANOVA with Tukey's multiple comparisons test. b) RT-qPCR was used to measure the expression of *Il1b*, in spleen of post MI EGFR<sup>mylKO</sup> mice and controls, normalized to *Gapdh*. \*P<0.05, one-way ANOVA with Tukey's multiple comparisons test.

Altogether, these data suggest a role for EGFR in regulating inflammatory myeloid dynamics following cardiac injury.

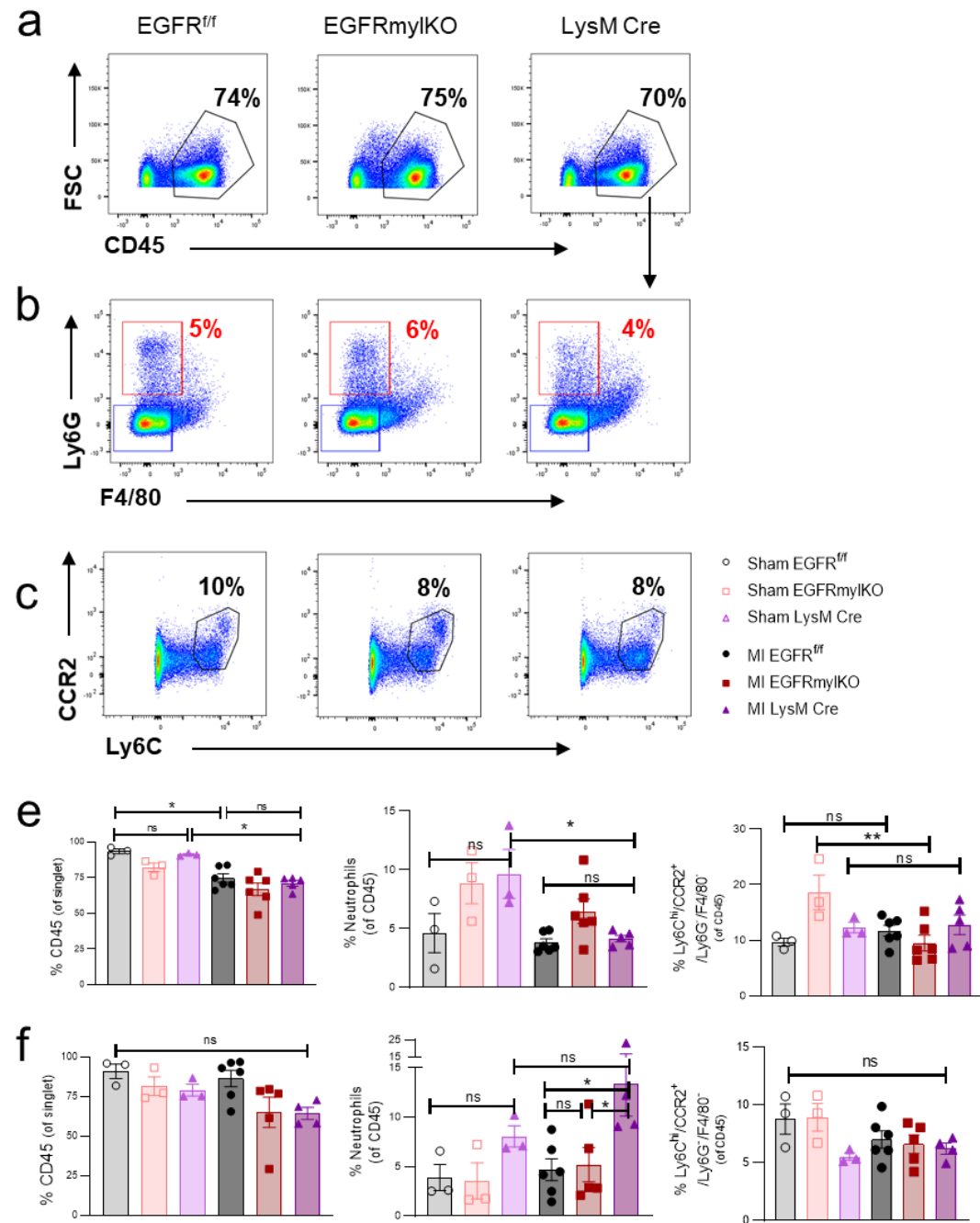


**Figure 37. Following MI, Myeloid-Cell Specific EGFR does not Significantly Impact Leukocyte Density in Spleen.** Representative flow cytometry plots showing a) live, CD45<sup>+</sup>, b) Ly6G<sup>+</sup>, F4/80<sup>+</sup>, c) Ly6C<sup>+</sup>, CCR2<sup>+</sup>, in the spleen 4 and 7 days following MI in EGFRmylKO versus EGFR<sup>f/f</sup> and Lys M Cre controls. Accompanying histogram details flow cytometry gated cell populations: total leukocytes (% CD45), neutrophils, and inflammatory recruited cells at d) 4, and e) 7 days pMI. N = 5-7, represented by individual bullets in histogram. ns, not significant using one-way ANOVA with Tukey's multiple comparisons test.

### 3.10 Myeloid-Cell Specific EGFR Promotes Pro-Repair Myeloid Polarization

Following MI, the distribution of inflammatory or resolving mf heavily informs the level of damage or repair (DeBerge et al., 2021; Mia et al., 2020). During the repair phase of injury resolution, mf gene expression and phenotypes are focused on facilitating scar stabilization, and angiogenesis (Ferraro et al., 2019; Gombozhapova et al., 2017). Since we observed a shift in the mf continuum in EGFRmylKO hearts at 7 days post MI, we investigated mf gene expression during the repair phase. We isolated CD11b cells from infarcted hearts, and confirmed cardiac mf enrichment (Figure 38a-b). The percentage of CD11b cells that were also CD64 positive was lower than basal hearts (95 vs 65) due to the presence of monocytes and neutrophils within infarcted hearts (Figure 32a-d). Post-MI cardiac CD11b cells were then subject to gene expression analyses. We confirmed that even in injury cardiac myeloid cells maintained EGFR deletion (Figure 38c). In EGFRmylKO cells, reduced levels of *Cd206*, *Il10*, and *Vegfa* transcripts were observed relative to control (Figure 38c). Levels of *Angptl4*, and *Cxcl12* remained unchanged (Figure 38c).

Reparative mf rely on the upregulation of signaling networks and TFs like STAT3 in order to mediate their physiological functions (Mouton et al., 2018). EGFR has been shown to engage in crosstalk with these pathways, so we investigated whether EGFR in mf would contribute to anti-inflammatory pathway activation (Zhao G et al., 2016). We isolated and cultured BMDM from control and EGFRmylKO, and stimulated with IL4, a potent inducer of reparative mf polarization (Viola et al., 2019). We confirmed polarization through enhanced expression of arginase 1 (*Arg1*) in treated cells relative to naive cells (Figure 39a) (Viola et al., 2019). Consistent with previous findings, EGFR

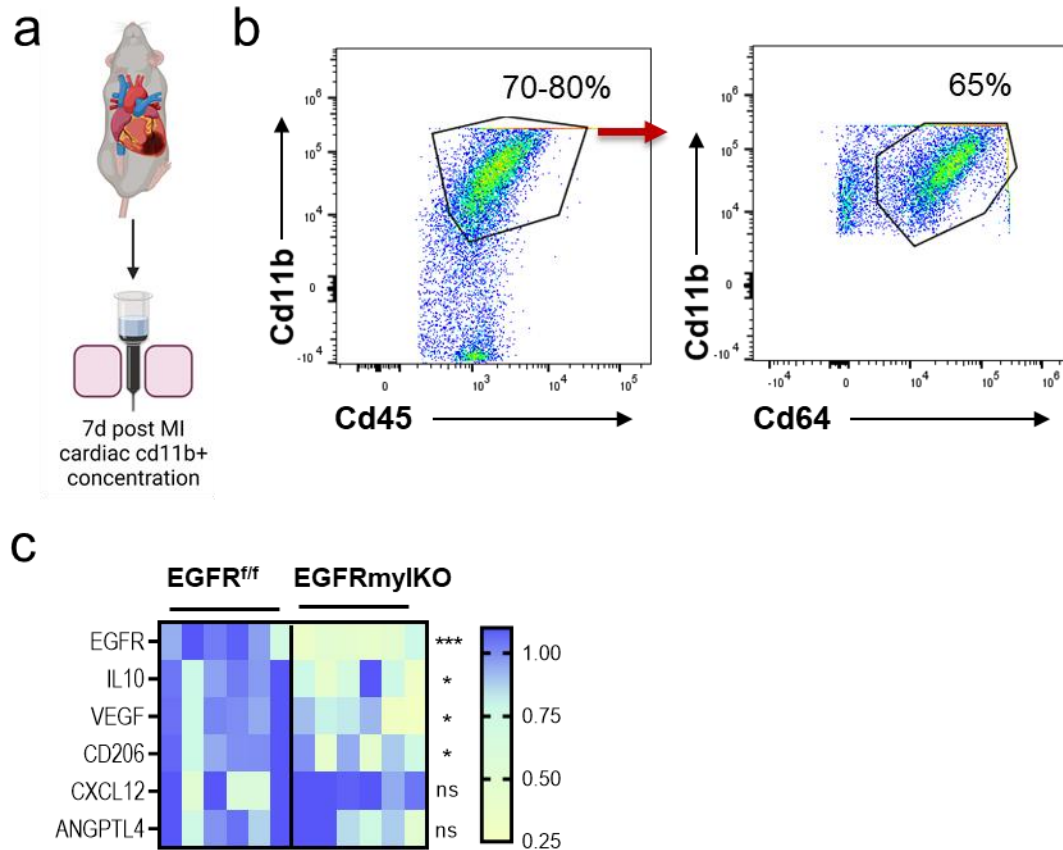


**Figure 38. Myeloid-Cell Specific EGFR Deletion Results in Reduced Expression of Repair Promoting Factors Post Injury.** a) Cardiac non-myocytes were subject to CD11b cell column isolation 7 days following MI. b) 7 days post MI CD11b<sup>+</sup> cells were subject to flow cytometry to verify and estimate cardiac macrophage concentration in isolates from EGFR<sup>fl/fl</sup> vs EGFR<sup>mylKO</sup> hearts using CD45, CD11b, and CD64. c) 7 days post MI, RT-qPCR was used to measure gene expression of *Egfr*, *Cd206*, *Il10*, *Vegfa*, *Angptl4*, *Cxcl12*, and *Gapdh* in cardiac Cd11b<sup>+</sup> cells from EGFR<sup>mylKO</sup>, versus EGFR<sup>fl/fl</sup>. N = 5-6 per group, represented by individual boxes in heatmap. \*\*\*P<0.001, \*P<0.05, ns, not significant using one-way ANOVA with Tukey's multiple comparisons test.

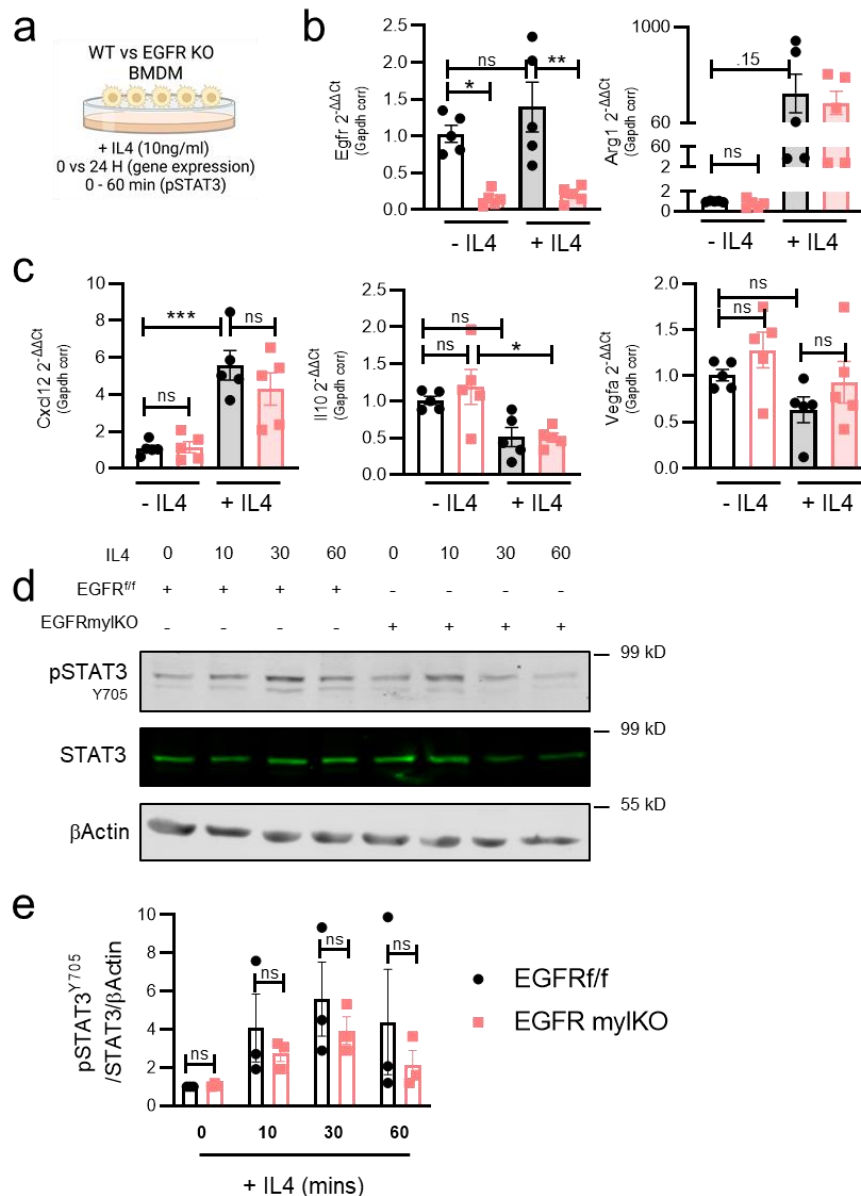


**Figure 39. EGFR Deletion in BMDM May Result in Reduced STAT3 activation following IL4 Induced Polarization.** a) schematic depicting bmdm polarization in vitro. RT-qPCR was used to measure b) *Egfr*, and *Arg1* c) *Vegf*, *Il10*, and *Cxcl12* expression in IL4 treated (24 hr, 10 ng/ml) bmdmf from EGFRmylKO, versus EGFR<sup>f/f</sup>, normalized to Gapdh. N = 5, represented by individual bullets in histogram. \*\*P<0.01, \*\*\*P<0.001, ns, not significant using one-way ANOVA with Tukey's multiple comparisons test. d) Representative immunoblot analysis of STAT3 expression and activation in EGFRmylKO versus EGFR<sup>f/f</sup> IL4 (10 ng/ml) treated bmdm e) Phosphorylated STAT3 (Y705) normalized to total STAT3 and  $\beta$ -Actin expression. N = 3 individual isolations, represented in histogram by individual bullets. ns not significant using one-way ANOVA with Tukey's multiple comparisons test.

deficient BMDM had reduced transcripts of *Arg1* compared to control, though here, this reduction was not significant (Figure 39a). We then sought to determine how EGFR deficiency in BMDM affected transcript levels of *Il10*, *Vegfa*, *Angptl4*, and *Cxcl12* in IL4 treatment. We observed reduced levels of these transcripts, though not to the same degree as in post-MI cells (Figure 39b). Since STAT3 is a major TF regulating the expression of angiogenic cytokines, we examined its activation in control or EGFR deficient BMDM. We observed following IL4 stimulation, an increase in STAT3 phosphorylation in control BMDM (Figure 39C-D). This was slightly reduced in EGFR deficient cells, though not significantly (Figure 39c-d). In total, these findings provide some indication of how EGFR may regulate myeloid and mf phenotypes within the context of injury repair.

**CHAPTER 4**  
**KEY FINDINGS AND SIGNIFICANCE, DISCUSSION, AND FUTURE**  
**DIRECTIONS**

**4.1 Summary and Significance**

In recent years, there has been great interest to understand the intricacies of cardiac mf biology. Through mouse models, this has resulted in defining their origin, characterizing their distribution, and niche, and lastly, uncovering their novel homeostatic functions (Williams et al., 2018). Cardiac mf derive from a combination of embryonic yolk sac precursors, fetal liver precursors, and post natal circulating mon (Alvarez-Argote et al., 2021). Embryonic TRMs develop in a manner independent of myeloblastosis oncogene (c-Myb), a TF critical to hematopoiesis, and renew through proliferation (Schulz et al., 2012; Alvarez-Argote et al., 2021). Mechanisms that contribute to their renewal continue to be investigated, though the activation of ERK1/2 has been shown to be involved in mf proliferation (Sager et al., 2016; Alvarez-Argote et al., 2021). Cardiac mf that develop from circulating mon are maintained through continued recruitment of mon from extramedullary sites, primarily through CCR2 and its chemokine, CCL2 signaling (Alvarez-Argote et al., 2021). EGFR is a growth factor receptor which initiates ERK1/2 activation to enhance cell proliferation (Wee et al., 2017). Here, we identified that the absence of EGFR in mf did not result in significant changes in embryonic mf subsets, marked by Tim4 expression. Further, EGFR deficiency did not lead to alterations in mon derived mf subsets; CCR2 expressing mf were similar across all groups, Figure 40A.

Since TRMs can be identified early during embryogenesis, prior to hematopoiesis, there has been a push to investigate their homeostatic functions, beyond mediating inflammatory events (Williams et al., 2018; Alvarez-Argote et al., 2021). To date, noted TRM functions include, but are not limited to capillary and vascular development, lymphatic vessel growth and maturation, maintenance of cardiac cell turnover, and maintenance of cardiac cell integrity (Leid et al., 2016; Cahill et al., 2021; Nicolas-Avila et al., 2020; Hulsmans et al., 2017). Some identified factors contributing to these processes include IGF1, VEGFC, MERTK, and CX43 respectively (Leid et al., 2016; Cahill et al., 2021; Nicolas-Avila et al., 2020; Hulsmans et al., 2017). Though EGFR is implicated in the regulation of some of these factors, how EGFR contributes to TRM homeostatic function had not been explored (Sakuma et al., 2021; Guo et al., 2021; Zhang et al., 2020). Our findings indicate that EGFR is critical to normal TRM function, and homeostatic roles. In hearts with EGFR-deficient TRM, we observed enhanced stress and inflammation. This was characterized by elevated cm size, enhanced fetal gene transcripts, and an upregulation in stress associated cardiac myeloid cell genes. The shift in cardiac myeloid gene expression included a significant decrease in the expression of *Igfbp5* and *Igfbp7*, both of which have been shown to regulate the activation of cell surface receptors that directly enhance cm growth (Evdokimova et al., 2012; Hwang et al., 2011). In hearts with EGFR deficient TRMs, we also observed enhanced phosphorylation of ERK1/2, a kinase downstream of growth inducing receptors, Figure 40A (Heineke et al., 2006).

In response to injury, like MI, TRMs aid in initiating inflammatory responses, though they are mostly cleared out by ischemia (Dick et al., 2019). To mount an immune

response, resolve injury, and engage repair, circulating CCR2 mon infiltrate injured hearts, differentiating into mf (Prabhu et al., 2016; Swirski et al., 2018). They secrete numerous immune modulators, and are critical to mitigating severe HF outcomes (Adamo (b) et al., 2020; Swirski et al., 2018). As EGFR has been implicated in mediating inflammatory gene programs, we investigated its definitive role in post MI mf function. Here, we show that EGFR is critical to regulating inflammatory responses in injury during acute inflammation and resolution and repair. EGFR deletion in myeloid cells results in enhanced accumulation of inflammatory mf earlier following injury. During resolution and repair, inflammatory mf, relative to resolving mf were much higher in hearts with EGFR deficient mf. This resulted in reduced mf transcripts of *Il10* and *Vegfa*. *Il10* was also significantly reduced in the ventricle, in addition to fewer post injury capillaries. Injured hearts lacking myeloid EGFR also experienced aggravated hypertrophic remodeling. Together, deficient remodeling in these hearts was coupled to systolic dysfunction Figure 40B.

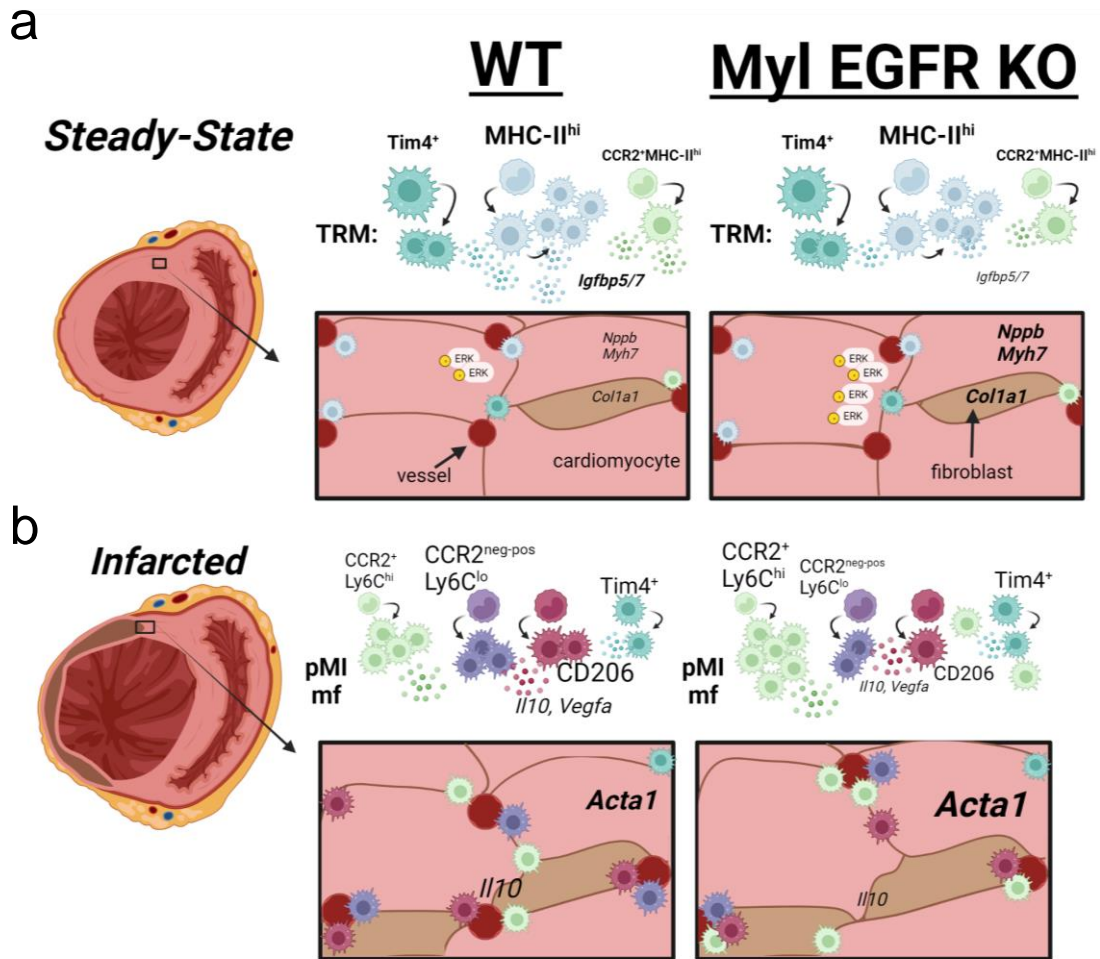


**Figure 40. Summary: Myeloid EGFR in Cardiac Homeostasis and Injury Repair.** a) In steady state, cardiac mf, distributed through the ventricle, can be stratified by expression of MHC-II, Tim4 and CCR2 (orderd by abundance). They express transcripts like Igfbps, which aid in maintaining cardiac homeostasis. The deletion of myeloid EGFR does not shift mf abundance or subtype, but results in differential expression of over 700 transcripts, including Igfbp5/7. These transcriptional changes are accompanied by increased levels of ERK1/2 activation, fetal gene transcripts, collagen, and cell size. b) Following ischemic injury, mf in the heart help promote repair. A deletion of myeloid EGFR increases proinflammatory mf densities, and reduces resolving mf subtypes. This results in reduced repair promoting transcripts, leading to limited injury resolution, and worsened HF outcomes.

## 4.2 Extended Discussion

### *Lys M Cre Strategy:*

HF remains a major public health burden that affects over 6 million Americans; HF leads to a significant amount of hospitalization in US adults, and aggravates healthcare costs in the US (Virani et al., 2021). Currently, there is tremendous interest to uncover the cellular and molecular changes that contribute to HF pathogenesis, especially within the context of inflammation, in order to identify novel, feasible targets against its progression. Cardiac mf have been in focus due to their ability to regulate normal physiology and post injury outcomes (Swirski et al., 2018; Dick et al., 2019). Specifically, a major research goal of the last few years has been to investigate how they contribute to heart health in order to understand if they can be targeted in HF to improve patient outcomes (Williams et al., 2018; Lavine et al., 2018).

Here, we examined if and how EGFR, a critical regulator of cell signaling, contributes to cardiac mf function. To manipulate EGFR in mf, we employed a model of myeloid cell-specific EGFR deletion. *LysM Cre*-mediated EGFR deletion should result in deletion of EGFR within all myeloid cells highly expressing *lyz2* (Shi et al., 2019). Though this model was not exclusive to mf, it provided significant EGFR deletion in cells of interest, namely BMDM and cardiac myeloid cells. Our model also did not result in any significant compensatory changes in EGFR signaling partners, or pathways. In baseline hearts, we identified that the majority of cardiac CD11b-expressing myeloid cells were also positive for CD64, indicating significant mf populations. Targeting deletion in mf specifically can be quite challenging, likely due to shared precursors, and consequently, genes, among many myeloid cells (Shi et al., 2019). Additionally, because

we wanted to evaluate the contribution of EGFR in mon-derived mf, both basally, and following injury, *lyz2* mediated deletion was preferred, over other models like F4/80 Cre (Shi et al., 2019). We did verify EGFR deletion in a subset of BM mon, data not shown.

***EGFR Contribution to Maintenance of TRM Subsets:***

Our first major objective was to determine whether EGFR contributes to TRM maintenance. The current understanding is that mf in the steady-state heart are maintained in part via proliferation, or monocyte recruitment (Zaman et al., 2020; Molawi et al., 2014). To date, very few published studies have addressed TRM renewal mechanisms and dynamics in the steady-state heart (Sansone et al., 2020; Alvarez-Argote et al., 2021; Zaman et al., 2020). Following injury however, when surviving TRM proliferation occurs at more noticeably, ERK1/2 has been shown to be activated, and involved in mf proliferation (Sager et al., 2016). This led us to question the involvement of EGFR in steady state mf maintenance. We examined TRM percentages in control and EGFR-deficient cardiac nonmyocytes, using Tim4, MHC-II, and CCR2 to define populations, and identified no significant changes in TRM subtypes. These findings suggest that EGFR may not play a role in TRM maintenance in adulthood, however, this interpretation requires additional considerations. Namely, though Tim4, and CCR2 are expressed by distinct TRM subtypes, it is not known if over time, expression of these markers can become common across types of mf. An explicit investigation of whether EGFR regulates TRM proliferation or survival is still required. Beyond this, it is also necessary to consider that other factors, like colony stimulating factor 1 (CSF) may play more central roles in mf proliferation, resulting in maintained TRM subsets even in the absence of EGFR (Guilliams et al., 2020).

### ***Myeloid EGFR Contribution to Cardiac Homeostasis***

We then asked if TRM EGFR resulted in any functional changes in TRM, and subsequently cardiac homeostasis. We addressed this objective by first assaying the structure and function of hearts with EGFR-deficient myeloid cells. We identified in these hearts increased CM size, especially when compared to LysM Cre transgenic control hearts. These hearts also exhibited elevated fetal gene transcripts, which were indicative of the development of cardiac hypertrophy (Heineke et al., 2006; Nakamura et al., 2018). Interestingly, we identified a modest increase in collagen 1 gene expression in these hearts, here, it is possible that CM which expand may require additional ECM support (Eguchi et al., 2021; Khalil et al., 2019). We measured cardiac systolic function in these hearts, finding no significant changes. These findings were in line with other studies where pathological hypertrophy does not result in significantly reduced systolic function (Zaman et al., 2021; Eguchi et al., 2021; Nakamura et al., 2018). Together, these data served as an indication that EGFR was critical to normal TRM function, and cardiac homeostasis.

### ***EGFR-Dependent Regulation of Cardiac Myeloid Transcriptome***

To investigate how EGFR deficient myeloid cells resulted in cardiac stress, we chose to examine global myeloid gene expression in control vs EGFR knockout cells. Using total CD11b concentrated cardiac myeloid cells was preferred to understand translational significance. RNAseq analysis highlighted the role of EGFR in regulating an extensive network of genes. We first processed our results through IPA, which clustered several differentially expressed genes into pathways indicating the contribution of myeloid EGFR to regulating the link between innate and adaptive immunity.

Surprisingly, some of the most upregulated genes from EGFR lacking cells were immunoglobulin heavy and light chain subunits and complement factors. Additionally, EGFR-deficient myeloid cells more highly expressed markers of activated, or stressed mf (Huang et al., 2014; Fuchs et al., 2018; Dick et al., 2019). Together, these suggested the enhanced inflammatory nature of EGFR-deficient cells, where notably, there was significantly enhanced expression of chemokines and cytokines including *Il12*. This also included an upregulation of chemokines like *Cxcl13*, important in lymphocyte recruitment and maturation (Carlsen et al., 2004). B cells are the second largest class of immune cells in the steady-state heart, and interestingly, have also been shown to regulate CM size (Adamo (a) et al., 2020). Their depletion has been shown to result in decreased CM size and increased cardiac function in baseline hearts (Adamo (a) et al., 2020). Whether B cell densities are elevated in response to myeloid EGFR deletion remains to be determined. Though we cannot definitively rule out their contribution to gene expression patterns identified in RNAseq experiments, due to the expression of Cd11b in a subset of B cells, LysM Cre GFP reporter studies have revealed miniscule expression in B cells (Kantor et al., 1992; McCubbrey et al., 2017). As such, elevated cardiac hypertrophy, and altered Cd11b gene expression is most likely the result of the loss of EGFR in TRM and cardiac myeloid subsets.

Next, a sizable number of differentially expressed genes from EGFR knockout myeloid cells were clustered by IPA into pathways related to coronary development, maturation, vasculogenesis, and angiogenesis. This was of interest to us, given cardiac mf roles in coronary development (Leid et al., 2016). Hearts with EGFR deficient mf did not have significant alterations in capillary density, though it remains to be determined how

the loss of EGFR in these mf regulates global coronary development, and vascular morphology through adulthood. Further, it still remains unclear how long-term inhibition of vasculogenic factors in EGFR-deficient mf will impact endothelial function, angiogenesis, and adaptation in hypertrophied hearts, though, we predict that over time EGFRmylKO hearts may experience increased signs of stress (Gogiraju et al., 2019).

EGFR has been linked to regulating Cx43, and in our EGFR knockout myeloid cells, Cx43 levels were significantly reduced (Sakuma et al., 2021; Guo et al., 2021). Mf Cx43 has been studied in the context of regulating CM membrane potential, and may contribute to normal conduction mechanisms in the heart, but connexin gap junction proteins are involved in a number of other cell processes. Connexins allow intercellular communication through the transfer of ions and other signaling molecules (Rodjakovic et al., 2021). The role of mf Cx43 in regulating other CM or cardiac cell function is still unexplored, but its reduction in EGFR-deficient myeloid cells could contribute to enhanced stress in basal hearts (Rodjakovic et al., 2021).

Recent works highlight TRM expression of IGFBP4, and implicate its reduction in the initiation of AngII mediated hypertrophy (Zaman et al., 2021). Here, IGFBP4 is posited to act as a negative regulator of IGF1, with its reduction resulting in enhanced IGF1/IGF1R activation (Zaman et al., 2021). Though *Igfbp4* was not significantly reduced in EGFR deficient myeloid cells, we observed significant reductions in *Igfbp 5* and *7* which similarly impact growth factor (IGF1R) and cytokine (TNFR1) signaling (Evdokimova et al., 2012; Hwang et al., 2011). Specifically, IGFBP7 has been shown to directly interact with IGF1R, therefore impeding IGF1-mediated activation (Evdokimova et al., 2012). Similarly, IGFBP5 has been shown to compete with TNFa for TNFR1

binding, resulting in reduced TNFR1 activation (Hwang et al., 2011). Based on these functions, we propose a working model where reduced myeloid Igfbp transcripts may result in enhanced signaling in neighboring CM. To critically consider this model, we first assayed cardiac non-myocytes, depleted of all myeloid cells for expression of *Igfbp 5* and *7*, finding much lower levels than in myeloid cells (data not shown). These results suggested that myeloid cells are a large source of IGFBP5 and 7 in the adult myocardium. IGFBP protein levels of secretion in EGFRmylKO hearts still remains to be determined. We then assayed hearts for activation of hypertrophy associated pathways downstream of IGF1R and TNFR1, these included AKT and the MAPK cascade of kinases (Fernandez et al., 2021; Sabio et al., 2014; Miao et al., 2020). We identified enhanced ERK1/2 phosphorylation in EGFRmylKO hearts. These findings suggest enhanced signaling in EGFRmylKO hearts, though it is not yet established exactly how reduced IGFBP leads to these outcomes, and whether these changes in ERK1/2 activation can be attributed to CM signaling. Whether reduced IGFBPs result in enhanced CM IGF1R or TNFR1 signaling in CM is still being elucidated. Further, which signaling mechanism and pathway is most contributing to hypertrophic phenotypes observed in EGFRmylKO hearts remains to be determined.

### ***Does Myeloid EGFR Regulate Cardiac Ageing***

Mouse models of TRM distribution and subtype have indicated that they begin to change with age (Dick et al., 2022; Alvarez-Argote et al., 2021; Hulsmans et al., 2018). A recent study has examined all TRM subsets at up to 52 weeks of age in mice, and CCR2<sup>mf</sup> appear to increase in age (Dick et al., 2022). This is further supported by 2 additional studies that show decreased CX3CR1, or increased CCR2<sup>mf</sup> with ageing (Molawi et al.,

2014; Hulsmans et al., 2018). During aging, mice experience increased LV mass, and a decline in diastolic dysfunction. Though how mf, and a change in mf distribution contributes to this is still being explored. We questioned whether mf EGFR would play a significant role in functional or structural parameters in aged hearts. Echocardiography analyses suggested comparable increases in total LV mass in either group, with similar LV dilation. These results suggest myeloid EGFR may not play a role in typical features seen during physiological ageing. How myeloid EGFR deletion alters CM size and TRM subsets at this aged timepoint still remains unknown.

### ***Myeloid EGFR Regulates Myeloid Inflammation in the Infarcted Heart***

In our study, we observed that the loss of myeloid expressed EGFR was of grave detriment to injured hearts, and resulted in enhanced inflammation, limited repair, and ultimately decreased systolic function. Earlier works have examined the role of myeloid and mf EGFR in the development of colitis and colitis-associated cancer (Srivatsa et al., 2017; Hardbower et al., 2017). These studies highlight the complex and context-dependent nature of myeloid EGFR in disease pathology. For example, myeloid EGFR has been shown to be protective against the development of colitis, though it has also been shown to enhance tumor burden in colon cancer (Srivatsa et al., 2017; Hardbower et al., 2017). Here, in response to a model of colitis, mice lacking myeloid EGFR experience a significant decline in body weight, accompanied with severe colon inflammation (Srivatsa et al., 2017). In this model, EGFRmylKO colons exhibit increased percentages of CD45<sup>+</sup> leukocytes, Ly6C<sup>hi</sup> monocytes, and Ly6G neutrophils (Srivatsa et al., 2017). However, tumor burden in colitis associated cancer is reduced in mice lacking myeloid EGFR (Srivatsa et al., 2017; Hardbower et al., 2017). It is plausible that at the

onset of colitis development, myeloid cell-expressed EGFR may promote the production of cytokines and growth factors that protect the colon epithelium, thereby limiting continued inflammatory responses. However, once colons begin to develop tumors, growth factors produced in response to myeloid EGFR activation can enhance tumor growth and burden.

This complexity in disease outcomes observed with EGFR-deficient myeloid cells also extends to cardiovascular related injuries. Here, it is important to consider a recent study looking to understand the role of macrophages in systemic injury, and injury complications secondary to MI. This study identifies that in response to MI, alveolar and interstitial lung mf levels rise, peaking between 1 and 4 days post MI, and declining thereafter (Hoyer et al., 2019). This rise in mf levels can be attributed to enhanced proliferation (alveolar mf) or recruitment (interstitial mf), and is accompanied by significant transcriptional changes at 4 days post MI, reflecting for instance, enhanced proliferation (Hoyer et al., 2019). Specifically, MI results in an upregulation of EGFR in alveolar lung mf. To understand if this increase in EGFR might regulate inflammatory outcomes in the case of secondary complications, mice lacking myeloid EGFR were subject to MI, then 4 days after, bacterial pneumonia (Hoyer et al., 2019). In this context, myeloid EGFR deletion resulted in improved survival in pneumonia following MI (Hoyer et al., 2019). Lungs from EGFRmylKO animals exhibited lower levels of inflammatory cytokines like *Il1b* and *Tnfa*, accompanied with lower neutrophils, but significantly elevated alveolar mf (Hoyer et al., 2019). Similar analyses of inflammatory cytokines in MI and pneumonia injured interstitial mf revealed EGFR deletion had no impact, and in pneumonia alone, EGFR deletion did not change inflammatory cytokine levels in alveolar

mf (Hoyer et al., 2019). These findings suggest that EGFR-dependent regulation of inflammation in myeloid subsets is not uniform, and can result in distinct cell phenotypes, and ultimately, disease outcomes.

Given these previous findings we chose to characterize inflammatory responses in the heart post MI at 3 distinct phases. Recent studies have shown early mf phagosome activities can heavily influence post-injury repair (DeBerge et al., 2017; Dehn et al., 2018). IPA analyses from cardiac myeloid cells deficient in EGFR highlighted significant reductions in transcripts involved in phagosome formation. We reasoned that this may result in improper clearance of dying CM 24 hours post-MI. When we assessed levels of apoptotic CM at this time, we didn't observe any differences. This could point to compensatory mechanisms in EGFR-deficient myeloid cells, allowing them to still clear dead cells at this point in injury. Though we did not directly examine the phagocytic activity of EGFRmylKO mf, they have been shown to not significantly regulate bacterial phagocytosis (Hardbower et al., 2016). Unsurprisingly, we then observed similar levels of neutrophils in blood and infarcts at this timepoint. We quantified inflammatory monocytes at the peak of inflammation, 4 days following MI, finding greater percentages in EGFRmylKO hearts, especially relative to EGFR<sup>f/f</sup> controls. The enhanced presence of inflammatory monocytes in EGFRmylKO hearts continued 7 days into the injury. At this time, resolving mf subsets initiate transcriptional programs to stabilize cardiac repair (Mouton et al., 2018). To understand the level of inflammatory and resolving mf, we stratified mf by Ly6C, and observed a greater number of high expressing Ly6C cells relative to low in EGFRmylKO hearts. Though we recognize mf phenotypes and functions can exist beyond this paradigm, it allows us to draw initial conclusions about

how EGFR regulates mf polarization, and is also still accepted in the literature (Nicolas-Avila et al., 2020; Glington et al., 2022). We also quantified levels of Tim4 myeloid cells at this timepoint during injury. The dynamics of this resident mf subset following injury are still being understood, but is thought to be dependent on proliferation, which begins around 2-4 days post MI (Dick et al., 2019). Our results here suggest that EGFR is not critical to the initial proliferative burst in this mf subset.

Since we saw increased levels of recruited inflammatory cells, we sought to understand their source. We first examined BM and spleen to understand if myeloid EGFR deletion would result in a greater number of monocytes in response to injury. Here, we observed that MI resulted in an increase in these cells in the BM relative to sham only at 4 days, though there was no difference in EGFRmylKO animals. Though we observed elevated spleen weights in EGFRmylKO 7 days following MI, analyses of *Il1b* transcripts or inflammatory monocytes did not reveal any post-MI EGFR-dependent changes. We did not assay blood for levels of inflammatory monocytes, or extensively check cell death and survival in post MI recruited mf, making it difficult to conclude the reason for elevated recruited, inflammatory mf in EGFRmylKO hearts. This can be further explored, along with a more robust analysis of myelopoiesis in EGFRmylKO spleens or BM post MI.

### ***Myeloid EGFR Regulates Myeloid Polarization in the Infarcted Heart***

In injured hearts, we observed significantly reduced transcripts of *Il10* in EGFR deficient cardiac myeloid cells, and EGFRmylKO left ventricles. These findings were consistent to prior studies showing reduced levels of *Il10* and *Vegfa* in anti-inflammatory polarized EGFR deficient mf (Hardbower et al., 2017). Recently, RNAseq analyses have

shown that day 7 post-MI mf more highly express TF like STAT3 to enhance transcription of cytokines and growth factors that favor cardiac repair (Mouton et al., 2018). Since we observed reduced repair associated transcripts in EGFRmylKO post-MI cardiac myeloid cells at this timepoint, we wondered whether EGFR was important to this pathway. We investigated the contribution of EGFR to this pathway using a more traditional model of anti-inflammatory mf polarization: IL4 stimulation (Ying et al., 2013). We observed enhanced M2 mf polarization in IL4-treated control or EGFR deficient BMDM, indicated by increased levels of *Arg1* (Viola et al, 2019; Ying et al., 2013). EGFR KO mf have been reported to produce less *Arg1* in these conditions, and though our experiments suggested that the differences were not significant (Hardbower et al., 2016). These mf did not phenocopy EGFR KO myeloid cells post-MI, and no significant changes in STAT3 activation were observed between control and KO IL4 stimulated BMDM. Although EGFR has been reported to be transactivated by IL4, these data indicate that mf polarization in culture cannot appropriately recapitulate inflammatory events occurring post-MI (Zhao G et al., 2016; Lu et al., 2014). It is also important to consider that the large scope of gene programs and protein pathways that change in IL4-treated cells within a 24 hour period cannot be fully predicted, especially in the absence of EGFR (He et al., 2021). As a result, to fully examine mechanistically how myeloid EGFR contributes to post-MI inflammatory phenotypes, it may be necessary to consider mf polarization in response to more translationally relevant models. For example, assessing mf activation and changes in transcription during efferocytosis by coculture with apoptotic cells might be more indicative of EGFR dependent signaling in post MI (Glinton et al., 2022).

### ***Translational Perspectives: Myeloid EGFR Promotes Healing in the Infarcted Heart***

Our study emphasizes the significant roles that mf play in cardiac repair, and in contributing to HF outcomes and severity. Interestingly, it was recently identified that in HF patients receiving an LVAD, improved systolic function, as measured by EF, was associated with having a lower percentage of CCR2<sup>+</sup> mf in the myocardium, both pre- and post-LVAD implantation (Bajpai et al., 2018). EGFRmylKO hearts experienced worse cardiac function following injury, here, mice lost a greater percentage of systolic function in comparison to either control group. This decline in cardiac function was accompanied with aggravated remodeling. Specially, the loss of myeloid EGFR resulted in limited angiogenesis and excessive hypertrophic growth. These findings suggest that mf, and mf EGFR may be critical in HF outcomes. Long-term consequences post-MI in EGFRmylKO hearts still remain to be determined. Additionally, how mf EGFR may regulate nonischemic models of HF are still not understood. Further, because myeloid EGFR deletion results in elevated stress in hearts before injury, it is important to understand how myeloid EGFR deletion purely after injury may impact HF outcomes.

#### **4.3 Future Directions**

Altogether, our study indicates myeloid expressed EGFR as a critical regulator of cardiac homeostasis and post injury repair. Considering our findings, there are additional questions to be answered. First, it is critical to understand through what mechanisms EGFR regulates Igfbp 5 and 7 transcript levels in cardiac myeloid cells. Next, do decreased levels of Igfbp 5 and 7 in EGFR deficient mf result in enhanced hypertrophic signaling in CM? Preliminary evidence might suggest this to be the case, though whether this is dependent on TNFR1 or IGFR1R still remains to be determined. Using BMDM,

which produce IGF1 and IGF1R (Figure 41a), we have preliminarily established a model where exposing NRVM to conditioned media from mf may enhance phosphorylation of AKT and ERK comparable to direct activation of IGF1R for instance (Figure 41b). Whether EGFR deficient mf would produce an even stronger response can be explored in the future. Additionally, understanding explicitly how mf EGFR contributes to ageing and senescence is a required future direction. For instance, does EGFR deletion in this model of cardiac stress similarly result in a greater percentage of CCR2 inflammatory cells? If so, is this unique to heart muscle, or are these changes global, resulting in a multi organ shift in mf distribution. Lastly, it is important to understand how EGFR deletion disturbs the post MI mf equilibrium. Studies point to mitochondrial bioenergetic flux as a major contributor to mf phenotypes, and EGFR has been shown to influence mitochondrial oxygen consumption rates (OCR) (Zhang et al., 2019; Huang et al., 2020). Interestingly, EGFR-deficient BMDM treated with lipopolysaccharide (LPS) or IL4 display altered OCR in comparison to control (Figure 42). It would be meaningful to understand if this is reflected in post-MI mf, and whether this contributes to the shift in mf phenotypes post MI. Addressing these outstanding questions would help to uncover a complete understanding of myeloid EGFR in the regulation of cardiac homeostasis and injury repair.

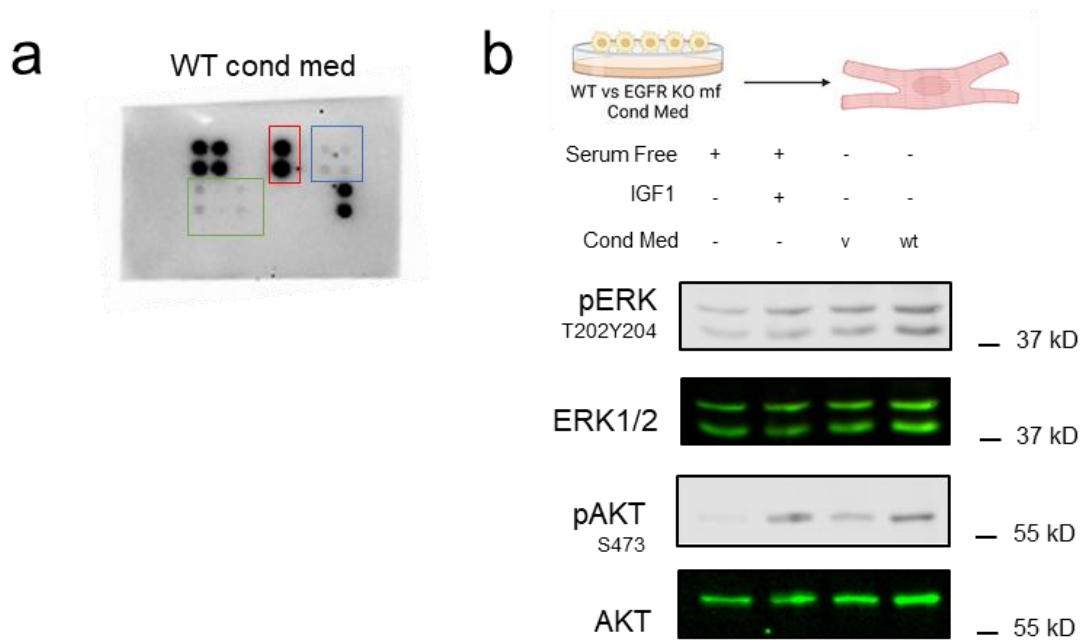


**Figure 41. Mf Secretome May Enhance Growth Factor Signaling in NRVMs.** a) Representative antibody array showing levels of Igf1 (red), Igfbp1, Igfbp2 (blue), Igfbp3, Igfbp5, Igfbp6, and Igfbp7 (green) from BMDM of EGFR<sup>f/f</sup> control. b) Immunoblot showing levels of total AKT, pAKT at serine 473, and total ERK 1/2, pERK 1/2 at threonine 202/tyrosine 204 in NRVM incubated for 2h with serum free (plus or minus 5 ng/ml Igf1 for 10 min), or 5% fbs in rpmi (v), or 5% fbs in rpmi exposed to wt bmdm for 48H.

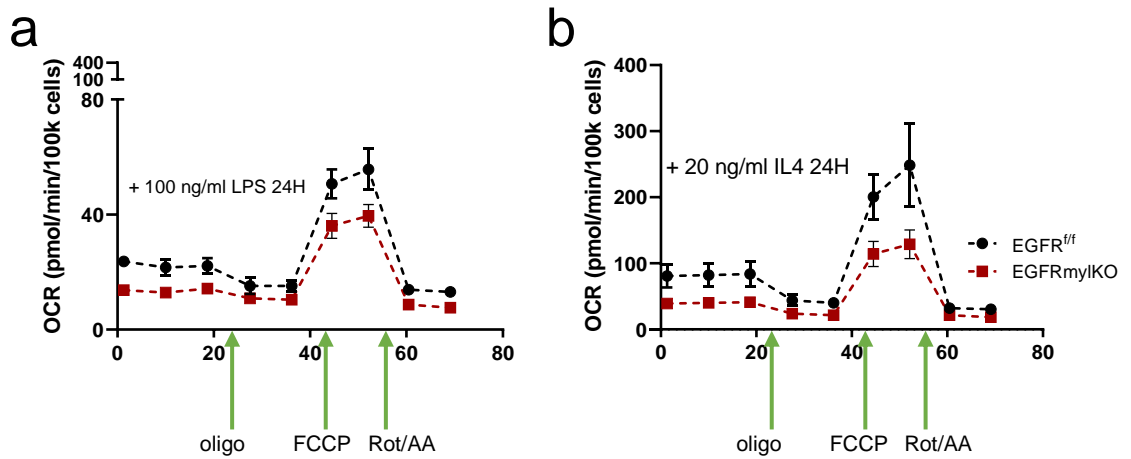


**Figure 42. EGFRmylKO Mf Display Altered OCR In Response to LPS or IL4, Relative to Control.** Day 6 bmdm were seeded at 100,000, and treated with a) 100 ng/ml LPS or b) 20 ng/ml IL4 for 24 hours. Bmdm were then subject to mitochondrial stress tests using the seahorse XF96 analyzer. 3 basal readings were recorded, then cells were subject to oligomycin (1ug/ml), FCCP (1uM), and rotenone (Rot)/antimycin a (AA) (1uM/20uM).

## REFERENCES CITED

Abram, C. L., Roberge, G. L., Hu, Y., & Lowell, C. A. (2014). Comparative analysis of the efficiency and specificity of myeloid-Cre deleting strains using ROSA-EYFP reporter mice. *J Immunol Methods*, 408, 89-100. <https://doi.org/10.1016/j.jim.2014.05.009>

Adamo (a), L., Rocha-Resende, C., Lin, C. Y., Evans, S., Williams, J., Dun, H., . . . Mann, D. L. (2020). Myocardial B cells are a subset of circulating lymphocytes with delayed transit through the heart. *JCI Insight*, 5(3). <https://doi.org/10.1172/jci.insight.134700>

Adamo (b), L., Rocha-Resende, C., Prabhu, S. D., & Mann, D. L. (2020). Reappraising the role of inflammation in heart failure. *Nat Rev Cardiol*, 17(5), 269-285. <https://doi.org/10.1038/s41569-019-0315-x>

Allard, J. B., & Duan, C. (2018). IGF-Binding Proteins: Why Do They Exist and Why Are There So Many? *Front Endocrinol (Lausanne)*, 9, 117. <https://doi.org/10.3389/fendo.2018.00117>

Alvarez-Argote, S., & O'Meara, C. C. (2021). The Evolving Roles of Cardiac Macrophages in Homeostasis, Regeneration, and Repair. *Int J Mol Sci*, 22(15). <https://doi.org/10.3390/ijms22157923>

Andronic, A. A., Mihaila, S., & Cinteza, M. (2016). Heart Failure with Mid-Range Ejection Fraction - a New Category of Heart Failure or Still a Gray Zone. *Maedica (Bucur)*, 11(4), 320-324.

Azevedo, P. S., Polegato, B. F., Minicucci, M. F., Paiva, S. A., & Zornoff, L. A. (2016). Cardiac Remodeling: Concepts, Clinical Impact, Pathophysiological Mechanisms and Pharmacologic Treatment. *Arq Bras Cardiol*, 106(1), 62-69. <https://doi.org/10.5935/abc.20160005>

Bai, B., Yang, W., Fu, Y., Foon, H. L., Tay, W. T., Yang, K., . . . Wang, Y. (2019). Seipin Knockout Mice Develop Heart Failure With Preserved Ejection Fraction. *JACC Basic Transl Sci*, 4(8), 924-937. <https://doi.org/10.1016/j.jacbts.2019.07.008>

Bajpai, G., Bredemeyer, A., Li, W., Zaitsev, K., Koenig, A. L., Lokshina, I., . . . Lavine, K. J. (2019). Tissue Resident CCR2- and CCR2+ Cardiac Macrophages Differentially Orchestrate Monocyte Recruitment and Fate Specification Following Myocardial Injury. *Circ Res*, 124(2), 263-278. <https://doi.org/10.1161/CIRCRESAHA.118.314028>

Bajpai, G., Schneider, C., Wong, N., Bredemeyer, A., Hulsmans, M., Nahrendorf, M., . . . Lavine, K. J. (2018). The human heart contains distinct macrophage subsets with

divergent origins and functions. *Nat Med*, 24(8), 1234-1245.  
<https://doi.org/10.1038/s41591-018-0059-x>

Barrick, C. J., Roberts, R. B., Rojas, M., Rajamannan, N. M., Suitt, C. B., O'Brien, K. D., . . . Threadgill, D. W. (2009). Reduced EGFR causes abnormal valvular differentiation leading to calcific aortic stenosis and left ventricular hypertrophy in C57BL/6J but not 129S1/SvImJ mice. *Am J Physiol Heart Circ Physiol*, 297(1), H65-75.  
<https://doi.org/10.1152/ajpheart.00866.2008>

Barrick, C. J., Yu, M., Chao, H. H., & Threadgill, D. W. (2008). Chronic pharmacologic inhibition of EGFR leads to cardiac dysfunction in C57BL/6J mice. *Toxicol Appl Pharmacol*, 228(3), 315-325. <https://doi.org/10.1016/j.taap.2007.12.012>

Bergmann, O., Zdunek, S., Felker, A., Salehpour, M., Alkass, K., Bernard, S., . . . Frisé, J. (2015). Dynamics of Cell Generation and Turnover in the Human Heart. *Cell*, 161(7), 1566-1575. <https://doi.org/10.1016/j.cell.2015.05.026>

Blanton, R. M., Carrillo-Salinas, F. J., & Alcaide, P. (2019). T-cell recruitment to the heart: friendly guests or unwelcome visitors? *Am J Physiol Heart Circ Physiol*, 317(1), H124-H140. <https://doi.org/10.1152/ajpheart.00028.2019>

Brand, T. M., Iida, M., Luthar, N., Starr, M. M., Huppert, E. J., & Wheeler, D. L. (2013). Nuclear EGFR as a molecular target in cancer. *Radiother Oncol*, 108(3), 370-377.  
<https://doi.org/10.1016/j.radonc.2013.06.010>

Buijttendijk, M. F. J., Barnett, P., & van den Hoff, M. J. B. (2020). Development of the human heart. *Am J Med Genet C Semin Med Genet*, 184(1), 7-22.  
<https://doi.org/10.1002/ajmg.c.31778>

Burchfield, J. S., Xie, M., & Hill, J. A. (2013). Pathological ventricular remodeling: mechanisms: part 1 of 2. *Circulation*, 128(4), 388-400.  
<https://doi.org/10.1161/CIRCULATIONAHA.113.001878>

Burgess, A. W. (2008). EGFR family: structure physiology signalling and therapeutic targets. *Growth Factors*, 26(5), 263-274. <https://doi.org/10.1080/08977190802312844>

Cahill, T. J., Sun, X., Ravaut, C., Villa Del Campo, C., Klaourakis, K., Lupu, I. E., . . . Riley, P. R. (2021). Tissue-resident macrophages regulate lymphatic vessel growth and patterning in the developing heart. *Development*, 148(3).  
<https://doi.org/10.1242/dev.194563>

- Califano, G., Ouzaid, I., Verze, P., Hermieu, J. F., Mirone, V., & Xylinas, E. (2021). Immune checkpoint inhibition in upper tract urothelial carcinoma. *World J Urol*, 39(5), 1357-1367. <https://doi.org/10.1007/s00345-020-03502-7>
- Carapetis, J. R. (2007). Rheumatic heart disease in developing countries. *N Engl J Med*, 357(5), 439-441. <https://doi.org/10.1056/NEJMp078039>
- Carlsen, H. S., Bækkevold, E. S., Morton, H. C., Haraldsen, G., & Brandtzaeg, P. (2004). Monocyte-like and mature macrophages produce CXCL13 (B cell-attracting chemokine 1) in inflammatory lesions with lymphoid neogenesis. *Blood*, 104(10), 3021-3027. <https://doi.org/10.1182/blood-2004-02-0701>
- Che, T. F., Lin, C. W., Wu, Y. Y., Chen, Y. J., Han, C. L., Chang, Y. L., . . . Yang, P. C. (2015). Mitochondrial translocation of EGFR regulates mitochondria dynamics and promotes metastasis in NSCLC. *Oncotarget*, 6(35), 37349-37366. <https://doi.org/10.18632/oncotarget.5736>
- Chen, B., Huang, S., Su, Y., Wu, Y. J., Hanna, A., Brickshawana, A., . . . Frangogiannis, N. G. (2019). Macrophage Smad3 Protects the Infarcted Heart, Stimulating Phagocytosis and Regulating Inflammation. *Circ Res*, 125(1), 55-70. <https://doi.org/10.1161/CIRCRESAHA.119.315069>
- Chen, G., & Goeddel, D. V. (2002). TNF-R1 signaling: a beautiful pathway. *Science*, 296(5573), 1634-1635. <https://doi.org/10.1126/science.1071924>
- Clausen, B. E., Burkhardt, C., Reith, W., Renkawitz, R., & Förster, I. (1999). Conditional gene targeting in macrophages and granulocytes using LysMcre mice. *Transgenic Res*, 8(4), 265-277. <https://doi.org/10.1023/a:1008942828960>
- Daub, H., Weiss, F. U., Wallasch, C., & Ullrich, A. (1996). Role of transactivation of the EGF receptor in signalling by G-protein-coupled receptors. *Nature*, 379(6565), 557-560. <https://doi.org/10.1038/379557a0>
- De Ponti, F. F., & Scott, C. L. (2021). In matters of the heart, (cellular) communication is key. *Immunity*, 54(9), 1906-1908. <https://doi.org/10.1016/j.immuni.2021.08.004>
- DeBerge, M., Grinton, K., Subramanian, M., Wilsbacher, L. D., Rothlin, C. V., Tabas, I., & Thorp, E. B. (2021). Macrophage AXL receptor tyrosine kinase inflames the heart after reperfused myocardial infarction. *J Clin Invest*, 131(6). <https://doi.org/10.1172/JCI139576>

- Dehn, S., & Thorp, E. B. (2018). Myeloid receptor CD36 is required for early phagocytosis of myocardial infarcts and induction of Nr4a1-dependent mechanisms of cardiac repair. *FASEB J*, 32(1), 254-264. <https://doi.org/10.1096/fj.201700450R>
- Deller, M. C., & Yvonne Jones, E. (2000). Cell surface receptors. *Curr Opin Struct Biol*, 10(2), 213-219. [https://doi.org/10.1016/s0959-440x\(00\)00072-5](https://doi.org/10.1016/s0959-440x(00)00072-5)
- Demory, M. L., Boerner, J. L., Davidson, R., Faust, W., Miyake, T., Lee, I., . . . Parsons, S. J. (2009). Epidermal growth factor receptor translocation to the mitochondria: regulation and effect. *J Biol Chem*, 284(52), 36592-36604. <https://doi.org/10.1074/jbc.M109.000760>
- Dick, S. A., Macklin, J. A., Nejat, S., Momen, A., Clemente-Casares, X., Althagafi, M. G., . . . Eelman, S. (2019). Self-renewing resident cardiac macrophages limit adverse remodeling following myocardial infarction. *Nat Immunol*, 20(1), 29-39. <https://doi.org/10.1038/s41590-018-0272-2>
- Dick, S. A., Wong, A., Hamidzada, H., Nejat, S., Nechanitzky, R., Vohra, S., . . . Eelman, S. (2022). Three tissue resident macrophage subsets coexist across organs with conserved origins and life cycles. *Sci Immunol*, 7(67), eabf7777. <https://doi.org/10.1126/sciimmunol.abf7777>
- Dirkx, E., da Costa Martins, P. A., & De Windt, L. J. (2013). Regulation of fetal gene expression in heart failure. *Biochim Biophys Acta*, 1832(12), 2414-2424. <https://doi.org/10.1016/j.bbadis.2013.07.023>
- Eguchi, A., Coleman, R., Gresham, K., Gao, E., Ibetti, J., Chuprun, J. K., & Koch, W. J. (2021). GRK5 is a regulator of fibroblast activation and cardiac fibrosis. *Proc Natl Acad Sci U S A*, 118(5). <https://doi.org/10.1073/pnas.2012854118>
- EJ, M., & SL, L. (2021). *Physiology, Cellular Receptor*. StatPearls Publishing.
- Engström, A., Erlandsson, A., Delbro, D., & Wijkander, J. (2014). Conditioned media from macrophages of M1, but not M2 phenotype, inhibit the proliferation of the colon cancer cell lines HT-29 and CACO-2. *Int J Oncol*, 44(2), 385-392. <https://doi.org/10.3892/ijo.2013.2203>
- Eelman, S., Lavine, K. J., Beaudin, A. E., Sojka, D. K., Carrero, J. A., Calderon, B., . . . Mann, D. L. (2014). Embryonic and adult-derived resident cardiac macrophages are maintained through distinct mechanisms at steady state and during inflammation. *Immunity*, 40(1), 91-104. <https://doi.org/10.1016/j.immuni.2013.11.019>

Evdokimova, V., Tognon, C. E., Benatar, T., Yang, W., Krutikov, K., Pollak, M., . . . Seth, A. (2012). IGFBP7 binds to the IGF-1 receptor and blocks its activation by insulin-like growth factors. *Sci Signal*, 5(255), ra92. <https://doi.org/10.1126/scisignal.2003184>

Fernández, C., Torrealba, N., Altamirano, F., Garrido-Moreno, V., Vásquez-Trincado, C., Flores-Vergara, R., . . . Lavandero, S. (2021). Polycystin-1 is required for insulin-like growth factor 1-induced cardiomyocyte hypertrophy. *PLoS One*, 16(8), e0255452. <https://doi.org/10.1371/journal.pone.0255452>

Ferraro, B., Leoni, G., Hinkel, R., Ormanns, S., Paulin, N., Ortega-Gomez, A., . . . Soehnlein, O. (2019). Pro-Angiogenic Macrophage Phenotype to Promote Myocardial Repair. *J Am Coll Cardiol*, 73(23), 2990-3002. <https://doi.org/10.1016/j.jacc.2019.03.503>

Fine, N., Tasevski, N., McCulloch, C. A., Tenenbaum, H. C., & Glogauer, M. (2020). The Neutrophil: Constant Defender and First Responder. *Front Immunol*, 11, 571085. <https://doi.org/10.3389/fimmu.2020.571085>

Fu, X., Khalil, H., Kanisicak, O., Boyer, J. G., Vagnozzi, R. J., Maliken, B. D., . . . Molkentin, J. D. (2018). Specialized fibroblast differentiated states underlie scar formation in the infarcted mouse heart. *J Clin Invest*, 128(5), 2127-2143. <https://doi.org/10.1172/JCI98215>

Fuchs, T., Hahn, M., Ries, L., Giesler, S., Busch, S., Wang, C., . . . Neumaier, M. (2018). Expression of combinatorial immunoglobulins in macrophages in the tumor microenvironment. *PLoS One*, 13(9), e0204108. <https://doi.org/10.1371/journal.pone.0204108>

Galuppo, P., Vettorazzi, S., Hövelmann, J., Scholz, C. J., Tuckermann, J. P., Bauersachs, J., & Fraccarollo, D. (2017). The glucocorticoid receptor in monocyte-derived macrophages is critical for cardiac infarct repair and remodeling. *FASEB J*, 31(11), 5122-5132. <https://doi.org/10.1096/fj.201700317R>

Gao, E., Lei, Y. H., Shang, X., Huang, Z. M., Zuo, L., Boucher, M., . . . Koch, W. J. (2010). A novel and efficient model of coronary artery ligation and myocardial infarction in the mouse. *Circ Res*, 107(12), 1445-1453. <https://doi.org/10.1161/CIRCRESAHA.110.223925>

Gibb, A. A., Lazaropoulos, M. P., & Elrod, J. W. (2020). Myofibroblasts and Fibrosis: Mitochondrial and Metabolic Control of Cellular Differentiation. *Circ Res*, 127(3), 427-447. <https://doi.org/10.1161/CIRCRESAHA.120.316958>

Glinton, K. E., Ma, W., Lantz, C. W., Grigoryeva, L. S., DeBerge, M., Liu, X., . . . Thorp, E. B. (2022). Macrophage-produced VEGFC is induced by efferocytosis to

ameliorate cardiac injury and inflammation. *J Clin Invest*.  
<https://doi.org/10.1172/JCI140685>

Gogiraju, R., Bochenek, M. L., & Schäfer, K. (2019). Angiogenic Endothelial Cell Signaling in Cardiac Hypertrophy and Heart Failure. *Front Cardiovasc Med*, 6, 20.  
<https://doi.org/10.3389/fcvm.2019.00020>

Gombozhapova, A., Rogovskaya, Y., Shurupov, V., Rebenkova, M., Kzhyshkowska, J., Popov, S. V., . . . Ryabov, V. (2017). Macrophage activation and polarization in post-infarction cardiac remodeling. *J Biomed Sci*, 24(1), 13. <https://doi.org/10.1186/s12929-017-0322-3>

Grisanti, L. A., Guo, S., & Tilley, D. G. (2017). Cardiac GPCR-Mediated EGFR Transactivation: Impact and Therapeutic Implications. *J Cardiovasc Pharmacol*, 70(1), 3-9. <https://doi.org/10.1097/FJC.0000000000000462>

Grisanti, L. A., Talarico, J. A., Carter, R. L., Yu, J. E., Repas, A. A., Radcliffe, S. W., . . . Tilley, D. G. (2014).  $\beta$ -Adrenergic receptor-mediated transactivation of epidermal growth factor receptor decreases cardiomyocyte apoptosis through differential subcellular activation of ERK1/2 and Akt. *J Mol Cell Cardiol*, 72, 39-51.  
<https://doi.org/10.1016/j.yjmcc.2014.02.009>

Guilliams, M., Thierry, G. R., Bonnardel, J., & Bajenoff, M. (2020). Establishment and Maintenance of the Macrophage Niche. *Immunity*, 52(3), 434-451.  
<https://doi.org/10.1016/j.immuni.2020.02.015>

Guo, S., Okyere, A. D., McEachern, E., Strong, J. L., Carter, R. L., Patwa, V. C., . . . Tilley, D. G. (2022). Epidermal growth factor receptor-dependent maintenance of cardiac contractility. *Cardiovasc Res*, 118(5), 1276-1288. <https://doi.org/10.1093/cvr/cvab149>

Halade, G. V., Norris, P. C., Kain, V., Serhan, C. N., & Ingle, K. A. (2018). Splenic leukocytes define the resolution of inflammation in heart failure. *Sci Signal*, 11(520).  
<https://doi.org/10.1126/scisignal.aao1818>

Hardbower, D. M., Coburn, L. A., Asim, M., Singh, K., Sierra, J. C., Barry, D. P., . . . Wilson, K. T. (2017). EGFR-mediated macrophage activation promotes colitis-associated tumorigenesis. *Oncogene*, 36(27), 3807-3819. <https://doi.org/10.1038/onc.2017.23>

Hardbower, D. M., Singh, K., Asim, M., Verriere, T. G., Olivares-Villagómez, D., Barry, D. P., . . . Wilson, K. T. (2016). EGFR regulates macrophage activation and function in bacterial infection. *J Clin Invest*, 126(9), 3296-3312. <https://doi.org/10.1172/JCI83585>

Hawkins, N. M., Petrie, M. C., Jhund, P. S., Chalmers, G. W., Dunn, F. G., & McMurray, J. J. (2009). Heart failure and chronic obstructive pulmonary disease: diagnostic pitfalls and epidemiology. *Eur J Heart Fail*, 11(2), 130-139. <https://doi.org/10.1093/eurjhf/hfn013>

He, L., Huang, X., Kanisicak, O., Li, Y., Wang, Y., Pu, W., . . . Zhou, B. (2017). Preexisting endothelial cells mediate cardiac neovascularization after injury. *J Clin Invest*, 127(8), 2968-2981. <https://doi.org/10.1172/JCI93868>

He, L., Jhong, J. H., Chen, Q., Huang, K. Y., Strittmatter, K., Kreuzer, J., . . . Marneros, A. G. (2021). Global characterization of macrophage polarization mechanisms and identification of M2-type polarization inhibitors. *Cell Rep*, 37(5), 109955. <https://doi.org/10.1016/j.celrep.2021.109955>

Heineke, J., & Molkentin, J. D. (2006). Regulation of cardiac hypertrophy by intracellular signalling pathways. *Nat Rev Mol Cell Biol*, 7(8), 589-600. <https://doi.org/10.1038/nrm1983>

Hilgendorf, I., Gerhardt, L. M., Tan, T. C., Winter, C., Holderried, T. A., Chousterman, B. G., . . . Swirski, F. K. (2014). Ly-6Chigh monocytes depend on Nr4a1 to balance both inflammatory and reparative phases in the infarcted myocardium. *Circ Res*, 114(10), 1611-1622. <https://doi.org/10.1161/CIRCRESAHA.114.303204>

Holbro, T., & Hynes, N. E. (2004). ErbB receptors: directing key signaling networks throughout life. *Annu Rev Pharmacol Toxicol*, 44, 195-217. <https://doi.org/10.1146/annurev.pharmtox.44.101802.121440>

Howangyin, K. Y., Zlatanova, I., Pinto, C., Ngkelo, A., Cochain, C., Rouanet, M., . . . Silvestre, J. S. (2016). Myeloid-Epithelial-Reproductive Receptor Tyrosine Kinase and Milk Fat Globule Epidermal Growth Factor 8 Coordinately Improve Remodeling After Myocardial Infarction via Local Delivery of Vascular Endothelial Growth Factor. *Circulation*, 133(9), 826-839. <https://doi.org/10.1161/CIRCULATIONAHA.115.020857>

Hoyer, F. F., Naxerova, K., Schloss, M. J., Hulsmans, M., Nair, A. V., Dutta, P., . . . Nahrendorf, M. (2019). Tissue-Specific Macrophage Responses to Remote Injury Impact the Outcome of Subsequent Local Immune Challenge. *Immunity*, 51(5), 899-914.e897. <https://doi.org/10.1016/j.immuni.2019.10.010>

Huang, C. Y., Hsu, L. H., Chen, C. Y., Chang, G. C., Chang, H. W., Hung, Y. M., . . . Kao, S. H. (2020). Inhibition of Alternative Cancer Cell Metabolism of EGFR Mutated Non-Small Cell Lung Cancer Serves as a Potential Therapeutic Strategy. *Cancers (Basel)*, 12(1). <https://doi.org/10.3390/cancers12010181>

- Huang, J., Sun, X., Gong, X., He, Z., Chen, L., Qiu, X., & Yin, C. C. (2014). Rearrangement and expression of the immunoglobulin  $\mu$ -chain gene in human myeloid cells. *Cell Mol Immunol*, 11(1), 94-104. <https://doi.org/10.1038/cmi.2013.45>
- Hulsmans, M., Clauss, S., Xiao, L., Aguirre, A. D., King, K. R., Hanley, A., . . . Nahrendorf, M. (2017). Macrophages Facilitate Electrical Conduction in the Heart. *Cell*, 169(3), 510-522.e520. <https://doi.org/10.1016/j.cell.2017.03.050>
- Hulsmans, M., Sager, H. B., Roh, J. D., Valero-Muñoz, M., Houstis, N. E., Iwamoto, Y., . . . Nahrendorf, M. (2018). Cardiac macrophages promote diastolic dysfunction. *J Exp Med*, 215(2), 423-440. <https://doi.org/10.1084/jem.20171274>
- Hwang, J. R., Huh, J. H., Lee, Y., Lee, S. I., Rho, S. B., & Lee, J. H. (2011). Insulin-like growth factor-binding protein-5 (IGFBP-5) inhibits TNF- $\alpha$ -induced NF- $\kappa$ B activity by binding to TNFR1. *Biochem Biophys Res Commun*, 405(4), 545-551. <https://doi.org/10.1016/j.bbrc.2011.01.064>
- Hänninen, A., Maksimow, M., Alam, C., Morgan, D. J., & Jalkanen, S. (2011). Ly6C supports preferential homing of central memory CD8<sup>+</sup> T cells into lymph nodes. *Eur J Immunol*, 41(3), 634-644. <https://doi.org/10.1002/eji.201040760>
- Ito, H., Hiroe, M., Hirata, Y., Tsujino, M., Adachi, S., Shichiri, M., . . . Marumo, F. (1993). Insulin-like growth factor-I induces hypertrophy with enhanced expression of muscle specific genes in cultured rat cardiomyocytes. *Circulation*, 87(5), 1715-1721. <https://doi.org/10.1161/01.cir.87.5.1715>
- Ivey, M. J., Kuwabara, J. T., Pai, J. T., Moore, R. E., Sun, Z., & Tallquist, M. D. (2018). Resident fibroblast expansion during cardiac growth and remodeling. *J Mol Cell Cardiol*, 114, 161-174. <https://doi.org/10.1016/j.yjmcc.2017.11.012>
- Ivey, M. J., & Tallquist, M. D. (2016). Defining the Cardiac Fibroblast. *Circ J*, 80(11), 2269-2276. <https://doi.org/10.1253/circj.CJ-16-1003>
- Jakubzick, C. V., Randolph, G. J., & Henson, P. M. (2017). Monocyte differentiation and antigen-presenting functions. *Nat Rev Immunol*, 17(6), 349-362. <https://doi.org/10.1038/nri.2017.28>
- Jura, N., Endres, N. F., Engel, K., Deindl, S., Das, R., Lamers, M. H., . . . Kuriyan, J. (2009). Mechanism for activation of the EGF receptor catalytic domain by the juxtamembrane segment. *Cell*, 137(7), 1293-1307. <https://doi.org/10.1016/j.cell.2009.04.025>

Kantor, A. B., Stall, A. M., Adams, S., & Herzenberg, L. A. (1992). Differential development of progenitor activity for three B-cell lineages. *Proc Natl Acad Sci U S A*, 89(8), 3320-3324. <https://doi.org/10.1073/pnas.89.8.3320>

Khalil, H., Kanisicak, O., Vagnozzi, R. J., Johansen, A. K., Maliken, B. D., Prasad, V., . . . Molkenkin, J. D. (2019). Cell-specific ablation of Hsp47 defines the collagen-producing cells in the injured heart. *JCI Insight*, 4(15), e128722. <https://doi.org/10.1172/jci.insight.128722>

Kondo, M. (2010). Lymphoid and myeloid lineage commitment in multipotent hematopoietic progenitors. *Immunol Rev*, 238(1), 37-46. <https://doi.org/10.1111/j.1600-065X.2010.00963.x>

Kotlyarov, S. (2022). Involvement of the Innate Immune System in the Pathogenesis of Chronic Obstructive Pulmonary Disease. *Int J Mol Sci*, 23(2). <https://doi.org/10.3390/ijms23020985>

Kovacs, T., Zakany, F., & Nagy, P. (2022). It Takes More than Two to Tango: Complex, Hierarchical, and Membrane-Modulated Interactions in the Regulation of Receptor Tyrosine Kinases. *Cancers (Basel)*, 14(4). <https://doi.org/10.3390/cancers14040944>

Lafuse, W. P., Wozniak, D. J., & Rajaram, M. V. S. (2020). Role of Cardiac Macrophages on Cardiac Inflammation, Fibrosis and Tissue Repair. *Cells*, 10(1). <https://doi.org/10.3390/cells10010051>

Lanaya, H., Natarajan, A., Komposch, K., Li, L., Amberg, N., Chen, L., . . . Sibilina, M. (2014). EGFR has a tumour-promoting role in liver macrophages during hepatocellular carcinoma formation. *Nat Cell Biol*, 16(10), 972-977. <https://doi.org/10.1038/ncb3031>

Lavine, K. J., Epelman, S., Uchida, K., Weber, K. J., Nichols, C. G., Schilling, J. D., . . . Mann, D. L. (2014). Distinct macrophage lineages contribute to disparate patterns of cardiac recovery and remodeling in the neonatal and adult heart. *Proc Natl Acad Sci U S A*, 111(45), 16029-16034. <https://doi.org/10.1073/pnas.1406508111>

Lavine, K. J., Pinto, A. R., Epelman, S., Kopecky, B. J., Clemente-Casares, X., Godwin, J., . . . Kovacic, J. C. (2018). The Macrophage in Cardiac Homeostasis and Disease: JACC Macrophage in CVD Series (Part 4). *J Am Coll Cardiol*, 72(18), 2213-2230. <https://doi.org/10.1016/j.jacc.2018.08.2149>

Lee, J. S., Jeong, S. J., Kim, S., Chalifour, L., Yun, T. J., Miah, M. A., . . . Cheong, C. (2018). Conventional Dendritic Cells Impair Recovery after Myocardial Infarction. *J Immunol*, 201(6), 1784-1798. <https://doi.org/10.4049/jimmunol.1800322>

- Lee, T. C., & Threadgill, D. W. (2009). Generation and validation of mice carrying a conditional allele of the epidermal growth factor receptor. *Genesis*, 47(2), 85-92. <https://doi.org/10.1002/dvg.20464>
- Leid, J., Carrelha, J., Boukarabila, H., Epelman, S., Jacobsen, S. E., & Lavine, K. J. (2016). Primitive Embryonic Macrophages are Required for Coronary Development and Maturation. *Circ Res*, 118(10), 1498-1511. <https://doi.org/10.1161/CIRCRESAHA.115.308270>
- Lemmon, M. A., Schlessinger, J., & Ferguson, K. M. (2014). The EGFR family: not so prototypical receptor tyrosine kinases. *Cold Spring Harb Perspect Biol*, 6(4), a020768. <https://doi.org/10.1101/cshperspect.a020768>
- Leuschner, F., Rauch, P. J., Ueno, T., Gorbatov, R., Marinelli, B., Lee, W. W., . . . Nahrendorf, M. (2012). Rapid monocyte kinetics in acute myocardial infarction are sustained by extramedullary monocytopoiesis. *J Exp Med*, 209(1), 123-137. <https://doi.org/10.1084/jem.20111009>
- Lin, S. Y., Makino, K., Xia, W., Matin, A., Wen, Y., Kwong, K. Y., . . . Hung, M. C. (2001). Nuclear localization of EGF receptor and its potential new role as a transcription factor. *Nat Cell Biol*, 3(9), 802-808. <https://doi.org/10.1038/ncb0901-802>
- Litviňuková, M., Talavera-López, C., Maatz, H., Reichart, D., Worth, C. L., Lindberg, E. L., . . . Teichmann, S. A. (2020). Cells of the adult human heart. *Nature*, 588(7838), 466-472. <https://doi.org/10.1038/s41586-020-2797-4>
- Liu, M., Yan, M., He, J., Lv, H., Chen, Z., Peng, L., . . . Ai, D. (2021). Macrophage MST1/2 Disruption Impairs Post-Infarction Cardiac Repair via LTB4. *Circ Res*, 129(10), 909-926. <https://doi.org/10.1161/CIRCRESAHA.121.319687>
- Lother, A., Bergemann, S., Deng, L., Moser, M., Bode, C., & Hein, L. (2018). Cardiac Endothelial Cell Transcriptome. *Arterioscler Thromb Vasc Biol*, 38(3), 566-574. <https://doi.org/10.1161/ATVBAHA.117.310549>
- Loukov, D., Naidoo, A., Puchta, A., Marin, J. L., & Bowdish, D. M. (2016). Tumor necrosis factor drives increased splenic monopoiesis in old mice. *J Leukoc Biol*, 100(1), 121-129. <https://doi.org/10.1189/jlb.3MA0915-433RR>
- Lu, N., Wang, L., Cao, H., Liu, L., Van Kaer, L., Washington, M. K., . . . Yan, F. (2014). Activation of the epidermal growth factor receptor in macrophages regulates cytokine production and experimental colitis. *J Immunol*, 192(3), 1013-1023. <https://doi.org/10.4049/jimmunol.1300133>

Luck, H., Khan, S., Kim, J. H., Copeland, J. K., Revelo, X. S., Tsai, S., . . . Winer, D. A. (2019). Gut-associated IgA. *Nat Commun*, 10(1), 3650. <https://doi.org/10.1038/s41467-019-11370-y>

Lázár, E., Sadek, H. A., & Bergmann, O. (2017). Cardiomyocyte renewal in the human heart: insights from the fall-out. *Eur Heart J*, 38(30), 2333-2342. <https://doi.org/10.1093/eurheartj/ehx343>

Ma, Y., Mouton, A. J., & Lindsey, M. L. (2018). Cardiac macrophage biology in the steady-state heart, the aging heart, and following myocardial infarction. *Transl Res*, 191, 15-28. <https://doi.org/10.1016/j.trsl.2017.10.001>

Machaj, F., Dembowska, E., Rosik, J., Szostak, B., Mazurek-Mochol, M., & Pawlik, A. (2019). New therapies for the treatment of heart failure: a summary of recent accomplishments. *Ther Clin Risk Manag*, 15, 147-155. <https://doi.org/10.2147/TCRM.S179302>

Makki, N., Thiel, K. W., & Miller, F. J. (2013). The epidermal growth factor receptor and its ligands in cardiovascular disease. *Int J Mol Sci*, 14(10), 20597-20613. <https://doi.org/10.3390/ijms141020597>

Mangoni, M. E., & Nargeot, J. (2008). Genesis and regulation of the heart automaticity. *Physiol Rev*, 88(3), 919-982. <https://doi.org/10.1152/physrev.00018.2007>

Manning, B. D., & Toker, A. (2017). AKT/PKB Signaling: Navigating the Network. *Cell*, 169(3), 381-405. <https://doi.org/10.1016/j.cell.2017.04.001>

Mascolo, A., di Mauro, G., Cappetta, D., De Angelis, A., Torella, D., Urbanek, K., . . . Rossi, F. (2022). Current and future therapeutic perspective in chronic heart failure. *Pharmacol Res*, 175, 106035. <https://doi.org/10.1016/j.phrs.2021.106035>

McCubbrey, A. L., Allison, K. C., Lee-Sherick, A. B., Jakubzick, C. V., & Janssen, W. J. (2017). Promoter Specificity and Efficacy in Conditional and Inducible Transgenic Targeting of Lung Macrophages. *Front Immunol*, 8, 1618. <https://doi.org/10.3389/fimmu.2017.01618>

Mia, M. M., Cibi, D. M., Abdul Ghani, S. A. B., Song, W., Tee, N., Ghosh, S., . . . Singh, M. K. (2020). YAP/TAZ deficiency reprograms macrophage phenotype and improves infarct healing and cardiac function after myocardial infarction. *PLoS Biol*, 18(12), e3000941. <https://doi.org/10.1371/journal.pbio.3000941>

Miao, K., Zhou, L., Ba, H., Li, C., Gu, H., Yin, B., . . . Wang, D. W. (2020). Transmembrane tumor necrosis factor alpha attenuates pressure-overload cardiac

hypertrophy via tumor necrosis factor receptor 2. *PLoS Biol*, 18(12), e3000967.  
<https://doi.org/10.1371/journal.pbio.3000967>

Mildner, A., & Jung, S. (2014). Development and function of dendritic cell subsets. *Immunity*, 40(5), 642-656. <https://doi.org/10.1016/j.immuni.2014.04.016>

Miyanishi, M., Tada, K., Koike, M., Uchiyama, Y., Kitamura, T., & Nagata, S. (2007). Identification of Tim4 as a phosphatidylserine receptor. *Nature*, 450(7168), 435-439.  
<https://doi.org/10.1038/nature06307>

Molawi, K., Wolf, Y., Kandalla, P. K., Favret, J., Hagemeyer, N., Frenzel, K., . . . Sieweke, M. H. (2014). Progressive replacement of embryo-derived cardiac macrophages with age. *J Exp Med*, 211(11), 2151-2158. <https://doi.org/10.1084/jem.20140639>

Moran, A. E., Forouzanfar, M. H., Roth, G. A., Mensah, G. A., Ezzati, M., Flaxman, A., . . . Naghavi, M. (2014). The global burden of ischemic heart disease in 1990 and 2010: the Global Burden of Disease 2010 study. *Circulation*, 129(14), 1493-1501.  
<https://doi.org/10.1161/CIRCULATIONAHA.113.004046>

Mouton, A. J., DeLeon-Pennell, K. Y., Rivera Gonzalez, O. J., Flynn, E. R., Freeman, T. C., Saucerman, J. J., . . . Lindsey, M. L. (2018). Mapping macrophage polarization over the myocardial infarction time continuum. *Basic Res Cardiol*, 113(4), 26.  
<https://doi.org/10.1007/s00395-018-0686-x>

Nakamura, M., & Sadoshima, J. (2018). Mechanisms of physiological and pathological cardiac hypertrophy. *Nat Rev Cardiol*, 15(7), 387-407. <https://doi.org/10.1038/s41569-018-0007-y>

Nakou, E. S., Parthenakis, F. I., Kallergis, E. M., Marketou, M. E., Nakos, K. S., & Vardas, P. E. (2016). Healthy aging and myocardium: A complicated process with various effects in cardiac structure and physiology. *Int J Cardiol*, 209, 167-175.  
<https://doi.org/10.1016/j.ijcard.2016.02.039>

Nicolás-Ávila, J. A., Lechuga-Vieco, A. V., Esteban-Martínez, L., Sánchez-Díaz, M., Díaz-García, E., Santiago, D. J., . . . Hidalgo, A. (2020). A Network of Macrophages Supports Mitochondrial Homeostasis in the Heart. *Cell*, 183(1), 94-109.e123.  
<https://doi.org/10.1016/j.cell.2020.08.031>

Ogiso, H., Ishitani, R., Nureki, O., Fukai, S., Yamanaka, M., Kim, J. H., . . . Yokoyama, S. (2002). Crystal structure of the complex of human epidermal growth factor and receptor extracellular domains. *Cell*, 110(6), 775-787. [https://doi.org/10.1016/s0092-8674\(02\)00963-7](https://doi.org/10.1016/s0092-8674(02)00963-7)

Oh, G. C., & Cho, H. J. (2020). Blood pressure and heart failure. *Clin Hypertens*, 26, 1. <https://doi.org/10.1186/s40885-019-0132-x>

Okada, T., Miyagi, H., Sako, Y., Hiroshima, M., & Mochizuki, A. (2022). Origin of diverse phosphorylation patterns in the ERBB system. *Biophys J*, 121(3), 470-480. <https://doi.org/10.1016/j.bpj.2021.12.031>

Okyere, A. D., Song, J., Patwa, V., Carter, R. L., Enjamuri, N., Lucchese, A. M., . . . Tilley, D. G. (2022). Pepducin ICL1-9-Mediated  $\beta$ 2-Adrenergic Receptor-Dependent Cardiomyocyte Contractility Occurs in a G. *Cardiovasc Drugs Ther*. <https://doi.org/10.1007/s10557-021-07299-4>

Okyere, A. D., & Tilley, D. G. (2020). Leukocyte-Dependent Regulation of Cardiac Fibrosis. *Front Physiol*, 11, 301. <https://doi.org/10.3389/fphys.2020.00301>

Overland, A. C., & Insel, P. A. (2015). Heterotrimeric G proteins directly regulate MMP14/membrane type-1 matrix metalloprotease: a novel mechanism for GPCR-EGFR transactivation. *J Biol Chem*, 290(16), 9941-9947. <https://doi.org/10.1074/jbc.C115.647073>

Park, D. S., & Fishman, G. I. (2017). Development and Function of the Cardiac Conduction System in Health and Disease. *J Cardiovasc Dev Dis*, 4(2). <https://doi.org/10.3390/jcdd4020007>

Patwa, V., Guo, S., Carter, R. L., Kraus, L., Einspahr, J., Teplitsky, D., . . . Tilley, D. G. (2021). Epidermal growth factor receptor association with  $\beta$ 1-adrenergic receptor is mediated via its juxtamembrane domain. *Cell Signal*, 78, 109846. <https://doi.org/10.1016/j.cellsig.2020.109846>

Peet, C., Ivetic, A., Bromage, D. I., & Shah, A. M. (2020). Cardiac monocytes and macrophages after myocardial infarction. *Cardiovasc Res*, 116(6), 1101-1112. <https://doi.org/10.1093/cvr/cvz336>

Pfleger, J., Coleman, R. C., Ibetti, J., Roy, R., Kyriazis, I. D., Gao, E., . . . Koch, W. J. (2020). Genomic Binding Patterns of Forkhead Box Protein O1 Reveal Its Unique Role in Cardiac Hypertrophy. *Circulation*, 142(9), 882-898. <https://doi.org/10.1161/CIRCULATIONAHA.120.046356>

Pinto, A. R., Ilinykh, A., Ivey, M. J., Kuwabara, J. T., D'Antoni, M. L., Debuque, R., . . . Tallquist, M. D. (2016). Revisiting Cardiac Cellular Composition. *Circ Res*, 118(3), 400-409. <https://doi.org/10.1161/CIRCRESAHA.115.307778>

- Prabhu, S. D., & Frangogiannis, N. G. (2016). The Biological Basis for Cardiac Repair After Myocardial Infarction: From Inflammation to Fibrosis. *Circ Res*, 119(1), 91-112. <https://doi.org/10.1161/CIRCRESAHA.116.303577>
- Prenzel, N., Fischer, O. M., Streit, S., Hart, S., & Ullrich, A. (2001). The epidermal growth factor receptor family as a central element for cellular signal transduction and diversification. *Endocr Relat Cancer*, 8(1), 11-31. <https://doi.org/10.1677/erc.0.0080011>
- Purba, E. R., Saita, E. I., & Maruyama, I. N. (2017). Activation of the EGF Receptor by Ligand Binding and Oncogenic Mutations: The "Rotation Model". *Cells*, 6(2). <https://doi.org/10.3390/cells6020013>
- Riedemann, J., & Macaulay, V. M. (2006). IGF1R signalling and its inhibition. *Endocr Relat Cancer*, 13 Suppl 1, S33-43. <https://doi.org/10.1677/erc.1.01280>
- Rodjakovic, D., Salm, L., & Beldi, G. (2021). Function of Connexin-43 in Macrophages. *Int J Mol Sci*, 22(3). <https://doi.org/10.3390/ijms22031412>
- Roth, G. A., Mensah, G. A., Johnson, C. O., Addolorato, G., Ammirati, E., Baddour, L. M., . . . Group, G.-N.-J. G. B. o. C. D. W. (2020). Global Burden of Cardiovascular Diseases and Risk Factors, 1990-2019: Update From the GBD 2019 Study. *J Am Coll Cardiol*, 76(25), 2982-3021. <https://doi.org/10.1016/j.jacc.2020.11.010>
- Sabio, G., & Davis, R. J. (2014). TNF and MAP kinase signalling pathways. *Semin Immunol*, 26(3), 237-245. <https://doi.org/10.1016/j.smim.2014.02.009>
- Sager, H. B., Hulsmans, M., Lavine, K. J., Moreira, M. B., Heidt, T., Courties, G., . . . Nahrendorf, M. (2016). Proliferation and Recruitment Contribute to Myocardial Macrophage Expansion in Chronic Heart Failure. *Circ Res*, 119(7), 853-864. <https://doi.org/10.1161/CIRCRESAHA.116.309001>
- Sansonetti, M., Waleczek, F. J. G., Jung, M., Thum, T., & Perbellini, F. (2020). Resident cardiac macrophages: crucial modulators of cardiac (patho)physiology. *Basic Res Cardiol*, 115(6), 77. <https://doi.org/10.1007/s00395-020-00836-6>
- Savarese, G., & Lund, L. H. (2017). Global Public Health Burden of Heart Failure. *Card Fail Rev*, 3(1), 7-11. <https://doi.org/10.15420/cfr.2016:25:2>
- Savarese, G., Stolfo, D., Sinagra, G., & Lund, L. H. (2022). Heart failure with mid-range or mildly reduced ejection fraction. *Nat Rev Cardiol*, 19(2), 100-116. <https://doi.org/10.1038/s41569-021-00605-5>

Schreier, B., Rabe, S., Schneider, B., Bretschneider, M., Rupp, S., Ruhs, S., . . . Gekle, M. (2013). Loss of epidermal growth factor receptor in vascular smooth muscle cells and cardiomyocytes causes arterial hypotension and cardiac hypertrophy. *Hypertension*, 61(2), 333-340. <https://doi.org/10.1161/HYPERTENSIONAHA.112.196543>

Schreier, B., Stern, C., Dubourg, V., Nolze, A., Rabe, S., Mildenerger, S., . . . Gekle, M. (2021). Endothelial epidermal growth factor receptor is of minor importance for vascular and renal function and obesity-induced dysfunction in mice. *Sci Rep*, 11(1), 7269. <https://doi.org/10.1038/s41598-021-86587-3>

Schulz, C., Gomez Perdiguero, E., Chorro, L., Szabo-Rogers, H., Cagnard, N., Kierdorf, K., . . . Geissmann, F. (2012). A lineage of myeloid cells independent of Myb and hematopoietic stem cells. *Science*, 336(6077), 86-90. <https://doi.org/10.1126/science.1219179>

Segers, V. F. M., Brutsaert, D. L., & De Keulenaer, G. W. (2018). Cardiac Remodeling: Endothelial Cells Have More to Say Than Just NO. *Front Physiol*, 9, 382. <https://doi.org/10.3389/fphys.2018.00382>

Sen, B., & Johnson, F. M. (2011). Regulation of SRC family kinases in human cancers. *J Signal Transduct*, 2011, 865819. <https://doi.org/10.1155/2011/865819>

Severino, P., D'Amato, A., Pucci, M., Infusino, F., Adamo, F., Birtolo, L. I., . . . Fedele, F. (2020). Ischemic Heart Disease Pathophysiology Paradigms Overview: From Plaque Activation to Microvascular Dysfunction. *Int J Mol Sci*, 21(21). <https://doi.org/10.3390/ijms21218118>

Shi, J., Hua, L., Harmer, D., Li, P., & Ren, G. (2018). Cre Driver Mice Targeting Macrophages. *Methods Mol Biol*, 1784, 263-275. [https://doi.org/10.1007/978-1-4939-7837-3\\_24](https://doi.org/10.1007/978-1-4939-7837-3_24)

Shostak, K., & Chariot, A. (2015). EGFR and NF- $\kappa$ B: partners in cancer. *Trends Mol Med*, 21(6), 385-393. <https://doi.org/10.1016/j.molmed.2015.04.001>

Sibilia, M., Steinbach, J. P., Stingl, L., Aguzzi, A., & Wagner, E. F. (1998). A strain-independent postnatal neurodegeneration in mice lacking the EGF receptor. *EMBO J*, 17(3), 719-731. <https://doi.org/10.1093/emboj/17.3.719>

Skelly, D. A., Squiers, G. T., McLellan, M. A., Bolisetty, M. T., Robson, P., Rosenthal, N. A., & Pinto, A. R. (2018). Single-Cell Transcriptional Profiling Reveals Cellular Diversity and Intercommunication in the Mouse Heart. *Cell Rep*, 22(3), 600-610. <https://doi.org/10.1016/j.celrep.2017.12.072>

- Song, J., Frieler, R. A., Whitesall, S. E., Chung, Y., Vigil, T. M., Muir, L. A., . . . Mortensen, R. M. (2021). Myeloid interleukin-4 receptor  $\alpha$  is essential in postmyocardial infarction healing by regulating inflammation and fibrotic remodeling. *Am J Physiol Heart Circ Physiol*, 320(1), H323-H337. <https://doi.org/10.1152/ajpheart.00251.2020>
- Sorkin, A., & Goh, L. K. (2009). Endocytosis and intracellular trafficking of ErbBs. *Exp Cell Res*, 315(4), 683-696. <https://doi.org/10.1016/j.yexcr.2008.07.029>
- Sousa, L. P., Lax, I., Shen, H., Ferguson, S. M., De Camilli, P., & Schlessinger, J. (2012). Suppression of EGFR endocytosis by dynamin depletion reveals that EGFR signaling occurs primarily at the plasma membrane. *Proc Natl Acad Sci U S A*, 109(12), 4419-4424. <https://doi.org/10.1073/pnas.1200164109>
- Squire, J. M. (1971). General model for the structure of all myosin-containing filaments. *Nature*, 233(5320), 457-462. <https://doi.org/10.1038/233457a0>
- Srivatsa, S., Paul, M. C., Cardone, C., Holcman, M., Amberg, N., Pathria, P., . . . Sibilio, M. (2017). EGFR in Tumor-Associated Myeloid Cells Promotes Development of Colorectal Cancer in Mice and Associates With Outcomes of Patients. *Gastroenterology*, 153(1), 178-190.e110. <https://doi.org/10.1053/j.gastro.2017.03.053>
- Stevens, S. M., von Gise, A., VanDusen, N., Zhou, B., & Pu, W. T. (2016). Epicardium is required for cardiac seeding by yolk sac macrophages, precursors of resident macrophages of the adult heart. *Dev Biol*, 413(2), 153-159. <https://doi.org/10.1016/j.ydbio.2016.03.014>
- Sugita, J., Fujiu, K., Nakayama, Y., Matsubara, T., Matsuda, J., Oshima, T., . . . Komuro, I. (2021). Cardiac macrophages prevent sudden death during heart stress. *Nat Commun*, 12(1), 1910. <https://doi.org/10.1038/s41467-021-22178-0>
- Swirski, F. K., & Nahrendorf, M. (2018). Cardioimmunology: the immune system in cardiac homeostasis and disease. *Nat Rev Immunol*, 18(12), 733-744. <https://doi.org/10.1038/s41577-018-0065-8>
- Sylva, M., van den Hoff, M. J., & Moorman, A. F. (2014). Development of the human heart. *Am J Med Genet A*, 164A(6), 1347-1371. <https://doi.org/10.1002/ajmg.a.35896>
- Tallquist, M. D. (2018). Cardiac fibroblasts: from origin to injury. *Curr Opin Physiol*, 1, 75-79. <https://doi.org/10.1016/j.cophys.2017.08.002>
- Tirziu, D., Giordano, F. J., & Simons, M. (2010). Cell communications in the heart. *Circulation*, 122(9), 928-937. <https://doi.org/10.1161/CIRCULATIONAHA.108.847731>

Tucker, N. R., Chaffin, M., Fleming, S. J., Hall, A. W., Parsons, V. A., Bedi, K. C., . . . Ellinor, P. T. (2020). Transcriptional and Cellular Diversity of the Human Heart. *Circulation*, 142(5), 466-482. <https://doi.org/10.1161/CIRCULATIONAHA.119.045401>

Van den Bossche, J., Baardman, J., & de Winther, M. P. (2015). Metabolic Characterization of Polarized M1 and M2 Bone Marrow-derived Macrophages Using Real-time Extracellular Flux Analysis. *J Vis Exp*(105). <https://doi.org/10.3791/53424>

Van der Borgh, K., & Lambrecht, B. N. (2018). Heart macrophages and dendritic cells in sickness and in health: A tale of a complicated marriage. *Cell Immunol*, 330, 105-113. <https://doi.org/10.1016/j.cellimm.2018.03.011>

van der Laan, A. M., Hirsch, A., Robbers, L. F., Nijveldt, R., Lommerse, I., Delewi, R., . . . Piek, J. J. (2012). A proinflammatory monocyte response is associated with myocardial injury and impaired functional outcome in patients with ST-segment elevation myocardial infarction: monocytes and myocardial infarction. *Am Heart J*, 163(1), 57-65.e52. <https://doi.org/10.1016/j.ahj.2011.09.002>

Vanhaesebroeck, B., Stephens, L., & Hawkins, P. (2012). PI3K signalling: the path to discovery and understanding. *Nat Rev Mol Cell Biol*, 13(3), 195-203. <https://doi.org/10.1038/nrm3290>

Viola, A., Munari, F., Sánchez-Rodríguez, R., Scolaro, T., & Castegna, A. (2019). The Metabolic Signature of Macrophage Responses. *Front Immunol*, 10, 1462. <https://doi.org/10.3389/fimmu.2019.01462>

Virani, S. S., Alonso, A., Aparicio, H. J., Benjamin, E. J., Bittencourt, M. S., Callaway, C. W., . . . Subcommittee, A. H. A. C. o. E. a. P. S. C. a. S. S. (2021). Heart Disease and Stroke Statistics-2021 Update: A Report From the American Heart Association. *Circulation*, 143(8), e254-e743. <https://doi.org/10.1161/CIR.0000000000000950>

Walklate, J., Ferrantini, C., Johnson, C. A., Tesi, C., Poggesi, C., & Geeves, M. A. (2021). Alpha and beta myosin isoforms and human atrial and ventricular contraction. *Cell Mol Life Sci*, 78(23), 7309-7337. <https://doi.org/10.1007/s00018-021-03971-y>

Waugh, M. G., & Hsuan, J. J. (2001). EGF receptors as transcription factors: ridiculous or sublime? *Nat Cell Biol*, 3(9), E209-211. <https://doi.org/10.1038/ncb0901-e209>

Wee, P., & Wang, Z. (2017). Epidermal Growth Factor Receptor Cell Proliferation Signaling Pathways. *Cancers (Basel)*, 9(5). <https://doi.org/10.3390/cancers9050052>

Weirather, J., Hofmann, U. D., Beyersdorf, N., Ramos, G. C., Vogel, B., Frey, A., . . . Frantz, S. (2014). Foxp3+ CD4+ T cells improve healing after myocardial infarction by

modulating monocyte/macrophage differentiation. *Circ Res*, 115(1), 55-67.  
<https://doi.org/10.1161/CIRCRESAHA.115.303895>

Weischenfeldt, J., & Porse, B. (2008). Bone Marrow-Derived Macrophages (BMM): Isolation and Applications. *CSH Protoc*, 2008, pdb.prot5080.  
<https://doi.org/10.1101/pdb.prot5080>

Williams, J. W., Giannarelli, C., Rahman, A., Randolph, G. J., & Kovacic, J. C. (2018). Macrophage Biology, Classification, and Phenotype in Cardiovascular Disease: JACC Macrophage in CVD Series (Part 1). *J Am Coll Cardiol*, 72(18), 2166-2180.  
<https://doi.org/10.1016/j.jacc.2018.08.2148>

Wolf, A. A., Yáñez, A., Barman, P. K., & Goodridge, H. S. (2019). The Ontogeny of Monocyte Subsets. *Front Immunol*, 10, 1642. <https://doi.org/10.3389/fimmu.2019.01642>

Wong, N. R., Mohan, J., Kopecky, B. J., Guo, S., Du, L., Leid, J., . . . Lavine, K. J. (2021). Resident cardiac macrophages mediate adaptive myocardial remodeling. *Immunity*, 54(9), 2072-2088.e2077. <https://doi.org/10.1016/j.immuni.2021.07.003>

Wu, L., Dalal, R., Cao, C. D., Postoak, J. L., Yang, G., Zhang, Q., . . . Van Kaer, L. (2019). IL-10-producing B cells are enriched in murine pericardial adipose tissues and ameliorate the outcome of acute myocardial infarction. *Proc Natl Acad Sci U S A*, 116(43), 21673-21684. <https://doi.org/10.1073/pnas.1911464116>

Yin, H., Favreau-Lessard, A. J., deKay, J. T., Herrmann, Y. R., Robich, M. P., Koza, R. A., . . . Ryzhov, S. (2021). Protective role of ErbB3 signaling in myeloid cells during adaptation to cardiac pressure overload. *J Mol Cell Cardiol*, 152, 1-16.  
<https://doi.org/10.1016/j.yjmcc.2020.11.009>

Ying, W., Cheruku, P. S., Bazer, F. W., Safe, S. H., & Zhou, B. (2013). Investigation of macrophage polarization using bone marrow derived macrophages. *J Vis Exp*(76).  
<https://doi.org/10.3791/50323>

Yokoyama, T., Nakano, M., Bednarczyk, J. L., McIntyre, B. W., Entman, M., & Mann, D. L. (1997). Tumor necrosis factor-alpha provokes a hypertrophic growth response in adult cardiac myocytes. *Circulation*, 95(5), 1247-1252.  
<https://doi.org/10.1161/01.cir.95.5.1247>

Yoon, S., & Seger, R. (2006). The extracellular signal-regulated kinase: multiple substrates regulate diverse cellular functions. *Growth Factors*, 24(1), 21-44.  
<https://doi.org/10.1080/02699050500284218>

Zaman, R., Hamidzada, H., Kantores, C., Wong, A., Dick, S. A., Wang, Y., . . . Epelman, S. (2021). Selective loss of resident macrophage-derived insulin-like growth factor-1 abolishes adaptive cardiac growth to stress. *Immunity*, 54(9), 2057-2071.e2056. <https://doi.org/10.1016/j.immuni.2021.07.006>

Zeboudj, L., Giraud, A., Guyonnet, L., Zhang, Y., Laurans, L., Esposito, B., . . . Ait-Oufella, H. (2018). Selective EGFR (Epidermal Growth Factor Receptor) Deletion in Myeloid Cells Limits Atherosclerosis-Brief Report. *Arterioscler Thromb Vasc Biol*, 38(1), 114-119. <https://doi.org/10.1161/ATVBAHA.117.309927>

Zhang, S., Weinberg, S., DeBerge, M., Gainullina, A., Schipma, M., Kinchen, J. M., . . . Thorp, E. B. (2019). Efferocytosis Fuels Requirements of Fatty Acid Oxidation and the Electron Transport Chain to Polarize Macrophages for Tissue Repair. *Cell Metab*, 29(2), 443-456.e445. <https://doi.org/10.1016/j.cmet.2018.12.004>

Zhang, X., Gureasko, J., Shen, K., Cole, P. A., & Kuriyan, J. (2006). An allosteric mechanism for activation of the kinase domain of epidermal growth factor receptor. *Cell*, 125(6), 1137-1149. <https://doi.org/10.1016/j.cell.2006.05.013>

Zhang, Y., Yang, X., Liu, H., Cai, M., & Shentu, Y. (2020). Inhibition of Tumor Lymphangiogenesis is an Important Part that EGFR-TKIs Play in the Treatment of NSCLC. *J Cancer*, 11(1), 241-250. <https://doi.org/10.7150/jca.35448>

Zhao, G., Liu, L., Peek, R. M., Hao, X., Polk, D. B., Li, H., & Yan, F. (2016). Activation of Epidermal Growth Factor Receptor in Macrophages Mediates Feedback Inhibition of M2 Polarization and Gastrointestinal Tumor Cell Growth. *J Biol Chem*, 291(39), 20462-20472. <https://doi.org/10.1074/jbc.M116.750182>

Zhao, L., Cheng, G., Jin, R., Afzal, M. R., Samanta, A., Xuan, Y. T., . . . Dawn, B. (2016). Deletion of Interleukin-6 Attenuates Pressure Overload-Induced Left Ventricular Hypertrophy and Dysfunction. *Circ Res*, 118(12), 1918-1929. <https://doi.org/10.1161/CIRCRESAHA.116.308688>

Ziaeeian, B., & Fonarow, G. C. (2016). Epidemiology and aetiology of heart failure. *Nat Rev Cardiol*, 13(6), 368-378. <https://doi.org/10.1038/nrcardio.2016.25>

Zouggari, Y., Ait-Oufella, H., Bonnin, P., Simon, T., Sage, A. P., Gu erin, C., . . . Mallat, Z. (2013). B lymphocytes trigger monocyte mobilization and impair heart function after acute myocardial infarction. *Nat Med*, 19(10), 1273-1280. <https://doi.org/10.1038/nm.3284>